

***Controlled Assembly of Supramolecular  
Nanofibers and Their Applications***

**Dissertation**

zur Erlangung des akademischen Grades eines  
Doktors der Naturwissenschaften (Dr. rer. nat.)  
an der Bayreuther Graduiertenschule für Mathematik  
und Naturwissenschaften (BayNAT) der Universität Bayreuth

vorgelegt von

**Daniel Weiß**

Hannover

Bayreuth, 2015



Die vorliegende Arbeit wurde in der Zeit von Oktober 2012 bis Juni 2016 in Bayreuth am Lehrstuhl Makromolekular Chemie I unter Betreuung von Herrn Professor Dr. Hans-Werner Schmidt angefertigt

Dissertation eingereicht am: 28.06.2016

Zulassung durch das Leitungsgremium: 26.07.2016

Wissenschaftliches Kolloquium: 09.11.2016

Amtierender Direktor: Prof. Dr. Stephan Kümmel

Prüfungsausschuss:

Prof. Dr. Hans-Werner Schmidt	(Erstgutachter)
Prof. Dr. Andreas Greiner	(Zweitgutachter)
Prof. Dr. Stefan Förster	(Vorsitz)
Prof. Dr. Thomas Scheibel	



## TABLE OF CONTENTS

<b>1</b>	<b>INTRODUCTION.....</b>	<b>1</b>
1.1	PREPARATION OF MICRO- AND NANOFIBERS.....	1
	Electrospinning.....	2
	Melt-blowing.....	4
	Centrifugal spinning.....	5
1.2	SUPRAMOLECULAR CHEMISTRY.....	7
	Interactions in supramolecular systems.....	7
	Ion-dipole interactions.....	7
	Cation- $\pi$ interactions.....	8
	Hydrogen bonds.....	9
1.3	MATERIALS CLASS OF 1,3,5-BENZENETRISAMIDES.....	11
	Formation of columnar stacks in the solid state.....	12
	Formation of one-dimensional structures from solution.....	14
	Applications of 1,3,5-benzenetrisamides.....	15
1.4	PRINCIPLES OF FILTRATION TECHNOLOGY.....	17
	Separation by filtration.....	17
	Mechanisms of filtration.....	18
	Depth filtration.....	20
	Characterization of filter media.....	21
	Applications of filters.....	23
<b>2</b>	<b>AIM AND MOTIVATION.....</b>	<b>25</b>
	Self-assembly of alkoxy-substituted 1,3,5-benzenetrisamides under controlled conditions.....	25
	Supramolecular nanofibers for air filtration applications.....	26
	Sand - supramolecular nanofiber filters for the removal of bacteria from water.....	27
<b>3</b>	<b>SELF-ASSEMBLY OF ALKOXY-SUBSTITUTED 1,3,5-BENZENETRISAMIDES UNDER CONTROLLED CONDITIONS.....</b>	<b>29</b>
3.1	INTRODUCTION.....	29
	Methods to self-assemble 1,3,5-benzenetrisamides from solution.....	29
	Industrial crystallization from solution.....	30
	Approach in this thesis.....	31
3.2	EXPERIMENTAL SETUP FOR SELF-ASSEMBLY UPON COOLING.....	34
3.3	EXPERIMENTAL DETAILS FOR MATERIALS SELECTION.....	40
	Implementation of preliminary self-assembly experiments.....	40
	Determination of solubility.....	40

3.4	MATERIALS SELECTION FOR A SUITABLE SELF-ASSEMBLY SYSTEM.....	42
	Self-assembly screening experiments.....	43
	Temperature dependent solubility of selected BTAs.....	45
3.5	SELF-ASSEMBLY UNDER CONTROLLED CONDITIONS.....	49
	Implementation of self-assembly experiments from solution under controlled conditions .....	49
	Sample preparation for scanning electron microscopy .....	49
	Evaluation of SEM-images .....	50
3.6	MORPHOLOGY OF SUPRAMOLECULAR FIBERS FROM DIFFERENT EXPERIMENTS UNDER CONTROLLED CONDITIONS.....	52
	Influence of stirring velocities on temperature profiles .....	52
	Sample preparation .....	54
	Influence of applied cooling temperature on fiber morphology .....	58
3.7	CONCLUSION .....	61
<b>4</b>	<b>SUPRAMOLECULAR NANOFIBERS FOR AIR FILTRATION APPLICATIONS .....</b>	<b>63</b>
4.1	INTRODUCTION .....	63
	Fine particulate air-pollution .....	63
	Preparation of nanofibers for filtration applications .....	64
4.2	EXPERIMENTAL.....	68
	Materials.....	68
	Preparation of nanofiber-microfiber composites .....	70
	Sample preparation for SEM investigations.....	72
	Determination of supramolecular fiber content.....	72
	Air filtration test rig setup.....	72
	Implementation of filtration tests .....	74
	Turbidity measurements.....	74
	Infrared spectroscopy .....	75
	Capillary flow porometry .....	75
4.3	RESULTS AND DISCUSSION .....	77
	4.3.1 <i>Nanofiber-microfiber composites based on 1,3,5-benzenetrisamides with branched alkyl chains.</i> 77	
	Turbidity measurements.....	77
	Reproducibility of nanofiber-microfiber preparation process .....	80
	Concentration dependent preparation of nanofiber-microfiber composites.....	82
	Filtration efficiencies of composites prepared from BTA solution with different concentrations.....	86
	Capillary flow porometry .....	90
	Solvent dependent preparation of nanofiber-microfiber composites.....	91
	Filtration efficiencies of composites prepared from different solvents.....	95
	Infrared spectroscopy of nanofiber-microfiber composites .....	98
	Conclusion .....	100

4.3.2	<i>Nanofiber-microfiber composites based on BTA 4</i> .....	101
	Concentration dependent preparation of nanofiber-microfiber composites .....	101
	Mass fraction of supramolecular nanofibers in nanofiber-microfiber composites.....	103
	Filtration efficiencies of composites prepared from BTA solution with different concentrations .....	103
	Conclusion .....	105
4.4	CONCLUSION .....	106
<b>5</b>	<b>SAND - SUPRAMOLECULAR NANOFIBER FILTERS FOR THE REMOVAL OF BACTERIA FROM WATER .....</b>	<b>107</b>
5.1	INTRODUCTION .....	107
	Current situation in water treatment .....	107
5.2	PREPARATION OF FILTER UNITS COMPOSED OF SAND AND SUPRAMOLECULAR NANOFIBERS .....	112
	Materials .....	112
	Preparation of sand beds with supramolecular nanofibers .....	114
	Characterization of sand - supramolecular nanofiber filters .....	115
5.3	DEVELOPMENT OF A LIQUID FILTRATION TEST SETUP .....	118
	Setup for liquid filtration experiments.....	118
	Sample holder .....	120
	Filtration of polymer micro-particles as model system .....	124
	Filtration performance of polymer micro-particles from water .....	126
	Differential pressure during the filtration process.....	128
	Preparation of sand - supramolecular nanofiber filters from solutions with different concentrations.....	131
5.4	FILTRATION OF <i>E. COLI</i> BACTERIA FROM WATER .....	134
	Implementation of filtration process .....	134
	Time dependent bacterial growth curves .....	136
	Colony counting experiments .....	138
	Results of filtration experiments to remove <i>E. coli</i> bacteria from water .....	138
5.5	CONCLUSION .....	143
<b>6</b>	<b>SUMMARY .....</b>	<b>145</b>
<b>7</b>	<b>ZUSAMMENFASSUNG .....</b>	<b>149</b>
<b>8</b>	<b>APPENDIX .....</b>	<b>153</b>
8.1	MATERIALS AND METHODS .....	153
8.2	SYNTHESIS AND ANALYTICAL DATA OF <i>N,N',N''</i> -TRIS(2-ETHOXYETHYL)BENZENE-1,3,5-TRICARBOXAMIDE .....	154
8.3	SYNTHESIS AND ANALYTICAL DATA OF <i>N,N',N''</i> -TRIS(2-METHOXYETHYL)BENZENE-1,3,5-TRICARBOXAMIDE.....	157
8.4	SYNTHESIS AND ANALYTICAL DATA OF <i>N,N',N''</i> -TRIS(1-METHOXYPROPAN-2-YL)BENZENE-1,3,5-TRICARBOXAMIDE ..	160

8.5	SYNTHESIS AND ANALYTICAL DATA OF <i>N,N',N''</i> -TRIS(1-METHOXYBUTAN-2-YL)BENZENE-1,3,5-TRICARBOXAMIDE ....	163
8.6	SYNTHESIS AND ANALYTICAL DATA OF <i>N,N',N''</i> -TRIS(2-ISOPROPOXYETHYL)BENZENE-1,3,5-TRICARBOXAMIDE .....	166
8.7	SYNTHESIS AND ANALYTICAL DATA OF <i>N,N',N''</i> -TRIS(2-ETHYLHEXYL)BENZENE-1,3,5-TRICARBOXAMIDE .....	169
8.8	SYNTHESIS AND ANALYTICAL DATA OF <i>N,N',N''</i> -TRIS(6-METHYLHEPTYL)BENZENE-1,3,5-TRICARBOXAMIDE .....	171
8.9	SYNTHESIS AND ANALYTICAL DATA OF <i>N,N',N''</i> -TRIS(3-METHYL BUTYL)BENZENE-1,3,5-TRICARBOXAMIDE .....	173
<b>9</b>	<b>REFERENCES.....</b>	<b>175</b>
	<b>DANKSAGUNG.....</b>	<b>189</b>

### 1 Introduction

Scientific work performed in the course of this thesis is divided into three parts with individual goals that are all related to the controlled self-assembly of supramolecular micro- and nanofibers. The introduction of this thesis provides a brief overview of selected topics that will be essential to the individual parts presented later. Each of these parts is concerned with the preparation of fibers with diameters down to the nanometer range. So called “*top-down*” approaches that are commonly used in industrial fiber production for the preparation of mostly polymer microfibers as well as nanofibers will therefore be introduced briefly. Research carried out in the course of this thesis focuses on a very different “*bottom-up*” approach and the preparation of supramolecular fibers with diameters in the nanometer range. In this context, the field of supramolecular chemistry and the self-assembly of low molecular weight compounds into nanostructures will be discussed. In particular, work presented in chapter 3 focuses on the controlled preparation of supramolecular nanofibers from solution under defined conditions. However, the parts presented in chapters 4 and 5 are mostly concerned with the adaption of supramolecular nanofibers to potential real-life applications such as filtration of gases or liquids. Principles of separation technology will also be discussed in the introduction with special emphasis on the field of filtration.

#### 1.1 Preparation of micro- and nanofibers

Many technologies affecting everyday life rely on the controlled preparation of micro- and nanofibers with defined morphology such as filtration applications, protective clothing, or tissue engineering.<sup>[1-6]</sup> Much academic and industrial research focuses on the development of a variety of different fiber preparation methods to obtain tailored fibers exhibiting the desired dimensions and morphology as well as chemical and physical properties.<sup>[7,8]</sup>

In principle, preparation methods of micro- and nanofibers can be divided into two conceptually different approaches as shown in **Figure 1.1**. The first approach relies on so called “*top-down*” processes. Here, polymers are transformed from the macroscale into fibers with diameters in the range of micro- or nanometers by spinning and a mechanical deformation process. Common production methods are based on spinning processes, whereas “*spinning*” refers to an extrusion process of a liquid material (spinning dope) through a small spinneret to obtain continuous fibers. This spinning dope typically consists of a polymer melt or solution. Among others, melt-blowing, centrifugal spinning and

electrospinning are well-established examples of top-down processes to obtain micro- and/or nanofibers.<sup>[8]</sup>

In contrast, supramolecular chemistry provides a “bottom-up” approach for the preparation of fibers with dimensions in the micro- and nanometer scale. Systems consisting of low molecular weight compounds assemble into nano- or microfibers driven by the formation of non-covalent intermolecular interactions, such as hydrogen bonding or  $\pi$ - $\pi$  interactions.<sup>[9]</sup> However, it has to be mentioned that structures that can be obtained from such processes are not limited to the formation of fibrillary structures, also two dimensional objects (sheets) are possible.

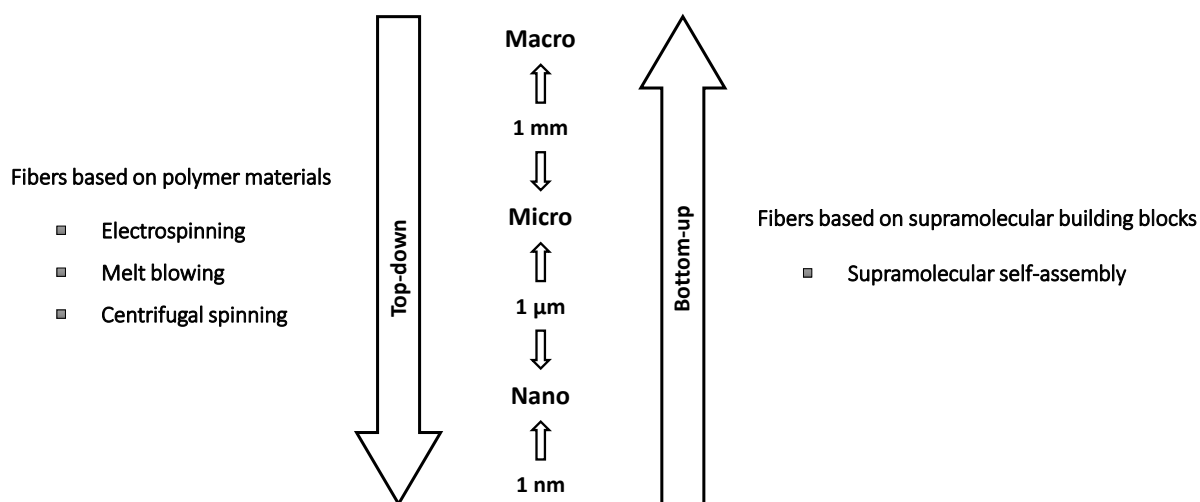


**Figure 1.1:** Schematic representation of so-called “top-down” and “bottom-up” approaches for the preparation of fibers with diameters ranging from the macro- to the nanoscale.

### Electrospinning

One well-established top-down preparation method of polymer micro- and nanofibers is given by electrospinning.<sup>[2,4-6,8]</sup> Therein, charged liquid materials are transformed into solid fibers with diameters in the nanometer range. A schematic illustration of the basic experimental setup is displayed in **Figure 1.2**. The spinning dope, which can either be a polymer melt or a solution, is filled into a syringe equipped with a metal needle usually featuring an inner diameter of less than 1 mm. High voltage needs to be applied between the needle of the syringe and a suitable collector, for example aluminum foil. By applying pressure on the plunger of the syringe, the spinning dope is forced through the metal needle and the spinning process starts. As the spinning dope leaves the needle, a so-called “jet” forms that moves from the needle to the collector. Charges carried by the liquid material interact with the generated electric field and result in a tensile force on the spinning jet. Thereby, the diameter of the jet constantly decreases during the spinning process. In case of solution electrospinning, the solvent

evaporates during the spinning process to yield a solid polymer fiber, while during melt electrospinning cooling of the polymer results in solidification.<sup>[6,8]</sup> Electrospun nanofibers have been investigated in different potential applications including tissue engineering,<sup>[10]</sup> heterogeneous catalysis<sup>[11,12]</sup> or filtration applications.<sup>[2,13,14]</sup>

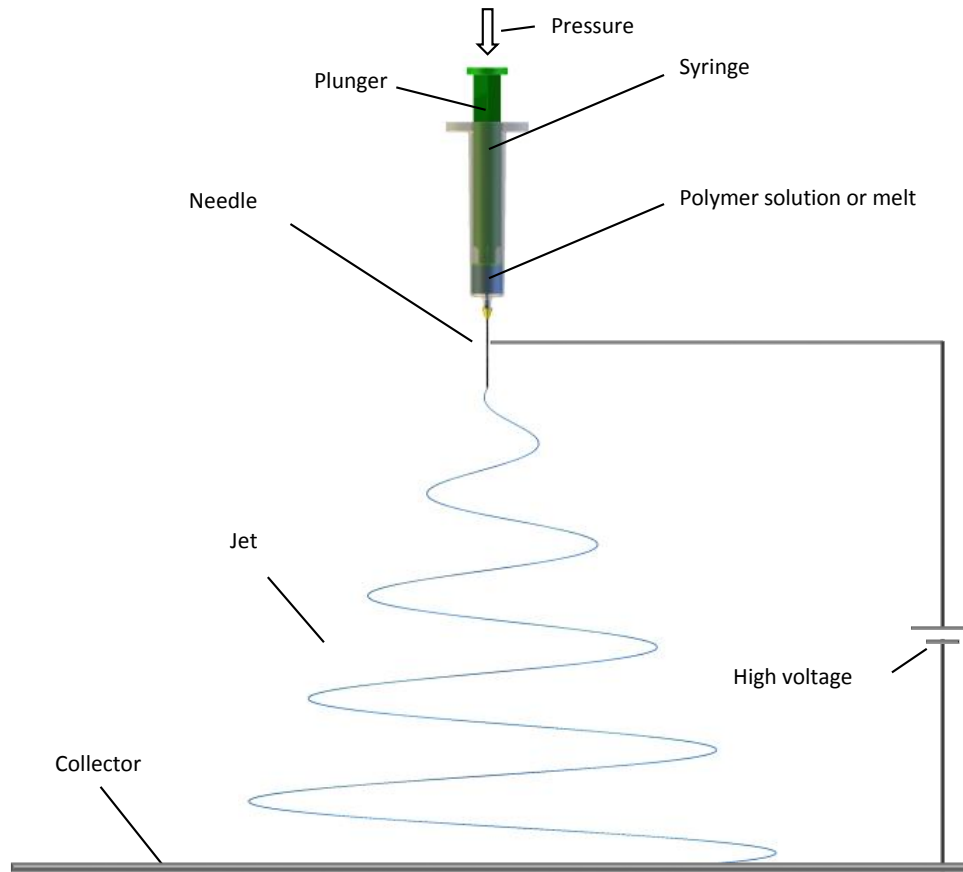


**Figure 1.2:** Schematic representation of the general electrospinning setup. A syringe is filled with the spinning dope such as polymer melt or solution. High voltage is applied between the needle and the collector. Upon applying pressure on the syringe, a spinning jet forms that moves from the tip of the needle to the collector. (Figure is based on ref<sup>[6]</sup>)

However, in many cases the transfer from laboratory scale to large scale applications is limited due to the low cost to yield efficiencies of the process.<sup>[8]</sup> For example, issues like interference between neighboring jets were observed in upscaling.<sup>[15]</sup> In solution electrospinning, one major drawback of the process is the utilization of solvents, which are volatile organic compounds in most cases.<sup>[5]</sup>

*Melt-blowing*

The preparation of polymer micro- and nanofibers by melt-blowing is another example for one of the most established processes.<sup>[5,8,16,17]</sup> Mostly used in the production of polymer fibers, melt-blowing is a gas-assisted extrusion process of a low viscosity polymer melt. **Figure 1.3** displays a schematic representation of the general setup of a spinning die used in melt blowing that is typically used for fiber production. After extrusion of the polymer melt through the spinning die, elongation of the polymer is achieved by dragging forces on the melt by two air streams exhibiting high velocities of up to 250 m/s.<sup>[7]</sup> Among others, the resulting fiber morphology obtained by this process is dependent on many different parameters such as the feeding rate, viscosity of the polymer melt, extrusion temperature as well as the velocity of the assisting air streams. Besides, the technical difficulties of the melt-blowing process are in the number of different polymers that can be processed and mostly polyolefines are industrially processed this way.

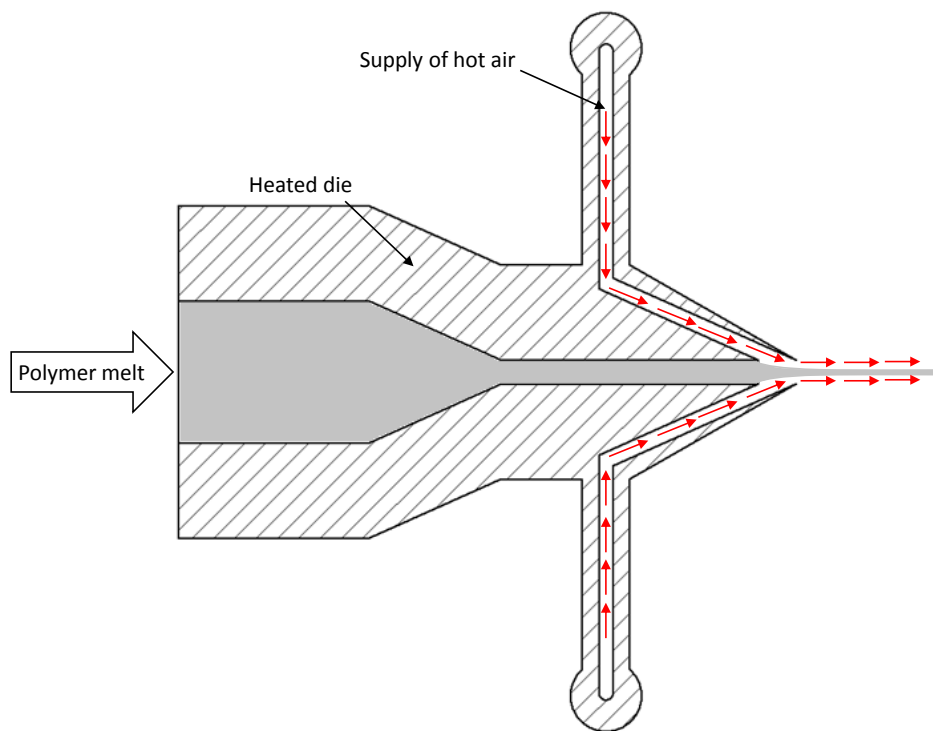


**Figure 1.3:** Schematic illustration of a melt-blowing spinning die. The polymer melt is fed into the heated die under application of pressure. Once the polymer melt leaves the die, the melt deformation is assisted by a continuous strong flow of hot air through two separate channels (red arrows). (Figure is based on ref<sup>[16]</sup>)

Due to the difficult control of the fiber diameters, a lot of research effort has been put on the design of novel geometries of spinning dies and the spinning process for the preparation of fibers in the

nanometer-range.<sup>[18,19]</sup> Polymer fibers produced by melt-blowing can be found in different applications such as in filtration or for medical purposes.<sup>[7,20–22]</sup>

### *Centrifugal spinning*

The preparation method of centrifugal spinning is also based on an extrusion process of a polymer melt or solution through a spinneret. This drawing process is additionally enhanced only by application of centrifugal forces.<sup>[8,23]</sup> **Figure 1.4** schematically illustrates a typical experimental setup utilized for the preparation of polymer fibers by centrifugal spinning. The liquid material for the spinning process is fed continuously into the rotating reservoir from the top of the system. Upon rotation, the resulting centripetal force drives the spinning dope out of the spinnerets, which are located at the sides of the reservoir. The resulting fibers shown in red are then deposited on the collector in the periphery of the system. A flexible foil ensures air-turbulences inside the setup during the spinning process.<sup>[24]</sup>

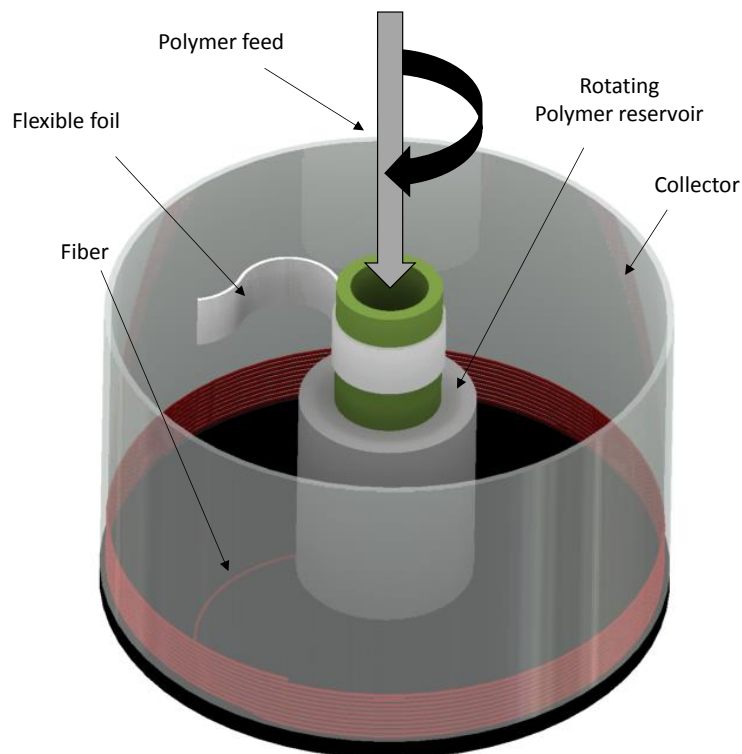


**Figure 1.4:** Schematic representation of the general experimental setup of a centrifugal spinning process. A rotating polymer reservoir is fed with the spinning dope from the top of the system. A flexible foil ensures air turbulences during the process. Upon rotation, the liquid material is forced through the spinnerets and fibers are deposited on the collector. (Figure is based on ref<sup>[8]</sup>)

Important parameters are temperature of the spinning dope, the geometrical dimensions of the reservoir, the applied rotational speed and the distance between the spinneret and the collector.<sup>[8]</sup>

Parameter studies of centrifugal spun fibers comprising polymers such as polyacrylonitrile, polyvinylpyrrolidone or polyethylene oxide confirmed the accessibility of fibers with diameters in the nanometer range.<sup>[24,25]</sup>

In contrast to the three described *top-down* processes for the preparation of micro-and nanofibers, this thesis is based on a different *bottom-up* approach utilizing controlled self-assembly of small molecules. Therefore, a brief introduction of supramolecular chemistry and the corresponding concepts are introduced in the following. Due to the fact that chapters 4 and 5 are additionally concerned with the utilization of these supramolecular fibers for filtration applications, the principles of separation technology, in particular filtration, are discussed in the course of this introduction.

### 1.2 Supramolecular Chemistry

The field of supramolecular chemistry refers to the build-up of chemical systems that are mainly based on non-covalent interactions between individual molecules. It is a fast growing scientific discipline, often inspired by the chemistry of living biological systems such as enzyme catalysis.<sup>[9]</sup> The field of supramolecular chemistry encompasses a large variety of different systems, which are exemplarily illustrated by the literature references.<sup>[26–29]</sup> A lot of scientific effort is put on the employment of supramolecular chemistry in various research areas such as for example catalysis,<sup>[30–32]</sup> photochemistry,<sup>[33]</sup> gelation of organic solvents or water<sup>[34]</sup> and electronics.<sup>[35]</sup>

#### *Interactions in supramolecular systems*

Apart from the classic covalent bond, non-covalent interactions involve a variety of different effects between individual molecules including hydrogen bonding, ion-ion, dipole-dipole, ion-dipole, cation- $\pi$ , anion- $\pi$ ,  $\pi$ - $\pi$  interactions as well as van-der-Waals forces. However, these interactions differ significantly in their binding energy. In many cases, combinations of two or more of these interactions are present in supramolecular systems.<sup>[9]</sup> To illustrate the diversity of supramolecular chemistry, one example of supramolecular systems is briefly introduced for ion-dipole interactions as well as cation- $\pi$  interactions and hydrogen bonds.

#### *Ion-dipole interactions*

One example for an ion-dipole interaction that was utilized to design a system that self-assembles into linear chain-like structures involves host-guest interactions between a crown-ether and a dialkylammonium-ion.<sup>[36]</sup> **Figure 1.5** displays the molecular structure of the individual molecular building block of this supramolecular system and a schematic representation of the resulting self-assembly into linear chains. The building block has two functional units that allow for a defined ion-dipole interaction between the individual molecules to yield an A-B-type monomer capable of forming a linear supramolecular polymer. The benzo-21-crown-7 group (red) can coordinate to the dialkylammonium-ion (blue) resulting in highly viscous solutions of chloroform indicating the self-assembly. Concentration dependent <sup>1</sup>H-NMR analysis proofed the formation of linear chains.<sup>[36]</sup>

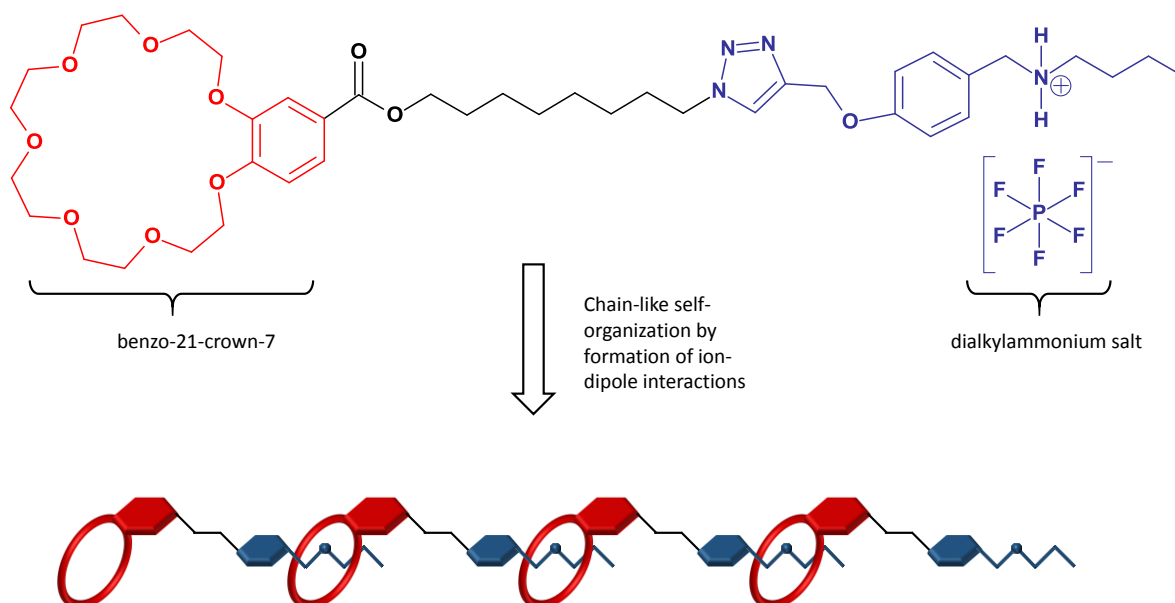


**Figure 1.5:** Example of a supramolecular system that self-assembles via a host-guest coordination of a dialkylammonium-ion by a crown-ether in solution. Top: Molecular structure of the individual building blocks that self-assemble into large linear structures. The highlighted parts of the structure serve as the host (red) and the guest (blue). Bottom: Schematic representation of four individual molecules that self-organize by the ion-dipole interaction to a linear chain. (Figure is based on ref<sup>[36]</sup>)

It has been shown that solutions containing these supramolecular structures can be electrospun to obtain fibers with diameters in the nanometer range. Further investigations focused on the formation of shape-persistent gels of solutions containing the linear structures and additionally a metal-crosslinker  $[\text{PdCl}_2(\text{PhCN})_2]$ .<sup>[37]</sup> These systems are responsive to different external stimuli such as variations in temperature or pH-value. In addition to the presented example for ion-dipole interactions in supramolecular chemistry, for example other systems have been reported featuring such interactions.<sup>[38–40]</sup> In contrast to classical polymers, these systems are fully based on non-covalent interactions.

### *Cation- $\pi$ interactions*

Supramolecular systems have been reported that utilize cation- $\pi$  interactions between individual molecules. Such interactions are part of many different systems and are investigated for example as artificial receptors and found in many biology systems.<sup>[41]</sup> In analogy to the previously displayed system in **Figure 1.5**, another linear self-assembly system yielding a supramolecular polymer based on non-covalent interactions was achieved by cation- $\pi$  interactions. **Figure 1.6** displays the molecular structure of an A-B-type building block that exhibits two functional groups that allow for a controlled

intermolecular host-guest coordination.<sup>[42]</sup> Concentration dependent <sup>1</sup>H-NMR studies in chloroform showed that the pillar[5]arene-unit (host) can incorporate the imidazole-unit (guest) resulting in high viscosities of the corresponding solutions in chloroform. By pH-dependent viscosity measurements, also pH-responsiveness was demonstrated.

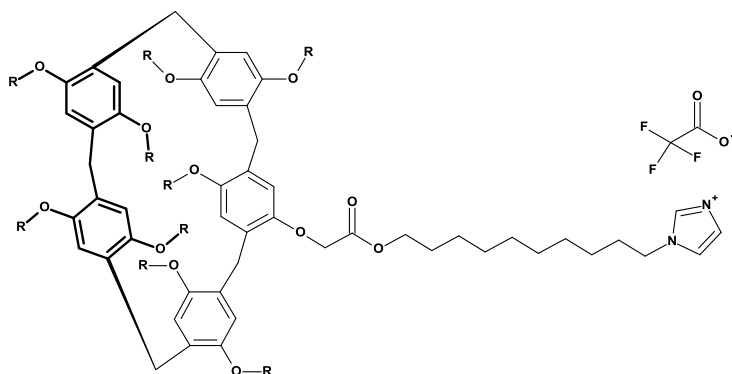


**Figure 1.6:** Example of a multifunctional molecule that exhibits a charged imidazole-unit (guest) and a pillar[5]arene-unit (host) consisting of 5 hydroquinone-derivatives linked via methylene units in para-position. This supramolecular A-B-type monomer is capable of forming linear supramolecular polymers. (Figure is based on ref<sup>[42]</sup>)

### *Hydrogen bonds*

A very prominent example of supramolecular interactions is the formation of hydrogen bonds. These interactions can be regarded as a special kind of dipole-dipole interaction, hydrogen bonds involve a hydrogen-atom that is attracted to an electronegative atom such as oxygen or nitrogen. The presence of interactions strongly influences the physical properties of a compound.<sup>[9,43]</sup> One example for a supramolecular system that is capable of self-assembly into one-dimensional structures by formation of hydrogen bonds are cyclic peptides with alternating D- and L-amino acids.<sup>[44]</sup> As schematically shown in **Figure 1.7**, these compounds form supramolecular columns of individual molecules that are arranged parallel to each other. Thereby, each molecule forms four hydrogen bonds to neighboring molecules into the direction of the individual column. The glutamine side chains contribute additional hydrogen bonds that stabilize the arrangement of the columns by intracolumnar interactions. Furthermore, the primary amide groups in the periphery of the molecular structure result in the formation of hydrogen bonds between adjacent columns stabilizing the parallel arrangement.

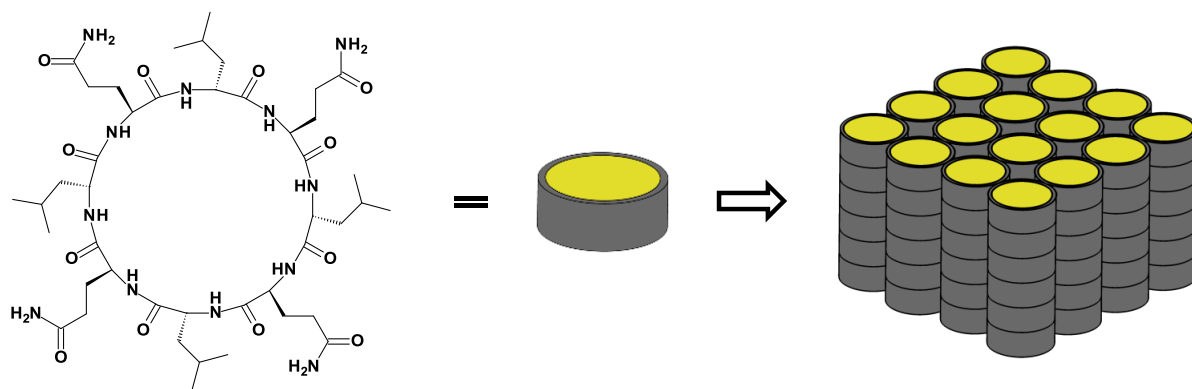


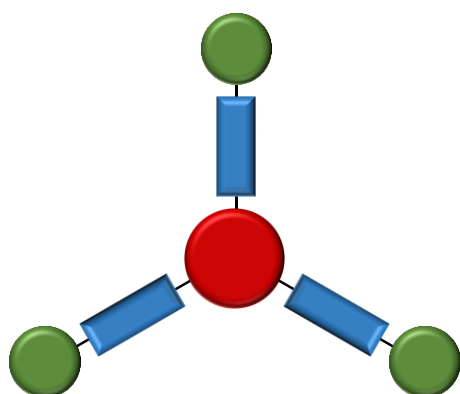
**Figure 1.7:** Example of a supramolecular system that is based on the formation of intermolecular hydrogen bonds between cyclic peptides consisting of alternating D-Leucine and L-Glutamine amino acids. This supramolecular building block can self-assemble from solution into parallel arrays of solid nanotubes. (Figure is based on ref<sup>[44]</sup>)

Apart from the displayed example, many other cyclic peptides have been synthesized and investigated.<sup>[44–46]</sup> These compounds have even been identified to exhibit antiviral activity against hepatitis C viruses.<sup>[47]</sup>

A very versatile motif in supramolecular chemistry are 1,3,5-benzenetrisamides. This thesis focuses on the controlled preparation of supramolecular nanofibers based on the formation of directed threefold hydrogen bonds between these molecules. Therefore, this class of supramolecular building blocks will be discussed in more detail in the following.

### 1.3 Materials class of 1,3,5-benzenetrisamides

One well-established supramolecular motif that is capable of forming ordered structures by the formation of hydrogen bonds is given by the materials class of 1,3,5-trisamides. The general molecular structure of such compounds is schematically shown in **Figure 1.8** and consists of a central core (red), which can be for example a benzene- or a cyclohexane-ring. This core is symmetrically substituted by three amide groups (blue), which can be connected to the ring-structure in two different ways. They can be either be attached with the carbon-atom of the C=O-bond or with the nitrogen-atom to the core. In the periphery of the molecular structure, substituents are connected to the amide groups that control the solubility and aggregation behavior as well as the thermal properties of the system. The amide groups are able to form directed threefold hydrogen bonds between individual molecules that can result into the formation of one-dimensional supramolecular columns either in the solid-state, in the liquid crystalline state or in dilute solution. <sup>[48–51]</sup>



#### central core

- benzene- or cyclohexane-ring
- symmetrically substituted

#### amide groups

- formation of hydrogen bonds to adjacent molecules
- enabling one-dimensional growth into supramolecular columns

#### substituents in the periphery

- large variety of different substituents possible
- tailoring of solubility and aggregation behavior

**Figure 1.8:** General molecular structure of 1,3,5-trisamides. The amide groups (blue) are connected to the central core (red) either by the carbon-atom of the C=O-bond or by the nitrogen-atom to the core. The amide moiety can be substituted by a variety of different substituents (green) in the periphery allowing for a very large number of different molecules.

Work performed in the course of this thesis focused on the utilization of this self-assembly motif with a benzene-core in the center and amide groups that are connected to the central ring by the carbon-atom. Therefore, supramolecular systems based on 1,3,5-benzenetrisamides (BTAs) will be introduced in more detail in the following.

In the past decades, a lot of research activities have been put on the synthesis and characterization of BTAs featuring a variety of different substituents in the periphery. Matsunaga et al. reported for the

first time on the liquid crystalline behavior of alkyl-substituted 1,3,5-benzenetrisamides.<sup>[52]</sup> In addition, the phase behavior of a variety of different alkyl-substituted BTAs was investigated and compared to analogue trisamide-structures with the cyclohexane-core. Even small changes in molecular structure resulted in significant changes of the thermal behavior of the investigated compounds.<sup>[50]</sup> Detailed work on alkyl-substituted BTAs has been reported recently comparing the properties and self-assembly behavior of N-centered and C=O centered compounds utilizing different analytical methods such as differential scanning calorimetry, polarization optical microscopy and IR-spectroscopy.<sup>[53]</sup> Further, supramolecular systems of BTAs exhibiting aryl-substituents in the periphery have been reported.<sup>[54,55]</sup> In particular, the impact of additional  $\pi$ - $\pi$ -interactions between individual molecules by introducing aryl-substituents into the molecular structure of BTAs was studied by van Gorp et al.<sup>[56]</sup> Among many others, further reported 1,3,5-benzenetrisamides feature a variety of different substituents and functionalities for example amino acids<sup>[57]</sup> or benzo-crown ethers.<sup>[58]</sup>

### *Formation of columnar stacks in the solid state*

The formation of supramolecular columns can be observed for many BTA systems either in the bulk material or in dilute solution. As mentioned before, the aggregation behavior of the individual molecular building blocks is very dependent on the selected substituents in the periphery.<sup>[51]</sup> Crystal structure analysis of many BTAs have been performed to give more insight on the non-covalent interactions between individual molecules in the solid state.<sup>[59–64]</sup>

For instance, Lightfoot et al. reported the crystal structure of *N,N',N''*-tris(2-methoxyethyl)benzene-1,3,5-tricarboxamide that was recrystallized from ethanol.<sup>[60]</sup> The molecular structure as well as the hydrogen bond formation between adjacent molecules in the crystal structure is shown in **Figure 1.9**. The BTA molecule does not exhibit coplanarity of the benzene-ring and the amide groups. Instead, the amide groups are tilted out of plane to form hydrogen bonds with amide groups of the neighboring molecule. As a result of threefold hydrogen bonding, the BTA molecules form helical supramolecular columns, while all amide groups of one molecule point into the same direction. Along the axis of the column of BTA molecules a crystallographic  $2_1$  screw axis can be found.

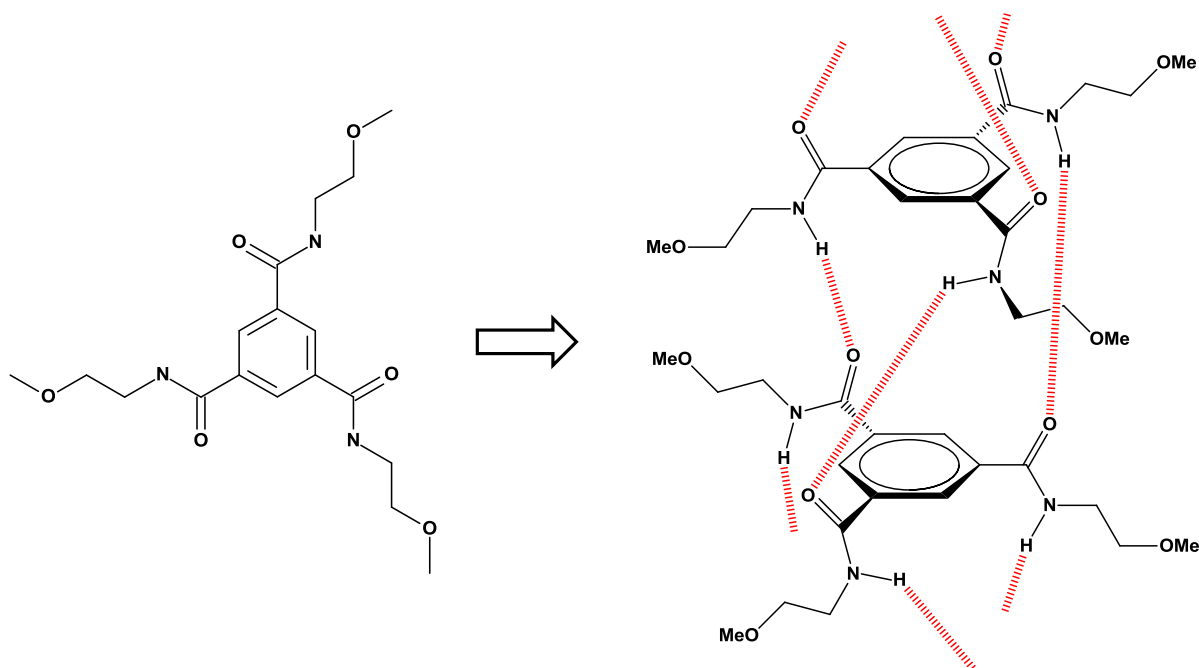


**Figure 1.9:** Left: Molecular structure of *N,N,N''*-tris(2-methoxyethyl)benzene-1,3,5-tricarboxamide. Right: Formation of threefold directed hydrogen bonds between two neighboring molecules in the solid state of the bulk material recrystallized from ethanol. (Figure is based on ref<sup>[60]</sup>)

Theoretical investigations on supramolecular columns consisting of 1,3,5-benzenetrisamides as well as 1,3,5-cyclohexanetrisamides have been performed.<sup>[65]</sup> It was found that each individual building block exhibits a dipolar moment, because all amide groups point into the same direction. The aggregation of molecules by directed threefold hydrogen bonds leads to the formation of a macrodipole belonging to the supramolecular column. Depending on the molecular structure of the building block, the resulting macrodipole may vary significantly. In molecules containing a cyclohexane-core, the amide groups point more along the axis of the column compared to molecules with benzene-cores resulting in larger values for the macrodipoles. By aggregation of two or more supramolecular columns, these macrodipoles can interact.

In addition, the crystal structure of a very prominent BTA has been reported by utilization of a combination of X-Ray powder diffraction and solid-state NMR spectroscopy.<sup>[66]</sup> In industry, 1,3,5-tris(2,2-dimethylpropionylamino)benzene is used as a very efficient clarifying agent for isotactic polypropylene. This material also forms supramolecular columns exhibiting a  $2_1$  screw axis and threefold directed hydrogen bonds. However, in the resulting crystal structure, the supramolecular columns are arranged anti-parallel to each other leading to a net-dipolar moment of zero.

Though many of the BTAs show formation of directed threefold hydrogen bonds, it was found that the BTA crystal structures are not limited to threefold directed hydrogen bond formation to yield

supramolecular columns as shown in **Figure 1.9**. For example, the crystal structure of *N,N,N'*-trimethyl-benzene-1,3,5-tricarboxamide revealed the formation of hydrogen bonds that interact with molecules within one column as well as with molecules from adjacent columns.<sup>[59]</sup> This is only observed for very small substituents. Also a BTA containing fluorine-atoms in the periphery of the molecular structure has been found to exhibit amide groups pointing in different directions inside individual columns.<sup>[64]</sup>

#### *Formation of one-dimensional structures from solution*

The formation of threefold directed hydrogen bonds allows under defined processing conditions for the preparation of one-dimensional supramolecular structures by self-assembly of 1,3,5-benzenetrisamides from solution with dimensions on the nanoscale. Such self-assembled nanostructures from solutions of BTAs are usually obtained from the preparation of a clear BTA solution in a given solvent and subsequent application of an external influence to the system to trigger the self-assembly process. **Figure 1.10** schematically displays such a self-assembly process.

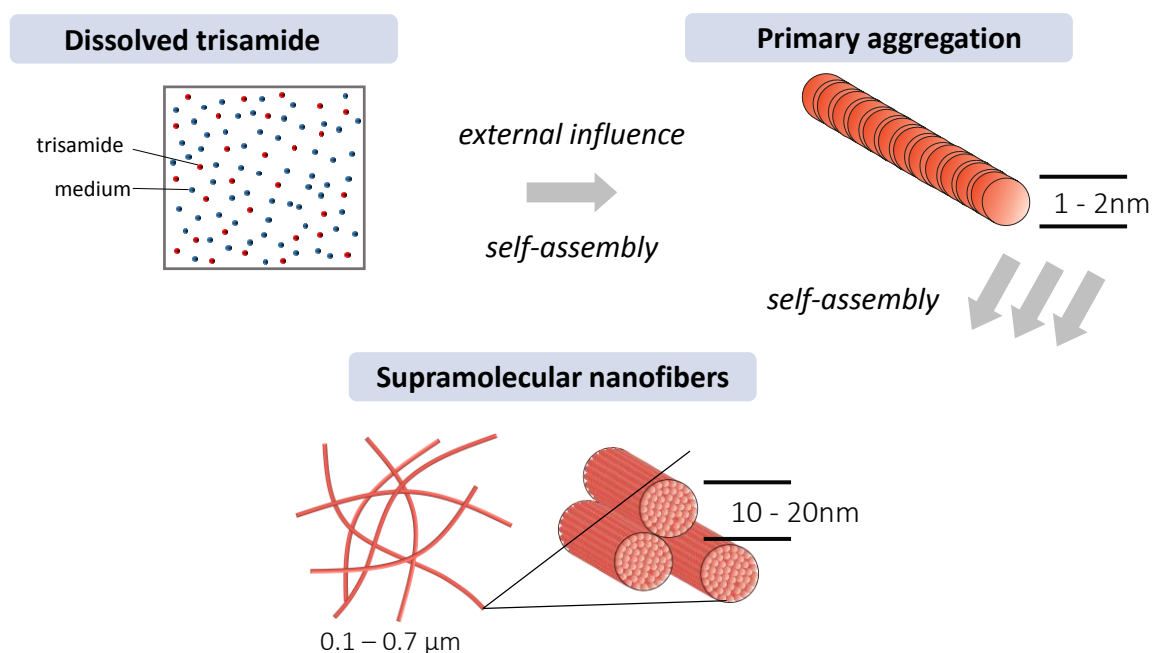


**Figure 1.10:** Schematic representation of a self-assembly process of a 1,3,5-benzenetrisamide from solution. Upon some external influence to a clear solution of the BTA in a given solvent, primary aggregation of the BTA molecules occurs, which further assemble into larger one-dimensional structures.

Possible methods to initiate the self-assembly process are changes in temperature of the BTA solution, evaporation of the solvent resulting in a change of BTA-concentration, changes of the pH-value,

addition of a non-solvent to the solution or a combination of these possibilities. Some examples of self-assembly systems from a BTA solution will be introduced in the following. One of the most common approaches in self-assembly experiments utilizing BTAs to gelate a given solvent is by varying the temperature of a BTA solution. Lee et al. reported on a self-assembly system applying a BTA exhibiting diacetylenic substituents in the periphery of the molecular structure. By heating and subsequent cooling, gelation of a solvent-mixture of THF and cyclohexane was achieved. Transmission electron microscopy (TEM) revealed the presence of supramolecular nanofibers with diameters of down to 50 nm.<sup>[67]</sup> In analogy, self-assembly experiments based on temperature changes were reported using BTA featuring ester groups in the molecular structure to obtain organogels of different solvents.<sup>[68]</sup> Other BTA systems have been developed that are capable of forming gels of organic solvents.<sup>[56,59,69,70]</sup>

For the investigation of mechanical properties of supramolecular BTA nanofibers featuring different alkyl substituents, self-assembly experiments were conducted by heating of a BTA solution and subsequent cooling at a constant cooling rate. The resulting suspension was dried at ambient conditions and the remaining supramolecular structures were subjected to mechanical analysis<sup>[71,72]</sup> It was found that supramolecular fibers of different alkyl-substituted BTAs exhibit Young's moduli in the lower GPa range.

In addition to gelation of organic solvents, BTA systems have been developed to enable gelation of water to form hydrogels by varying the temperature of a BTA solution.<sup>[73,74]</sup> The morphology of the resulting supramolecular material was verified to be fibrous structures by Cryo-TEM analysis.

Apart from changes in temperature, Bernet et al. reported on a self-assembly system using a BTA with *p*-carboxylphenyl-substituents in water that forms hydrogels upon variation of the pH-value.<sup>[55]</sup>

Upon addition of water to a solution of a BTA with an ethyl cinnamate substituent in *N,N*-dimethylformamide, a thermo-reversible gelation of the resulting aqueous mixture was obtained.<sup>[75]</sup> By utilization of scanning electron microscopy (SEM), fibrous structures were found featuring diameters in the nanometer range.

### *Applications of 1,3,5-benzenetrisamides*

Supramolecular nanostructures of 1,3,5-benzenetrisamides with well-defined morphology are suitable for a variety of applications. As previously mentioned, many self-assembly BTA systems exist that are capable of forming organo-<sup>[56,59,67-70]</sup> or hydrogels.<sup>[55,73,74,76]</sup> In consequence, it opens applications ranging from the manipulation of organic fluids to tissue engineering.

In biological studies, a BTA system with mannose as part of the molecular structure was found to be capable to binding and detecting *E. coli* bacteria in water.<sup>[77]</sup>

Furthermore, this materials class has been investigated as additives to improve the electret properties of polypropylene.<sup>[78,79]</sup> One way to improve the electret performance of a given polymer material is to insert additives that act as traps for electrical charges.<sup>[80]</sup> The selected 1,3,5-benzenetrisamide with cyclohexyl-substituents was soluble in the polypropylene melt at 260 °C. During preparation of the polymer film, a cooling process triggered the self-assembly in the polymer melt resulting in the formation of supramolecular fibrous structures throughout the polymer material. The result demonstrated that 1,3,5-benzenetrisamides have a potential to serve as additives to prepare efficient electret materials.

Furthermore, 1,3,5-benzenetrisamides have been found to be efficient nucleation and clarification agents for different polymers. Blomenhofer et al. investigated the applicability of 18 different BTAs to function as a nucleating agent for isotactic polypropylene yielding a highly transparent polymer material, which normally appears to be very turbid. By introducing about 0.02 – 0.2 wt.-% of selected BTAs, different modifications of the crystal structures of the polypropylene can be obtained.<sup>[81]</sup> Additional work was performed on selected systems to provide a deeper understanding on the nucleation and clarification of isotactic polypropylene by 1,3,5-benzenetrisamides.<sup>[61,82,83]</sup>

Apart from isotactic polypropylene, the utilization of 1,3,5-benzenetrisamides has also been transferred to other polymers. For example, Abraham et al. reported on the nucleation of polyvinylidene fluoride by screening experiments of a variety of different 1,3,5-benzenetrisamides.<sup>[84]</sup> In addition, nucleation studies of polybutylene terephthalate and polylactide by 1,3,5-benzenetrisamides were reported.<sup>[85–87]</sup>

Recently, supramolecular nanofibers based on the self-assembly of 1,3,5-benzenetrisamides from solution were prepared inside a polymer nonwoven to yield a nanofiber-microfiber composite material. These composites with nanofibers featuring diameters of around 500 nm were subjected to air-filtration experiments to remove particulate matter from air.<sup>[88,89]</sup> It was found that supramolecular nanofibers have a great potential to be used in filtration applications.

### 1.4 Principles of filtration technology

One of the unit operations in process engineering refers to the separation of a mixture containing at least two components into two distinct fractions.<sup>[90]</sup> In general, separation processes can be classified into two main categories, namely *thermal* and *mechanical separation* processes.

*Thermal separation* processes are based on the utilization of mass and/or heat transfer that occurs at interfaces between two different phases that are far from being at equilibrium state.<sup>[91]</sup> For example during distillation processes, a homogenous liquid phase tries to achieve equilibrium state with a gas phase by mass transfer from the liquid into the gas phase. By mass exchange between these two phases a separation effect can be achieved. Mostly homogenous mixtures containing different components are separated by thermal separation processes. Such processes encompass different techniques like liquid-liquid solvent extraction, distillation and rectification, adsorption and absorption. In chemical industry, distillation processes are one of the most commonly used separation techniques.<sup>[92,93]</sup> A possible application of adsorption and absorption processes is the purification of gases.

In contrast, *mechanical separation* processes are based on the application of mechanical forces to heterogeneous mixtures of different components. Examples of such processes are sedimentation, centrifugation or filtration. Due to the time required for sedimentation processes, centrifugation or filtration is often preferred in chemical industry.<sup>[92]</sup> Due to the fact that much of the work performed in the course of this thesis is closely related to filtration processes to remove solid particles from a fluid, the principles of filtration will be introduced in the following.

#### *Separation by filtration*

Filtration processes are used for the separation of heterogeneous mixtures of at least two different phases. Although many filtration operations exist that correspond to the separation of a liquid phase from a gas, in most cases filtration is referred to the separation of a solid phase from a fluid phase, while the fluid can either be a liquid or a gas.<sup>[94]</sup> In general, filtration processes are performed for different reasons in industrial applications. For example, a valuable fluid may be treated to remove a solid impurity or a desired solid may be collected from a fluid. Depending on the purpose of the process different kinds of filters or filtration systems have to be applied. A typical filtration operation normally exhibits different individual stages such as pre-treatment, solids-concentration, separation and post-treatment. The pre-treatment step corresponds to a modification of the suspension that has to be filtered such as by adjustment of the pH-value or by addition of flocculant. During concentration of the

suspension, the liquid is partially removed to reduce the volume that has to be filtered. Post-treatment processes mostly refer to improvements of quality of the separated products.<sup>[95]</sup> However, the most essential part of a filtration operation is given by the separation stage based on the use of a filter medium. Purchas and Sutherland define a filter medium as follows:<sup>[1]</sup>

*“A filter medium is any material that, under the operating conditions of the filter, is permeable to one or more components of a mixture, solution or suspension, and is impermeable to the remaining components.”*

Filter media can be obtained from a variety of different materials such as polymer fibers, metals, glass, ceramic materials or carbon.<sup>[96–100]</sup> These materials are transformed into a permeable form to serve as filter media.<sup>[1]</sup> Each filter medium exhibits a set of characteristic properties that makes each medium suitable for a specific application. Among others, such properties include thermal and chemical stability, wettability, particle sizes that can be retained, filtration efficiency, dirt-holding capacity and resistance to flow of the fluid medium resulting in a pressure building up before and after the filter medium and finally cost.

In real life applications many compromises have to be made in the design of a filter medium for a specific application. A filter medium should meet the following requirements to be favorable for a specific application: 1. Capability of removing up to all undesired contaminants from the fluid regardless of the particle size. 2. Low resistance of the filter medium to an applied flow. 3. Large dirt holding capacity. 4. Very small in size. 5. Low costs for production of the filter medium.<sup>[3]</sup>

### *Mechanisms of filtration*

In general, separation of solid particles from a fluid can be classified into four different mechanisms. The first mechanism refers to the so-called *surface straining*. Thereby, the particles are greater than the pore size of the filter medium and once the particle, which is carried by the fluid flow, reaches the filter medium it is separated close to the surface and blocks a pore of the filter (see **Figure 1.11 (A)**). Particles separated by *cake filtration* (see **Figure 1.11 (B)**) can be smaller than the size of the individual pores. However, bridging processes lead to an accumulation of particles (filter cake) close to the surface without fully blocking them. As the filter cake builds up, an additional filtration effect is generated by the deposited particles. A filtration system that is based on *cake filtration* usually involves an initial period of time after the filtration operation started during which the filter does not reach the desired filtration efficiency. In contrast to the first two mechanisms, *depth filtration* (see **Figure 1.11 (C)**) is based on particle deposition inside the filter medium after the individual particle entered

through a pore. Thereby, particle sizes can be smaller than the pores of the filter medium. In most cases, a filtration process mostly consists of a combination of these three mechanisms. In addition, another separation process exists that corresponds to a combination of *surface straining* and *depth filtration*, the so-called *depth-straining*. It is based on variations of the pore diameter as the particle passes through the filter medium. The diameter of the pore might become too small for such a particle resulting in the blocking of the pore and deposition inside the filter medium.<sup>[3,95]</sup>

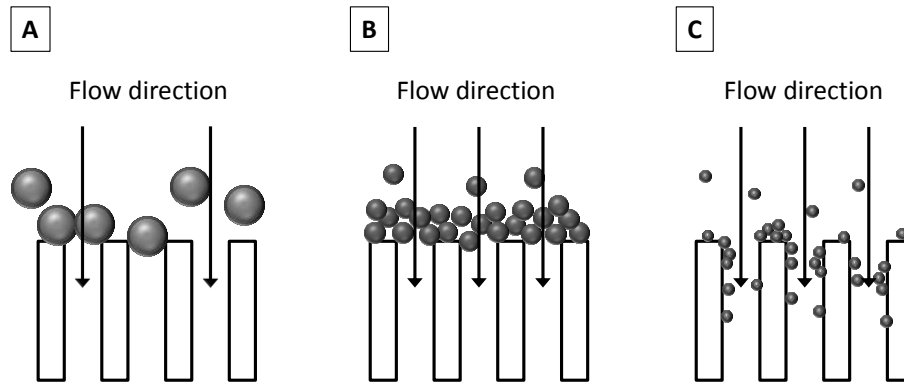


**Figure 1.11:** Basic filtration mechanisms for the separation of solid particles from a fluid stream. *Surface straining* (A) refers to the deposition of particles close to the surface of the filter if the particle size is larger than the pores of the filter medium. In *cake filtration* (B) the particles are smaller than the pores, but are gathered close to the surface by bridging of the pores. Accumulation results in filter cake formation. In case of *depth filtration* (C) the particles are smaller than the pore and attach to the wall of the pore inside the filter. (Figure is based on ref<sup>[95]</sup>)

Depending on the desired application for a filtration system, filters are designed to feature specific filtration mechanisms. For example, the recovery of a valuable solid from the fluid is usually accomplished by filtration systems that are based on *surface straining* or *cake filtration*. Due to the fact that the particles are deposited near the surface of the filter, the solid particles can easily be removed from the filter. In contrast, clarification of a fluid can also be achieved by *depth filtration* and *depth straining* mechanisms. Apart from the valuable fraction of the filtered mixture to be obtained from the process, other factors such as the particle concentration in the feed have to be considered.<sup>[95]</sup> Usually filters based on *cake filtration* mechanism are fed with high concentrations of solid material suspended in the fluid and the filtration system is cleaned after reaching a limiting resistance of the filter to the flow.

The complexity of important influences in the deposition of particles by *depth filtration* mechanism exceeds those for the other three processes. Most of the work performed is concerned with fibrous media. Thereby, depth filtration is one very important separation mechanism. In consequence, the concept of *depth filtration* will be introduced in more detail.

*Depth filtration*

Hutten describes four major influences that affect the separation by *depth filtration* mechanism.<sup>[3]</sup> Particles carried by the fluid transported through the filter medium generally follow the streamlines of the fluid. However, if a particle gets into contact with the material of the filter medium, it usually gets deposited due to physical attractive forces. **Figure 1.12** displays the major influences leading to particle deposition that will be introduced in the following. The *inertial impaction* (a) refers to particles that exhibit an inertia too high to be carried around an intersecting fiber. Therefore, the particle collides with the fiber and is deposited. The second way of particle deposition is given by *interception* (b). A particle does not particularly collide with a fiber, but approaches the fiber to the point where attractive forces capture the particle.<sup>[3,99]</sup>

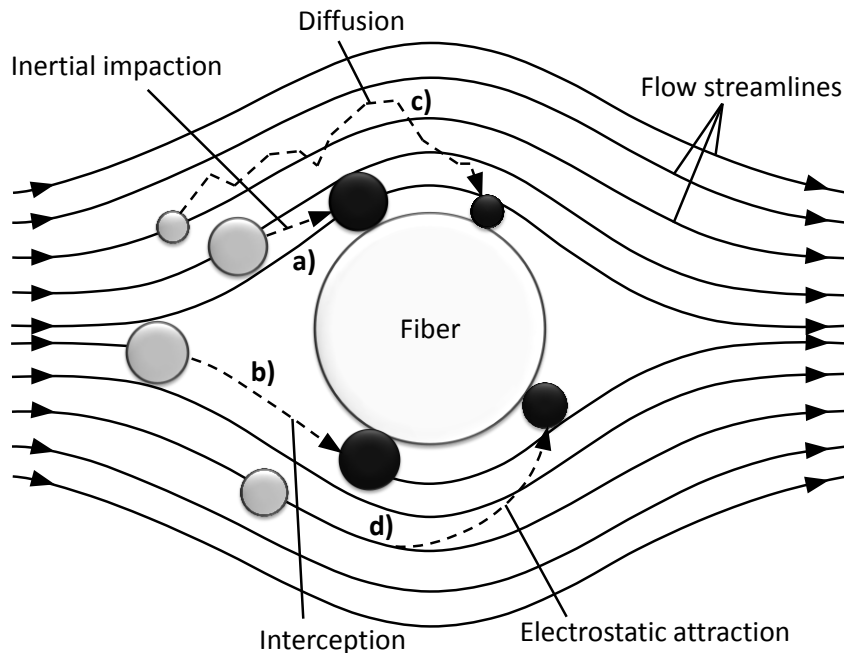


**Figure 1.12:** Schematic representation of influences contributing to particle deposition by *depth filtration* mechanism. (Figure is based on ref<sup>[3]</sup>)

Deposition by *diffusion* (c) is mainly based on the Brownian diffusion of small particles that allows for motion away from the streamlines of the fluid resulting in contact with the fibrous filter material. The last influence is given by *electrostatic attractions* (d) of the filter material and the particles. However, depending on the particle sizes, different influences in *depth filtration* dominate the separation process. Large particles with diameters of around 300 nm and higher are usually separated by interception, whereas particles with diameters of way below 100 nm are captured by diffusion. In most cases, filter media based on *depth filtration* exhibit the largest penetration of particles in the

intermediate region of particle diameters between the two influences. **Figure 1.13** displays a schematic correlation between the particle diameter and the penetration of a filter medium. The particle size corresponding to the most penetration is referred to as the “most penetration particle size” (MPPS).<sup>[3]</sup>

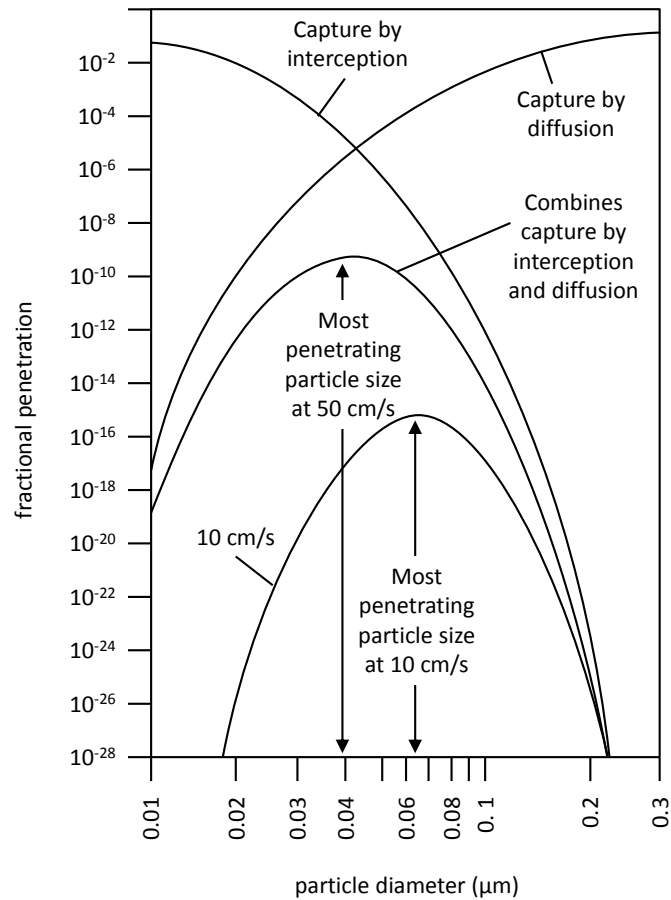


**Figure 1.13:** Correlation between the diameter of filtered particles and the penetration of a filter medium. Depending on the particle size, either interception or diffusion processes dominate the particle deposition. The combination of these influences yields the resulting penetration. The location of the most penetration particle size (MPPS) depends on the linear velocity of the filtration process. (Figure is based on ref<sup>[3]</sup>)

The particle size of the MPPS depends on many factors such as the flow velocity of the fluid during filtration or the material the particles are composed of. Apart from the particle deposition, additional effects like reentrainment have to be considered, whereas this process corresponds to the detachment of particles that were already captured by the filter medium due to mechanical forces of the fluid medium on the particle.<sup>[3]</sup>

#### *Characterization of filter media*

Among others, filter media are usually characterized by two main properties. The percentage of particles removed from the fluid is referred to as *filtration efficiency* ( $f$ ) and corresponds to the quality of separation that can be achieved by the selected filter medium. Values are typically given for defined particle diameters and are generally calculated according to equation 1.1. By investigation of the filtration efficiency of particles with different diameters, typically particle size dependent filtration efficiency curves are displayed.

$$f = \left(1 - \frac{N}{N^0}\right) \cdot 100\% \quad (1.1)$$

$N$  corresponds to the number of particles that penetrated the filter medium and  $N^0$  refers to the number of all particles that were applied to the filter.

The second property corresponds to the resistance of the filter to the fluid during the filtration process. The flow of the fluid through the filter medium requires some kind of driving force. Therefore, normally a pressure difference is applied to the filter to start the filtration process, which can be induced either by gravity, vacuum or utilization of a pump. In theory, the flow through a filter is sometimes compared with the flow through individual capillaries representing the individual pores. However, in many filter media, such as nonwovens, the so-called pores are rather void spaces inside the porous medium without a regular cross-section.<sup>[3,95]</sup>

One of the simplest approaches to describe the flow of a fluid through a porous medium is based on work by Darcy, who performed series of experiments of water flowing vertically through an iron pipe filled with sand representing a porous structure. The relationship between flow velocity and a permeability constant is given by equation 1.2.<sup>[95]</sup>

$$u = -\frac{k}{\mu} \cdot \frac{dp}{dz} = -\frac{k}{\mu} \cdot \Delta p \quad (1.2)$$

$u$  represents the linear flow velocity of the fluid measured in m/s.  $k$  is the permeability constant and  $\mu$  is the viscosity of the fluid.  $dp$  refers to changes in pressure over a porous medium with thickness  $dz$ , which can also be written as a pressure difference  $\Delta p$  before and after the filter. For nonwoven media, most systems can be described by Darcy's law. However, the exact form of the permeability constant is not clear and has to be investigated for each material separately. One of the most important information obtained by equation 1.2 is that the linear flow velocity  $u$  is directly proportional to the difference in pressure before and after the filter medium. Therefore, comparison between two different filter media is often difficult due to differences in setup and testing conditions. The so-called quality factor was established to allow for the evaluation and comparison of different filtration systems. The quality factor QF is given by equation 1.3. Here,  $N$  is the number of particles that

penetrated the filter medium,  $N^0$  refers to the number of all particles that were applied to the filter and  $\Delta p$  is the differential pressure before and after the filter.

$$QF = -\frac{\ln(N/N^0)}{\Delta p} \quad (1.3)$$

By taking into account the filtration efficiency of a filter and the corresponding differential pressure at defined operating conditions, different filters can be compared.

### *Applications of filters*

Filtration systems are applied in a variety of different technologies of the everyday life. In solid gas separation, filters can be found for example in living and working space purification systems, industrial dust removal or respirators. In liquid filtration, one of the most prominent examples for the application of filtration systems is the treatment of ground and surface water to obtain safe drinking water.<sup>[101]</sup> In addition, one of the most widespread technologies containing many different filters are automobiles involving the filtration of the air intake, fuel filtration and cabin air filtration.<sup>[3]</sup>

The choice of a suitable filter for a specific application mainly depends on the particles that have to be removed from the fluid. **Figure 1.14** provides an overview of contaminations that are often removed by liquid filtration applications. These applications are generally classified into four different filtration processes depending on the size of particles that need to be removed from the fluid. These are *microfiltration*, *ultrafiltration*, *nanofiltration* and *reverse osmosis*.<sup>[3]</sup> In general, the removal of small particles is associated with a higher differential pressure during operation of the filter, whereas less pressure is needed in filtration systems separating larger particles.

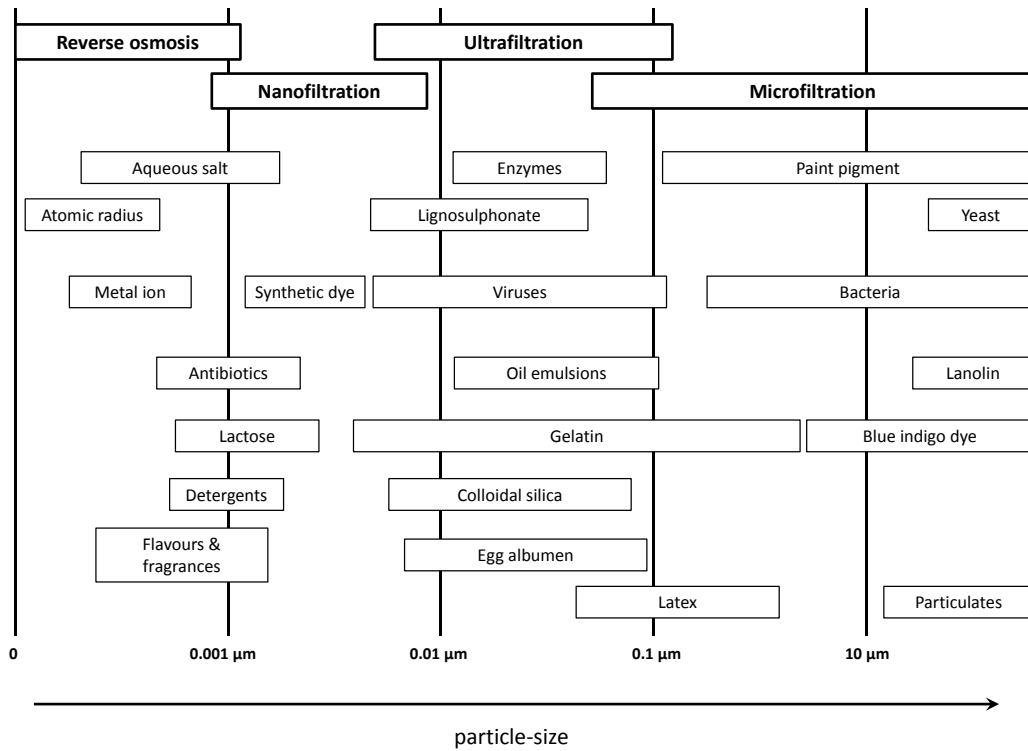


**Figure 1.14:** Schematic overview of contaminations with different particle sizes removed by *reverse osmosis*, *nanofiltration*, *ultrafiltration* and *microfiltration*. (Figure is based on ref<sup>[3]</sup>)

Based on the topics discussed in this chapter, the following chapters will present the work performed in the course of this thesis. In contrast to conventional top-down approaches, the self-assembly of small molecules provides a bottom-up approach for the preparation of supramolecular nanofibers. The influence of processing parameters on the morphology of the fibers was investigated under defined self-assembly conditions. In addition, prepared nanofibers were employed into support structures to obtain composites that were suitable for air- and liquid filtration applications.

## 2 Aim and Motivation

One essential goal within the scope of this thesis is the preparation of supramolecular nanofibers from solution based on the self-assembly of 1,3,5-benzenetrisamides (BTAs). This process is driven by the formation of controlled and directional non-covalent interactions between individual molecular building blocks. The resulting fiber morphology is governed by parameters such as the molecular structure of the BTA, the concentration, the used solvent and the selected processing conditions. The research of this thesis encompasses three different parts that are all related to the self-assembly process of BTAs. Each of these three parts will be introduced in more detail in the following:

### *Self-assembly of alkoxy-substituted 1,3,5-benzenetrisamides under controlled conditions*

Self-assembly of 1,3,5-benzenetrisamides from solution is an efficient way for the preparation of supramolecular nanofibers. During processing, different experimental parameters may influence the resulting nanofiber morphology such as the molecular structure of the BTA, the selected processing solvent, BTA concentration, operating temperature range and mechanical stirring of the BTA solution.

Therefore, this chapter of the thesis aims for a deeper understanding of the possibilities to control the resulting morphology of supramolecular fibers by performing a series of self-assembly experiments under controlled conditions and variations of the processing conditions.

Several objectives for this part are defined:

- Design of an experimental setup to conduct self-assembly experiments to control the number of influencing processing parameters, allowing for a series of experiments under defined conditions.
- Understanding of the experimental setup and operating conditions, in particular heat transfer processes.
- Implementation of a series of self-assembly experiments under variation of mechanical stirring velocity and the temperature range with the aim to control the resulting fiber diameter and the fiber diameter distribution.
- Analysis of the resulting fiber morphology by scanning electron microscopy (SEM) to evaluate the influences and correlate to the processing conditions.

### *Supramolecular nanofibers for air filtration applications*

Exposure to airborne particulate matter with particle diameters of less than 2.5  $\mu\text{m}$  has been identified as one major risk factor to human health.<sup>[102]</sup> Therefore, enormous interest exists on the development of novel filter media involving fibers with diameters in the nanometer range to remove such particles from ambient air.<sup>[22,99,103,104]</sup> Mostly, related research is based on fibers produced by common top-down-approaches such as electrospinning, melt-blowing or centrifugal spinning.<sup>[2,6,25,105]</sup> A very new approach, recently reported by our research group utilizes for the first time supramolecular fibers based on 1,3,5-benzenetrisamides for the preparation of supramolecular nanofiber-microfiber composites. Such composites have a great potential in air filtration applications.<sup>[89]</sup>

Beyond the initial findings, this thesis covers research to gain a deeper insight into the preparation of supramolecular nanofiber-microfiber composites and the influence of processing parameters on the morphology of the resulting composites related to their filtration performance.

This chapter encompasses the following goals:

- Influence of solvent and BTA concentration on the *in-situ* preparation of nanofiber-microfiber composites based on a polyester/viscose model nonwoven.
- Investigation of the temperature dependent solubility and self-assembly behavior of selected BTA and solvent combinations by turbidity measurements.
- Characterization of the prepared nanofiber-microfiber composites by different analytical methods such as SEM analysis, IR-spectroscopy or capillary flow porometry.
- Filtration test experiments to remove particulate matter from air to demonstrate the applicability of these composites for air filtration applications.
- Transfer of the concept from aliphatic substituted 1,3,5-benzenetrisamides to a system with alkoxy-substituents in the periphery of the molecular structure and implementation into a technical nonwoven.

### *Sand - supramolecular nanofiber filters for the removal of bacteria from water*

Ingestion of ground and surface water that is contaminated by microbial pathogens causes millions of people around the world to suffer from waterborne diseases such as acute diarrheas, typhoid fever, bacillary dysentery and cholera.<sup>[106]</sup> Interventions for the treatment of contaminated water have been proven to reduce the occurrences of infections by consumption of contaminated water. Many of those water treatment solutions are based on filtration processes by porous media such as ceramic materials or granulate materials.<sup>[97,100,107–109]</sup>

Recent results obtained by utilization of supramolecular nanofibers based on the *in-situ* self-assembly of 1,3,5-benzenetrisamides from solution to prepare nanofiber-microfiber composites demonstrated the enormous potential of supramolecular materials in filtration. Therefore, this chapter aims for the first time for the development of a filter that incorporates supramolecular nanofibers inside a granulate material to yield a filter unit that is capable of removing microbial contamination such as *E. coli* from water.

The main objectives of this chapter are:

- Development of a preparation process to obtain filter media containing supramolecular nanofibers inside a granulate material such as sea sand.
- Design of a filter unit containing a combination of sand and supramolecular nanofibers that can be subjected to liquid filtration test experiments.
- Characterization of such filter units by means of dimensional stability and SEM analysis.
- Development a liquid filtration test setup for the evaluation of prepared units by means of filtration performance to remove polymer particles from water.
- Monitoring of relevant operating parameters during the filtration process like for example differential pressures.
- Filtration experiments with *E. coli* bacteria from water.<sup>1</sup>

---

<sup>1</sup> In cooperation with the DWI – Leibniz Institute for Interactive Materials, RWTH Aachen, Germany



### 3 Self-assembly of alkoxy-substituted 1,3,5-benzenetrisamides under controlled conditions

#### 3.1 Introduction

##### *Methods to self-assemble 1,3,5-benzenetrisamides from solution*

The design of supramolecular nanostructures by self-assembly of low molecular weight building blocks from solution has attracted much research interest.<sup>[26,110–112]</sup> Most of these self-assembly systems are based on the formation of reversible non-covalent interactions such as hydrogen bonds,  $\pi$ - $\pi$ -stacking or metal-ligand coordination. A variety of studies have been reported on a very simple structural motif based on 1,3,5-benzenetrisamides (BTAs) and on the preparation of supramolecular nanostructures of these compounds from solution.<sup>[49,51,56]</sup> These materials are designed to form supramolecular columns by directed threefold hydrogen bonding of the amide moieties between the individual building blocks.<sup>[60,65,66]</sup> To obtain supramolecular BTA-nanostructures, usually a solution of BTA in a given solvent is prepared with a defined concentration. The self-assembly process is then triggered by an external influence to this solution to induce the formation of supramolecular columns, which can result in the formation of nanofibers. Change of the pH-value, changes of solvent quality, evaporation of the solvent or temperature changes are possible methods to initiate such a self-assembly process.

For instance, Bernet et al. reported on a *pH-sensitive* self-assembly system from water utilizing a BTA with three *p*-carboxylphenyl substituents. Thereby, the sodium-salt of the BTA is fully dissolved in a solution of NaOH in water and upon decreasing the pH-value the self-assembly process starts yielding a supramolecular hydrogel.<sup>[55]</sup> Another method of inducing the self-assembly of 1,3,5-benzenetrisamides is the *addition of a non-solvent* to a BTA solution. Shen et al. reported on the gelation of *N,N*-dimethylformamide containing a BTA with ethyl cinnamate-substituents upon addition of water to the system.<sup>[75]</sup> Another commonly used method to start the self-assembly of BTAs from solution is by *variation of temperature* for example upon cooling. The resulting supramolecular structures can subsequently be separated from the solvent. For example, a 1,3,5-benzenetrisamide with the methyl ester of  $\gamma$ -aminobutyric acid in the periphery of the molecular structure has been demonstrated to form organogels of aromatic solvents upon cooling of the system from a solution at elevated temperatures. The resulting gels were dried in vacuo to yield fibrous supramolecular structures.<sup>[70]</sup> Leenders et al. prepared a hydrogel by heating of a solution of a 1,3,5-benzenetrisamide in water to a temperature of 80 °C and subsequent cooling to 20 °C without any further specification

of the temperature profile or mechanical stirring of the solution during the cooling process.<sup>[73]</sup> The resulting structures were analyzed by Cryo-TEM. A combination of cooling and simultaneous evaporation of the solvent was used recently to prepare composites based on supramolecular nanofibers inside a polymer nonwoven scaffold.<sup>[89]</sup>

To investigate the mechanical properties of supramolecular BTA nanofibers featuring different alkyl substituents by nanomechanical bending experiments. Here, the BTA-fibers were prepared by cooling of a BTA solution at a constant linear cooling rate and subsequent drying at air.<sup>[71,72]</sup> In addition, it has been described that the morphology of supramolecular nanofibers prepared by cooling of a BTA solution can be strongly dependent on the applied temperature profile.<sup>[113]</sup>

Influences described earlier utilized to start self-assembly processes such as changes of temperature, evaporation of the solvent and changing solvent compositions exhibit many similarities to tools used in industrial crystallization processes. Therefore, the principles of industrial crystallization processes are briefly introduced in the following.

#### *Industrial crystallization from solution*

Crystallization from solution is an universal tool for the separation and purification of chemicals in fine chemical industry, food industry, and pharmaceuticals.<sup>[114]</sup> Each crystallization process starts by preparing a solution of the solid, which is supposed to be purified, in a selected solvent. Then, an external influence to generate supersaturation and to induce nucleation and crystal growth is applied to the system.

Solution crystallization is defined as a process, which yields a solid crystalline product from a liquid solution.<sup>[115,116]</sup> Such a solution is generated by adding a solid compound to a solvent resulting in a homogenous system. The maximum amount of solid dissolvable in a defined amount of solvent at a known temperature is called the solubility. Solutions containing this specific amount of solid are considered to be saturated.<sup>[116]</sup> Technically, crystallization processes can be performed in batch or continuous processes, whereas continuous crystallizers are usually preferred if large amounts of the desired product have to be prepared. In contrast, batch crystallizers can be adjusted easily to process a variety of different compounds in small amounts.

Three different types of batch crystallizers are commonly used: *cooling crystallizers*, *evaporation crystallizers*, and *salting-out crystallizers*. Each type of crystallizer applies a different influence to the system to create supersaturation of the solution.<sup>[116]</sup> In *evaporation crystallizers*, the concentration of a dissolved compound in a solution is increased by evaporation of the solvent to create supersaturation

of the system. Another way to achieve supersaturation of a solution is by addition of another liquid that reduces the solvent quality of the system. For instance, in *salting-out crystallizers*, a solution exhibiting a high ionic strength can be added to the system that causes the desired solid compound to crystallize. A very relevant type of crystallizer for this thesis is given by *cooling crystallizers*. These setups are suitable for systems exhibiting a strong temperature dependent solubility of the solid compound in the selected solvent. Therefore, it is essential to obtain accurate temperature dependent solubility data for the development of the crystallization process. Today, many research effort is put on the temperature dependent solubility behavior of various organic compounds in different solvents as well as of inorganic compounds for example sodium chromate.<sup>[117–120]</sup> In most cases, the solubility of a compound in a given solvent increases with increasing temperature, whereas the intensity of the temperature dependency itself may vary drastically between different compounds. Furthermore, the solubility of a compound may be significantly enhanced in solvent mixtures compared to the solubility in the pure solvents. For example, it was found that phenanthrene exhibits increased solubility in mixtures of diiodomethane and cyclohexane compared to the two individual pure solvents.<sup>[121]</sup> Precise control of the temperature profile during the cooling process can significantly influence the resulting particle size distribution.<sup>[122]</sup> Temperature controlled crystallizers are often combined with controlled seeding during the cooling process. This additional impact may influence the particle size distribution as much as differences in the temperature profiles.<sup>[123]</sup>

#### *Approach in this thesis*

This chapter reports on the design of an experiment under controlled conditions to prepare supramolecular fibers of 1,3,5-benzenetrisamides from solution by *application of a temperature change and mechanical stirring* of a hot BTA solution. In principle, the experimental setup to perform the self-assembly experiments can be compared to a simple batch cooling crystallizer. However, the work focused on the application of different conditions of mechanical stirring during the self-assembly process and, in consequence, different cooling characteristics, on the influence on the resulting fiber morphology. The underlying steps of the experiment are illustrated schematically in **Figure 3.1**. The fully dissolved BTA (red dots) in a selected solvent (blue dots) at elevated temperatures (A) is cooled against a constant cooling temperature on the outside of the system with a suitable cooling agent, while the overall concentration of the self-assembly system was kept constant by preventing evaporation of the solvent. The self-assembly system and the cooling agent are separated by a glass wall. The change in temperature leads to a supersaturation of the system resulting in the formation of supramolecular nanofibers (red fibers) suspended in the solvent (B). After the cooling process is

complete, the prepared fibers are separated from the solvent. The solvent of the suspension is evaporated at ambient conditions yielding supramolecular fibers.

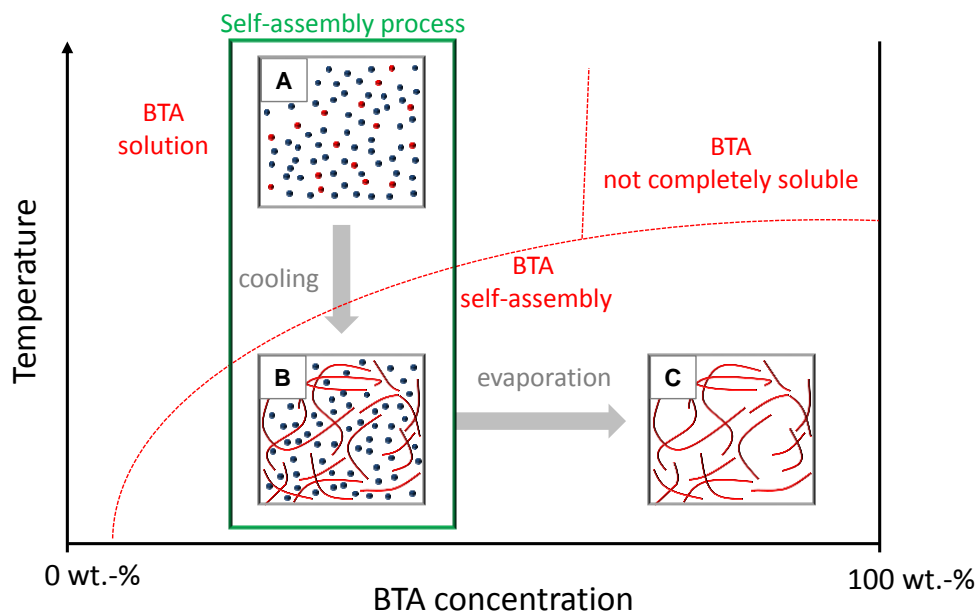


**Figure 3.1:** Schematic representation of thermally induced self-assembly to form supramolecular fibers upon cooling (solvent: blue dots; dissolved 1,3,5-benzenetrisamide: red dots; supramolecular nanofibers: red lines). At elevated temperatures, a solution of fully dissolved BTA (A) is cooled to induce the formation of supramolecular fibers via self-assembly, resulting in suspensions of supramolecular fibers in the solvent (B). Complete solvent evaporation yields the supramolecular fibers (C).

In a self-assembly system that is investigated by this experiment under controlled conditions, the solubility of the BTA in a given solvent needs to be strongly temperature dependent, while at low temperatures the solubility has to be negligible to ensure that the supramolecular fibers obtained from this experiment are only due to the cooling process. However, the self-assembly into supramolecular nanofibers needs to be inducible by a change in temperature. This process might be inhibited if the self-assembly system tends to strong supersaturation upon cooling resulting in a metastable solution.

In this thesis, the influence of shear forces during the self-assembly process on the resulting morphology of the supramolecular fibers will be analyzed by applying different conditions of mechanical stirring to the system. However, variation of the stirring speed of the BTA solution during the self-assembly process has a strong influence on the resulting temperature profiles. Since, it was already found that different cooling rates result in a change of the resulting nanofiber morphology, temperature profiles as well as the mechanical stirring have to be precisely monitored during the experiments.<sup>[113]</sup> A second experimental series in this thesis is the variation of the applied cooling

temperature to investigate the influence on the resulting fiber morphology apart from variations of conditions of mechanical stirring. A custom-made experimental setup was developed enabling the cooling and controlled stirring of a hot BTA solution while preventing evaporation of the solvent. The time dependent temperature profiles were monitored during each experiment. The detailed experimental setup, the selection of a suitable self-assembly system as well as the results of the self-assembly experiments are presented in the following.

### 3.2 Experimental setup for self-assembly upon cooling

One essential part of the work presented in this chapter is the design of a custom-made experimental setup fitting the task to investigate the self-assembly behavior of a selected 1,3,5-benzenetrisamide from solution. The process focused on temperature changes and simultaneously mechanical stirring during self-assembly. A change of the overall BTA concentration by evaporation of the solvent had to be avoided. **Figure 3.2** displays a schematic representation of the developed custom-made setup. The chosen vessel was a screw-mountable laboratory glass bottle (250 mL; Duran Group) with an outer-diameter of 70 mm and a height of 143 mm. A customized cap allowed for the insertion of a mechanical stirrer (RZR 2051; Heidolph) and a thermocouple (type K), while keeping the vessel sealed and avoiding any evaporation of the solvent. The selected mechanical stirrer ensured a reproducible mechanical stirring by enabling precise digital control of the stirring velocity measured in revolutions per minute (rpm). The thermocouple was linked to a Datalogger (PCE-T390; PCE-Instruments) to record time dependent temperature profiles of the self-assembly system inside the glass during the process ( $T_{\text{inside}}$ ).

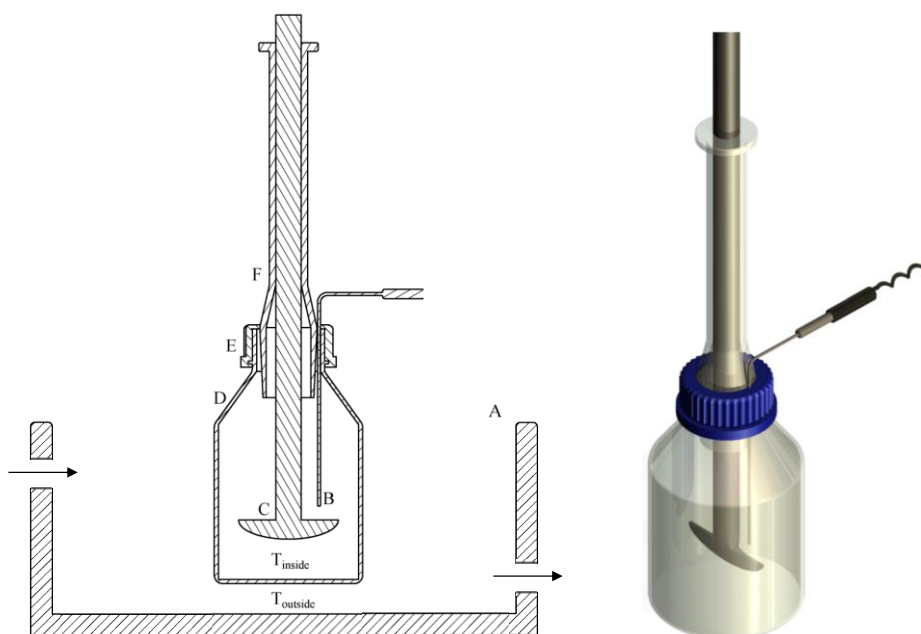


**Figure 3.2:** Schematic representation of the custom-made experimental setup for thermal induced self-assembly experiments consisting of a temperature control bath (A), a thermocouple (B), a mechanical stirrer (C), a screw-mountable vessel (D), a customized cap (E) and a guide for the mechanical stirrer (F).

The vessel can be heated from the outside with a water bath and cooled with a cooling bath of a cryostat (Haake F3; cooling agent: ethylene glycol/water (1:1)). The cooling agent inside the cryostat was circulated constantly to improve the heat exchange. The experimental setup is designed in a way that it was possible that the vessel could be placed quickly from the heating bath into the cooling bath. Heating and cooling temperatures ( $T_{\text{outside}}$ ) were being kept constant during each experiment, so no temperature profiles of the cooling agent outside the vessel were recorded. Since changes in temperature are one key parameter of this experimental setup, the mechanism of heat exchange between the BTA solution on the inside of the glass and the cooling agent on the outside has to be introduced.

Transport processes such as heat transfer are of great importance in many industrial operations.<sup>[92]</sup> The rate of heat flow  $\dot{Q}$  in this experimental setup is based on the indirect heat exchange between two liquid media through a wall. If the experiment is performed without any mechanical stirring, the movement of the fluid inside the vessel is governed by natural convection and due to insufficient mixing a temperature gradient arises from the glass wall to the inside of the vessel. Mechanical stirring during the cooling process enhances the heat transport from inside the vessel leading to a more homogenous temperature distribution throughout the liquid medium. Assuming an ideal mixing of the fluids, **Figure 3.3** displays a simplified schematic representation of the heat exchange through a wall for very small time intervals in which all parameters are assumed to be constant.<sup>[124]</sup> The process can basically be divided into three individual steps.<sup>[125]</sup> The first step consists of the heat transfer from the self-assembly system to the wall on the inside of the glass  $\dot{Q}_1$ . This transfer is directly proportional to the thermal conductivity coefficient  $\lambda_1$  of the BTA solution and to the surface area of the wall  $A_w$ .  $T_{\text{inside}}$  represents the temperature of the self-assembly system inside the vessel and  $T_{\text{outside}}$  corresponds to the constant cooling temperature outside the vessel.  $T_{w1}$  refers to the temperature of the wall on the inside of the laboratory glass. According to equation 3.1, the greater the difference between  $T_{\text{inside}}$  and  $T_{w1}$ , the greater is the resulting heat transfer  $\dot{Q}_1$ .

$$\dot{Q}_1 = \frac{\epsilon_1}{\alpha_1} \cdot A_w \cdot (T_{\text{inside}} - T_{w1}). \quad (3.1)$$

$\delta_1$  represents a boundary layer in which the heat transfer is mainly governed by thermal conduction.<sup>[126]</sup> On the one hand, a high thermal conductivity  $\lambda_1$  of the fluid inside the vessel leads to high values for the heat transfer, whereas on the other hand, a thick boundary layer  $\delta_1$  close to the wall reduces the heat flow  $\dot{Q}_1$ .

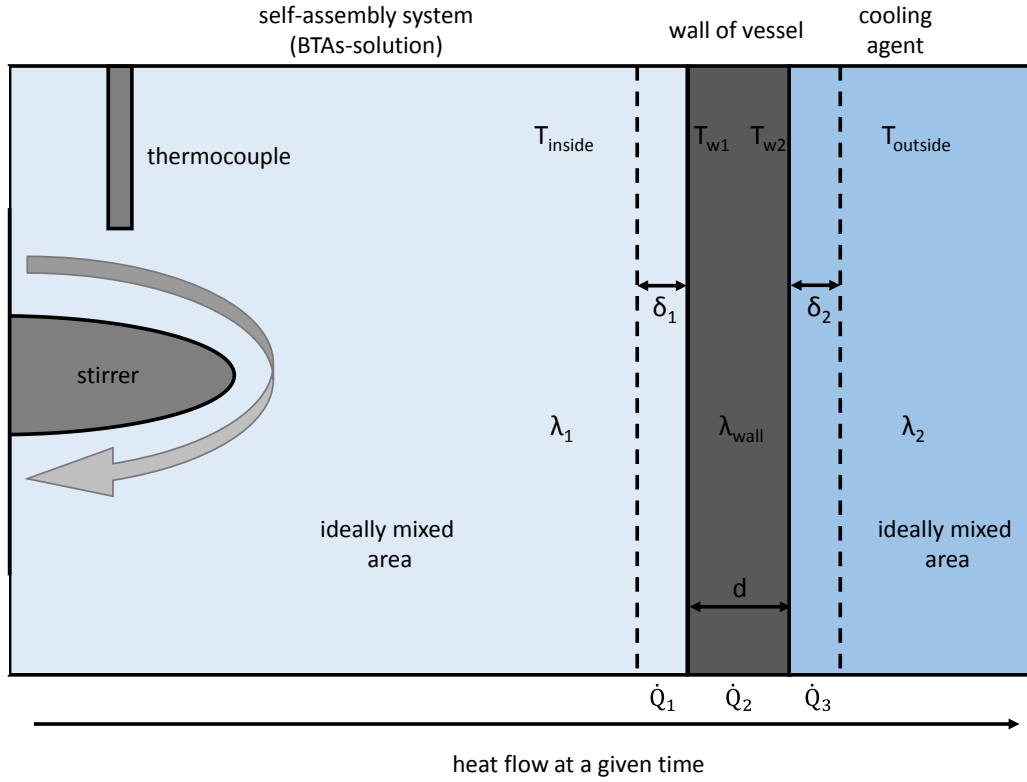


**Figure 3.3:** Schematic representation of the heat transfer from the self-assembly system on the cooling agent. The transfer consists of three individual steps: 1. Heat transfer from the self-assembly system on the wall. 2. Heat conduction through the wall. 3. Heat transfer from the wall to the cooling agent.  $\lambda_1$ : Thermal conductivity coefficient of the self-assembly system.  $\lambda_2$ : Thermal conductivity coefficient of the cooling agent.  $\lambda_{wall}$ : Thermal conductivity coefficient of the material of the wall.  $T_{inside}$ : Temperature inside the vessel.  $T_{outside}$ : Temperature of the cooling agent.  $T_{w1}$ : Temperature of the wall on the inside.  $T_{w2}$ : Temperature of the wall on the outside.  $\delta_1$ : Boundary layer between self-assembly system and wall.  $\delta_2$ : Boundary layer between cooling agent and wall.  $d$ : Thickness of the wall.

The second step in the cooling process is the transfer of heat through the wall of the vessel  $\dot{Q}_2$  which is given by equation 3.2.

$$\dot{Q}_2 = \frac{\dot{e}_{wall}}{d} \cdot A_w \cdot (T_{w1} - T_{w2}). \quad (3.2)$$

Even though the wall of the vessel is curved, differences in the surface area of the wall  $A_w$  between the inside and outside are assumed to be negligible.  $\lambda_{wall}$  is the thermal conductivity coefficient of the material of the wall and  $d$  corresponds to its thickness.  $T_{w2}$  describes the temperature of the wall on the outside of the vessel.

The third step of the heat exchange describes the transfer from the outside of the wall of the vessel to the cooling agent  $\dot{Q}_3$  through a boundary layer  $\delta_2$ . High thermal conductivity  $\lambda_2$  of the cooling agent allows for large values of heat being transferred.

$$\dot{Q}_3 = \frac{\ddot{e}_2}{\ddot{a}_2} \cdot A_w \cdot (T_{w2} - T_{\text{outside}}). \quad (3.3)$$

The total amount of heat exchanged is equal for all three individual steps, so that the overall heat exchange  $\dot{Q}$  from the solution inside the glass to the cooling agent on the outside can be represented by equation 3.4.<sup>[127]</sup>

$$\dot{Q} = \dot{Q}_1 = \dot{Q}_2 = \dot{Q}_3. \quad (3.4)$$

Transformation of equations 3.1 and 3.3 and substitution into equation 3.2 yields the overall heat flow rate  $\dot{Q}$  from the self-assembly system to the cooling agent under stationary conditions:

$$\dot{Q} = \frac{A_w}{\frac{\ddot{a}_1}{\ddot{e}_1} + \frac{d}{\ddot{e}_{\text{wall}}} + \frac{\ddot{a}_2}{\ddot{e}_2}} \cdot (T_{\text{inside}} - T_{\text{outside}}). \quad (3.5)$$

The temperature profile of the BTA solution during the cooling process is directly related to the overall heat flow  $\dot{Q}$ . While most variables are directly accessible such as thermal conductivities  $\lambda_1$  and  $\lambda_2$  as well as the differences in temperature, the thickness of the boundary layers  $\delta_1$  and  $\delta_2$  on the inside and on the outside of the system have to be derived from dimensionless quantities such as the *Nusselt number* (Nu), the *Reynolds number* (Re) and the *Prandtl number* (Pr), which are frequently used in chemical reaction engineering. The value of the Nusselt number is given by equation 3.6.<sup>[126]</sup>

$$\text{Nu} = \frac{\acute{a}_1 D}{\ddot{e}_1} \quad (3.6)$$

$$\acute{a}_1 = \frac{\ddot{e}_1}{\ddot{a}_1} \quad (3.7)$$

$\acute{a}_1$  is called the heat transfer coefficient and is given by the ratio of  $\ddot{e}_1$  and  $\ddot{a}_1$  as shown equation 3.7. D corresponds to a characteristic length depending on the geometry of the experimental setup. For a mechanically stirred batch reactor, this length corresponds to the inner diameter of the reactor. The Nusselt number depends on varying equations depending on the experimental boundary conditions. In case of no applied mechanical stirring inside the vessel, the Nusselt number is governed by a phenomenon called natural convection. Local differences in density of the fluid medium cause movement of the individual particles. However, most experiments were performed under constant stirring. In this case, Nusselt number can be described by equation 3.8, which can be used for forced flow conditions.<sup>[126]</sup>

$$\text{Nu} = C \text{Re}^m \text{Pr}^n \left(\frac{L}{d}\right)^p \quad (3.8)$$

The values of C, m, n and p have to be determined empirically for a certain experimental setup.

The *Reynolds number* (Re) is a dimensionless quantity that is frequently used in fluid mechanics, whereas the *Prandtl number* (Pr) corresponds to the ratio of the kinematic viscosity of the fluid and its thermal diffusivity. L and d represent characteristic lengths depending on the geometry of the selected setup. Equation 3.9 describes a possible relation for the Reynolds number of a mechanically stirred batch reactor.<sup>[126]</sup>

$$\text{Re} = \frac{N \cdot b^2}{\dot{\nu}} \quad (3.9)$$

N represents the stirring velocity in revolutions per minute and b is the geometric width of the stirrer.  $\dot{\nu}$  is the kinematic viscosity of the system.<sup>[126]</sup> Increasing the mechanical stirring velocity inside the vessel results in an increase of the Reynolds number and in consequence an increase of the Nusselt number. According to equation 3.6, an increase in the Nusselt number leads to higher values of  $\dot{a}_1$  and thereby a decrease of the boundary layer  $\ddot{a}_1$ . A low thickness of this boundary layer improves the cooling process of the BTA solution. In addition, high kinematic viscosities of the fluid result in high values for the boundary layer limiting the cooling rate. Therefore, a cooling agent with a rather low viscosity was used as cooling agent (water and ethylene glycol (1:1)). The viscosity of pure ethylene glycol is around 22 mPas (20 °C), whereas pure water only exhibits a viscosity of 1 mPas (20 °C).

During the experiment the temperature of the cooling agent is kept constant by the use of a cryostat, while the temperature of the self-assembly system changes with time. **Figure 3.4** displays schematically an estimated theoretical temperature profile of the self-assembly system during the cooling process. Thereby, the cooling rate of the system changes continuously as the temperature difference between the BTA solution inside the vessel and the cooling agent on the outside becomes smaller. However, during the cooling process, the variation in temperature results also in significant changes of the viscosity of the BTA solution, which also influences the thickness of the boundary layer  $\ddot{a}_1$  and yet the heat exchange.

Two series of experiments will be conducted in the course of this work. The first series will focus on the variation of mechanical stirring velocities during the self-assembly process to investigate the influence of different mechanical conditions on the resulting morphology of supramolecular structures. This change in stirring will also lead to a change in the temperature profiles. During the second series of experiments, the cooling temperatures on the outside of the glass will be varied and therefore change temperature profiles by constant influence of shear force.

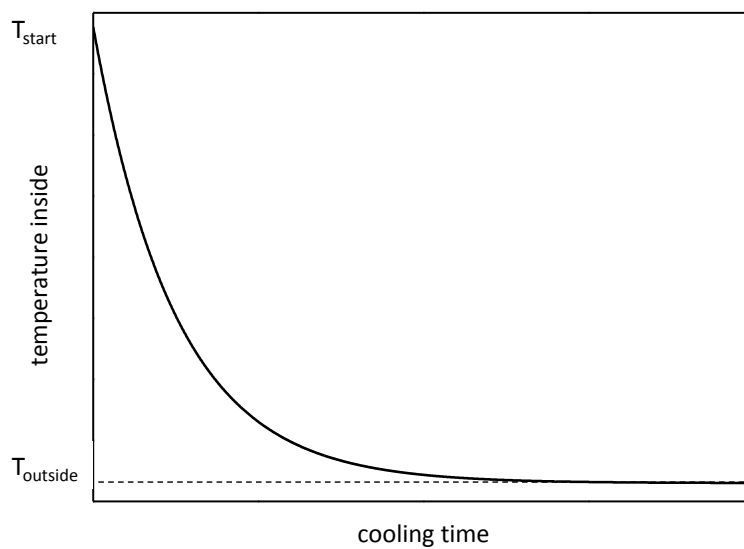


**Figure 3.4:** Schematic representation of an expected temperature profile of a liquid inside the glass based on equation 3.5 if the temperature of the cooling agent is kept at a constant value.

### 3.3 Experimental details for materials selection

This section provides the experimental details for section 3.4 “Materials selection of a suitable self-assembly system”, which presents screening self-assembly experiments and results of temperature dependent solubility and self-assembly experiments on a series of 5 alkoxy-substituted 1,3,5-benzenetrisamides. A suitable BTA and solvent combination is identified to be subjected to a series of experiments under controlled conditions. Experimental details on the materials selection are described in the following.

#### *Implementation of preliminary self-assembly experiments*

In order to identify the most suitable self-assembly system for the developed experimental setup under controlled conditions, screening experiments were performed to evaluate the tendency of each alkoxy-substituted 1,3,5-benzenetrisamide to form supramolecular fibers from solution. Therefore, solutions of each BTA at a concentration of 0.1 wt.-% were prepared and heated to a temperature of 50 °C, respectively. The total mass of each sample corresponded to a value of 20 g. Subsequently, these solutions were cooled to a temperature of 0 °C without further control of the temperature profile for 30 min and a few droplets of each BTA suspension were transferred into an aluminum pan normally used in differential scanning calorimetry. Evaporation of the solvent at ambient conditions yielded supramolecular structures. Samples were sputtered with platinum with a thickness of 2 nm and analyzed by utilization of a Scanning Electron Microscope (SEM) from Zeiss 1530 equipped with a field emission cathode. Images were taken using a SE2 detector and an accelerating voltage of 2 kV.

#### *Determination of solubility*

The identification of a suitable self-assembly system required knowledge about the temperature dependent solubility of a selected BTA in a given solvent. Each solubility measurement was started by suspending a defined amount of solid BTA in a given solvent or solvent mixture. The obtained suspension was then stirred at constant temperature. After 30 min the system was assumed to be at equilibrium state and investigated for remaining particles in the solvent. Based on the Tyndall effect, a Laser pointer was used to verify that no microscopic particles remained in the solvent that were not visible to the unaided eye. If no particles were detected, the suspended amount of BTA was considered to be soluble at the corresponding temperature. In this case, additional solid BTA was added to the solution and the procedure was repeated. If particles of solid BTA remained, the corresponding

amount of BTA was considered to be partially insoluble. Temperature dependent solubility may be obtained by performing a series of experiments at different temperatures.

### 3.4 Materials selection for a suitable self-assembly system

Temperature dependent solubility in water and aqueous mixtures as well as the tendency to form supramolecular fibers by self-assembly from solution of a selection of five different 1,3,5-benzenetrisamides were investigated with the procedures described before. **Figure 3.5** displays the molecular structures of the alkoxy-substituted 1,3,5-benzenetrisamides (BTA **1** – **5**). Instead of frequently used alkyl substituents in the periphery of the molecular structure, alkoxy groups were introduced to enhance solubility of the BTAs in water and aqueous solvent mixtures. Therefore, investigations in terms of temperature dependent solubility and self-assembly behavior mainly focused on the use of water and water/isopropanol mixtures. The synthesis and characterization of these 1,3,5-benzenetrisamides is described in detail in the appendix. They are synthesized based on the reaction between the acid chloride of trimesic acid and the corresponding amine. BTA **2** has already been reported in the literature.<sup>[60,128–130]</sup> All other alkoxy-substituted 1,3,5-benzenetrisamides are not known to the literature to this point.

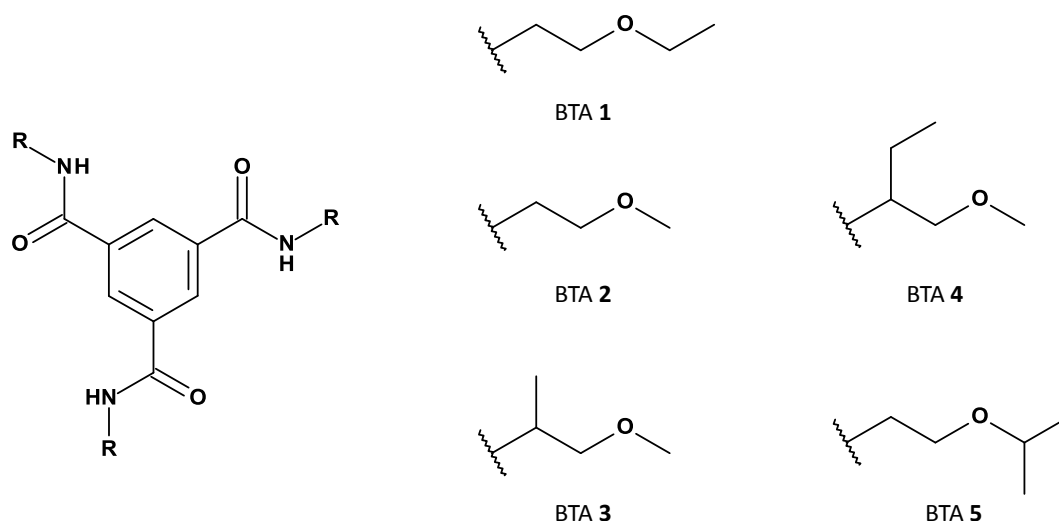


**Figure 3.5:** Chemical structures of selected 1,3,5-benzenetrisamides (BTAs **1** – **5**) with different branched substituents containing ether groups to enhance solubility in water and aqueous systems.

For the selection of a proper BTA and solvent combination, two key characteristics of each system have to be investigated. Knowledge about the solubility behavior and the tendency to form supramolecular fibrous structures from solution are essential in order to evaluate whether a system BTA and solvent combination can be investigated by the developed experiment under controlled conditions.

Therefore, screening experiments were performed to first determine the solubility behavior at room temperature of the selected alkoxy-substituted 1,3,5-benzenetrisamides in aqueous systems. Based

on these first results, the tendency to form supramolecular fibers from solution was investigated by self-assembly screening experiments. The BTA and solvent combinations exhibiting the most promising results were then subjected to deeper temperature dependent solubility studies to identify the self-assembly system that is most suitable for the investigation in self-assembly experiments under controlled conditions.

#### *Self-assembly screening experiments*

Investigations on the formation of supramolecular fibers by self-assembly of the selected BTAs from solution were performed. First, a 0.1 wt.-% solution of each selected BTA had to be prepared involving basic experiments concerning the solubility in a given solvent. Due to the introduction of alkoxy groups in the periphery of the BTAs, the first selected solvent for solubility measurements was water. Experiments were performed to determine the solubility of each BTA in pure water at room temperature. Table 3.1 presents the resulting solubility of BTAs **1** – **5** in water at room temperature in weight percentages. The values demonstrate that BTAs **1**, **2** and **5** are already soluble to a significant amount in pure water. Based on the Tyndall-effect, even at very low concentrations, remaining microscopic particles of BTA **3** and **4** were visible in water. Therefore, above these concentrations only partial solubility was obtained.

Table 3.1: Solubility of selected 1,3,5-benzenetrisamides in water at room temperature.

BTA	Solubility at 25 °C
1	≤ 1.50 wt.-%
2	≤ 0.70 wt.-%
3	≤ 0.01 wt.-%
4	≤ 0.01 wt.-%
5	≤ 0.50 wt.-%

Isopropanol was found to be a better solvent for BTAs **3** and **4**. Therefore, the preparation of solutions of BTA **3** and **4** with a concentration of 0.1 wt.-% required a water/isopropanol (60:40) solvent mixture. To perform the screening self-assembly experiments, each solution was heated to a temperature of 50 °C and subsequently cooled to 0 °C.

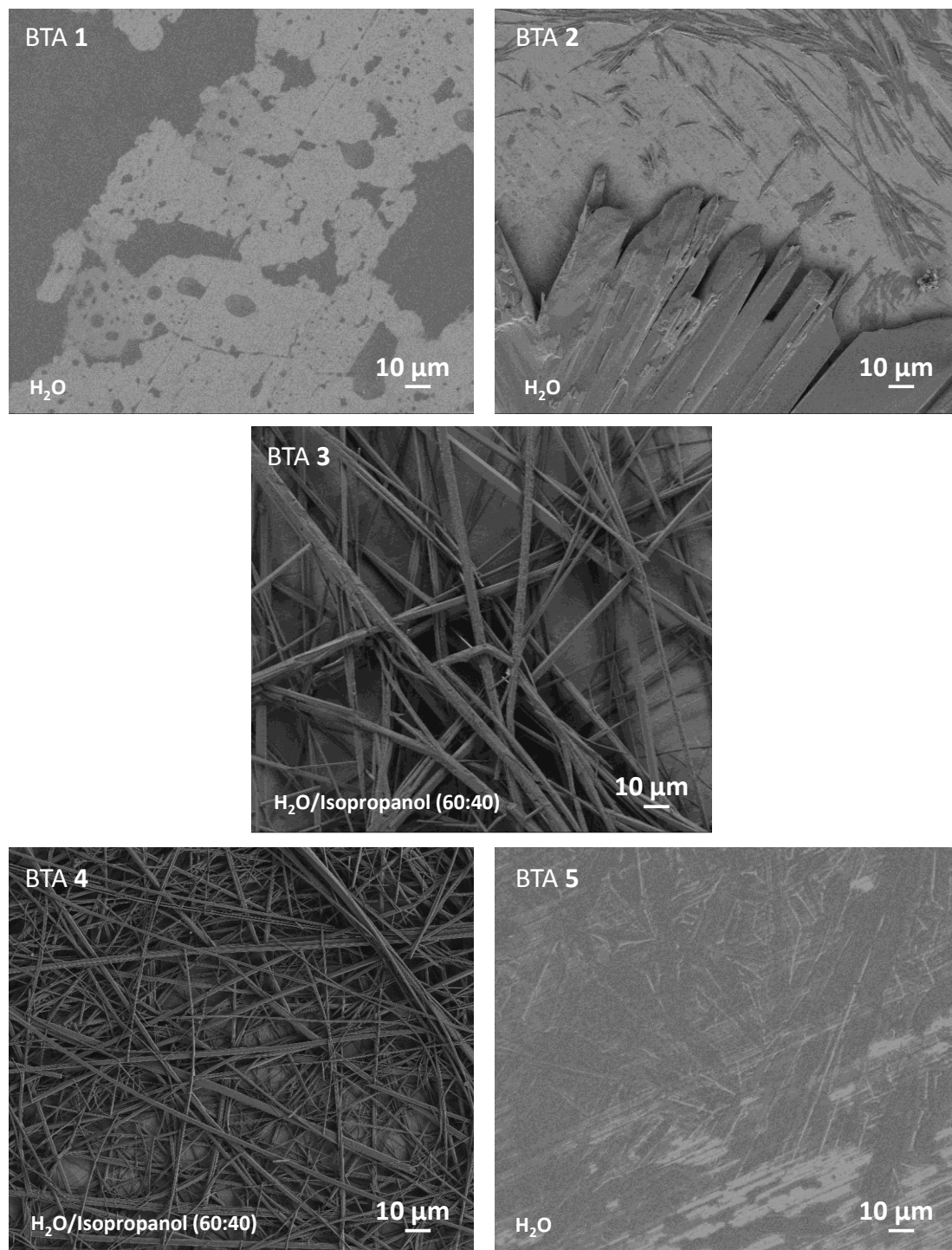


**Figure 3.6:** SEM-images showing the resulting morphology of self-assembled structures of BTA **1** to **5** from screening self-assembly experiments from solution. The BTA concentration in all experiments was 0.1 wt.-%. Due to the low solubility of BTA **3** and BTA **4** in pure water, the corresponding experiments were performed from a water/isopropanol mixture (60:40).

Samples of each solution were taken and dried at ambient conditions on aluminum pans typically used in differential scanning calorimetry (DSC). Overview images of dried samples of each BTA were taken by scanning electron microscopy (SEM) and are displayed in **Figure 3.6**. The self-assembly experiment

of BTA **1** from water yielded a film-like structure partially covering the surface of the aluminum DSC-pan. Formation of supramolecular fibers was not observed for BTA **1**. The corresponding experiment of a solution BTA **2** in water resulted in a very different morphology. Large ribbon-type structures were formed that were connected to each other covering large areas of the aluminum surface. In addition, smaller ribbon-type structures with a width of about 1-3  $\mu\text{m}$  appeared. The length of these structures was around 10 to 30  $\mu\text{m}$ . The mass fraction of the large structures appeared to be significantly higher compared to the smaller structures. In contrast, self-assembly of BTA **3** from water/isopropanol (60:40) resulted in the formation of supramolecular fibers with diameters of around 10  $\mu\text{m}$ . For BTA **4**, formation of more supramolecular fibers with even smaller fiber-diameters was observed. In contrast, the self-assembly experiment of BTA **5** resulted in the formation of a patterned and flat film-like structure. Due to good solubility in isopropanol even at room temperature, no fiber formation of BTAs **1**, **2** and **5** was investigated from water/isopropanol solvent mixtures. Only experiments utilizing BTA **3** and BTA **4** resulted in the formation of supramolecular fibrous structures. Based on these experiments results, BTAs **3** and **4** appear to be the most promising compounds to be subjected to further investigations, due to the low solubility at room temperature as well as the formation of fibrous structures.

#### *Temperature dependent solubility of selected BTAs*

Since SEM sample preparation required a drying process of suspended supramolecular structures in the solvent, the low solubility of BTAs **3** and **4** were favorable for further experiments. Therefore, temperature dependent solubility in pure water was studied for these two alkoxy-substituted BTAs. During the drying process additional self-assembly based on changes in concentration could not be excluded and might influence the resulting morphology of supramolecular fibers. Apart from that, fiber formation of BTAs **1**, **2** and **5** could not be observed. Due to a significant solubility of BTAs **1**, **2** and **5** in pure water at room temperature, these BTA and solvent combinations were not applicable.

**Figure 3.7** displays the results concerning temperature dependent solubility behavior of BTA **3** in pure water for temperatures ranging from 25  $^{\circ}\text{C}$  to 50  $^{\circ}\text{C}$ . While the solubility of the BTA **3** at room temperature is less than 0.01 wt.-%, it increases upon heating to a value of around 0.12 wt.-% at 50  $^{\circ}\text{C}$ . This temperature dependency basically fits very well the conditions of the developed experiment under controlled conditions. However, upon cooling of such a solution no formation of supramolecular fibers occurred. The system tends to strong supersaturation resulting in a metastable solution. Since the formation of fibrous structures is not inducible by a change in temperature, no further investigations on the self-assembly behavior of BTA **3** were performed.

Therefore, the temperature dependent solubility of BTA **4** in water was measured. The results are presented in **Figure 3.8**. Upon increasing the temperature of the system, the solubility remains very close to zero and only a slight increase is observed. However, the temperature dependence of the solubility behavior of BTA **4** in pure water was found too small to be applied to the experiment under controlled conditions.

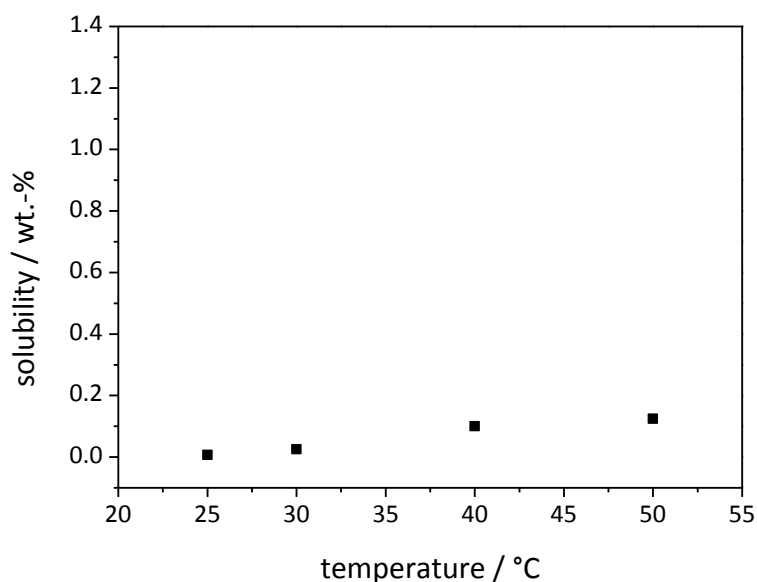


**Figure 3.7:** Temperature dependent solubility of BTA **3** in pure water.

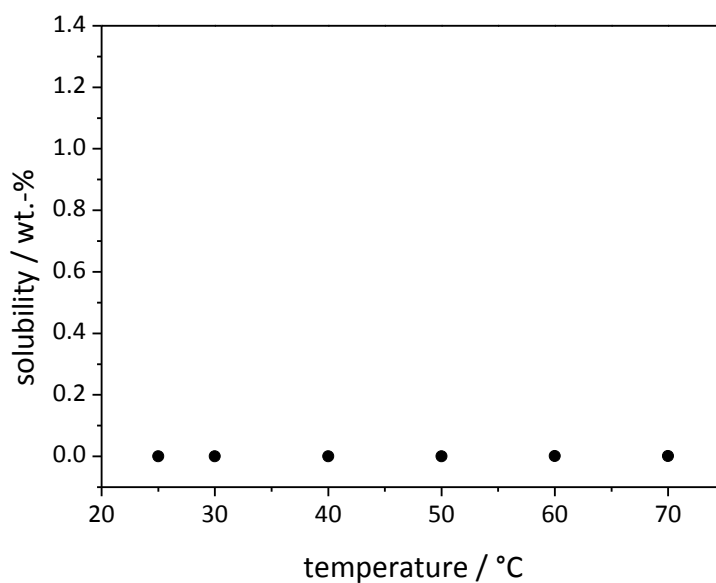


**Figure 3.8:** Temperature dependent solubility of BTA **4** in pure water.

To modify the solubility behavior of BTA **4**, additional experiments were performed with water/isopropanol mixtures of varying compositions. **Figure 3.9** presents results from temperature dependent solubility measurements of BTA **4** in different water/isopropanol mixtures. An increasing isopropanol content in the solvent mixtures results in an increased temperature dependency of the solubility. Almost no differences in solubility behavior can be observed between pure water and a mixture of water/isopropanol (90:10), whereas a mixture of 80 wt.-% water and 20 wt.-% isopropanol exhibits a solubility of 0.002 wt.-% at 25 °C and increases to a value of 0.06 wt.-% at 70 °C. This corresponds to an increase by a factor of 30. In case of a water/isopropanol mixture of 70 wt.-% water and 30 wt.-% isopropanol, the solubility at room temperature corresponds to a value of 0.025 wt.-%. However, it was found that upon cooling, the BTA solutions become hazy and fiber formation starts. In consequence, the self-assembly system consisting of BTA **4** and a solvent mixture of water and isopropanol is the most suitable to be investigated in the developed custom-made experiment. The temperature dependent change in solubility of BTA **4** in solvent mixtures containing 30 wt.-% and 40 wt.-% isopropanol was smaller considering the solubility at room temperature compared to a mixture of water and isopropanol (80:20). For instance, solubility of BTA **4** in water/isopropanol (60:40) only increased by a factor of 10 in a temperature range from 25 °C up to 70°C. Therefore, these mixtures were not selected for further investigations. Due to the very low solubility at room temperature of BTA **4** in the solvent mixture water/isopropanol (80:20), this system was found to fit the best for further investigations in experiments under controlled conditions. The next section (3.5) describes the experimental details of the series of self-assembly experiments using the combination of BTA **4** and the solvent mixture of water and isopropanol (80:20)

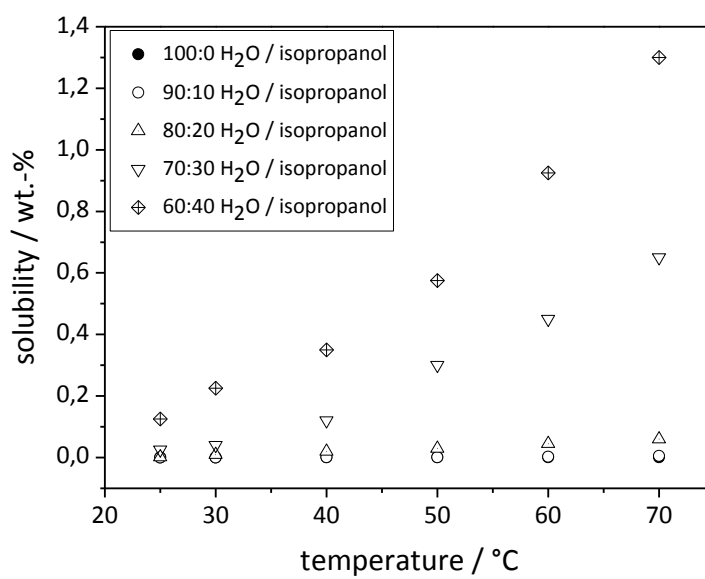


**Figure 3.9:** Temperature dependent solubility of BTA **4** in water/isopropanol mixtures with varying compositions ranging from 0 to 40 wt.-% isopropanol.

### 3.5 Self-assembly under controlled conditions

After a suitable BTA and solvent self-assembly system was identified. A series of experiments under controlled conditions using the experimental setup discussed before was conducted. The relevant experimental details on all performed investigations are described in this section.

#### *Implementation of self-assembly experiments from solution under controlled conditions*

The experimental setup described in section 3.2 was utilized to investigate the thermal controlled self-assembly of *N,N',N''*-tris(1-methoxybutan-2-yl)benzene-1,3,5-tricarboxamide (BTA **4**) from solution. First, BTA **4** was suspended in a water/isopropanol mixture (80:20) at a concentration of 0.05 wt.-% featuring a total mass of 200 g. The obtained mixture was then filled into the glass vessel and heated to 70 °C under constant stirring until a clear solution was obtained. The custom-made cap kept the vessel sealed to avoid evaporation of the solvent. Subsequently, the vessel was quickly removed from the water heating bath and placed into the cooling bath of the cryostat. The selected cooling agent was a mixture of ethylene glycol and water (1:1). The temperature of the cooling bath was kept constant during one experiment. All samples remained in the cooling bath for 2 h at a constant stirring velocity. Experiments were performed with cooling bath temperatures ranging from -15 °C to 25 °C and mechanical stirring velocities between 0 and 450 rpm. The vessel was then removed from the cooling bath and allowed to warm to room temperature overnight. Due to the very low solubility at room temperature, the self-assembled BTA remained unchanged in the water/isopropanol mixture.

#### *Sample preparation for scanning electron microscopy*

In order to characterize the resulting supramolecular nanostructures by means of scanning electron microscopy (SEM), 2 mL of the obtained suspension were dropped on a clean glass object slide and dried at room temperature under ambient pressure. After complete removal of the solvent, a SEM sample holder equipped with adhesive and conductive foil was used to pick up the supramolecular nanostructures. **Figure 3.10** shows this sample preparation. Each sample was sputtered with platinum with a thickness of 2 nm.

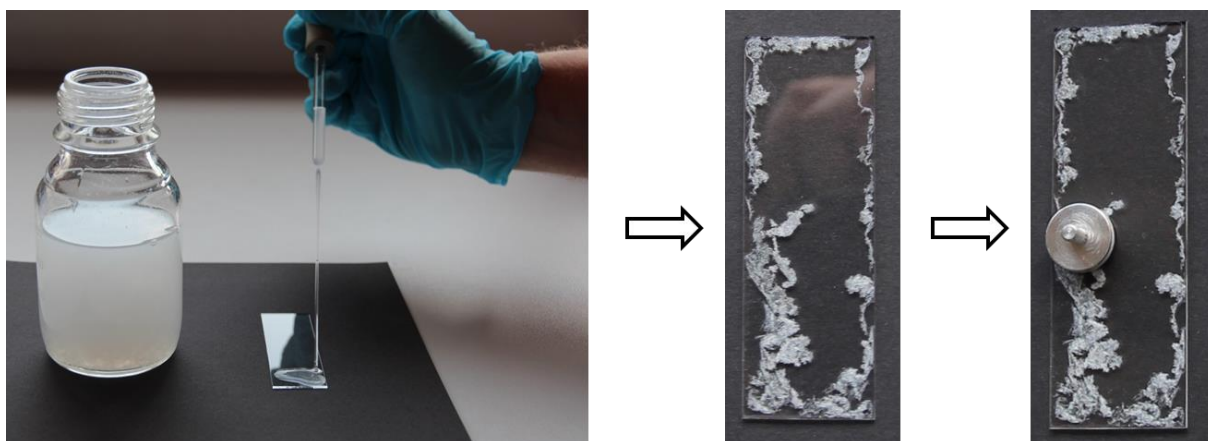


**Figure 3.10:** Sample preparation for SEM investigations of supramolecular nanostructures with a Pasteur pipette around 2 mL of the suspension were dropped on a glass object slide and dried at room temperature and ambient pressure. The nanostructures were collected via a SEM sample holder.

#### *Evaluation of SEM-images*

SEM investigations of prepared samples of supramolecular structures were performed on a Zeiss 1530 equipped with a field emission cathode. Images were taken utilizing a SE2 detector and an accelerating voltage of 2 kV. Images of each sample were recorded at different positions and different magnifications. Typically, SEM-images with a magnification of a factor of at least 5000 were used to determine the fiber diameters. A suitable software (Axiovision Release 4.8.3; Carl Zeiss) was utilized for the determination of fiber diameters of supramolecular nanofibers. **Figure 3.11** shows exemplarily a SEM image. The displayed fiber diameters show the fiber diameter determination assisted by the software. The fiber diameter distribution of a sample as well as the mean fiber diameter is based on at least 150 individual measured supramolecular fibers. Normalized histograms were generated with intervals of 100 nm. **Figure 3.12** shows exemplarily a fiber diameter histogram of supramolecular nanofibers of *N,N',N''*-tris(1-methoxybutan-2-yl)benzene-1,3,5-tricarboxamide (BTA **4**) prepared from a mixture of water/isopropanol (80:20) with a BTA-concentration of 0.05 wt.-%. The sample was mechanically stirred with a velocity of 300 rpm. The starting temperature was 70 °C and the applied cooling temperature was 5 °C.

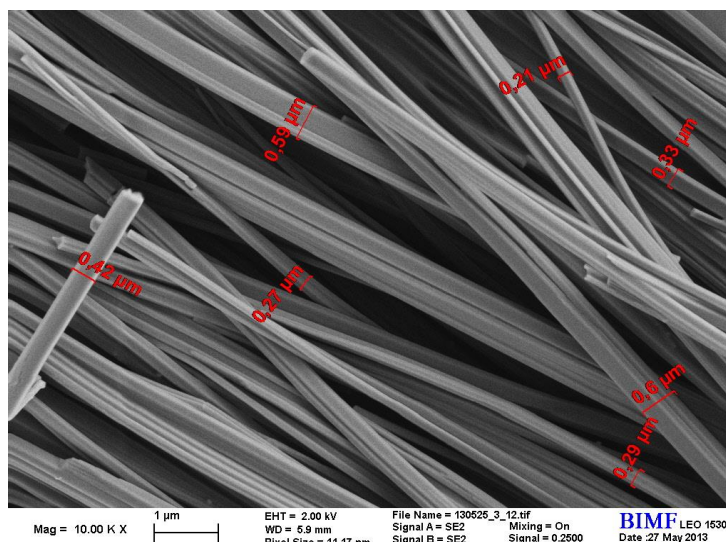


**Figure 3.11:** SEM-image of supramolecular nanofibers for the evaluation of the fiber-diameter. The determination of the fiber diameter utilizing a suitable software is exemplarily shown for three different fibers. The fibers of BTA **4** were prepared from a solvent mixture of water/isopropanol (80:20) with a concentration of 0.05 wt.-%. The temperature range was from 70 °C to 5 °C with a total mass of the sample of 200 g. The cooling agent was ethylene glycol/water (1:1). The mechanical stirring velocity was 300 rpm.

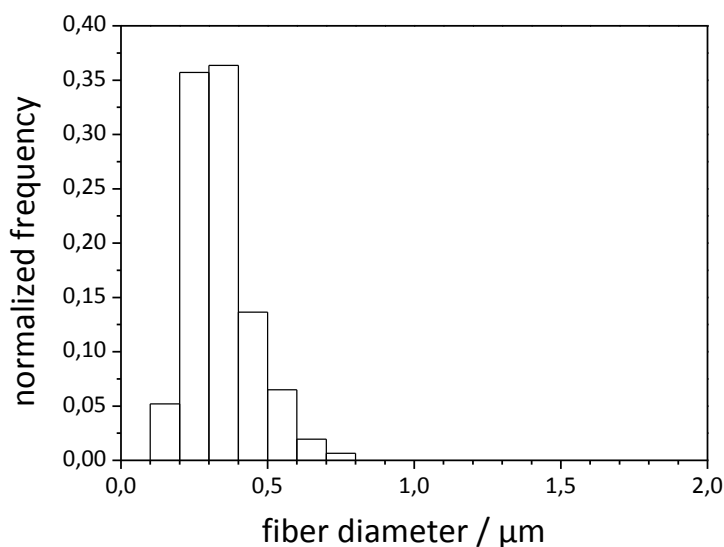


**Figure 3.12:** Exemplarily fiber diameter histogram of supramolecular nanofibers of BTA **4** prepared by utilization of the developed experimental setup. The fibers of BTA **4** were prepared from a solvent mixture of water/isopropanol (80:20) with a concentration of 0.05 wt.-%. The temperature range was from 70 °C to 5 °C with a total mass of the sample of 200 g. The cooling agent was ethylene glycol/water (1:1). The mechanical stirring velocity was 300 rpm. The histogram is based on fiber diameters of at least 150 individual supramolecular nanofibers.

### 3.6 Morphology of supramolecular fibers from different experiments under controlled conditions

The combination of BTA **4** and a mixture of water/isopropanol (80:20) with a concentration of 0.05 wt.-% was identified to be the most suitable system for the self-assembly experiments. Two experimental series were performed. The first series was conducted in a *temperature range from 70 °C to 5 °C with varying mechanical stirring velocities ranging from 0 rpm to a maximum of 450 rpm*, while the temperature profiles of these experiments were recorded. In the second experimental series, the applied *cooling temperature on the outside of the vessel was varied between 25 °C and –5 °C at a constant stirring velocity of 300 rpm*. The results concerning the morphology of the supramolecular fibers are based on SEM investigations will be presented in the following.

#### *Influence of stirring velocities on temperature profiles*

Even though the experiments are designed to enable self-assembly of a BTA in a given solvent just by a change in temperature and by application of different mechanical stirring velocities, a variety of parameters have to be additionally considered. Apart from the selected molecular structure of BTA **4** and the solvent system, parameters such as BTA concentration, temperature range, total mass of the sample, composition of the cooling agent, thickness of the wall of the vessel and the material can have an effect. These parameters may also indirectly influence the cooling process. Furthermore, one key parameter during the cooling process is given by the flow conditions inside the vessel and these conditions can be significantly influenced by changes in mechanical stirring velocity of the BTA solution. Therefore, temperature profiles during the cooling process were recorded at different stirring velocities ranging from 0 rpm up to a value of 450 rpm. The results displayed in **Figure 3.13** show that stirring the BTA solution inside the vessel yields a significant acceleration of the cooling process compared to the results corresponding to no mechanical stirring. If no stirring is applied to the system, the flow conditions inside the vessel are dominated by natural convection occurring due to local differences in density of the BTA solution. This variation exhibits the slowest cooling process compared to an ideally mixed system. The temperature profile recorded at a stirring velocity of 50 rpm already shows a strong acceleration. Further increase of the stirring velocity to a value of 150 rpm also results in faster cooling rates but the difference compared to the curve at 50 rpm is less distinct. Even less differences in the temperature profiles are observed between velocities of 150 rpm and 300 rpm, whereas the temperature profiles of at 300 rpm and 450 rpm are almost identical. These results can be explained by the correlation of flow conditions and the heat exchange from the inside of the glass to the cooling agent described by equation 3.5.

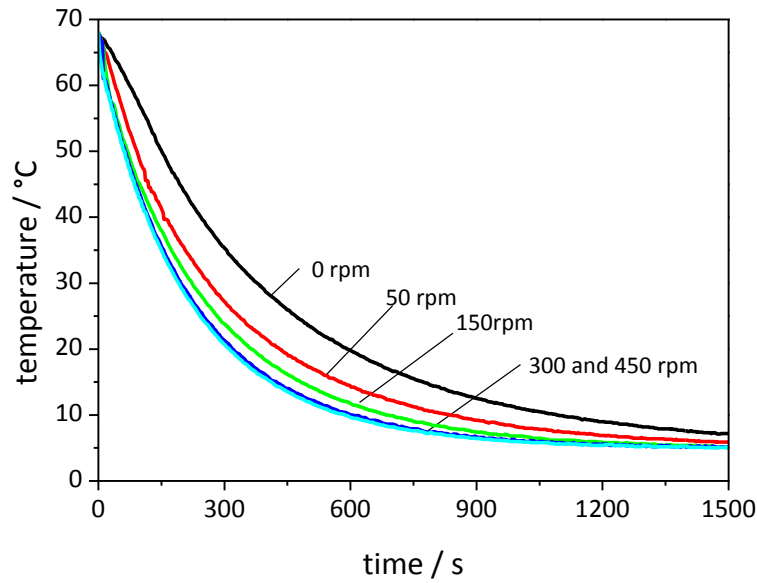


**Figure 3.13:** Exemplary temperature profiles during thermal induced self-assembly experiments with different stirring velocities ranging from 0 rpm to 450 rpm. *Preparation conditions* - Solvent: water/isopropanol (80:20); temperature range: 70 – 5 °C; BTA-concentration: 0.05 wt.-%; total mass of sample: 200 g; cooling time: 2 h; cooling agent: ethylene glycol/water (1:1).

By increasing the stirring velocity, the Reynolds number of the system is also increased corresponding to equation 3.9. In consequence, the value of the Nusselt number also rises as well as the value of  $\alpha_1$ . If the thermal conductivity  $\ddot{e}_1$  of the self-assembly system is assumed to be independent of the stirring velocity, the thickness of the boundary layer  $\delta_1$  close to the wall of the vessel is decreased. Evaluation of equation 3.5 shows that a decrease of  $\delta_1$  yields an increase of the amount of heat exchanged through the wall and results in an accelerated cooling process. However, by stirring the BTA solution, only flow conditions inside the vessel can be changed. If the thickness of the boundary layer  $\delta_1$  becomes very small, equation 3.5 may be reduced to equation 3.10.

$$\dot{Q} = \frac{A_w}{\frac{d}{\ddot{e}_{wall}} + \frac{\ddot{a}_2}{\ddot{e}_2}} \cdot (T_{inside} - T_{outside}) \quad \text{if:} \quad \frac{\ddot{a}_1}{\ddot{e}_1} \ll \frac{d}{\ddot{e}_{wall}} + \frac{\ddot{a}_2}{\ddot{e}_2} \quad (3.10)$$

At this point, the cooling process of the self-assembly system inside the vessel cannot be accelerated anymore because the thermal conductivity of the wall, the wall thickness, the thermal conductivity of the cooling agent and the thickness of the boundary layer on the outside of the vessel become rate-determining. In consequence, the stirring velocities exceeding a value of 150 rpm do not result in significant changes of the cooling process.

*Sample preparation*

The supramolecular BTA-fibers prepared under controlled conditions were dried and fixed on a SEM sample holder. **Figure 3.14** shows exemplarily an overview image of fibers obtained from a solution of BTA 4 in water/isopropanol (80:20) and a concentration of 0.05 wt.-%.

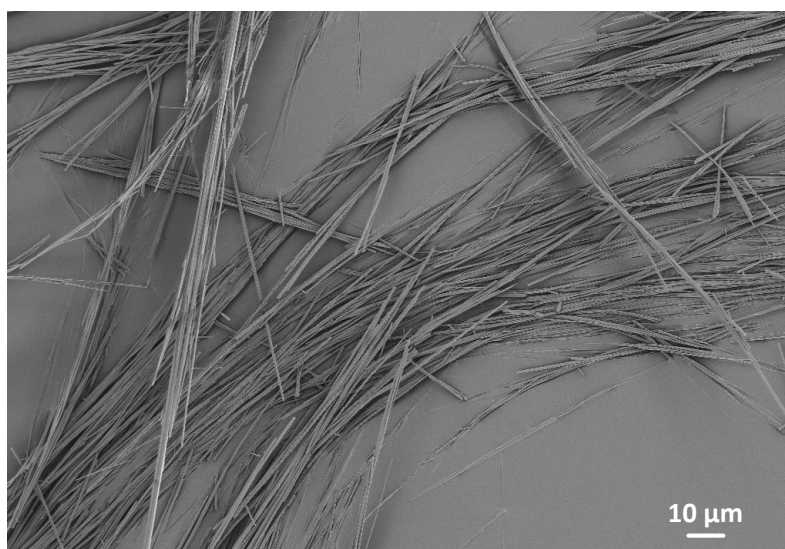


**Figure 3.14:** SEM-Image showing supramolecular fibers prepared by thermal induced self-assembly. *Preparation conditions* - Solvent: water/isopropanol (80:20); temperature range: 70 – 5 °C; BTA-concentration: 0.05 wt.-%; stirring velocity: 150 rpm; total mass of sample: 200 g; cooling time: 2 h; cooling agent: ethylene glycol/water (1:1).

The starting temperature for the cooling process was 70 °C and the cooling temperature applied on the outside of the vessel was 5 °C. The stirring velocity was 150 rpm and the total mass of the sample corresponded to a value of 200 g. While the morphology of most fibers appears to be rather like a straight line, many fibers are aligned parallel to each other. This alignment of the structures might result from the drying process during sample preparation for SEM analysis during which the fibers are pushed together. **Figure 3.15** displays a series of photographs taken of a suspension of BTA 4 in the water/isopropanol (80:20) mixture at different times during the drying process. Right after the suspension was placed on the object slide, the solid particles in the suspension appear mostly to be equally distributed throughout the solvent. As the drying process continues, the BTA starts to further aggregate. Upon complete solvent removal, the solid supramolecular structures mostly gather close to the edges of the object slide. It is assumed that the formation of larger aggregates as shown in **Figure 3.14** during the drying process corresponds to the alignment of individual fibers.

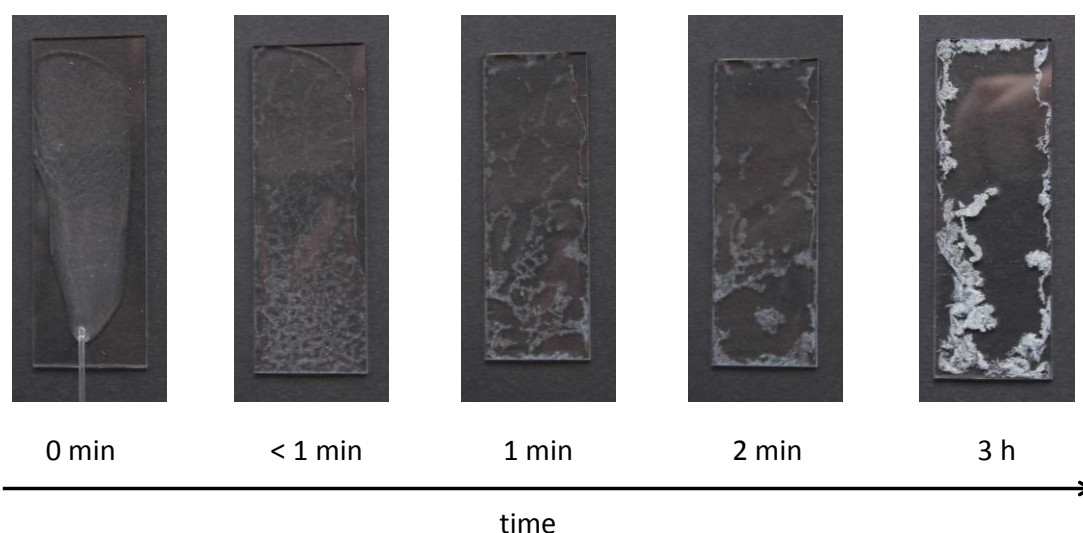


**Figure 3.15:** Series of photographs displaying drying of a suspension of supramolecular fibers in water/isopropanol (80:20) on a glass object slide. Over time, the supramolecular fibers aggregate during the drying process towards the edge of the object slide.

#### *Influence of stirring velocity on fiber morphology*

A series of different experiments was performed to prepare supramolecular fibers of BTA **4** from solution with different stirring velocities. Subsequently, suspensions containing the prepared fibers were dried and the morphology of the supramolecular fibers was investigated by SEM analysis. **Figure 3.16** displays exemplarily a series of SEM micrographs of BTA-fibers self-assembled at different mechanical stirring velocities during the cooling process. Apart from differences in stirring velocity, these fibers were prepared under identical conditions. The self-assembly process was performed in a temperature range between 70 °C and 5 °C. Fibers displayed on SEM micrographs in **Figure 3.16** already show a visible decrease in fiber diameters with increasing stirring velocity as evidenced by fiber diameter histograms. Each fiber diameter histogram was prepared in 100 nm intervals and is based on fiber diameters of at least 150 individual fibers. It was found that supramolecular fibers prepared without any mechanical treatment during the self-assembly process feature a very broad fiber diameter distribution. The corresponding mean fiber diameter of the presented sample was 1459 nm. However, the sample prepared with a stirring velocity of 50 rpm exhibits a mean fiber diameter of 617 nm and a narrower fiber diameter distribution compared to the corresponding sample at 0 rpm. Additional increase of mechanical stirring up to 300 rpm leads to a further decrease of fiber diameters and an even narrower fiber diameter distribution. The mean fiber diameter of the displayed sample corresponds to a value of 344 nm.

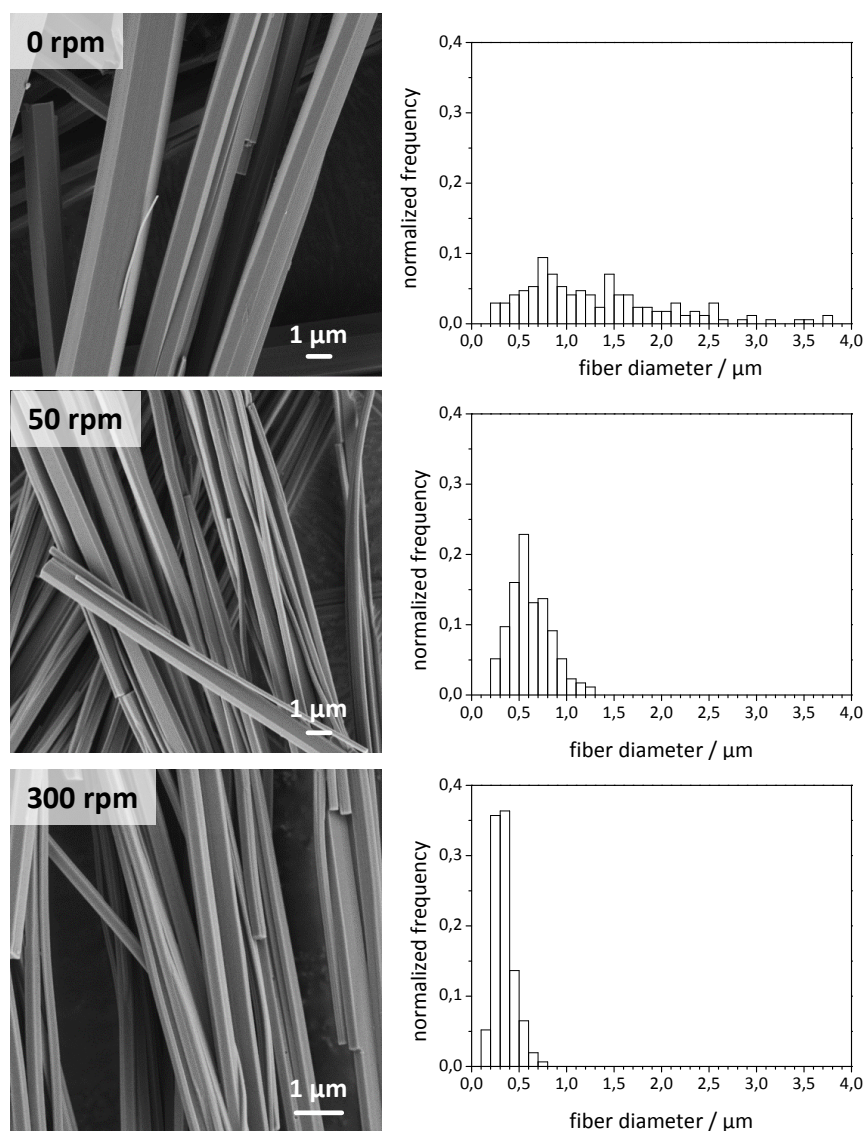


**Figure 3.16:** SEM micrographs of supramolecular nanofibers of BTA **4** prepared by thermal induced self-assembly and varying stirring velocities of 0 rpm, 50 rpm and 300 rpm. Corresponding fiber diameter histograms are based on at least 150 fibers. *Preparation conditions* - Solvent: water/isopropanol (80:20); temperature range: 70 – 5 °C; BTA-concentration: 0.05 wt.-%; total mass of sample: 200 g; cooling time: 2 h; cooling agent: ethylene glycol/water (1:1).

It has already been reported that the morphology of supramolecular fibers based on the self-assembly of a 1,3,5-benzenetrisamide with tert-butyl substituents in the periphery of the molecular structure can be significantly influenced by variations of linear temperature profiles.<sup>[113]</sup> These self-assembly experiments were performed with 2,2,4,4,6,8,8-heptamethylnonane as solvent at linear cooling rates of 10 and 60 K/min. It was found that faster cooling rates result in smaller fiber diameters. However, the changes in morphology of prepared supramolecular fibers in the current study may be attributed to an acceleration of the cooling process, due to differences of the flow conditions by application of mechanical forces to the system or to a combination of both influences.

Therefore, additional experiments were conducted with stirring velocities of 150 rpm and 450 rpm. To ensure the results to be reproducible, three individual experiments were performed for each set of conditions. **Figure 3.17** shows the values of mean fiber diameters of supramolecular fibers as a function of mechanical stirring velocity in the range from 0 to 450 rpm. Each displayed data point is the average of three experiments. The error bars correspond to the standard deviation of the three individual mean fiber diameters and do not reflect the distribution widths of the prepared fiber diameter histograms. The size of the error bars demonstrates the high reproducibility of the experiments under controlled conditions.

The largest decrease of the mean fiber diameters on the stirring velocity is observed from 0 to 150 rpm. For experiments at 300 and 450 rpm, no significant additional decrease in the mean fiber diameter was observed. As described earlier, it was found that only for stirring velocities in the range from 0 to 150 rpm, the cooling process of the self-assembly process is significantly accelerated. Beyond values of 150 rpm, only minor differences in the temperature profiles could be observed. Even though the stirring velocity was increased by a factor of three from 150 rpm to 450 rpm, no change in the morphology of the fibers was observed. These results clearly indicate that the resulting morphology of supramolecular fibers based on the self-assembly of BTA 4 from water/isopropanol mixtures is mainly dependent on the temperature profile during the cooling process. A possible influence of shearing forces on the morphology was not observed.

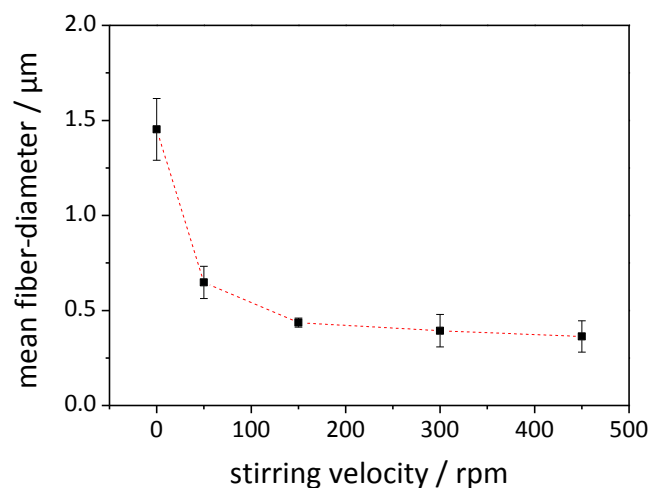


**Figure 3.17:** Influence of the stirring velocities on the resulting mean fiber diameters of supramolecular fibers of BTA 4. Each data point displayed is based on three independent experiments. The error bars represent the standard deviation of the three obtained mean fiber diameters. Each individual mean fiber diameter takes into account at least 150 fibers. *Preparation conditions* - Solvent: water/isopropanol (80:20); temperature range: 70 – 5 °C; BTA-concentration: 0.05 wt.-%; total mass of sample: 200 g; cooling time: 2 h; cooling agent: ethylene glycol/water (1:1).

*Influence of applied cooling temperature on fiber morphology*

A second experimental series was performed by variation of the applied cooling temperatures of the cooling agent on the outside of the glass, while the other experimental conditions were kept constant. A reduction of the cooling temperature leads to greater temperature differences and according to equation 3.5 to an increasing heat exchange. The influence of changes in the temperature profiles were verified by conducting experiments with varying cooling temperatures at constant flow conditions inside the vessel.

**Figure 3.18** shows exemplarily a series of three SEM micrographs of supramolecular BTA fibers prepared with different cooling temperatures. All other experimental conditions such as stirring velocity were kept constant. The SEM micrograph of the sample prepared in the temperature range from 70 °C to 25 °C exhibits thick fibers with diameters in the micrometer range. The corresponding fiber diameter histogram shows a very broad fiber diameter distribution with a mean fiber diameter of 1013 nm. By decreasing the temperature of the cooling agent to a value of 15 °C and therefore increasing the heat exchange, the mean fiber diameter equals to 544 nm and the fiber diameter distribution becomes less broad. The SEM image at the bottom of **Figure 3.18** shows supramolecular fibers of a sample prepared at a cooling temperature of 5 °C and the corresponding histogram features the narrowest fiber diameter distribution with an average of 344 nm. In addition, a series of three independent experiments was performed for each set of experimental parameters for cooling temperatures of 25, 15, 5 and -5 °C.

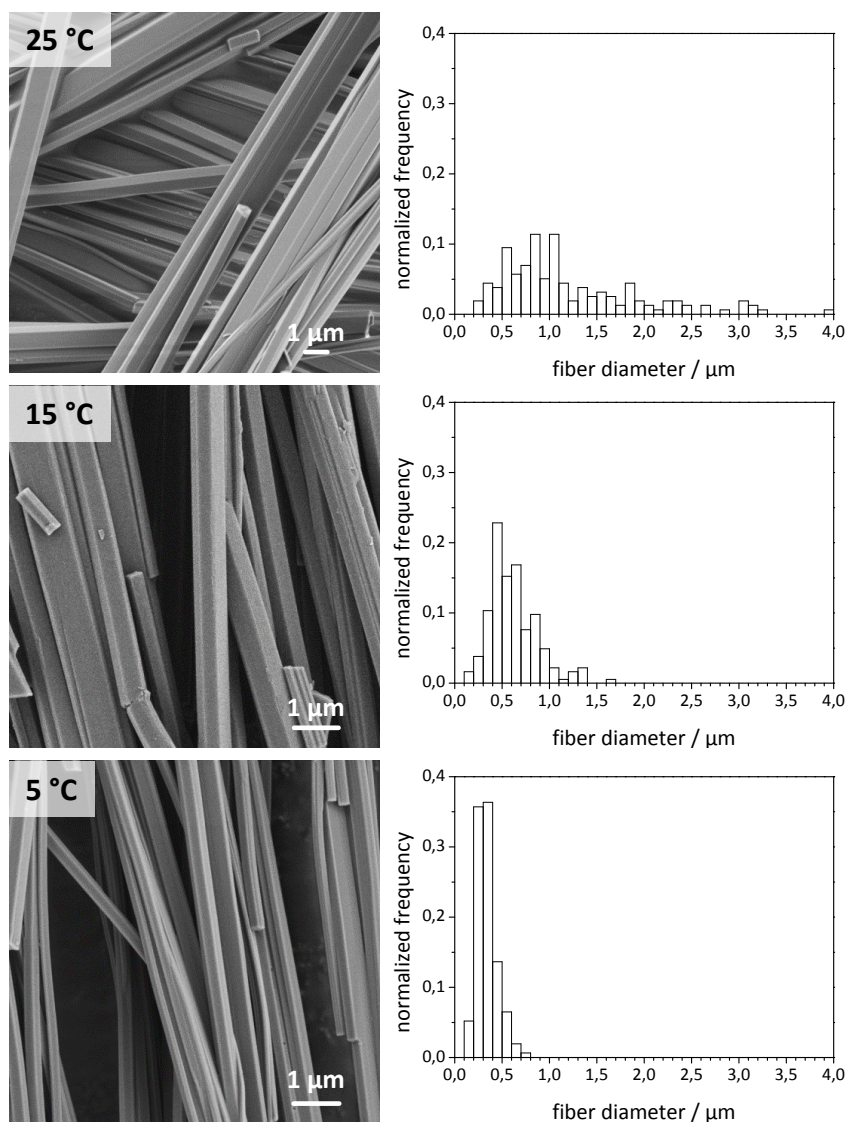


**Figure 3.18:** SEM micrographs of supramolecular nanofibers of BTA **4** prepared by thermal induced self-assembly and varying cooling temperatures of 25 °C, 15 °C and 5 °C. Corresponding fiber diameter histograms are based on at least 150 fibers. *Preparation conditions* - Solvent: water/isopropanol (80:20); stirring velocity 300 rpm; BTA-concentration: 0.05 wt.-%; total mass of sample: 200 g; cooling time: 2 h; cooling agent: ethylene glycol/water (1:1).

**Figure 3.19** shows the obtained mean fiber diameters as a function of the applied cooling temperature. Each displayed data point is based on three individual experiments. The error bars correspond to the standard deviation of the three individual mean fiber diameters and do not reflect the distribution widths of the prepared fiber diameter histograms. The results clearly show that apart from changes in mechanical conditions, changing the applied cooling temperature has a strong impact on the resulting morphology of supramolecular fibers of BTA **4**.

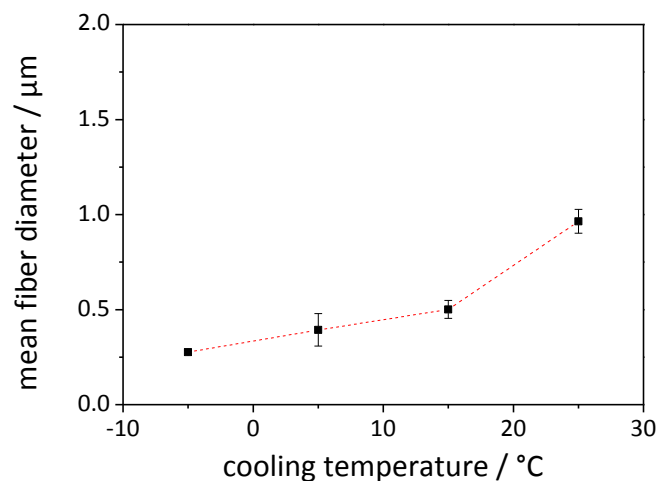


**Figure 3.19:** Influence of the applied cooling temperature on the resulting mean fiber diameters of supramolecular fibers of BTA 4. Each data point (error bars represent the standard deviation) displayed is based on three independent experiments. Each individual mean fiber diameter takes into account at least 150 fibers. *Preparation conditions* - Solvent: water/isopropanol (80:20); stirring velocity: 300 rpm; BTA-concentration: 0.05 wt.-%; total mass of sample: 200 g; cooling time: 2 h; cooling agent: ethylene glycol/water (1:1).

### 3.7 Conclusion

The work described in this chapter focused on the development of an experiment under controlled conditions to investigate the formation of supramolecular fibers based on 1,3,5-benzenetrisamides via self-assembly from solution upon changes in temperature and the impact of the variation of mechanical stirring velocities during the process. Screening experiments on a series of five alkoxy-substituted 1,3,5-benzenetrisamides revealed that the combination of BTA 4 and a solvent mixture of isopropanol and water (80:20) at a concentration of 0.05 wt.-% was the most suitable system for the developed experimental setup.

Two series of experiments under controlled conditions were performed and the results were found to be highly reproducible. In the course of the first experimental series upon variations in mechanical stirring, the morphology of obtained supramolecular fibers was strongly influenced. However, these influences only correlate to changes in the cooling process. Once no increase of the cooling performance was achieved by increasing the stirring velocity, the morphology of BTA fibers did not change further. Therefore, an influence of mechanical forces during the self-assembly process was not observed. In the second experimental series, the cooling temperature outside the vessel was varied and confirmed that an increased cooling performance leads to smaller fiber diameters and that the self-assembly process is strongly dependent on the cooling conditions.



## 4 Supramolecular nanofibers for air filtration applications

### 4.1 Introduction

#### *Fine particulate air-pollution*

Air-pollution has been recognized as a major risk factor for human health.<sup>[102]</sup> An air pollutant is defined as a substance that is released into the environment and exhibits the potential to harm humans as well as animals and vegetation. These pollutants can be divided into four different categories such as particulate matter, heavy metals (e.g. mercury), persistent organic compounds (e.g. dioxins) and gaseous pollutants (e.g. sulphur dioxide).<sup>[131]</sup> In particular, the exposure to ambient particulate matter has been identified to cause adverse effects to human health. Particulate matter comprises of a complex mixture of solid and liquid particles suspended in atmospheric air. However, for health related issues, particulate matter is usually subdivided into two main categories: Particulate matter with particles featuring diameters below 10  $\mu\text{m}$  ( $\text{PM}_{10}$ ) and fine particulate matter with diameters of less than 2.5  $\mu\text{m}$  ( $\text{PM}_{2.5}$ ).<sup>[132–134]</sup> Various emission sources contribute to air-pollution by particulate matter and are either based on natural sources<sup>[135]</sup> or on anthropogenic sources such as industrial processes (e.g. energy production, mining).<sup>[132]</sup> Apart from commonly known exhaust emissions of road traffic, vehicle use can even contribute to particulate matter emissions by resuspension of road dust which arises for example from wearing of brakes, tires and pavement.<sup>[136]</sup> In ambient air suspended particulate matter is inhalable and associated with serious health effects to the human body such as lung cancer, low birth weight and reduced life expectancy.<sup>[137–139]</sup> For instance, it was found that especially fine particulate matter exhibits more negative effects compared to larger particles like increased mutagenic activity<sup>[140,141]</sup> In 2010, 3.2 million human deaths were attributed to the exposure to fine particulate matter ( $\text{PM}_{2.5}$ ), whereas HIV-AIDS was considered to cause death of 1.5 million people. Even Malaria was accounted “only” for the death of 1.2 million people demonstrating that particulate matter really is a serious threat to human health.<sup>[142,143]</sup> In consequence, new approaches have to be developed to control the exposure of particulate matter including the design of novel filtration systems for the efficient removal of such small particles from ambient air.

### *Preparation of nanofibers for filtration applications*

In general, a vast number of different air filtration systems exist to separate solid and liquid particles from a gas. These systems are utilized in a variety of applications including air conditioning systems of living and office spaces, purification of the air intake of engines in automobiles, avoidance of air pollutants to enter vehicle cabins, respirators and vacuum cleaners.<sup>[1,3]</sup> For a specific application, a suitable filter medium has to be selected depending for example on the size of particles that have to be removed or the conditions of the filtration process such as the flow velocity of the fluid. Mostly in air filtration, the high efficiency removal of solid particles with diameters in the micrometer range is achieved by the use of fibrous filter media.<sup>[99]</sup> One example for frequently used systems in air filtration are nonwoven filter media, which are defined as porous fabrics comprised of fibers or filaments that are randomly arrayed and capable of removing solid or liquid particles from a gas stream.<sup>[3]</sup> Thereby, many research effort is put on the utilization of nanofibers, because of their highly beneficial surface to volume ratio compared to microfibers resulting in an increased probability of particle deposition on the surface of the fibers.<sup>[20,96,99]</sup> Typically, nanofibers are based on polymer materials and are fabricated via top-down processes such as electrospinning, melt blowing or centrifugal spinning.<sup>[2,6,25,105]</sup> Many studies have been conducted to evaluate the suitability of such fibers for air filtration applications. For instance, Qin et al. reported on the preparation of nanofibers of polyvinyl alcohol via electrospinning on top of a melt-blown polypropylene support and subsequent testing to remove uniform NaCl particles with diameters of 600 nm from an air stream.<sup>[13]</sup> Furthermore, it was demonstrated that electrospinning of various polyamides results in filter media capable of removing such small particles from air.<sup>[14,104]</sup> Apart from classical polymers, electrospinning of recombinant spider silk protein on top of a polymer support can be utilized to improve the filtration efficiency of existing filters to remove liquid droplets from air streams. Experiments were performed using different support materials such as polypropylene, polyamide and polyester.<sup>[144]</sup> Cho et al. demonstrated the improvement of cellulose filters by electrospun fibers incorporating titanium dioxide nanoparticles.<sup>[103]</sup> Apart from electrospinning, melt-blown fibers of polypropylene were investigated by means of air filtration efficiency of small particles and have proven to be suitable for air filtration applications.<sup>[20–22]</sup> Usually, the rate of production of the previously mentioned fabrication methods is significantly reduced with decreasing fiber diameters down to the nanometer range.

In contrast to previously described top-down approaches, supramolecular chemistry provides a bottom-up approach for the preparation of fibrous structures via self-assembly of small molecules.<sup>[26,110–112]</sup> One system based on this bottom-up approach was utilized for liquid filtration applications, demonstrating that supramolecular fibrous structures exhibit potential to be used as

filter media.<sup>[145–147]</sup> However, so far, little is known about the applicability of supramolecular fibers for air filtration applications. The formation of such structures is driven by secondary interactions such as hydrogen bonding,  $\pi$ - $\pi$ -stacking or metal ligand coordination. One intensively studied self-assembly motif that is capable of forming supramolecular nanofibers with diameters in the nanometer range is based on 1,3,5-benzenetrisamides (BTAs).<sup>[49,51,52,56]</sup> These compounds can form supramolecular columns by formation of directed threefold hydrogen bonds of the amide moieties.<sup>[60,65,66]</sup>

Recently it was demonstrated for the first time that supramolecular nanofibers based on a 1,3,5-benzenetrisamide can be employed in a nonwoven support to form a stable nanofiber-microfiber composite that can potentially be utilized in air filtration applications.<sup>[88,89]</sup>

The basic concept of this *in situ* preparation process is displayed in **Figure 4.1**. First, the BTA is fully dissolved at elevated temperatures in a suitable solvent to yield a clear solution with a defined concentration. A nonwoven scaffold is immersed into the solution until it is fully soaked (**Figure 4.1 A**). Subsequently, the nonwoven is removed from the solution resulting in a combination of cooling and drying of the soaked nonwoven (**Figure 4.1 B**). During this process, self-assembly of the BTA starts and supramolecular nanofibers inside the nonwoven scaffold are formed *in situ* connecting the individual microfibers of the support structure. Complete removal of the solvent yields a mechanically stable composite (**Figure 4.1 C**).

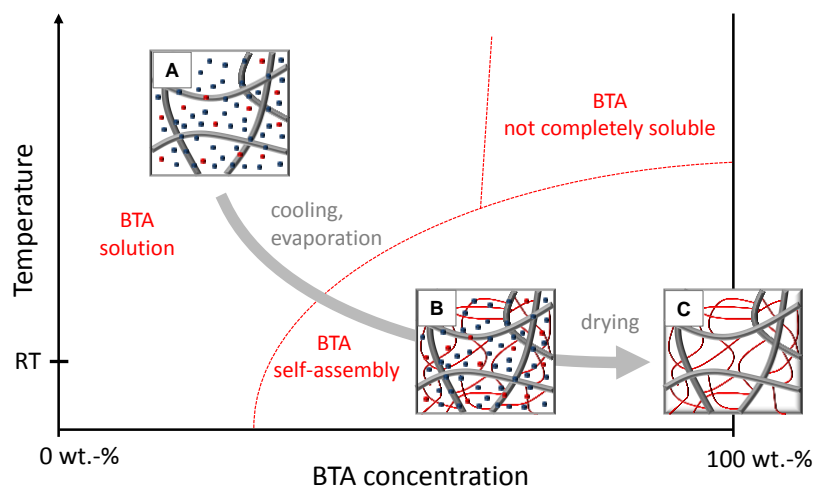


**Figure 4.1:** Schematic representation of the *in situ* preparation process of supramolecular nanofiber-microfiber composites (nonwoven scaffold: grey fibers; solvent: blue dots; dissolved 1,3,5-benzenetrisamide: red dots; supramolecular nanofibers: red fibers). The nonwoven microfiber scaffold is immersed into a 1,3,5-benzenetrisamide solution (A) at elevated temperatures and removed. During cooling and simultaneous solvent evaporation, self-assembly occurs and supramolecular nanofibers are formed within the nonwoven microfiber scaffold (B). Complete solvent evaporation yields the nanofiber-microfiber composite (C).

This bottom-up approach allows for the *in situ* preparation of fibers inside a support structure. In contrast, nanofibers prepared from top-down processes such as electrospinning are usually deposited on top of a support structure.<sup>[4,13,14,104,144]</sup> Typically, these processes do not allow to fully penetrate a porous support such as a nonwoven.

This chapter focuses on further investigations of nanofiber-microfiber composites containing supramolecular nanofibers based on 1,3,5-benzenetrisamides. This work is based on previous investigations by Misslitz and provides a deeper understanding of the preparation process.<sup>[88,89]</sup> Partially, previous experiments were repeated to ensure comparable results. **Figure 4.2** shows the chemical structure of investigated 1,3,5-benzenetrisamides. BTA **4** contains a methoxy group in the periphery of the molecular structure, while BTAs **6**, **7** and **8** exhibit branched alkyl substituents of different lengths. BTAs **6** and **7** are constitutional isomers.

This chapter is divided in two sections. The first section (4.3.1) describes experiments performed with BTAs **6**, **7** and **8** and focuses on the preparation of nanofiber-microfiber composites from solutions with different BTA concentrations as well as from different processing solvents such as 2-butanone, isopropanol and ethanol. A viscose/polyester model nonwoven was used for the preparation of these composites. In addition, temperature dependent turbidity measurements provide insight into the solubility and self-assembly behavior of these three BTAs in each of the solvents. Infrared spectroscopic investigations were performed to evaluate the formation of supramolecular columns by directed threefold hydrogen bonds. Capillary Flow Porometry of selected composite was used to evaluate the resulting pore-size distributions of the nanofiber-microfiber composites.

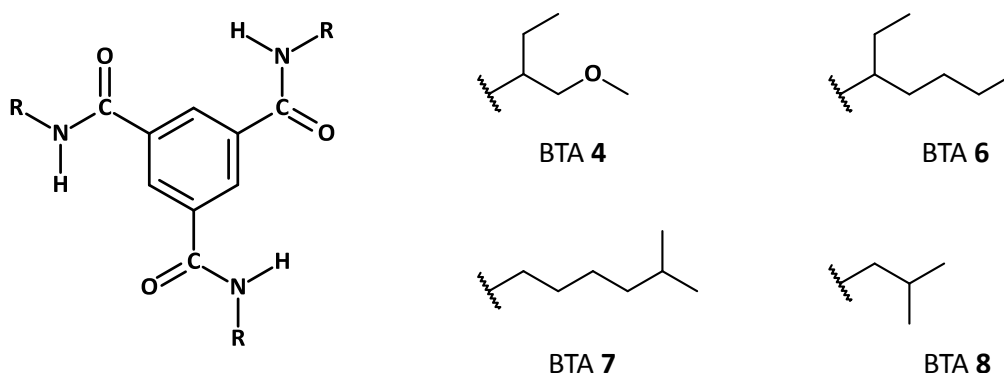


**Figure 4.2:** Chemical structures of 1,3,5-benzenetrisamides **4**, **6**, **7** and **8** with different peripheral substituents.

The second part of this chapter (4.3.2) focuses on the preparation of nanofiber-microfiber composites containing supramolecular nanofibers of BTA **4**. A solvent mixture of water and isopropanol (60:40) was selected as processing solvent. In contrast to the first part of this chapter, the selected nonwoven scaffold was a technical polyester nonwoven featuring microfibers with larger diameters and an increased overall thickness. Concentration dependent experiments to prepare nanofiber-microfiber composites with different nanofiber contents were performed and the resulting composites were tested in air filtration experiments.

## 4.2 Experimental

Many of the experimental details are applicable to both sections (4.3.1 and 4.3.2) such as the basic procedure for the preparation of nanofiber-microfiber composites containing supramolecular nanofibers based on 1,3,5-benzenetrisamides as well as the evaluation of the composites by means of filtration efficiency to remove particulate matter from air. Therefore, the experimental part of this chapter covers the experimental work performed for both sections. All materials used and the experimental details on the preparation and characterization of nanofiber-microfiber composites are described in the following.

### Materials

The synthesis and characterization of the selected 1,3,5-benzenetrisamides is described in detail in the appendix. BTAs utilized for the preparation of nanofiber-microfiber composites were *N,N,N''*-tris(1-methoxybutan-2-yl)benzene-1,3,5-tricarboxamide (BTA **4**), *N,N,N''*-tris(2-ethylhexyl)benzene-1,3,5-tricarboxamide (BTA **6**), *N,N,N''*-tris(6-methylheptyl)benzene-1,3,5-tricarboxamide (BTA **7**) and *N,N,N''*-tris(3-methylbutyl)benzene-1,3,5-tricarboxamide (BTA **8**) All solvents were commercially available from Aldrich and used without further purification.

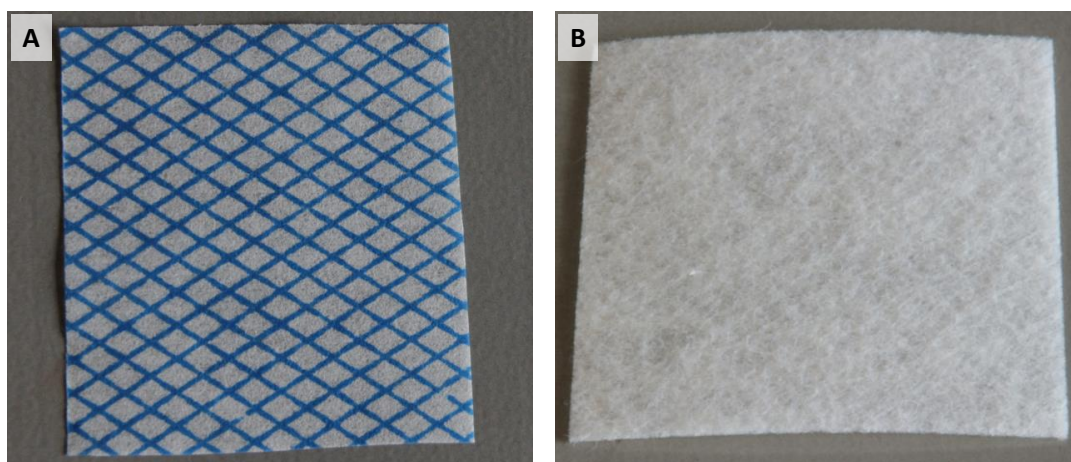


**Figure 4.3:** Selected nonwoven scaffolds for the preparation of composites containing supramolecular nanofibers. A viscose/polyester nonwoven with a thickness of 0.15 mm and a basis weight of 32.2 g/m<sup>2</sup> (A). Polyester nonwoven with a thickness between 2 and 2.6 mm and a basis weight of 120 g/m<sup>2</sup> (B).

For the preparation of nanofiber-microfiber composites two different nonwoven scaffolds were utilized. **Figure 4.3** shows photographic images of the selected nonwovens. A microfiber viscose/polyester nonwoven (see **Figure 4.3 A**) was used for the preparation of nanofiber-microfiber composites with 1,3,5-benzenetrisamides featuring different alkyl substituents in the periphery. This

nonwoven was commercially available with a basis weight of 32.2 g/m<sup>2</sup> and a thickness of 0.15 mm (AmPri). Results of experiments performed using this nonwoven are described in section 4.3.1. **Figure 4.4** shows a SEM micrograph displaying the morphology of this selected nonwoven scaffold. The average fiber diameter of the microfibers was 13 μm. Consolidation of this nonwoven was achieved by a binder that forms layers partially connecting the individual microfibers.

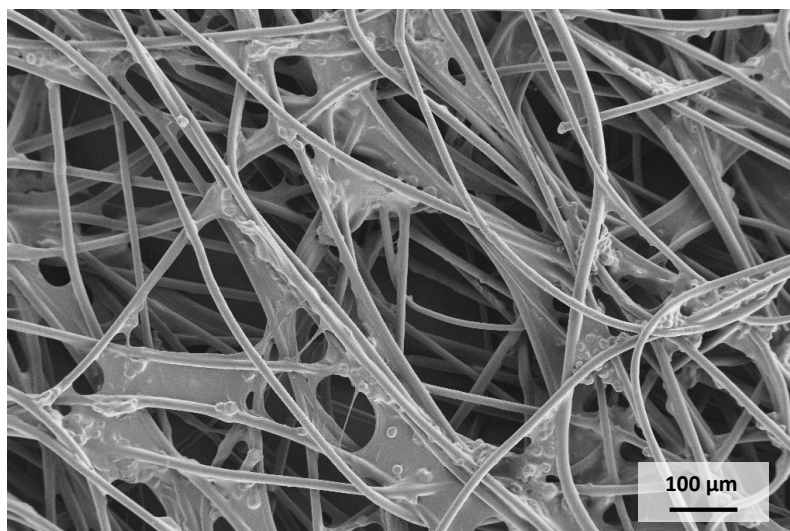


**Figure 4.4:** Overview SEM micrograph of the selected viscose/polyester nonwoven for the preparation of nanofiber-microfiber composites.

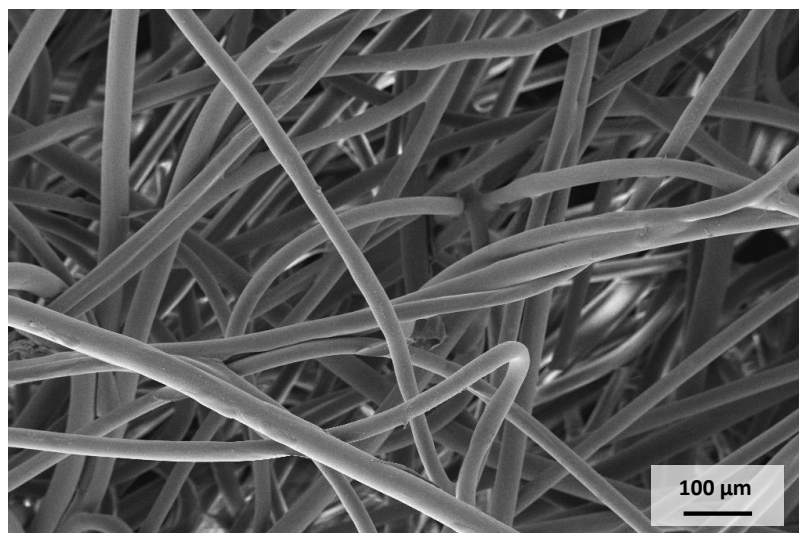


**Figure 4.5:** Overview SEM micrograph of the selected technical polyester nonwoven for the preparation of nanofiber-microfiber composites.

A second technical nonwoven (see **Figure 4.3 B**) was selected for the preparation of nanofiber-microfiber composites from a water/isopropanol mixture (60:40) with a 1,3,5-benzenetrisamide with an alkoxy substituent in the periphery of the molecular structure. This nonwoven featured thicknesses

between 2 and 2.6 mm and a basis weight corresponding to a value of 120 g/m<sup>2</sup>. Results obtained by using this nonwoven are presented in section 4.3.2. **Figure 4.5** shows a SEM micrograph of the microfiber morphology with fiber diameters between 25 and 30 μm. The nonwoven was mechanically and thermally bonded to ensure consolidation.

### *Preparation of nanofiber-microfiber composites*

First, a solution of the selected BTA in a given solvent and with a defined concentration was prepared at elevated temperatures. Results presented in section 4.3.1 are based on experiments utilizing solutions of BTAs **6**, **7** and **8** in 2-butanone, isopropanol and ethanol, respectively. Clear BTA solutions with concentrations between 0.6 and 1.0 wt.-% were prepared at a temperature of 50 °C.

Each individual solutions was filled into a custom-made immersion bath with a volume of about 200 mL and kept at the corresponding elevated temperature. The immersion bath was placed in a thermostat to ensure temperature control. Besides, it was sealable to avoid solvent evaporation and thereby changes in concentration of the 1,3,5-benzenetrisamide.

**Figure 4.6** illustrates the four step preparation process of the composites exemplarily utilizing the viscose/polyester nonwoven used for experiments presented in section 4.3.1. First, a nonwoven was fixed in a holding frame featuring an open area of 8.5 cm x 8.5 cm (see **Figure 4.6 A**). Subsequently, the fixed nonwoven was then vertically immersed into the prepared immersion bath containing the hot BTA solution (see **Figure 4.6 B**). To ensure complete soaking of the nonwoven scaffold, it was kept inside the immersion solution for 30 s. To avoid evaporation of the solvent during the preparation process, the immersion bath was sealable by the supporting frame. (see **Figure 4.6 C**). The frame containing the soaked nonwoven was removed from the solution and placed in a horizontal position. The samples were dried at ambient conditions for at least 30 min (see **Figure 4.6 D**). After complete removal of the solvent nanofiber-microfiber composites were obtained. Due to the solvent uptake of the nonwovens, the filling level of the immersion bath decreased after each prepared sample. Therefore, the BTA solution was replaced with 200 mL of a freshly prepared solution after a maximum of 6 individual samples.

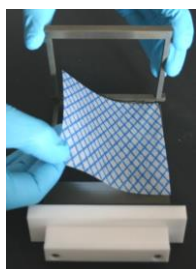
For filtration applications, a homogenous distribution of supramolecular nanofibers throughout the entire nonwoven is essential. Therefore, nonwoven scaffolds had to be fixed evenly in the supporting frame during the drying process. If the position of the sample in the supporting frame was shifted during the immersion process, the corresponding sample was discarded. During the drying process,

the nonwoven had no contact to any other object or surface, besides the supporting frame, to prevent dewetting.

Work performed in section 4.3.2 was based on the preparation of composites containing supramolecular nanofibers of BTA **4** from a solvent mixture of water/isopropanol (60:40). Corresponding BTA solutions were heated to 75 °C with concentrations of 0.2, 0.4, 0.6, 0.8 and 1.0 wt.-%, respectively.

### A: Mounting of nonwoven scaffold in metal frame

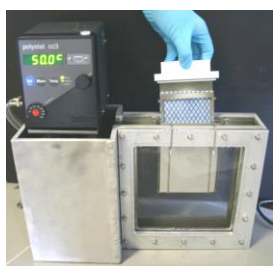
---



- Dimensions of nonwoven: 9.5 x 9.5 cm
- Accessible area in frame: 8.5 x 8.5 cm
- Nonwoven was fixed on the edges of metal frame

### B: Immersion of nonwoven in BTA solution

---



- BTA solution was filled in immersion bath and kept at elevated temperatures
- Vertical immersion of metal frame and nonwoven into BTA solution

### C: Complete soaking of nonwoven by BTA solution

---



- Immersion of the nonwoven for 30 s
- To avoid solvent evaporation, immersion bath was sealable by handle of metal frame

### D: Drying process

---



- Drying of nonwovens at ambient conditions in horizontal position
- Drying time dependent on utilized solvents

**Figure 4.6:** Series of photographs displaying the experimental process for the *in situ* preparation of nanofiber-microfiber composites. The selected nonwoven scaffold (9.5 x 9.5 cm) is placed in a supporting frame (A). The mounted nonwoven support was immersed vertically into a BTA solution at elevated temperatures (B). The nonwoven was kept in the BTA solution for 30 s to ensure that the scaffold is fully soaked (C). Drying at ambient conditions yielded nanofiber-microfiber composites (D).

---

### *Sample preparation for SEM investigations*

For SEM investigations, a piece of a prepared composite of about 1 cm x 1 cm was fixed via double-sided adhesive conductive tape on a SEM sample holder and sputtered with carbon. The sputtering process was performed utilizing a MED 010 (Balzers Union) sputter coater. SEM micrographs were recorded by utilization of a Zeiss 1530 FESEM. The applied acceleration voltage was 2 kV and images were taken with a SE2 detector. As described in detail in the previous chapter (see section 3.3), images were taken at different positions of each sample. By utilization of a suitable software (Axiovision Release 4.8.3; Carl Zeiss), the fiber diameters of at least 150 individual fibers were determined. Based on the recorded data, fiber diameter histograms were prepared in intervals of 100 nm.

### *Determination of supramolecular fiber content*

The content of supramolecular nanofibers inside the prepared composites was determined gravimetrically. Therefore, the initial mass of the nonwoven support before the preparation process was measured and subsequently, the dried composite obtained by the preparation process was weighed. Considering these two values, the supramolecular nanofiber content can be calculated. In order to consider possible mass losses of the nonwoven support, experiments were performed without any 1,3,5-benzenetrisamide present in the solvents accordingly to the described process to prepare nanofiber-microfiber composites. Calculated BTA-fiber contents took these results into account.

### *Air filtration test rig setup*

Prepared nanofiber-microfiber composites were evaluated by means of filtration efficiency of particulate matter from air. The corresponding air filtration tests were conducted by utilization of a suitable air filtration test rig (MFP 2000, PALAS GmbH). This modular test system allows for the determination of the efficiency of flat filter media to remove particles depending on their size from an air stream. **Figure 4.7** displays schematically the experimental setup of the utilized test rig. Filtration performance of a filter can be investigated by applying varying aerosols. Therefore, different aerosol generators capable of suspending particles with a defined particle size distribution and at a constant concentration depending on the desired test conditions can be equipped to the test system. Experiments performed focused on the use of the generation of a solid fine test dust from Powder Technology Inc. (Iso 12103-1, A2). The main part of these test particles exhibited sizes in the range from 0.2 to 2  $\mu\text{m}$ . An initial volumetric air flow was fed into the aerosol generator (RBG 1000, PALAS GmbH). A cylindrical reservoir of the selected generator was filled with the selected test particles.

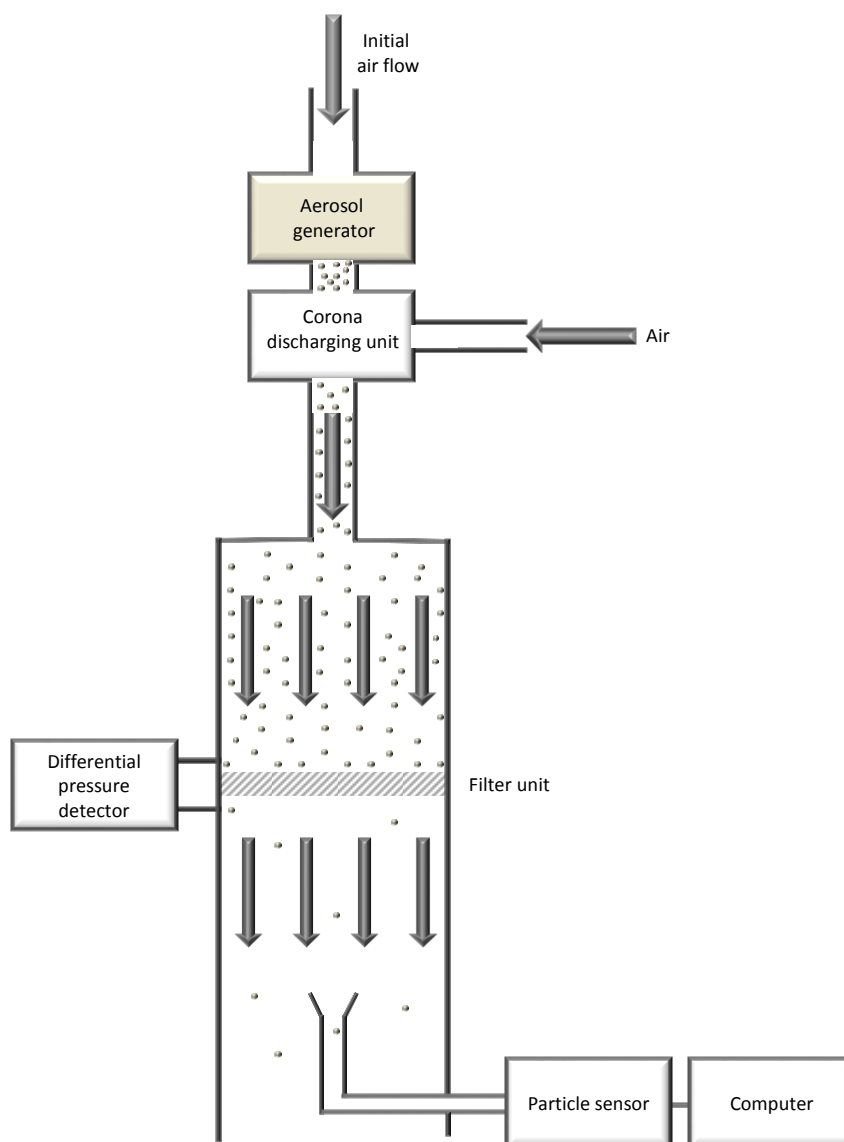


**Figure 4.7:** Schematic representation of the filter test rig utilized to test the filter performance of prepared nanofiber-microfiber composites to remove particulate matter from air. An aerosol generator was used to feed an aerosol of fine dust particles into an initial air flow. This aerosol was diluted by additional air, treated by a corona discharging unit to remove electrical charges from the dust particles and applied to a filter. A particle sensor in combination with a computer enabled monitoring of remaining particles in the air stream after the filtration process.

These particles were continuously suspended in small amounts in the initial air flow by a rotating brush. Subsequently, the initial air stream was combined with an additional volumetric air flow allowing for precise control of the particle concentration in the air stream that is applied to the filter. Due to the mechanical treatment of the suspended particles by the rotating brush, each individual particle exhibited an electrical charge on the surface, which may have influenced significantly the filtration efficiency of a tested filter. Therefore, the aerosol passed through a corona discharging unit (CD 2000, PALAS GmbH) to minimize electrical charges on the surface. After the discharging process, the aerosol

was fed into an air channel, which allowed for insertion of a flat filter medium. The circular filter area was around 28.3 cm<sup>2</sup>. Before and after the filter, pressure detectors were installed to monitor the differential pressure during the filtration process. After the aerosol passed through the channel, a representative sample of the air was collected and analyzed by a suitable light scattering detector (welas digital 2100, PALAS GmbH, detection range: 0.2 μm – 10 μm). The detector was capable of measuring the particle size distributions and the particle concentration in the air stream. A computer was used to control and monitor important parameters during a measurement such as the volumetric air flow and in consequence the linear flow velocity applied to the filter.

In addition, the measuring time was precisely controlled as well as the amount of particles generated by the aerosol generator. Acquired data of a filtration experiment were the amounts of particles counted depending on the size and the differential pressure before and after the measurement. Based on measurements performed with and without a filter, particle size dependent filtration efficiencies were accessible. Tested filter media had to be inserted manually into the air channel by opening the channel for a short period of time.

### *Implementation of filtration tests*

Prepared composites were tested by utilization of the previously described air filtration test rig. First, operation conditions of the test rig had to be adjusted. The volumetric flow rate was around 42.5 L/min and considering the size of the diameter of the air channel, the resulting linear flow velocity was approximately 25 cm/s. The particle concentration was around 30000 particles/cm<sup>3</sup>. Once constant operating parameters were reached, the amount of particles and the corresponding particle size distribution in the gas stream was measured for 30 s without any filter inserted in the test rig. This measurement served as reference. Subsequently, a filter was placed manually in the air filtration test rig and the aerosol was applied to the filter for 30 s at identical conditions. Remaining particles in the air stream after the filtration process were quantified by the detector. The differential pressure was recorded at the beginning and at the end of the measurement.

### *Turbidity measurements*

The solubility and self-assembly behavior of the selected 1,3,5-benzenetrisamides in different solvents was investigated by means of temperature dependent turbidity measurements. Therefore, BTA solutions in a given solvent with a concentration of 1.0 wt.-% were prepared.

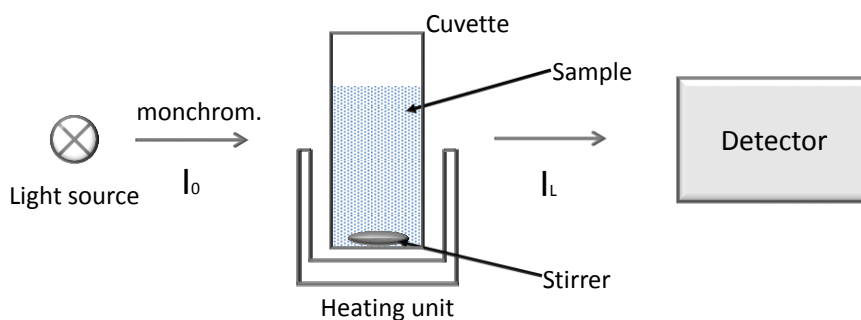


**Figure 4.8:** Schematic representation of a turbidity measurement. The BTS-solution is filled in a quartz glass cuvette and placed in a temperature control unit. Detector monitored the transmitted light through the sample emitted by a monochromatic light source. Each sample was continuously stirred during the experiment.

**Figure 4.18** displays a schematic representation of the experimental setup for temperature dependent turbidity measurements. These solutions were filled into quartz glass cuvettes (optical path length: 10 mm) through a syringe filter (Chromafil Xtra PTFE-20/13; pore size  $0.2 \mu\text{m}$ ). Turbidity experiments were conducted on a Jasco V-670 UV-Vis spectrometer. A multi cell sample holder (PAC-743R) enabled precise control of the sample temperature. The solubility behavior during cooling of the sample was investigated in a temperature range between 0 and  $50 \text{ }^\circ\text{C}$ . Samples were analyzed with cooling rates of  $1 \text{ K/min}$ . Determined cloud-points correspond to a transmittance of 50%. All samples were constantly stirred during the measurement.

#### *Infrared spectroscopy*

The presence of supramolecular columns based on threefold hydrogen bond formation inside the self-assembled nanofibers was investigated by means of infrared spectroscopy. Experiments were performed by attenuated total reflection (ATR) technique on a Fourier transform infrared spectrometer (PerkinElmer Spectrum 100 FT-IR). Background measurements were performed on ambient air. Spectra were recorded in the range from  $400 \text{ cm}^{-1}$  to  $4000 \text{ cm}^{-1}$

#### *Capillary flow porometry*

Pore size distributions of supramolecular nanofiber–microfiber composites were investigated by means of a capillary flow porometer (PSM 165, manufacturer: TOPAS). Each sample was placed in the sample holder with a circular opening (diameter: 6 mm). Volumetric flow rates ranging between 0 and  $7.5 \text{ L/min}$  were applied using compressed air, and the corresponding pressure was recorded online. As wetting liquid, TOPOR was used (supplier: TOPAS). The determination of the pore size distributions

was performed by two measurements. One measurement with wetting liquid and one without. Both measurements were carried out under identical parameters. Each pore size distribution is based on five individual samples and the resulting pore size distributions were calculated using PSM Win software (TOPAS).

### 4.3 Results and Discussion

The results based on the work conducted in this chapter will be presented and discussed in two different sections. The preparation of nanofiber-microfiber composites by utilization of 1,3,5-benzenetrisamides with different alkyl substituents (BTAs **6**, **7** and **8**) will be shown in section 4.3.1 as well as the corresponding characterization including fiber diameter histograms, mass content of supramolecular fibers in the composites and the filtration performance. Section 4.3.2 will focus on the use of a BTA exhibiting alkoxy substituents (BTA **4**) in the periphery of the molecular structure. The nanofiber-microfiber composites were processed from a water/isopropanol mixture (60:40) in a technical polyester nonwoven. Characterization involves mass content of supramolecular nanofibers, fiber diameter histograms based on SEM analysis and filtration experiments.

#### 4.3.1 Nanofiber-microfiber composites based on 1,3,5-benzenetrisamides with branched alkyl chains

The characterization of nanofiber-microfiber composites with alkyl-substituted 1,3,5-benzenetrisamides (BTAs **6**, **7** and **8**) prepared from solutions in 2-butanone, ethanol or isopropanol and by using the viscose/polyester model nonwoven will be described in the following.

##### *Turbidity measurements*

Turbidity measurements upon cooling of BTA solutions with a given concentration of 1.0 wt.-% were performed to evaluate the temperature dependent solubility behavior of the selected BTAs in the processing solvents. Therefore, solutions of either BTAs **6**, **7** or **8** were prepared at elevated temperatures in 2-butanone, ethanol and isopropanol, respectively. Each sample was sealed to prevent evaporation of the solvent and to ensure a constant overall BTA concentration. **Figure 4.9** shows the recorded cooling curves of the transmittance during the turbidity measurements of solutions containing BTA **6** in the three selected solvents. Experiments were performed in a temperature range from 0 to 50 °C with a constant cooling rate of 1 K/min. The y-axis represents the relative amount of transmitted light through the sample at each temperature in relation to the initial amount of transmitted light of the clear solution at 50 °C. All samples were continuously stirred during the measurement. Upon cooling, the intensity of transmitted light decreases significantly until no remaining light can be detected. Once a critical temperature is reached during the cooling process, the intensity almost instantaneously decreases to 0% for all three solvents.

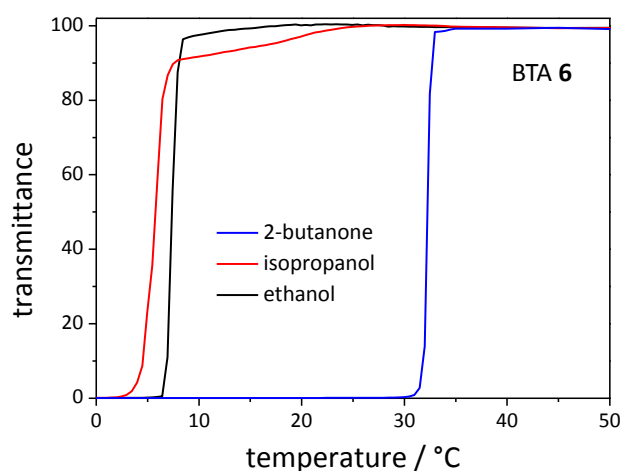


**Figure 4.9:** Turbidity measurements of BTA **6** upon cooling and constant stirring of solutions containing 1 wt.-% BTA. Experiments were performed in 2-butanone, isopropanol and ethanol, respectively. Each experiment started with a clear BTA solution corresponding to 100% transmittance. The curves represent the differential intensity detected at each temperature compared to the initial intensity at a wave length of 670 nm. Turbidity temperatures corresponding to a transmittance of 50% correspond to 32 °C for 2-butanone, 6 °C for isopropanol and 7 °C for ethanol.

The determined cloud points for the investigated solutions were 32 °C for 2-butanone, 6 °C for isopropanol and 7 °C for ethanol. These values correspond to a value of 50% transmitted light. Solubility behavior of BTA **6** in 2-butanone has been found to be very different compared to isopropanol and ethanol. Upon cooling a defined transition occurs from a clear solution to a suspension of solid BTA in the solvent for 2-butanone. In contrast, the intensity of transmitted light gradually decreases between 100 and 90% for BTA solutions in isopropanol and ethanol and subsequently a very fast transition with no remaining light occurs. While the solution in 2-butanone becomes opaque upon cooling above room temperature, solutions in isopropanol and ethanol have to be actively cooled to yield supramolecular structures below room temperature. **Figure 4.10** displays corresponding turbidity measurements of BTA solutions containing BTA **7** either in 2-butanone, isopropanol and ethanol. The results were found to be comparable to turbidity measurements of BTA **6** shown in **Figure 4.10**. Upon cooling, the transition from a clear solution in 2-butanone to an opaque solution occurs at much higher temperatures compared to isopropanol and ethanol. The corresponding values for the cloud points are 30 °C for 2-butanone, 6 °C for isopropanol and 6 °C for ethanol.

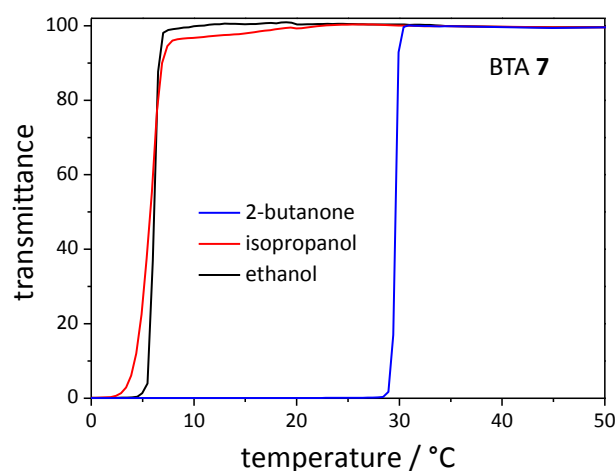


**Figure 4.10:** Turbidity measurements of BTA **7** upon cooling and constant stirring of solutions containing 1 wt.-% BTA. Experiments were performed in 2-butanone, isopropanol and ethanol, respectively. Each experiment started with a clear BTA solution corresponding to 100% transmittance. The curves represent the differential intensity detected at each temperature compared to the initial intensity at a wave length of 670 nm. Turbidity temperatures corresponding to a transmittance of 50% correspond to 30 °C for 2-butanone, 6 °C for isopropanol and 6 °C for ethanol.

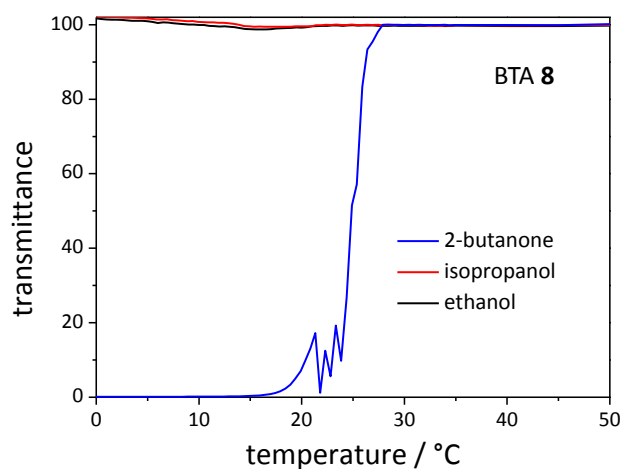


**Figure 4.11:** Turbidity measurements of BTA **8** upon cooling and constant stirring of solutions containing 1 wt.-% BTA. Experiments were performed in 2-butanone, isopropanol and ethanol, respectively. Each experiment started with a clear BTA solution corresponding to 100% transmittance. The curves represent the differential intensity detected at each temperature compared to the initial intensity at a wave length of 670 nm. Turbidity temperature corresponding to a transmittance of 50% corresponds to 25 °C for 2-butanone. In isopropanol and ethanol, no turbidity temperature was detected in the investigated temperature range.

As previously found for BTA **6**, experiments performed in isopropanol and ethanol also exhibit a gradually decrease of the intensity before a sharp transition occurs, but the effect is less intense

compared to the results of solutions containing BTA **6**. Only minor differences were found in the solubility behavior of the two constitutional isomers BTA **6** and **7** in the three selected processing solvents at a concentration of 1.0 wt.-%. **Figure 4.11** displays corresponding results from turbidity measurements of BTA solutions containing BTA **8** in all three selected solvents. In contrast to previous experiments with solutions in isopropanol or ethanol, no cloud points were determined in the investigated temperature range. The samples did not turn opaque upon cooling. The remaining solubility close to a temperature of 0 °C appeared to be still high enough to prevent the formation of supramolecular structures just by changes in temperature. However, the BTA solution with 2-butanone exhibits a cloud point at a temperature of 25 °C. Compared with results for BTAs **6** and **7** from 2-butanone, the value of the cloud point is slightly lower and the decrease in the intensity of transmitted light is not as defined. The results demonstrate that the temperature dependent solubility of all three BTAs in 2-butanone is very different to the behavior in isopropanol or ethanol.

### *Reproducibility of nanofiber-microfiber preparation process*

A key element in the development of a preparation process is whether or not the nanofiber-microfiber composites can be obtained in a reproducible quality. Apart from filtration testing, the characterization of composites relied mainly on SEM analysis of the supramolecular nanofiber morphology inside the nonwoven scaffold. Therefore, experimental series were performed to prepare nanofiber-microfiber composites and to evaluate the reproducibility of the preparation process by means of SEM analysis in repeated experiments. The work conducted involved the preparation of composites in different experimental series with varying parameters. To demonstrate the reproducibility of the process, three individual experiments were performed involving the preparation of the composite, the SEM sample preparation and the generation of a fiber diameter histogram for each set of preparation parameters. These parameters were the used 1,3,5-benzenetrisamide, the selected processing solvent, the BTA concentration, the immersion temperature and the time the nonwoven was immersed into the hot BTA solution. All samples were dried at ambient conditions. **Figure 4.12** shows exemplarily determined fiber diameter histograms of three individual experiments. Each composite was prepared by utilization of BTA **7** with a concentration of 1.0 wt.-% in 2-butanone. The fiber diameter histograms are based on at least 150 individual fibers and were prepared in intervals of 100 nm. Determined mean fiber diameters and corresponding standard deviations are 445 nm  $\pm$  202 nm for sample 1, 453 nm  $\pm$  182 nm for sample 2 and 424 nm  $\pm$  163 nm for sample 3. It was found that the developed preparation process features very high reproducibility of the obtained supramolecular fibers with respect to the mean fiber diameter. In addition, the corresponding standard deviations that represent the width of

the fiber diameter distributions are comparable. These results prove that the preparation process features very high reproducibility and based on that further experimental series to prepare nanofiber-microfiber composites were performed.

**Fiber histograms of BTA 7 processed from 2-butanone**

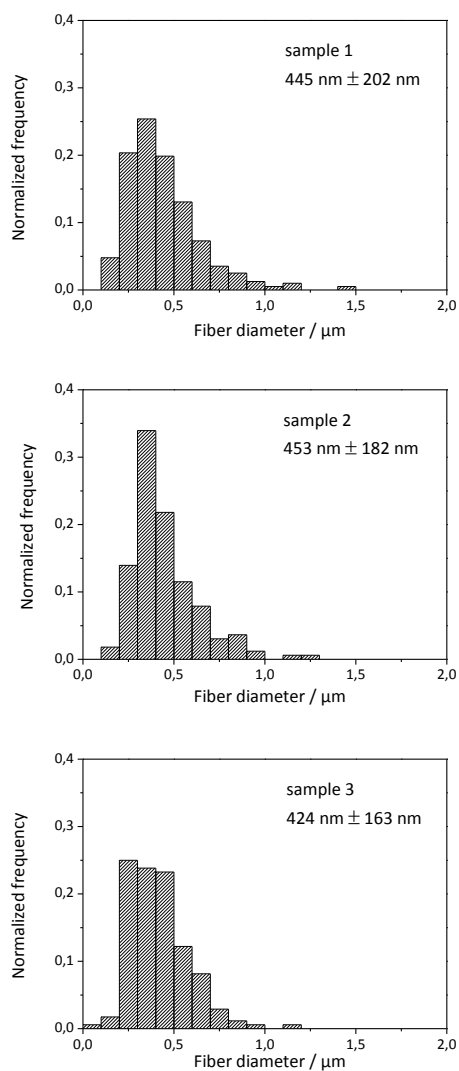


**Figure 4.12:** Supramolecular nanofiber diameter histograms of nanofiber-microfiber composites prepared from a solution of 1 wt.-% BTA 7 in 2-butanone. Each composite was prepared under identical conditions. The histograms correspond to independently prepared samples and are based on at least 150 individual supramolecular fiber diameters.

### *Concentration dependent preparation of nanofiber-microfiber composites*

To evaluate the influence of the BTA concentration in the immersion solution on the nanofiber morphology inside the composites as well as the corresponding filtration performance, experiments were performed to prepare nanofiber-microfiber composites from BTA solutions with different concentrations. The preparation of nanofiber-microfiber composites involved the full soaking of a nonwoven scaffold with a BTA solution. Upon solvent removal, the composite is obtained. In consequence, the BTA concentration in the immersion solution has to be directly related to the resulting mass content of BTA nanofibers in the composite. Experimental series were conducted using solutions of either BTA **6**, **7** or **8** with varying concentrations in the immersion solution. **Figure 4.13** shows exemplarily overview SEM images (left column) as well as magnified images (right column) of prepared samples with different BTA concentration in solution of 0.6, 0.8 and 1.0 wt.-%. Composites were prepared from 2-butanone at a temperature of 50 °C during the immersion process. According to previous investigations, it was found that for increasing concentrations of BTA **6** in 2-butanone, the nonwoven support becomes more densely filled with supramolecular nanofibers.<sup>[89]</sup> Obtained composites were characterized by means of nanofiber content, SEM analysis and filtration performance. The preparation of each sample was repeated two more times to prove reproducibility. While at a concentration of 0.6 wt.-% BTA in solution many pores of the nonwoven remain unfilled, supramolecular nanofibers appear to fully penetrate the entire nonwoven with almost no remaining openings for the composite prepared with a BTA concentration of 1.0 wt.-%. For each displayed sample, the corresponding fiber diameter histograms of supramolecular fibers based on the self-assembly process are shown. The average mean fiber diameters and the corresponding standard deviations of three individual experiments are 504 nm ± 28 nm at a concentration of 0.6 wt.-%, 446 nm ± 34 nm for 0.8 wt.-% and 457 nm ± 49 nm for 1.0 wt.-%. It has to be noted that these standard deviations do not represent the width of the fiber diameter distribution but correspond to the standard deviation of the mean fiber diameters between individual experiments. The mean fiber diameter of each individual experiment is based on at least 150 measured fiber diameters. In consequence, the given values represent an average over more than 450 fibers in repeated experiments. The results clearly show that only minor differences in the fiber diameter distributions can be found upon changes of the BTA concentration. These differences might be attributed to the accuracy of the fiber diameter determination. However, increasing BTA concentrations of the immersion solution yields more supramolecular fibers distributed throughout the nonwoven covering the distances between individual microfibers. Gravimetrically determined mass contents of BTA fibers and the standard deviations correspond to 5.9 wt.-% ± 0.6 wt.-% for samples prepared from a solution containing 0.6 wt.-% BTA **6**. The content increases to 6.5 wt.-% ± 0.5 wt.-% for a BTA **6** concentration in solution of

0.8wt.-% and to 7.3 wt.-%  $\pm$  0.7wt.-% for solutions containing 1.0 wt.-%. As expected, an increase in BTA concentration of the immersion solution, results in increased BTA content in the resulting composite.

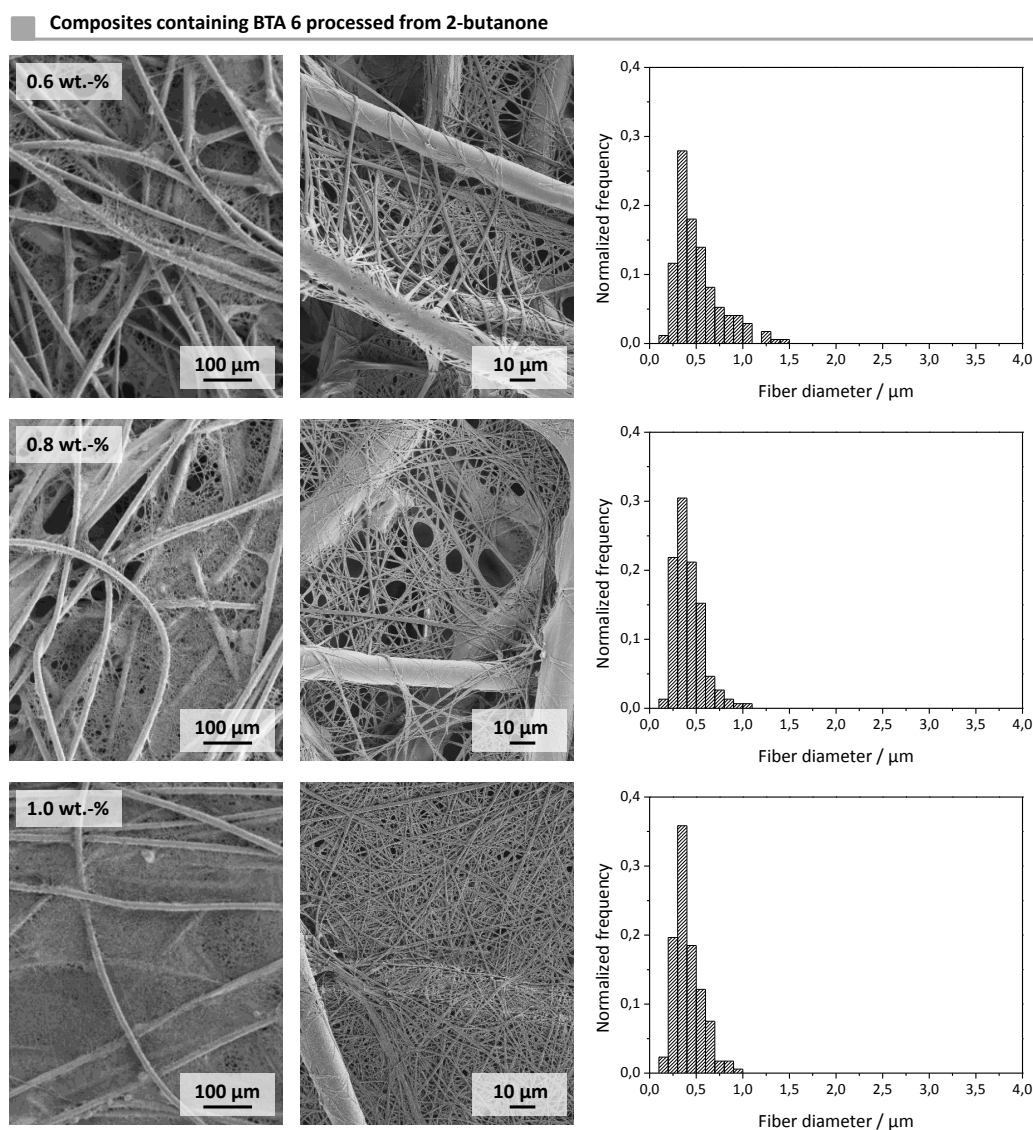


**Figure 4.13:** SEM micrographs of composites containing supramolecular nanofibers of BTA 6. Composites were prepared from 2-butanone with BTA concentrations of 0.6 wt.-%, 0.8 wt.-% and 1.0 wt.-%. The amounts of supramolecular nanofibers in composites prepared from 0.6 wt.-% solutions are 5.9 wt.-% and from 0.8 wt.-% solutions 6.5 wt.-%. A BTA concentration of 1.0 wt.-% in solution resulted in a supramolecular fiber content of 7.3 wt.-% in the dried composite. The corresponding histograms are based on at least 150 fibers.

A corresponding experimental series was performed utilizing solutions containing different amounts of BTA 7. SEM-images and corresponding fiber diameter histograms of nanofiber-microfiber composites containing BTA 7 are shown in **Figure 4.14**. The results were found to be comparable to those obtained by utilization of solutions of BTA 6. While many openings remain unfilled with

supramolecular nanofibers at a concentration of 0.6 wt.-%, the distribution of nanofibers throughout the nonwoven scaffold becomes more homogenous with increasing BTA concentrations in the immersion solution. The displayed fiber diameter histograms indicate that no significant difference in the mean fiber diameter as well as the fiber diameter distribution depending on the BTA concentration in the immersion solution. Corresponding values and standard deviations of three individual experiments for the mean fiber diameter are  $597 \text{ nm} \pm 124 \text{ nm}$  at a concentration of 0.6 wt.-%,  $443 \text{ nm} \pm 54 \text{ nm}$  for 0.8 wt.-% and  $441 \text{ nm} \pm 15 \text{ nm}$  for 1.0 wt.-%.

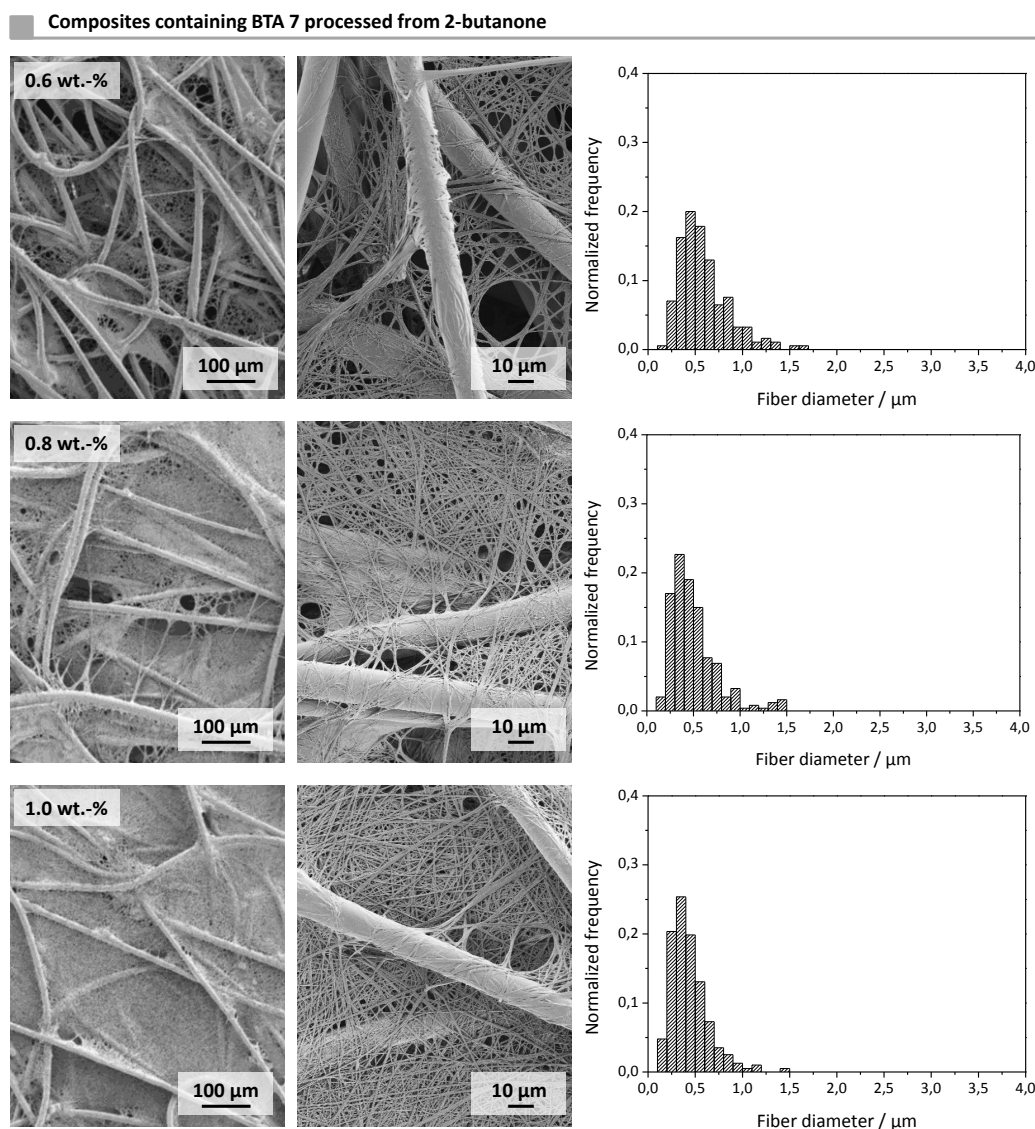


**Figure 4.14:** SEM micrographs of composites containing supramolecular nanofibers of BTA 7. Composites were prepared from 2-butanone with BTA concentrations of 0.6 wt.-%, 0.8 wt.-% and 1.0 wt.-%. The amounts of supramolecular nanofibers in composites prepared from 0.6 wt.-% solutions are 5.1 wt.-% and from 0.8 wt.-% solutions 6.2 wt.-%. A BTA concentration of 1.0 wt.-% in solution resulted in a supramolecular fiber content of 7.3 wt.-% in the dried composite. The corresponding histograms are based on at least 150 fibers.

Supramolecular nanofibers in composites prepared from 0.6 wt.-% solutions of BTA **7** exhibit slightly increased fiber diameters compared to higher concentrations. Upon an increase of the BTA concentration, the fiber distribution throughout the nonwoven becomes more homogeneous. Mass contents and standard deviations of self-assembled nanofibers in the resulting composites with BTA **7** were 5.1 wt.-%  $\pm$  0.6 wt.-% for samples prepared from a solution containing 0.6 wt.-%. The content increases to 6.2 wt.-%  $\pm$  0.6 wt.-% for a BTA **7** concentration in solution of 0.8 wt.-% and to 7.3 wt.-%  $\pm$  0.6 wt.-% for a concentration of 1.0 wt.-%. The mean values for the mass content are based on 9 independently prepared samples. According to results obtained for composites containing BTA **6**, the mass content increases with increasing BTA concentration in the immersion solution. Comparing composites with BTA **6** and **7**, no difference in the amount of supramolecular material was detected.

Furthermore, BTA **8** was used for the preparation of nanofiber-microfiber composites with varying BTA concentration in the immersion solution ranging from 0.6 to 1.0 wt.-%. SEM micrographs and corresponding fiber diameter histograms of the obtained composites are exemplarily shown in **Figure 4.15**.

In contrast to the previously shown results, supramolecular nanofibers cover only very few openings of the nonwoven support by application of a concentration of 0.6 wt.-% in solution. Mostly, small distances between the microfibers are covered, while large distances remain free of self-assembled fibers. Upon increasing the BTA **8** concentration in the immersion solution, the distribution of supramolecular fibers throughout the nonwoven becomes more homogenous. Although, composites prepared from 1.0 wt.-% solutions still exhibit larger remaining openings between the individual supramolecular fibers compared to composites containing BTA **6** and **7**. Corresponding values for mean fiber diameters and standard deviations of three individual experiments are 538 nm  $\pm$  64 nm for 0.6 wt.-%, 446 nm  $\pm$  14 nm for 0.8 wt.-% and 471 nm  $\pm$  56 nm for 1.0 wt.-%. Determined mass contents for composites containing BTA **8** and standard deviations are 5.5 wt.-%  $\pm$  0.4 wt.-% from a solution containing 0.6 wt.-% BTA **8**. For concentrations of 0.8 wt.-%, the resulting contents were 6.5 wt.-%  $\pm$  0.9 wt.-% and for 1.0 wt.-% the corresponding value was 7.3 wt.-%  $\pm$  0.7 wt.-%. These numbers are in very good agreement with previously presented results on the mass content of supramolecular nanofibers in prepared nanofiber-microfiber composites. For all investigated BTAs, a concentration of 1.0 wt.-% in the immersion solution was identified to be sufficient to yield homogeneously distributed supramolecular fibers throughout the nonwoven support. Independently of the utilized BTA, all composites prepared from the lowest BTA concentration in the immersion solution exhibit slightly increased values for the mean fiber diameters and feature the least homogeneous distribution of fibers

throughout the nonwoven scaffold. However, the morphology of supramolecular nanofibers with respect to the fiber diameter is comparable for all investigated BTAs.

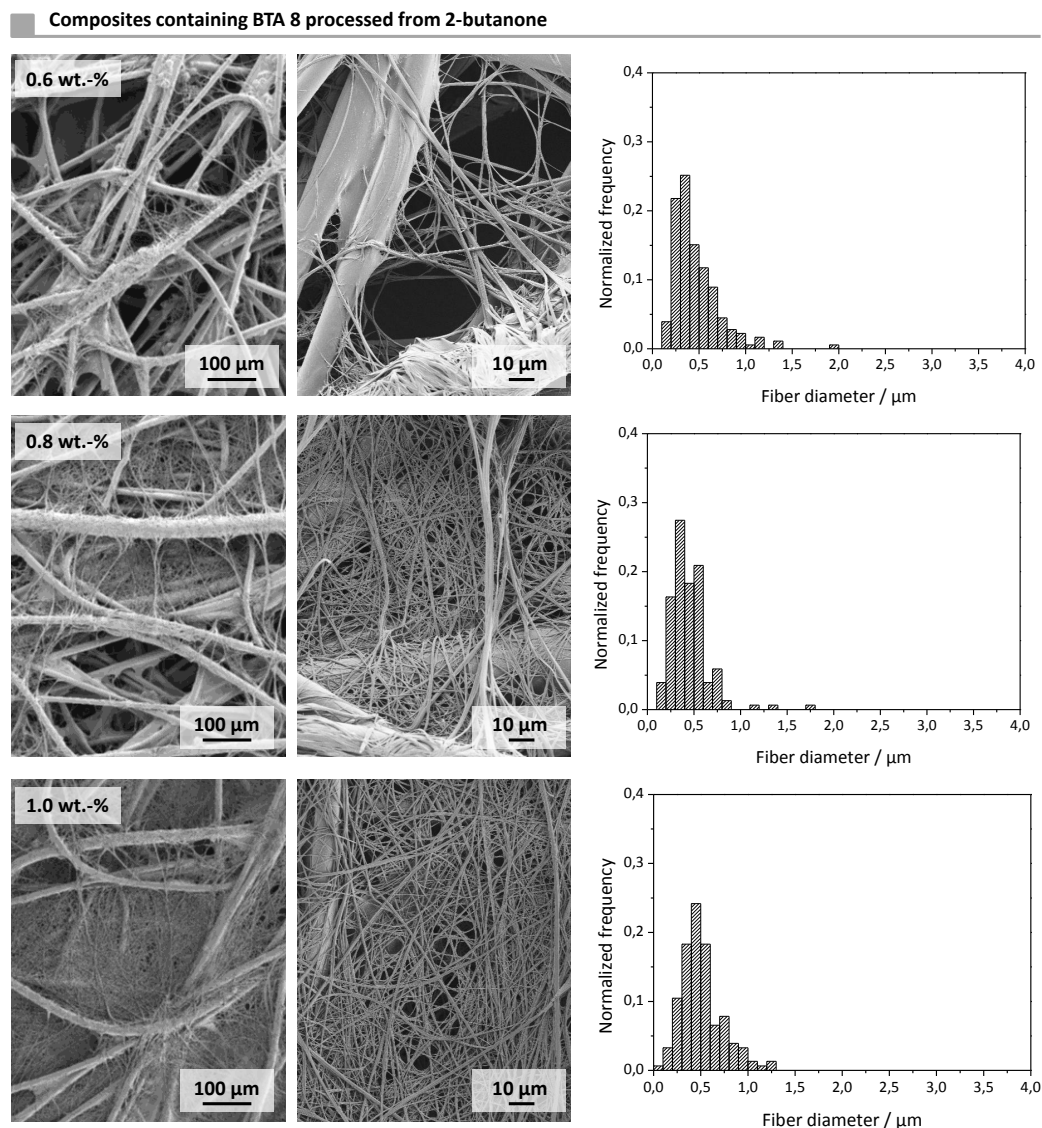


**Figure 4.15:** SEM micrographs of composites containing supramolecular nanofibers of BTA **8**. Composites were prepared from 2-butanone with BTA concentrations of 0.6 wt.-%, 0.8 wt.-% and 1.0 wt.-%. The amounts of supramolecular nanofibers in composites prepared from 0.6 wt.-% solutions are 5.5 wt.-% and from 0.8 wt.-% solutions 6.5 wt.-%. A BTA concentration of 1.0 wt.-% in solution resulted in a supramolecular fiber content of 7.3 wt.-% in the dried composite. The corresponding histograms are based on at least 150 fibers.

#### *Filtration efficiencies of composites prepared from BTA solution with different concentrations*

In addition to the characterization of prepared nanofiber-microfiber composites by means of SEM analysis, filtration experiments were conducted to evaluate the capability of removing particulate matter from air. Therefore, composites containing either BTA **6**, **7** or **8** prepared from 2-butanone with

varying concentrations between 0.6 and 1.0 wt.-% were subjected to filtration testing by utilization of the described air filtration test rig. The results of corresponding experiments are based on a minimum of at least six independently prepared samples. **Figure 4.16** shows particle size dependent filtration efficiencies in the range from 0.2  $\mu\text{m}$  to 2.0  $\mu\text{m}$  of prepared composites containing BTA **6** with varying BTA concentrations in the immersion solution. As reference, the filtration efficiency of the neat nonwoven scaffold is displayed (filled squares). It only exhibits very low efficiencies of mostly below 10% for the removal of particulate matter from air.

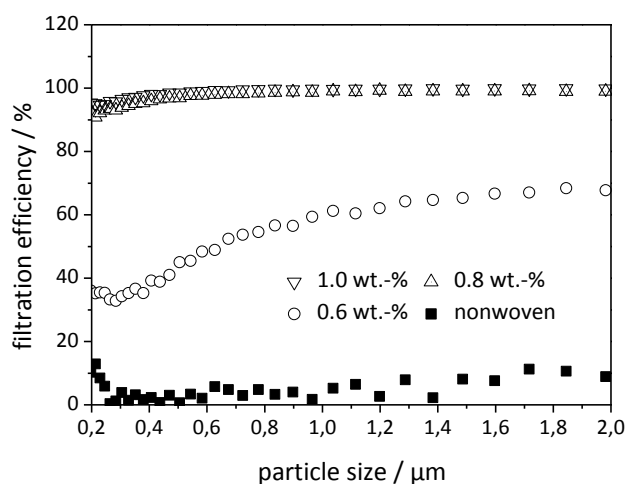


**Figure 4.16:** Particle size dependent filtration efficiencies of nanofiber-microfiber composites with BTA **6** prepared from 2-butanone with different BTA concentrations in the immersion solutions of 0.6 wt.-% (open circles), 0.8 wt.-% (triangles up) and 1.0 wt.-% (triangles down). As reference, the nonwoven scaffold without supramolecular nanofibers is shown (filled squares). The curves are based on an average of at least six independently prepared samples. Test conditions were: Filter area: 28.3  $\text{cm}^2$ ; flow velocity: 25  $\text{cm/s}$ ; test aerosol: iso fine dust; upstream aerosol concentration: 30000 Particles/ $\text{cm}^3$ ; measuring time: 30 s.

Nanofiber-microfiber composites prepared from solutions containing 0.6 wt.-% of BTA **6** already show a significant increase of the filtration efficiency ranging from 30 up to 60% depending on the particle size (open circles). The lowest efficiency was detected for particles with diameters of 0.3  $\mu\text{m}$ . Further increase of the supramolecular fiber content leads to efficiencies between 90 and 100%. Almost no difference can be observed between composites prepared from solutions either containing 0.8 wt.-% (triangles up) or 1.0 wt.-% (triangles down). Considering the applied flow velocity of 25  $\text{cm/s}$ , the neat nonwoven causes a differential pressure of 3 Pa. In contrast, the composites containing supramolecular fibers covering partially the spaces between the microfibers are associated with an increased differential pressure. Composites prepared from a solution with a BTA content of 0.6 wt.-% show an average differential pressure and standard deviation of 117 Pa  $\pm$  61 Pa. For 0.8 wt.-%, the differential pressure was 1380 Pa  $\pm$  637 Pa and for 1.0 wt.-% the differential pressure corresponded to

a value of  $1300 \text{ Pa} \pm 446 \text{ Pa}$ . It was found that within the accuracy of the measurement, no difference in the differential pressure between composites prepared from 0.8 wt.-% and 1.0 wt.-% solutions was detected. This finding might be attributed to an already homogeneous and dense filling of the spaces between the individual microfibers by utilization of a solution with a concentration of 0.8 wt.-%. Even though SEM analysis revealed remaining openings in the nonwoven support, the filtration efficiency of these two composites showed only minor differences. Thus, in this case, the remaining unfilled openings did not affect the filtration efficiency of the composites.

**Figure 4.17** displays corresponding filtration data for composites containing BTA **7** prepared from 2-butanone with varying concentrations. Recorded filtration efficiencies are very much alike those displayed in **Figure 4.16**. The composite preparation from a 0.6 wt.-% solution results in an increased filtration performance compared to the neat nonwoven with values varying between 30 and 60% depending on the particle size. Furthermore, almost no difference in filtration performance between composites prepared from 0.8 wt.-% solutions and 1.0 wt.-% solutions were observed featuring efficiencies between 90 and 100%.

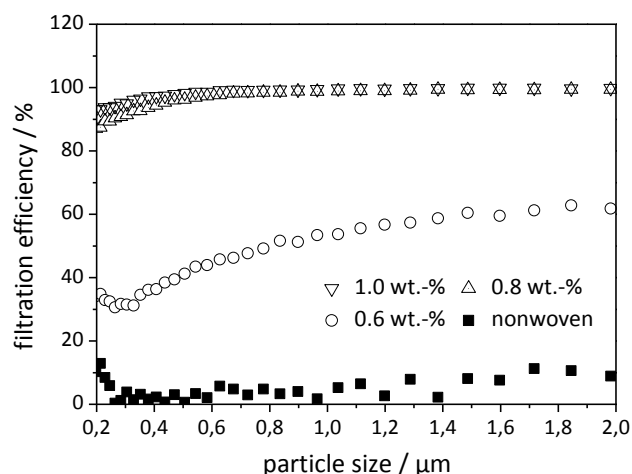


**Figure 4.17:** Particle size dependent filtration efficiencies of nanofiber-microfiber composites with BTA **7** prepared from 2-butanone with different BTA concentrations in the immersion solutions of 0.6 wt.-% (open circles), 0.8 wt.-% (triangles up) and 1.0 wt.-% (triangles down). As reference, the nonwoven scaffold without supramolecular nanofibers is shown (filled squares). The curves are based on an average of at least six independently prepared samples. Test conditions were: Filter area:  $28.3 \text{ cm}^2$ ; flow velocity:  $25 \text{ cm/s}$ ; test aerosol: iso fine dust; upstream aerosol concentration:  $30000 \text{ Particles/cm}^3$ ; measuring time:  $30 \text{ s}$ .

Values for the differential pressure and corresponding standard deviations are  $81 \text{ Pa} \pm 76 \text{ Pa}$  for composites prepared from 0.6 wt.-% solutions. For 0.8 wt.-%, the differential pressure was  $762 \text{ Pa} \pm 168 \text{ Pa}$  and for 1.0 wt.-% the average value was  $1529 \text{ Pa} \pm 594 \text{ Pa}$ . In contrast to results related with

composites containing BTA **6**, additional supramolecular material leads to even higher differential pressures.

Results of filtration experiments with composites containing BTA **8** are shown in **Figure 4.18**. While the neat nonwoven shows almost no filtration efficiency for particles with diameters of up to 2  $\mu\text{m}$ , composites prepared from BTA solutions with a concentration of 0.6 wt.-% do not show a significant improvement of the filtration performance. This may be attributed to the very inhomogeneous distribution of supramolecular fibers throughout the nonwoven scaffold as revealed by SEM analysis. Upon increasing the BTA concentration, the filtration performance can be improved. Composites prepared from solutions with a BTA concentration of 1.0 wt.-% are capable of removing between 60 and 80% of the particles from the air stream. Compared to previously shown results, the efficiency to remove particulate matter from air is lower than for composites which either contain BTA **6** or **7**. Even at a concentration of the BTA solution of 1.0 wt.-%, more remaining spaces between the individual supramolecular fibers were visible in SEM analysis, probably affecting the filtration performance. The corresponding values for the average differential pressure during the filtration process are 5 Pa  $\pm$  2 Pa (0.6 wt.-%), 46 Pa  $\pm$  23 Pa (0.8 wt.-%) and 348 Pa  $\pm$  110 Pa (1.0 wt.-%). The relative inhomogeneous distribution of self-assembled nanofibers inside composites compared to those containing BTA **6** and **7** probably results in less filtration performance.

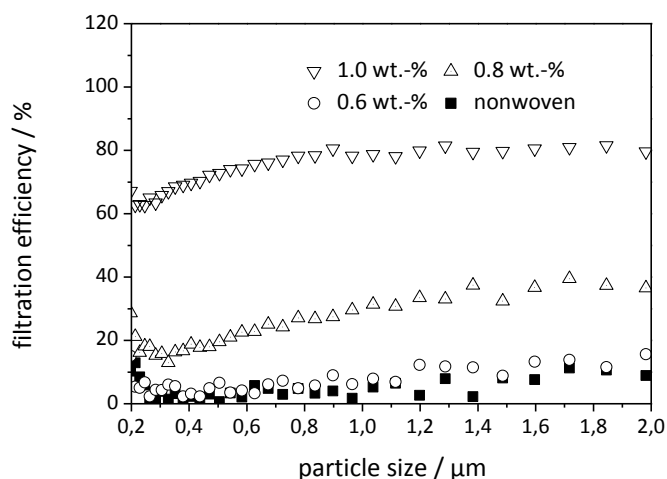


**Figure 4.18:** Particle size dependent filtration efficiencies of nanofiber-microfiber composites with BTA **8** prepared from 2-butanone with different BTA concentrations in the immersion solutions of 0.6 wt.-% (open circles), 0.8 wt.-% (triangles up) and 1.0 wt.-% (triangles down). As reference, the nonwoven scaffold without supramolecular nanofibers is shown (filled squares). The curves are based on an average of at least six independently prepared samples. Test conditions were: Filter area: 28.3  $\text{cm}^2$ ; flow velocity: 25  $\text{cm/s}$ ; test aerosol: iso fine dust; upstream aerosol concentration: 30000 Particles/ $\text{cm}^3$ ; measuring time: 30 s.

*Capillary flow porometry*

The filtration performances of composites containing BTA **6** or BTA **7** are very similar. However, composites containing BTA **8** feature rather low filtration efficiency values. Therefore, selected composites that either contained BTA **7** or BTA **8** were investigated by means of capillary flow porometry. **Figure 4.19** displays the pore size distribution of the neat nonwoven and of nanofiber-microfiber composites containing either BTA **7** or BTA **8**. The neat nonwoven exhibits rather large pores, while more than 99% of all pores are in the range from 20 to 92  $\mu\text{m}$ . The majority of pores (around 70%) correspond to values from 60 to 70  $\mu\text{m}$ . However, the introduction of supramolecular nanofibers of BTA **7** into the nonwoven scaffold leads to pore sizes between 6 and 20  $\mu\text{m}$ . 80% of these pores are in the range from 6 to 10  $\mu\text{m}$ . These results demonstrate that nanofibers of BTA **7** in the corresponding composites densely cover all pores of the microfiber nonwoven. In contrast, composites containing BTA **8**, show a very broad pore size distribution with remaining pores of 8 to 86  $\mu\text{m}$ . Only 62% of these pores are in the range from 18 to 38  $\mu\text{m}$ . This result indicates that the pore size distribution corresponds to a mixture between pores resulting from the microfiber scaffold as well as pores generated by supramolecular nanofibers. These differences are attributed to the complex drying process and the differences in temperature dependent solubility behaviors of BTA **7** and **8** as found by temperature dependent turbidity measurements.

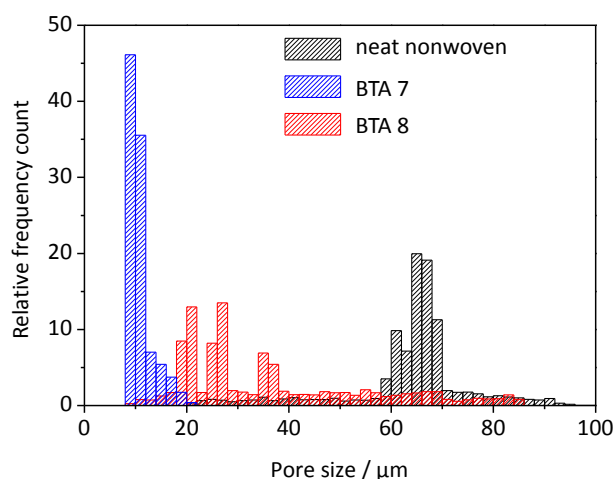


**Figure 4.19:** Pore size distributions of supramolecular nanofiber-microfiber composites containing either BTA **7** (blue) or BTA **8** (red) as measured by capillary flow porometry. As reference, the pore size distribution of the neat nonwoven is shown (black). Each pore size distribution is based on 5 independent measurements. Test conditions are: sample diameter: 6 mm, wetting liquid: TOPOR, fluid: compressed air, volumetric flow rate: 0 – 7.5 L/min.

*Solvent dependent preparation of nanofiber-microfiber composites*

Apart from concentration dependent experiments, nanofiber-microfiber composites were prepared from different processing solvents involving 2-butanone, isopropanol and ethanol to investigate the influence on the resulting nanofiber morphology with respect to the fiber diameter and the fiber diameter distribution by means of SEM analysis. Composites were prepared utilizing BTAs **6**, **7** and **8**, respectively. **Figure 4.20** shows overview and magnified SEM images of composites that contain BTA **6** and that were processed from either 2-butanone (top), isopropanol (middle) or ethanol (bottom).

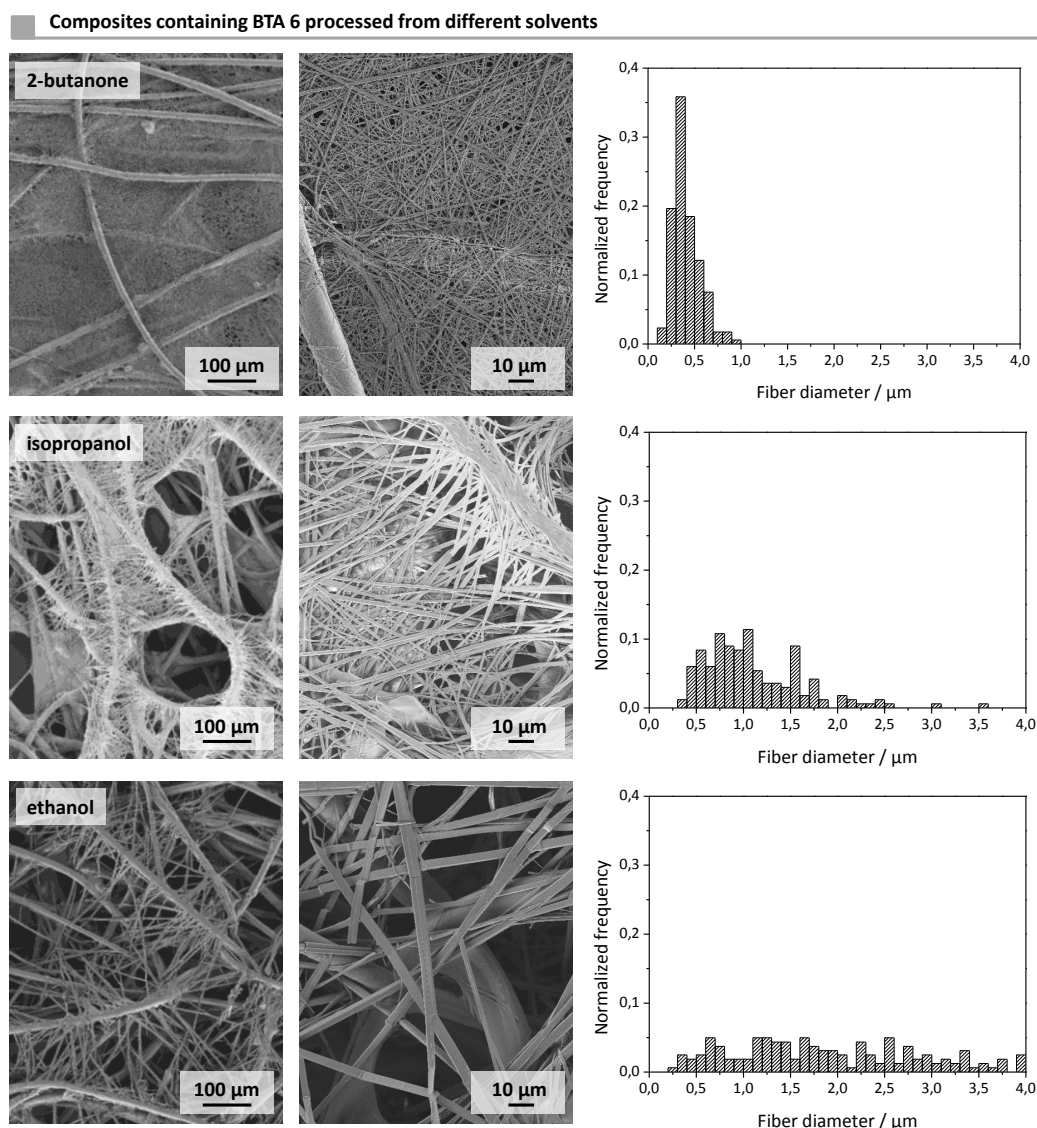


**Figure 4.20:** SEM micrographs of composites containing supramolecular nanofibers of BTA **6**. Composites were prepared from solutions containing 1 wt.-% BTA **6** in 2-butanone, isopropanol and ethanol, respectively. The amounts of supramolecular nanofibers in composites prepared from 2-butanone are 7.3 wt.-%. Processed from isopropanol the resulting supramolecular nanofiber content relates to 6.5 wt.-% and from ethanol 6.4 wt.-%. The corresponding histograms are based on at least 150 fibers.

All displayed samples were processed with a BTA concentration of 1.0 wt.-% in the immersion solution. The composite processed from 2-butanone corresponds to the sample already displayed in **Figure 4.13**. It was found that the distribution of supramolecular nanofibers throughout the entire nonwoven is most homogeneous when processed from 2-butanone. In contrast, the processing from isopropanol results in a gathering of supramolecular fibers in small spaces between the individual microfibers, while large openings remain unfilled. However, supramolecular fibers processed from ethanol appear to be fewer but with increased fiber diameters.

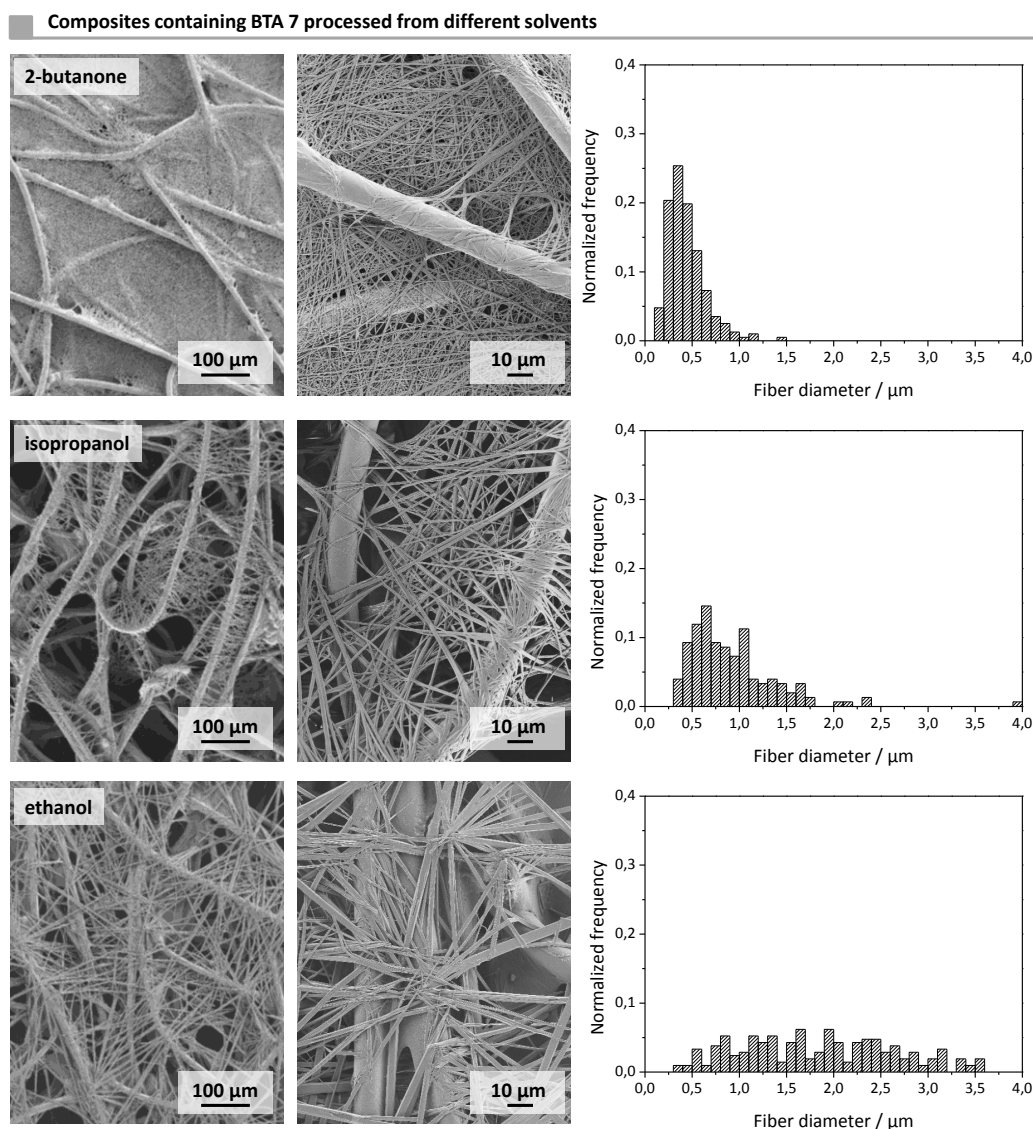


**Figure 4.21:** SEM micrographs of composites containing supramolecular nanofibers of BTA 7. Composites were prepared from solutions containing 1 wt.-% BTA 7 in 2-butanone, isopropanol and ethanol, respectively. The amounts of supramolecular nanofibers in composites prepared from 2-butanone are 7.3 wt.-%. Processed from isopropanol the resulting supramolecular nanofiber content relates to 7.0 wt.-% and from ethanol 6.2 wt.-%. The corresponding histograms are based on at least 150 fibers.

Evaluation of the corresponding fiber diameter histograms show that composites processed from 2-butanone exhibit the smallest mean fiber diameters as well as the most narrow fiber diameter distribution. Utilization of isopropanol as processing solvent leads to thicker fibers with a broader fiber diameter distribution. This effect becomes even larger when the composite is prepared from ethanol. Each histogram is based on at least 150 individual fibers. The resulting mean fiber diameters of three independently prepared samples and the corresponding standard deviations are 457 nm  $\pm$  49 nm processed from 2-butanone, 1139 nm  $\pm$  49 nm processed from isopropanol and 1942 nm  $\pm$  28 nm for ethanol. In addition, the mass contents of supramolecular fibers in the resulting composites are 7.3 wt.-%  $\pm$  0.7 wt.-% (2-butanone), 6.5 wt.-%  $\pm$  0.6 wt.-% (isopropanol) and 6.4 wt.-%  $\pm$  0.4 wt.-% (ethanol). Considering the accuracy of the measurements, only minor differences are determined in the nanofiber content in composites processed from different solvents.

Another experimental series was performed by utilization of BTA **7** for the preparation of nanofiber-microfiber composites. **Figure 4.21** exemplarily shows SEM images as well as corresponding fiber diameter histograms of composites processed from 2-butanone, isopropanol and ethanol, respectively. The obtained results are very much alike previously discussed data. The most homogeneous fiber distribution in the nonwoven scaffold as well as the smallest mean fiber diameter and the most narrow fiber diameter distribution can be obtained by processing from 2-butanone. In contrast, utilization of either isopropanol or ethanol yields composites with thicker supramolecular fibers. Supramolecular fibers prepared from isopropanol appear to gather mainly in the pores with small diameters, whereas the larger pores are not covered and many unfilled openings remain. Composites processed from ethanol feature a more homogeneous distribution in the nonwoven. However, these fibers exhibit increased fiber diameters and broader fiber diameter distributions. The corresponding values of the mean fiber diameters and the standard deviations of three independently prepared samples of each set of processing parameters are 441 nm  $\pm$  15 nm processed from 2-butanone, 1075 nm  $\pm$  165 nm processed from isopropanol and 1876 nm  $\pm$  137 nm for ethanol. Gravimetric evaluation of the mass content of supramolecular nanofibers in the prepared nanofiber-microfiber composites of nine independently prepared samples are 7.3 wt.-%  $\pm$  0.6 wt.-% (2-butanone), 7.0 wt.-%  $\pm$  0.4 wt.-% (isopropanol) and 6.2 wt.-%  $\pm$  0.6 wt.-% (ethanol). The results for BTA **7** were found to be very similar to those obtained by utilization of BTA **6**.

Furthermore, BTA **8** has been used to prepare nanofiber-microfiber composites from the different processing solvents. Exemplarily, SEM images of obtained composites and the fiber diameter histograms are shown in **Figure 4.22**. Partially, the results are in good agreement with previous findings. Smallest mean fiber diameters are obtained by preparation of composites from 2-butanone.

Utilization of isopropanol and ethanol yields supramolecular fibers with thicker fiber diameters and broader fiber diameter distribution. The distribution of supramolecular fibers throughout the nonwoven support appears to be even more inhomogeneous compared to composites containing either BTA 6 or 7. The corresponding mean fiber diameters of three individual experiments and the standard deviations are  $471 \text{ nm} \pm 56 \text{ nm}$  processed from 2-butanone,  $1147 \text{ nm} \pm 113 \text{ nm}$  processed from isopropanol and  $2382 \text{ nm} \pm 11 \text{ nm}$  for composites process from ethanol.

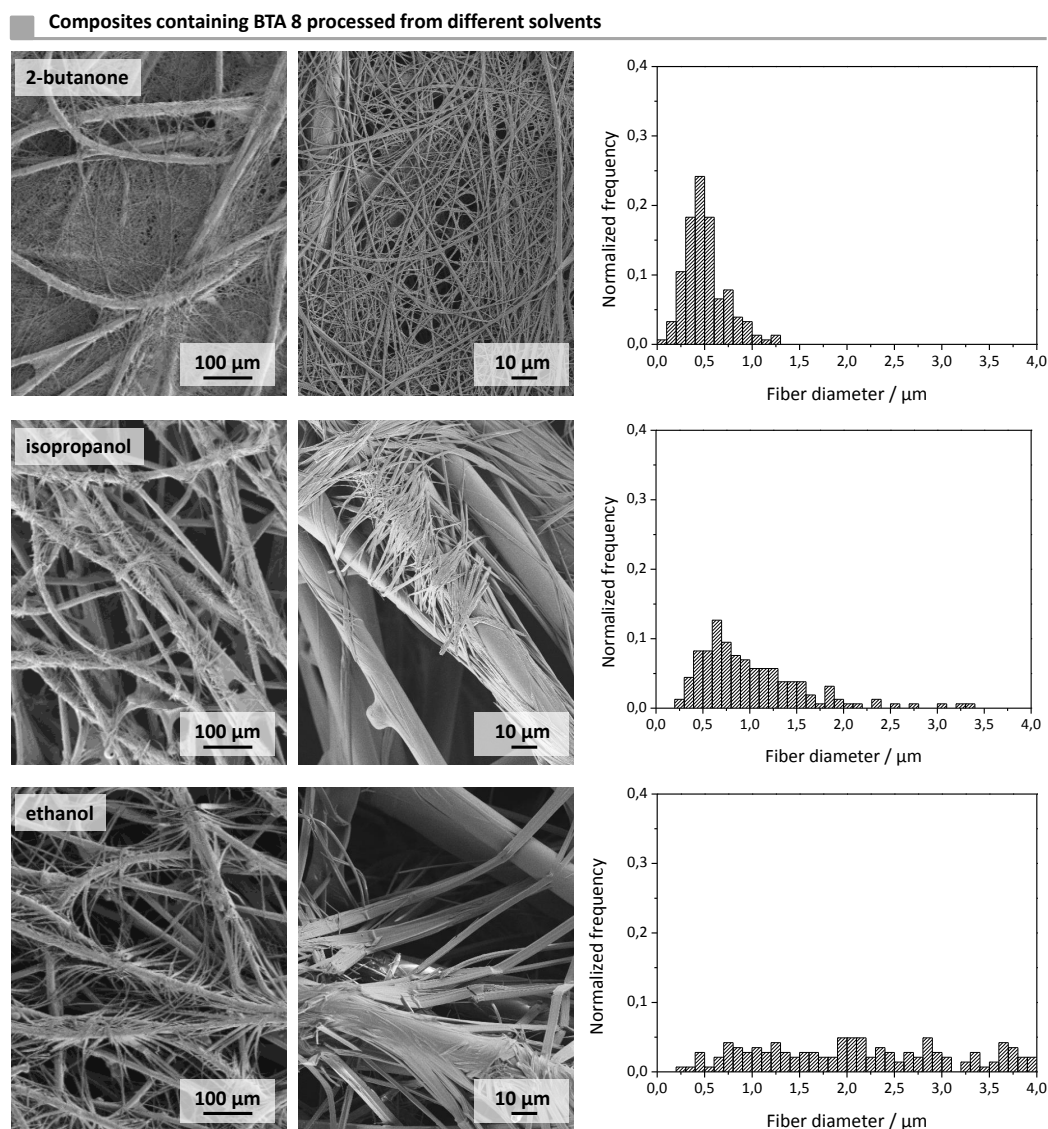


**Figure 4.22:** SEM micrographs of composites containing supramolecular nanofibers of BTA 8. Composites were prepared from solutions containing 1 wt.-% BTA 8 in 2-butanone, isopropanol and ethanol, respectively. The amounts of supramolecular nanofibers in composites prepared from 2-butanone are 7.3 wt.-%. Processed from isopropanol the resulting supramolecular nanofiber content relates to 6.1 wt.-% and from ethanol 6.4 wt.-%. The corresponding histograms are based on at least 150 fibers.

One major difference compared to results obtained by using BTAs **6** and **7** is the more inhomogeneous distribution of supramolecular material throughout the nonwoven, whereas the values of the mean fiber diameters are comparable. The mass content of BTA in the composites is 7.3 wt.-%  $\pm$  0.7 wt.-% (2-butanone), 6.1 wt.-%  $\pm$  0.5 wt.-% (isopropanol) and 6.4 wt.-%  $\pm$  0.5 wt.-% (ethanol). Within the accuracy of the measurements, no difference in the mass contents of supramolecular material in prepared composites was observed.

### *Filtration efficiencies of composites prepared from different solvents*

Prepared nanofiber-microfiber composites processed from different solvents were evaluated by means of filtration efficiency to remove particulate matter from air. The obtained samples were subjected to air filtration tests. Presented results of performed experiments are based on a minimum of at least six independently prepared samples. **Figure 4.23** shows particle size dependent filtration efficiencies in the range from 0.2  $\mu\text{m}$  to 2.0  $\mu\text{m}$  of prepared composites containing BTA **6** with varying processing solvents. Nanofiber-microfiber composites prepared from 2-butanone feature the highest observed filtration efficiencies between 90 and 100%. In contrast, supramolecular nanofibers inside the nonwoven scaffold based on the use of isopropanol or ethanol do not lead to significant improvements of the capability of removing particulate matter from air. This finding may be attributed to a combination of the inhomogeneous filling of the scaffold with self-assembled fibers and the differences in fiber diameters. Even though SEM analysis revealed that samples prepared from isopropanol appeared to exhibit more remaining openings, the filtration performance is slightly higher than for corresponding samples prepared from ethanol. The average values for the differential pressure are 1300 Pa  $\pm$  446 Pa for composites prepared from 2-butanone, 26 Pa  $\pm$  15 Pa from isopropanol and for composites from ethanol 16 Pa  $\pm$  3 Pa. These results correlate to previously discussed SEM analysis because of large remaining openings in the nonwoven that are not covered with any supramolecular fibers. However, another experimental series of filtration testing was performed on composites containing BTA **7** that were processed either from 2-butanone, isopropanol or ethanol. **Figure 4.24** displays the recorded filtration efficiency curves for particle sizes ranging from 0.2  $\mu\text{m}$  to 2.0  $\mu\text{m}$ . It was found that results obtained for composites with BTA **7** are much alike those recorded for BTA **6**. Samples processed from 2-butanone exhibit the highest values for the filtration efficiency, whereas samples with supramolecular fibers from isopropanol or ethanol show rather low efficiencies to remove particulate matter from air.

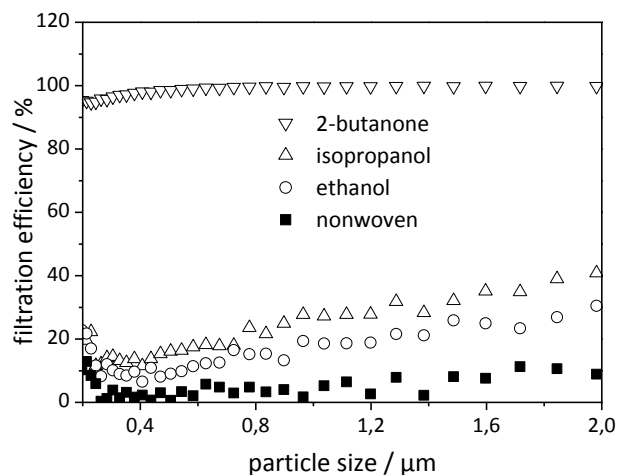


**Figure 4.23:** Particle size dependent filtration efficiencies of nanofiber-microfiber composites with BTA 6 prepared from 2-butanone (triangles down), isopropanol (triangles up) and ethanol (open circles), respectively. The BTA concentration in solution was 1 wt.-%. As reference, the nonwoven scaffold without supramolecular nanofibers is shown (filled squares). The curves are based on an average of at least six independently prepared samples. Test conditions were: Filter area: 28.3 cm<sup>2</sup>; flow velocity: 25 cm/s; test aerosol: iso fine dust; upstream aerosol concentration: 30000 Particles/cm<sup>3</sup>; measuring time: 30 s.

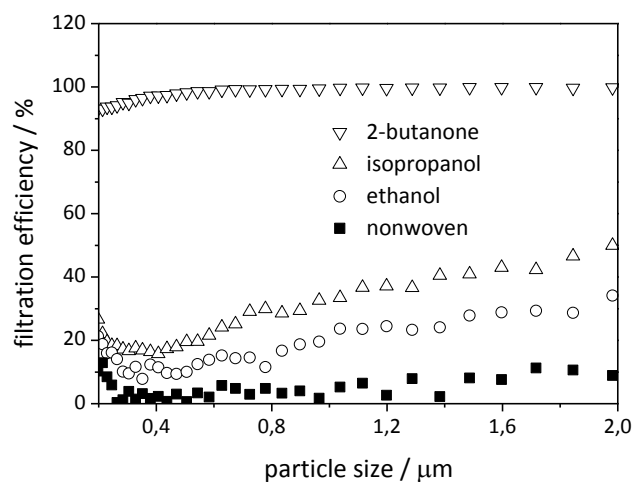


**Figure 4.24:** Particle size dependent filtration efficiencies of nanofiber-microfiber composites with BTA 7 prepared from 2-butanone (triangles down), isopropanol (triangles up) and ethanol (open circles), respectively. The BTA concentration in solution was 1 wt.-%. As reference, the nonwoven scaffold without supramolecular nanofibers is shown (filled squares). The curves are based on an average of at least six independently prepared samples. Test conditions were: Filter area: 28.3 cm<sup>2</sup>; flow velocity: 25 cm/s; test aerosol: iso fine dust; upstream aerosol concentration: 30000 Particles/cm<sup>3</sup>; measuring time: 30 s.

As revealed by SEM analysis, supramolecular fibers from isopropanol feature smaller fiber diameters compared to fibers from ethanol. Composites containing these fibers also show slightly higher filtration

performances even if the distribution of fibers throughout the nonwoven scaffold appears to be more inhomogeneous. Determined average differential pressures and corresponding standard deviations are 1529 Pa  $\pm$  594 Pa for composites prepared from 2-butanone, 31 Pa  $\pm$  9 Pa from isopropanol and for composites from ethanol 18 Pa  $\pm$  4 Pa.

**Figure 4.25** shows filtration efficiency curves obtained for composites prepared from the three selected solvents with BTA **8**. As SEM analysis already indicated, utilization of BTA **8** during the preparation process lead to nanofiber-microfiber composites with lower filtration efficiencies compared to composites containing BTA **6** and **7**. Samples prepared from 2-butanone exhibit the best results. In contrast, composites prepared from isopropanol or ethanol did not lead to any improvement of the filtration efficiency compared to the neat nonwoven. The corresponding average values for the differential pressure are 348 Pa  $\pm$  110 Pa for composites prepared from 2-butanone, 4 Pa  $\pm$  1 Pa from isopropanol and for composites from ethanol 8 Pa  $\pm$  3 Pa. The difference of the measured average differential pressure of prepared composites either from isopropanol or ethanol is very small compared to the neat nonwoven indicating that the pores of the nonwoven support are not sufficiently covered with supramolecular fibers to result in an improved filtration performance.

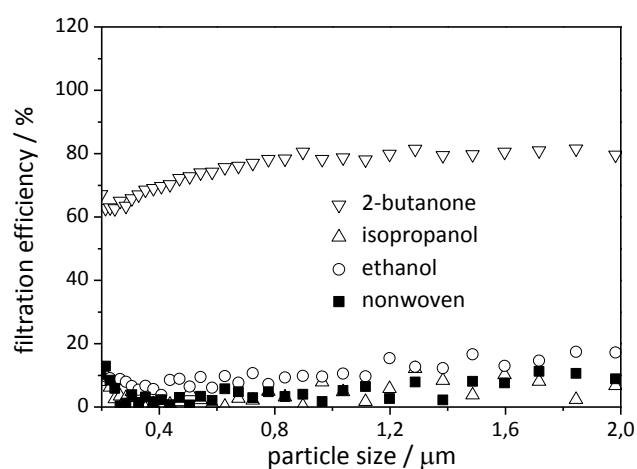


**Figure 4.25:** Particle size dependent filtration efficiencies of nanofiber-microfiber composites with BTA **8** prepared from 2-butanone (triangles down), isopropanol (triangles up) and ethanol (open circles), respectively. The BTA concentration in solution was 1 wt.-%. As reference, the nonwoven scaffold without supramolecular nanofibers is shown (filled squares). The curves are based on an average of at least six independently prepared samples. Test conditions were: Filter area: 28.3 cm<sup>2</sup>; flow velocity: 25 cm/s; test aerosol: iso fine dust; upstream aerosol concentration: 30000 Particles/cm<sup>3</sup>; measuring time: 30 s.

*Infrared spectroscopy of nanofiber-microfiber composites*

The formation of nanofibers based on the self-assembly of 1,3,5-benzenetrisamides involves the formation of supramolecular columns by threefold directed hydrogen bonding. To ensure that these intermolecular secondary interactions are present in the prepared supramolecular fibers inside the nonwoven scaffolds, infrared spectroscopic measurements of the composites were performed. According to the literature, BTAs organized in supramolecular columns feature characteristic IR signals for the N-H-stretch ( $3240\text{ cm}^{-1}$ ), the C=O-stretch ( $1640\text{ cm}^{-1}$ ) and the amide-II-stretch ( $1560\text{ cm}^{-1}$ ) vibrations.<sup>[51,129]</sup> Therefore, the composites were investigated by utilization of attenuated total reflection (ATR) technique enabling investigation of solid samples. **Figure 4.26** shows recorded normalized IR spectra in the range from  $1500\text{ cm}^{-1}$  to  $1800\text{ cm}^{-1}$ . The neat nonwoven (black curve) exhibits a strong signal at  $1730\text{ cm}^{-1}$  representing a carbonyl vibration of the polyester. In contrast the neat BTA **6** shows two signals at  $1640\text{ cm}^{-1}$  and  $1560\text{ cm}^{-1}$ . Another signal at  $3240\text{ cm}^{-1}$  can be also found but is not shown at this point due to reasons of clarity. Composites prepared from the different processing solvents at a BTA concentration of 1.0 wt.-% in the immersion solution also exhibit a very strong signal that belongs to the carbonyl vibration of the nonwoven scaffold. Corresponding signals of the BTA can clearly be observed for the composite processed from 2-butanone. In contrast, composites processed from isopropanol and ethanol only show very weak signals exhibiting the same wavelength. This finding may be attributed to the very inhomogeneous distribution of supramolecular fibers throughout the nonwoven scaffold.

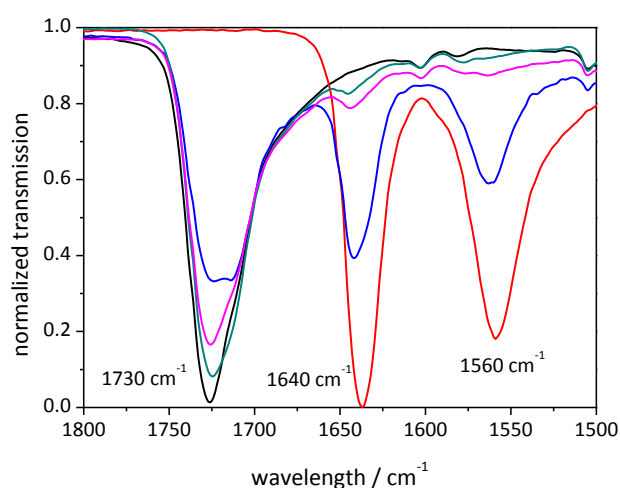


**Figure 4.26:** Normalized infrared spectra of the neat nonwoven scaffold (black), the neat BTA **6** (red) and nanofiber-microfiber composites prepared from three different processing solvents (2-butanone (blue), isopropanol (green) and ethanol (pink)) in the range of  $1500\text{ cm}^{-1}$  to  $1800\text{ cm}^{-1}$ .

Even though some signals are very weak, no other signals for the amide moieties can be found. Thus, it is assumed that the prepared supramolecular fibers contain supramolecular columns with directed threefold hydrogen bonds. In addition, infrared spectroscopic experiments were conducted on the neat BTAs **7** and **8** as well as the corresponding composites processed from the different solvents 2-butanone, isopropanol and ethanol. The top of **Figure 4.27** presents recorded IR spectra of BTA **7** and the corresponding composites, while the bottom of **Figure 4.27** shows the corresponding data obtained for BTA **8**.

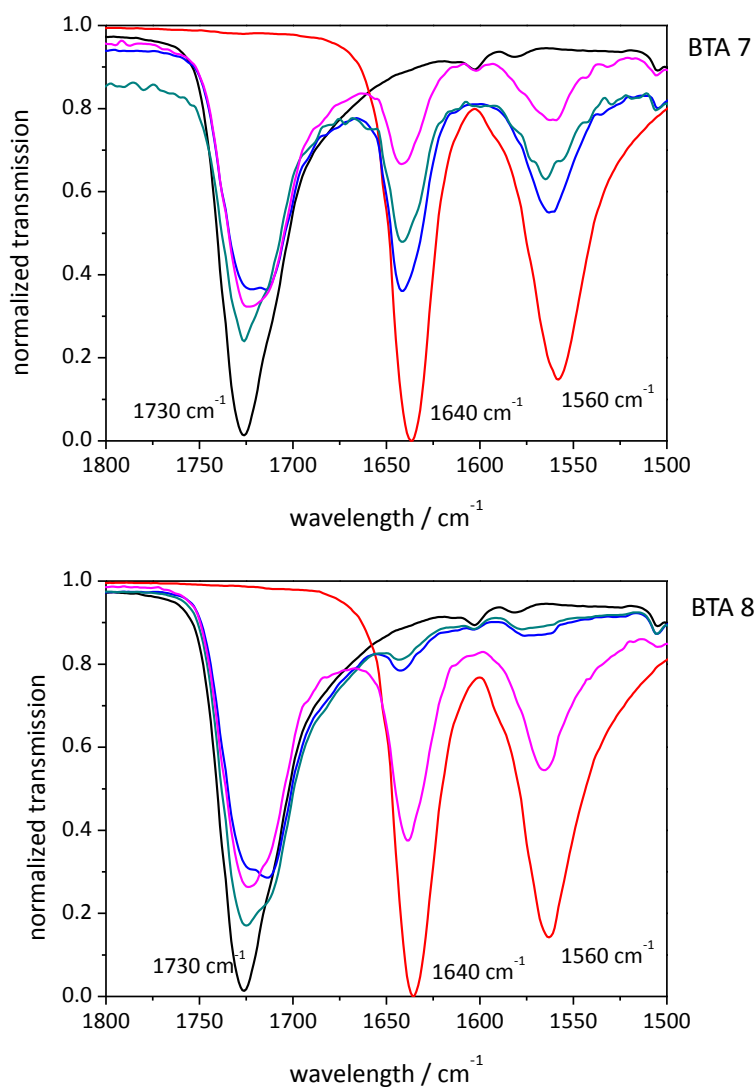


**Figure 4.27:** Normalized infrared spectra of the neat nonwoven scaffold (black), the neat BTA (red) and nanofiber-microfiber composites prepared from three different processing solvents (2-butanone (blue), isopropanol (green) and ethanol (pink)) in the range of 1500 cm<sup>-1</sup> to 1800 cm<sup>-1</sup>. Top: Composites containing BTA **7**. Bottom: Composites containing BTA **8**.

It was found that the corresponding signals at  $1640\text{ cm}^{-1}$  and  $1560\text{ cm}^{-1}$  were observed in all samples containing a 1,3,5-benzenetrisamide, although the intensity of the signals in samples processed from isopropanol and ethanol with BTA **8** appeared to be very weak but still visible. In all cases, the composites processed from 2-butanone exhibit the most visible signals for the BTA. This finding may be due to the most homogeneous distribution of the fibers throughout the nonwoven scaffold.

### *Conclusion*

Partially, the work performed in this chapter was reproduced based on previous work.<sup>[88]</sup> However, experiments were repeated and extended investigations provide a much deeper insight in the preparation of nanofiber-microfiber composites containing supramolecular nanofibers. The temperature dependent self-assembly behavior of the BTAs in all selected solvents was investigated by means of turbidity measurements correlating to results obtained by SEM analysis and filtration testing. It was shown that the developed preparation process for nanofiber-microfiber composites is highly reproducible and that prepared self-assembled nanofibers contain supramolecular columns featuring directed threefold hydrogen bonds connecting adjacent BTA molecules as evidenced by infrared spectroscopy. The morphology of supramolecular fibers based on 1,3,5-benzenetrisamides is very sensitive to processing parameters such as the selected solvent or the BTA concentration. It was demonstrated by capillary flow porometry that the homogeneity of supramolecular nanofiber distribution throughout the nonwoven is highly dependent on the selected BTA. Therefore, the nanofiber morphology can be influenced by selection of suitable processing parameters. One essential factor was found to be the temperature dependent solubility and self-assembly behavior, which has been investigated by means of turbidity measurements. BTA and solvent combinations that show formation of supramolecular structures during a cooling process at higher temperatures appear to be favorable for a more homogeneous preparation of nanofiber-microfiber composites compared to those exhibiting high solubility even at low temperatures. Filtration testing revealed that nanofiber-microfiber composites can be capable of removing more than 95% of particulate matter from air streams in air filtration. By proper selection of processing parameters, the *in situ* preparation of supramolecular nanofibers inside a nonwoven scaffold yields nanofiber-microfiber composites that have great potential for air filtration applications.

### 4.3.2 Nanofiber-microfiber composites based on BTA 4

Previously described results demonstrated that by utilization of alkyl-substituted 1,3,5-benzenetrisamides and a viscose/polyester model nonwoven, a nanofiber-microfiber composite can be prepared that is capable of efficiently removing particulate matter from air. So far, in all experiments the preparation process involved the use of polar organic solvents such as 2-butanone, isopropanol and ethanol. Therefore, work was conducted to adapt the preparation of nanofiber-microfiber composites from aqueous solvent systems to reduce the amount of these solvents towards aqueous solvent mixtures. Due to sufficient solubility of BTA 4 in a water/isopropanol mixture (60:40) at 75 °C and its self-assembly behavior, this BTA and solvent combination was selected for further investigations. In addition, a technical polyester nonwoven was utilized for the preparation of the composites. This nonwoven features an increased thickness compared to the previously used viscose/polyester model nonwoven and exhibits larger fiber diameters of the individual microfibers. Concentration dependent experiments to prepare nanofiber-microfiber composites using a technical polyester nonwoven were performed to evaluate the possibility to transfer this approach from the model nonwoven to a technical nonwoven scaffold.

#### *Concentration dependent preparation of nanofiber-microfiber composites*

Nanofiber-microfiber composites containing supramolecular nanofibers of BTA 4 were prepared from a water/isopropanol mixture (60:40) with varying BTA concentrations in the immersion solution ranging between 0.2 wt.-% and 1.0 wt.-%. The resulting nanofiber morphology was investigated by means of SEM analysis. **Figure 4.28** shows exemplarily SEM-images taken from nanofiber-microfiber composites as well as corresponding fiber diameter histograms.

It was found that increasing BTA concentrations in the immersion solution yield more densely filled composites with supramolecular fibers connecting the individual microfibers inside the nonwoven scaffold. The corresponding fiber diameter histograms are based on at least 150 individual fibers. Determined values for the mean fiber diameter of supramolecular nanofibers displayed in **Figure 4.28** are 567 nm for the composite prepared from a solution containing 0.2 wt.-% BTA. The corresponding value for the sample prepared from a 0.4 wt.-% solution is 540 nm. Remaining values are 563 nm (0.6 wt.-%), 553 nm (0.8 wt.-%) and 648 nm (1.0 wt.-%). It was found that changes of the BTA concentration in the immersion solution do not result in significant changes of the mean fiber diameter as well as the fiber diameter distribution. Only the sample prepared from a 1.0 wt.-% solution exhibited

a slightly increased value. In consequence, the fiber diameter of supramolecular nanofibers based on BTA 4 appears to be independent from the used concentration in the immersion solution.

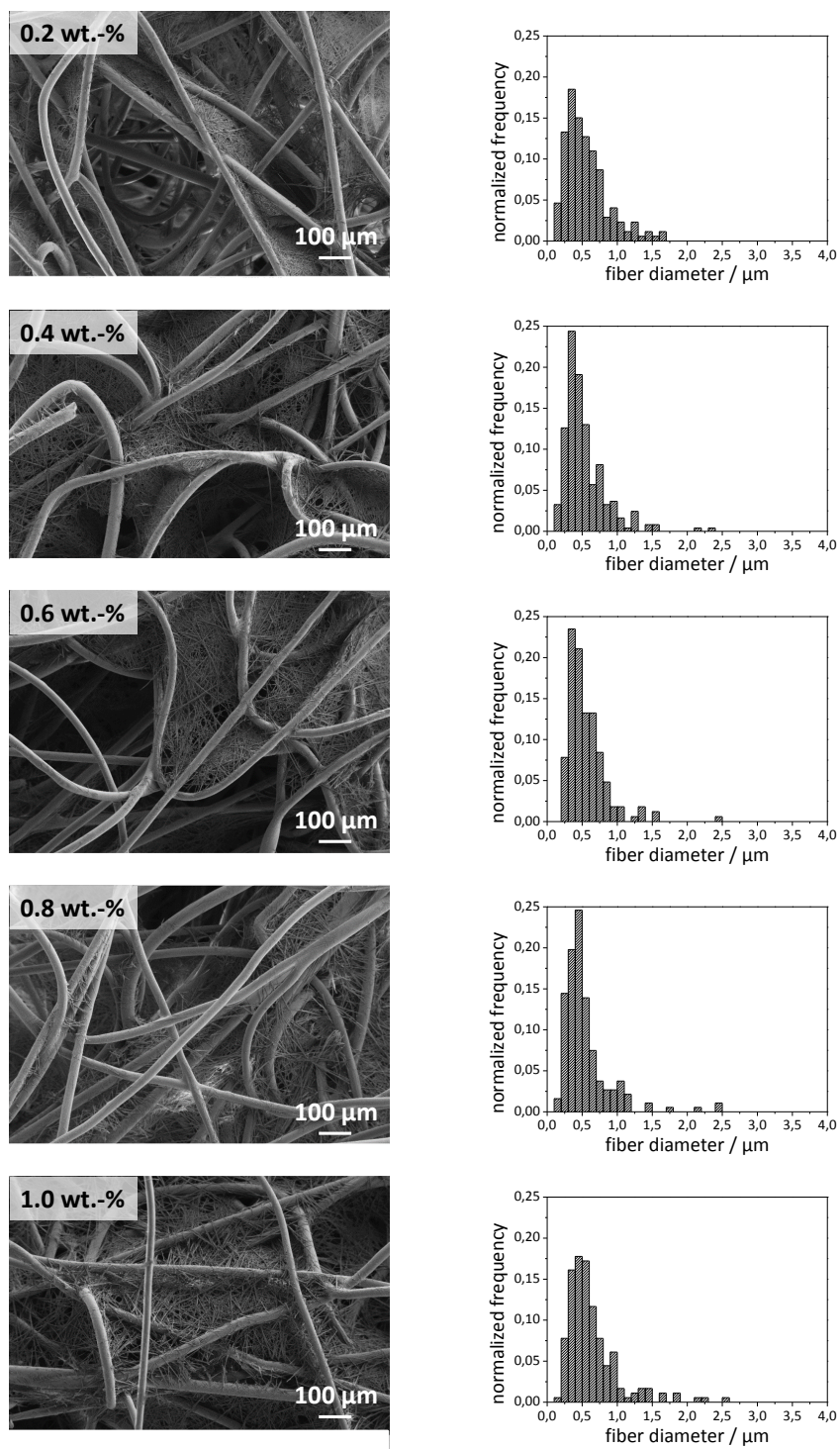


**Figure 4.28:** SEM micrographs of composites containing supramolecular nanofibers of BTA 4. Composites were prepared from a water/isopropanol mixture (60:40) containing different concentrations of BTA 8 between 0.2 wt.-% and 1.0 wt.-%. The corresponding histograms are based on at least 150 fibers.

*Mass fraction of supramolecular nanofibers in nanofiber-microfiber composites*

Differences in BTA concentration during the preparation process lead to varying mass content of supramolecular nanofibers in the resulting composites. Therefore, the amount of self-assembled fibers was determined gravimetrically in a series of experiments. **Figure 4.29** shows determined values for the BTA mass content depending on the BTA 4 concentration in the immersion solution. The results clearly show a linear correlation between the BTA concentration in the immersion solution and the resulting fiber content.

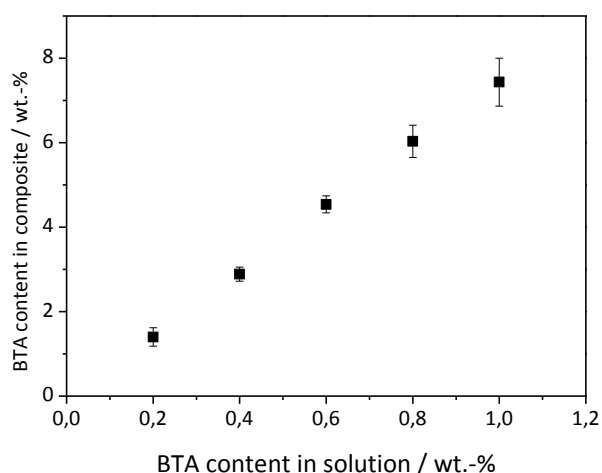


**Figure 4.29:** Content of BTA 4 in prepared nanofiber-microfiber composites as a function of BTA concentration in the immersion solution. Each data point displayed is based on the independent preparation of four composites.

The corresponding values and standard deviations of the mass content are 1.40 wt.-% ± 0.22 wt.-% (0.2 wt.-% in solution), 2.89 wt.-% ± 0.17 wt.-% (0.4 wt.-% in solution), 4.54 wt.-% ± 0.20 wt.-% (0.6 wt.-% in solution), 6.03 wt.-% ± 0.38 wt.-% (0.8 wt.-% in solution) and 7.43 wt.-% ± 0.58 wt.-% (1.0 wt.-% in solution). These values are based on 4 independently prepared nanofiber-microfiber composites.

*Filtration efficiencies of composites prepared from BTA solution with different concentrations*

Composites containing BTA 4 in different amounts were subjected to air filtration test experiments to evaluate the ability to remove particulate matter from air. **Figure 4.30** shows the recorded particle size dependent filtration efficiencies of composites prepared from solutions with different BTA concentration. Each curve represents an average of three independently prepared and tested samples. As reference, the filtration performance of the neat polyester nonwoven is displayed in **Figure 4.30** (filled squares). Without any supramolecular fibers inside the nonwoven, determined filtration

efficiencies were found to be mostly below 10%. By incorporating supramolecular nanofibers inside the scaffold, increased filtration efficiencies were observed. Even at low concentrations of BTA in the immersion solution of 0.2 wt.-%, the filtration efficiency increased to around 10%.

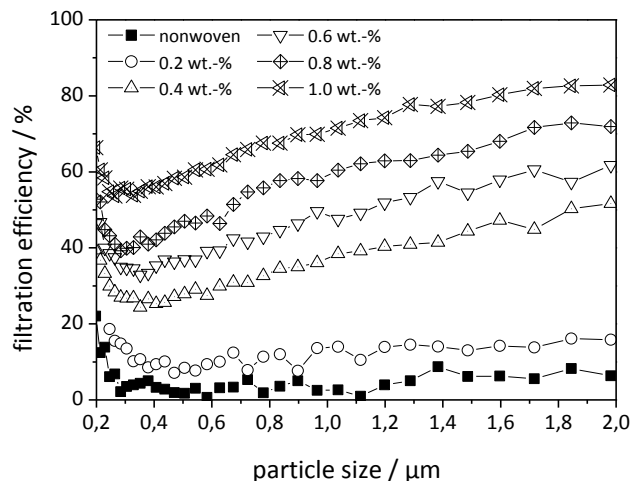


**Figure 4.30:** Particle size dependent filtration efficiencies of nanofiber-microfiber composites with BTA 4 prepared from water/isopropanol (60:40) with different BTA concentrations in the immersion solutions of 0.2 wt.-%, 0.4 wt.-%, 0.6 wt.-%, 0.8 wt.-% and 1.0 wt.-%. As reference, the nonwoven scaffold without supramolecular nanofibers is shown. The curves are based on an average of at least three independently prepared samples. Test conditions were: Filter area: 28.3 cm<sup>2</sup>; flow velocity: 25 cm/s; test aerosol: iso fine dust; upstream aerosol concentration: 30000 Particles/cm<sup>3</sup>; measuring time: 30 s.

Samples prepared from 1.0 wt.-% solutions exhibited efficiencies between 55 and 80% depending on the corresponding particle size, whereas the lowest values were recorded for particles with diameters between 0.3 and 0.4 μm. The neat nonwoven showed a differential pressure of 4 Pa ± 1 Pa. Corresponding values of the differential pressure and standard deviations are 7 Pa ± 2 Pa for samples prepared from 0.2 wt.-%, 26 Pa ± 10 Pa for 0.4 wt.-%, 35 Pa ± 10 Pa for 0.6 wt.-%, 47 Pa ± 16 Pa for 0.8 wt.-% and 57 Pa ± 6 Pa for a BTA concentration of 1.0 wt.-%. Even though the filtration efficiencies of these composites do not reach values as high as composites previously discussed in section 4.3.1, the corresponding differential pressures for these composites are about one and a half orders of magnitude lower than for composites containing either BTAs 6, 7 or 8 inside the viscose/polyester model nonwoven.

### *Conclusion*

The work performed in this section focused on the concentration dependent preparation of nanofiber-microfiber composites from an aqueous solution of BTA **4**. Replacement of pure organic solvents such as 2-butanone, isopropanol and ethanol by a mixture of water/isopropanol (60:40) demonstrates that the preparation process can be adapted to more environmentally friendly conditions. Furthermore, the process was transferred from the viscose/polyester model nonwoven to a technically relevant polyester nonwoven scaffold with differing morphology showing that the concept of preparation is not limited to a single support structure. The resulting composites were tested by means of air filtration efficiency and were found to exhibit improved filtration performances with very low differential pressures. The described results prove that supramolecular nanofiber based on 1,3,5-benzenetrisamides have a great potential to be used in air filtration applications and that further adaption of the preparation process may lead to even more efficient systems.

### 4.4 Conclusion

This chapter described within two main sections the preparation of nanofiber-microfiber composites containing supramolecular nanofibers of different 1,3,5-benzenetrisamides and the corresponding filtration performance of these composites in potential air filtration applications. In section 4.3.1, critical processing parameters such as the selected processing solvent were identified for the preparation of highly efficient composites to remove particulate matter from air. Solubility and self-assembly behavior of BTAs **6**, **7** and **8** have been investigated in three chosen solvents (2-butanone, isopropanol, and ethanol) by means of turbidity measurements. Composites prepared from 2-butanone exhibited the most homogeneous fiber distribution throughout the entire nonwoven resulting in composites with filtration efficiencies between 90 and 100% depending on the size of particles. Capillary flow porometry revealed that the pore sizes of the microfiber nonwoven can be significantly reduced by the incorporation of supramolecular nanofibers in the nonwoven scaffold. In addition, the preparation process has proven to be highly reproducible and infrared spectroscopic measurements confirmed the presence of supramolecular columns containing directed threefold hydrogen bonds in the resulting supramolecular structures.

In the second part of this chapter (4.3.2), the preparation process was transferred from the viscose/polyester model nonwoven to a technical polyester nonwoven and the self-assembly system has been adapted to the use of solvent systems featuring lower contents of organic solvents. The resulting composites exhibited high filtration efficiencies with low values for the differential pressure. Work presented within this chapter proves supramolecular nanofibers to have high potential for air filtration applications when employed inside a nonwoven scaffold.

## 5 Sand - supramolecular nanofiber filters for the removal of bacteria from water

### 5.1 Introduction

#### *Current situation in water treatment*

Due to the consumption of untreated ground or surface water that is contaminated with microbial pathogens, millions of people suffer each year from waterborne diseases. Especially children under the age of five as well as human immunodeficiency virus (HIV) –infected adults in developing countries are at risk of becoming infected by water transmitted microbial diseases.<sup>[106]</sup> Among others, acute diarrheas, bacillary dysentery, typhoid fever and even cholera can result from the consumption of such contaminated water.<sup>[148]</sup> Today, approximately 748 million people around the world do not have access to a source providing safe drinking water.<sup>[149]</sup> A field study in Lima, Peru revealed that the majority of patients with acute diarrheal diseases originate from regions of low socioeconomic status.<sup>[150]</sup> Interventions to improve water quality by removing microbial contamination have proven to reduce the number of occurring diarrheal diseases. Such interventions can be divided in two main categories. On the one hand, they can be based on a facility that treats the drinking water at one central location and the treated water has to be delivered to the individual households. Other approaches to treat water rely on the decontamination of water at the individual households.<sup>[151]</sup> Due to possible recontamination during delivery or storage, household based water treatment solutions appear to be potentially more effective. These solutions rely on the empowerment of people to treat their own drinking water right at the point of use (POU). Sobsey et al. reported that any water treatment technology at the point of use has to be integratable into the daily life of people using it. Besides the ability to efficiently remove pathogen bacteria from drinking water, many key characteristics have to be fulfilled by a possible solution such as low costs, quantities of water produced per time interval and the time a user has to spend to treat drinking water.<sup>[152]</sup> Apart from the pure development of a filter unit that is capable of removing microbial pathogens from water, successful application of products for point of use water disinfection has to be assessed by field studies and depends on many different parameters.<sup>[153,154]</sup>

A variety of different POU technologies have been developed and evaluated by means of social and economic sustainability.<sup>[101,155]</sup> For example, irradiation of untreated and aerated water with solar UV-light is a suitable method to treat microbial contamination in water. Therein, bottles comprised of polyethylene terephthalate (PET) are filled with source water and are exposed for several hours to

sunlight.<sup>[156]</sup> Even though this kind of treatment has been proven to reduce to the occurrence of diarrheal diseases, very turbid source water cannot be treated efficiently this way due to insufficient UV light penetration.<sup>[101,152]</sup> In addition, this method usually utilizes PET bottles with common volumes of 1 to 2 L and is therefore associated with a low yield compared to other technologies. However, further studies have been performed to investigate the combination of photocatalytic nanoparticles and UV light for the disinfection of water.<sup>[98,157–159]</sup>

Another common and inexpensive method to treat source water is by chlorination allowing for a fast preparation of large amounts of drinking water. By adding small amounts of a concentrated solution of hypochlorite to source water, most microbial pathogens are significantly reduced. Nevertheless, the disinfection of water with high contents of organic matter results in the generation of byproducts and decreases the efficiency. Due to the fact that for very turbid water no visible improvement of water quality can be observed by this method, many consumers tend to question the effectiveness.<sup>[101,152]</sup> Therefore, water treatment units have been reported that combine the concept of physical filtration and chlorination.<sup>[160]</sup> In addition, generation of byproducts usually also yield changes in taste of the treated water.

Apart from the previously described technologies, it was found that porous ceramic media can also be used as ceramic filter that can also be used to improve the quality of drinking water.<sup>[97,100,108]</sup> Thereby, the filter media can be produced in the developing countries close to the point of use and are usually operated by gravity driven filtration. To ensure constantly sufficient flow rates, the ceramic filters require periodic cleaning of the surface to prevent clogging. Comparing a central water treatment right at the source and in contrast the utilization of ceramic filters at the point of use, this household based solution was identified to be more cost-effective.<sup>[98,152]</sup>

In addition, biosand filters have been promoted as suitable point of use technology to treat drinking water. One of the most common setups utilizes a concrete housing that is filled with a sand material in large amounts. Over a period of around two weeks, a biofilm establishes inside the filter, which is essential to reach the maximum filtration efficiency.<sup>[107,109,161]</sup> It was found that the use of such filtration systems can lead to reduced occurrences of diarrheal diseases.<sup>[162]</sup>

Even though all of the described point of use water treatment technologies are capable of removing bacteria from water, all of these solutions feature strengths as well as weaknesses, for example with respect to cost, treatment time, yield or potential taste problems. Therefore, there is still a need for new ways to prepare filters that are capable of treating water by means of microbial contamination.

It was already demonstrated by Krieg et al. that a membrane comprised of supramolecular fibers that was deposited on top of a syringe filter can be utilized for liquid filtration applications. The supramolecular fibers can be used for the size-selective separation of nanoparticles from water.<sup>[145,146]</sup> Also biomolecules can be separated from water and immobilized enzymes still exhibit catalytic activity.<sup>[147]</sup>

In this thesis, a new approach utilizing supramolecular chemistry is developed to prepare a filter unit to remove microbial contamination from water. As shown before, supramolecular chemistry provides a bottom-up approach for the *in situ* preparation of supramolecular nanofibers via self-assembly of small molecules. Based on the previously conducted work on nanofiber-microfiber composites for air filtration applications, this chapter reports on the development of a sand bed that contains supramolecular nanofibers formed by the *in situ* self-assembly of 1,3,5-benzenetrisamides inside the voids of the granulate material. The underlying concept of the preparation of such a filter is schematically shown in **Figure 5.1**. A granulate material is placed in a suitable container and soaked with a clear solution of BTA at elevated temperatures (**Figure 5.1 (A)**). By applying a cooling step and a solvent replacement step, the supramolecular nanofibers inside the granulate material are formed *in situ*. The nanofibers interconnect the individual sand particles and are present in the voids of the granulate material (**Figure 5.1 (B)**).

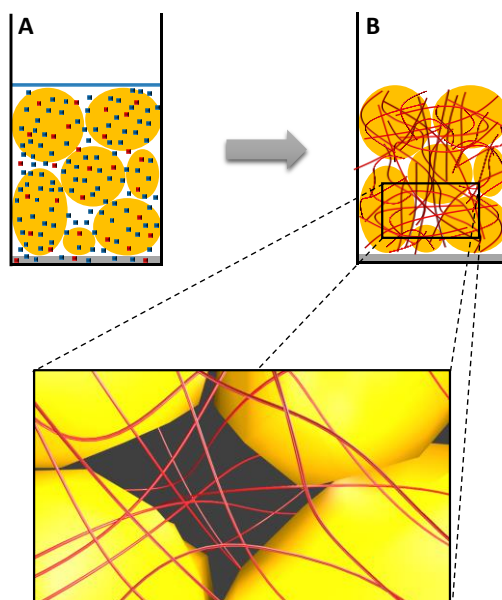


**Figure 5.1:** Schematic representation of the *in situ* preparation process of supramolecular nanofibers inside a granulate material. (granulate material: yellow grains; solvent: blue dots; dissolved 1,3,5-benzenetrisamide: red dots; supramolecular nanofibers: red fibers) First, the granulate material is fully soaked at elevated temperatures with a clear solution of a 1,3,5-benzenetrisamide (A). During cooling, self-assembly occurs and supramolecular nanofibers are formed within the granulate material (B).

The same 1,3,5-benzenetrisamides as used for the preparation of nanofiber-microfiber composites for air filtration applications (chapter 4) was selected to prepare the sand beds containing supramolecular nanofibers. The 1,3,5-benzenetrisamide (BTA **7**) exhibits a branched alkyl-substituent (**Figure 5.2**) and shows a temperature dependent solubility in 2-butanone. In contrast to the preparation of nanofiber-microfiber composites for air filtration, the approach for the preparation of supramolecular nanofibers in the voids of a granulate material is only based on a temperature change of a BTA solution and not on the additional evaporation of the solvent. Therefore, a strongly temperature dependent solubility behavior of the BTA in the selected solvent is essential.

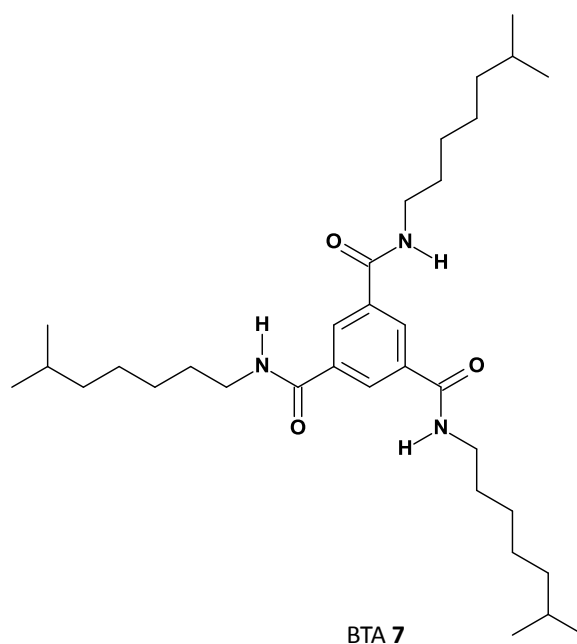


**Figure 5.2:** Molecular structure of the selected 1,3,5-benzenetrisamide (BTA **7**) with branched alkyl substituents.

The work presented in this chapter includes the development of a suitable preparation process to obtain mechanically stable filters with supramolecular nanofibers inside a granulate material that are applicable to liquid filtration processes. SEM analysis of the granulate material – supramolecular nanofiber material was performed to evaluate the resulting nanofiber morphology of supramolecular nanofibers inside the granulate bed. All filters were prepared inside a selected container with defined geometry. A filtration test setup and a filter test based on a suspension of polystyrene micro-particles in water was developed allowing to evaluate and optimize prepared sand beds with supramolecular nanofibers. In addition, the differential pressure during the filtration test experiments was monitored to investigate the stability of the filter units during the process. After optimization of the system by

filtration test experiments of polymer particles from water, the sand bed – nanofiber filters were subjected to further experiments to filter *E. coli* bacteria from water.

## 5.2 Preparation of filter units composed of sand and supramolecular nanofibers

Work performed in the course of this project involved the preparation and characterization of sand beds containing supramolecular nanofibers. All materials used and the experimental details on the preparation and characterization procedures are described in the following.

### *Materials*

*N,N',N''*-tris(6-methylheptyl)benzene-1,3,5-tricarboxamide (BTA **7**) was selected for the preparation of the filters with sand grains. The synthesis and the characterization are described in detail in the appendix (chapter 8.8). All solvents were commercially available from Aldrich and were used as received.

As granulate material, purified and calcinated sea sand (Grüssing, listed grain size: 0.3 mm, acid purified and calcinated) was selected. This granulate material was used without further purification. **Figure 5.3** shows an overview SEM image of the individual sand particles featuring various sizes mainly between 50 and 200  $\mu\text{m}$  with different shapes and surface roughness. This material is commonly used in liquid column chromatography and is free of any supporting additives.

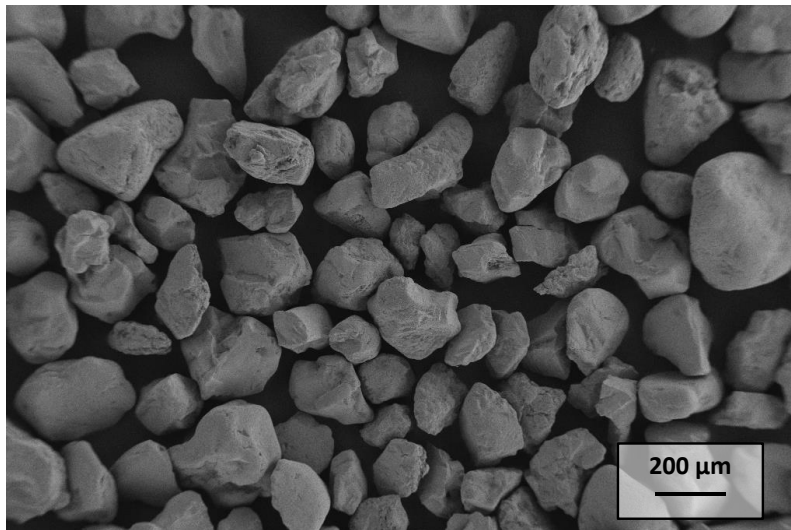


**Figure 5.3:** SEM-image of sea sand (Grüssing, listed grain size: 0.3 mm, acid purified and calcinated) utilized for the *in situ* preparation of sand bed - supramolecular nanofiber filters.

*Preparation and modification of the containers*

Each sand bed containing supramolecular nanofibers was prepared in a commercially available cylindrical film canister as shown in **Figure 5.4**. These containers comprised of HDPE were resistant to the utilized solvents. The inner diameter of the containers was 30 mm, the outer diameter was 32 mm and the height was 48 mm. The sand bed – supramolecular nanofiber filters were directly prepared inside these containers. Prior to the filter preparation process, the film canisters had to be modified.

As shown in **Figure 5.4 (A)**, in the bottom of the containers 30 to 40 homogeneously distributed holes were punched with a cannula with an outer diameter of around 0.9 mm. To prevent the sand from falling through the holes, the bottom of the container was covered with a filter paper (type: 601A) featuring a pore size of 5 – 13  $\mu\text{m}$  (see **Figure 5.4 (B)**). The diameter of this round filter paper was 30 mm corresponding to the inner diameter of the container. 25 g of commercially available sand were utilized as granulate material for the preparation of sand beds containing supramolecular nanofibers. **Figure 5.4 (C)** displays a finished container with a filter paper and 25 g of sand suitable for the *in situ* preparation process of supramolecular nanofibers in the voids of the sand bed.

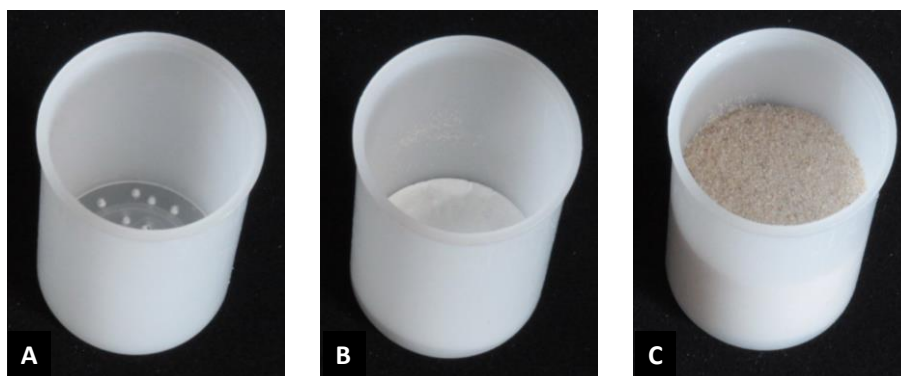


**Figure 5.4:** Film canisters utilized as filter containers for the preparation of sand beds with supramolecular nanofibers. The bottom of the containers was homogeneously equipped with around 30 to 40 holes with a diameter of around 0.9 mm (A). A filter paper was used to cover the bottom of the container (B). The containers were filled with 25 g of granulate material (C).

*Preparation of sand beds with supramolecular nanofibers*

First, 200 g of a solution of BTA **7** in 2-butanone with a concentration of 1.0 wt.-% was prepared in a 250 mL storage glass by dissolving solid BTA at a temperature of 50 °C. The mixture was constantly stirred until a clear solution was obtained. For the *in situ* preparation of supramolecular nanofibers inside the sand, a four step preparation process was developed. **Figure 5.5** illustrates schematically this process. During the first step, a prepared container with a filter paper on the bottom and 25 g of sand on top is immersed into a clear solution of BTA **7** in 2-butanone at 50 °C, until the sand is fully soaked. During this immersion process, the BTA solution fills the voids of the granulate material and penetrates the material through the holes on the bottom of the canister. The solution is not allowed to enter the canister through the top opening avoiding movement of the sand particles. The immersion process is exemplarily shown in **Figure 5.6**. The canister containing the soaked sand is placed in a polyethylene bag and the closed. The bag is cooled to a temperature of -78 °C for 30 min (Step 2) by use of a mixture of ethanol and dry ice. The cooling temperature was selected to ensure complete self-assembly of the BTA from the solution. After 30 min of cooling, the containers were allowed to warm to room temperature within 3 to 5 min. The change in temperature induces the formation of nanofibers that connect the individual sand particles forming a network throughout the entire granulate material. Due to the fact that the self-assembly process is very sensitive to the used solvent, the plastic bag ensured that 2-butanone remains the only solvent inside the canister. Mixing of the cooling agent with 2-butanone would result in drastic changes of the resulting nanofiber morphology.

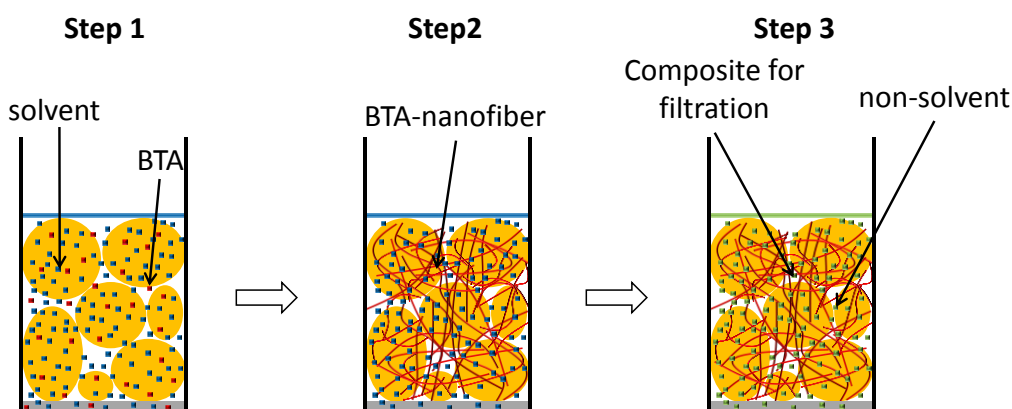


**Figure 5.5:** Schematic representation of the *in situ* preparation process of filter units containing supramolecular nanofibers inside a granulate material here sand. A container filled with a defined amount of sand is immersed into a clear BTA solution at elevated temperatures until the sand is fully soaked (Step 1). The system is cooled down to induce the *in situ* formation of supramolecular nanofibers within the voids of the granulate material (Step 2). The solvent of the BTA solution is replaced by water (non-solvent) without damage to the supramolecular nanofiber network (Step 3).

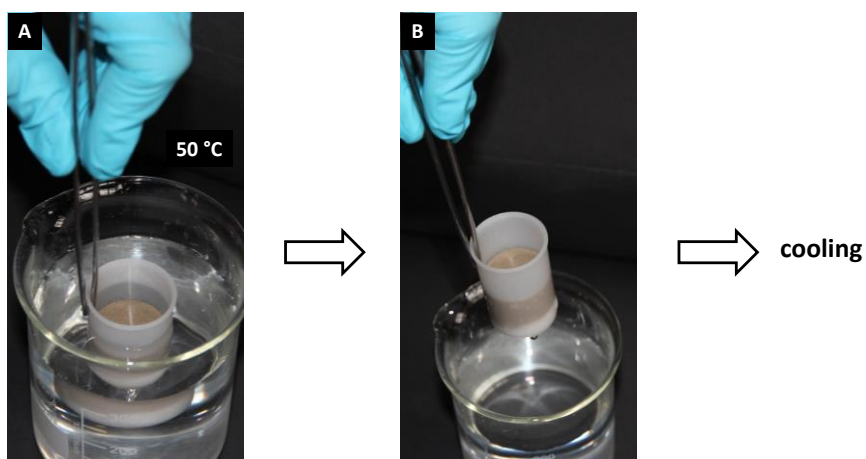


**Figure 5.6:** Photographs of the experimental immersion process of modified film canisters filled with sand in a clear BTA solution. The BTA solution is not allowed to swap over the edge of the container. The granulate material is fully soaked through the holes at the bottom of the container until the solvent reaches the surface.

In the third step, a solvent exchange was performed replacing 2-butanone by water, which is a non-solvent for the supramolecular nanofibers. The sand bed with supramolecular nanofibers is purged with pure water (around 50 mL) and a stable unit is obtained that can be sealed and stored for several days before filtration testing. During this step the supramolecular nanofiber network is preserved from being damaged during the storage at room temperature.

For further characterization of the unit's structure by SEM analysis, drying of the material is possible. A film canister containing the dried material was turned upside down and gently tapped until it loosened from the wall of the container. The remaining and dimensionally stable combination of sand and supramolecular nanofibers was then carefully divided into two pieces with a scalpel. Then, a SEM sample holder equipped with adhesive and conductive foil was utilized to pick up the supramolecular nanofibers and the sand particles from the cut surface.

#### *Characterization of sand - supramolecular nanofiber filters*

The characterization of the sand with supramolecular nanofibers can be divided into two parts. The first part corresponds to the characterization of the morphology of the supramolecular nanofibers in the voids of the sand by SEM analysis. The second part will be discussed in the following sections and refers to the analysis of units by means of liquid filtration performance.

One key requirement for a filter unit containing sand with supramolecular nanofibers is a homogenous distribution of fibers throughout the entire granulate material. An inhomogenous distribution might result in pathways through the unit that allows particles to penetrate the filter without being separated from the liquid phase.

The concept of the preparation of these filter units was already designed in a way that the individual particles can be fully connect resulting in a stable network. To prove that a stable material can be obtained, a sample was prepared with the following preparation parameters: Solvent: 2-butanone, BTA concentration: 1.0 wt.-%, immersion temperature: 50 °C, cooling temperature: -78 °C, cooling time: 30 min, non-solvent: water, total mass of granulate material: 25 g. After the filter unit was fully dried, it was removed from the container by turning it upside down and tapping on the outside of the container until the material left the container. **Figure 5.7** shows a comparison between 25 g of just plain sand (left) and the corresponding dried sand with BTA (right). It was found that the combination of sand and supramolecular nanofibers features dimensional stability upon removal from the container, whereas the plain granulate material without any supramolecular fibers falls apart. Only 50 mg of BTA **7** are already sufficient to stabilize an amount of 25 g of the sand, which corresponds roughly a nanofiber content of only 0.2 wt.-%. The material could even be lifted up by hand without any damage to the structure. This result indicates that supramolecular nanofibers were homogeneously distributed throughout the granulate material. An inhomogeneous distribution of nanofibers might have resulted in a far less stable material.



**Figure 5.7:** Photograph of 25 g of sea sand and a sand bed with supramolecular fibers consisting of 25 g of sand and about 50 mg BTA **7** demonstrating the dimensional stability of the prepared samples. Preparation parameters: Solvent: 2-butanone, BTA concentration: 1.0 wt.-%, immersion temperature: 50 °C, cooling temperature: -78 °C, cooling time: 30 min, non-solvent: water, total mass of granulate material: 25 g.

The sample displayed in **Figure 5.7** was investigated by means of SEM analysis. Therefore, it was cut horizontally in two equally sized pieces and a sample was taken from the inside of the granulate material utilizing a SEM sample holder that was equipped with adhesive and conductive tape. **Figure 5.8** shows an overview SEM image of two sand particles that are connected by supramolecular nanofibers based on the self-assembly of BTA **7** and the corresponding fiber-diameter histogram.

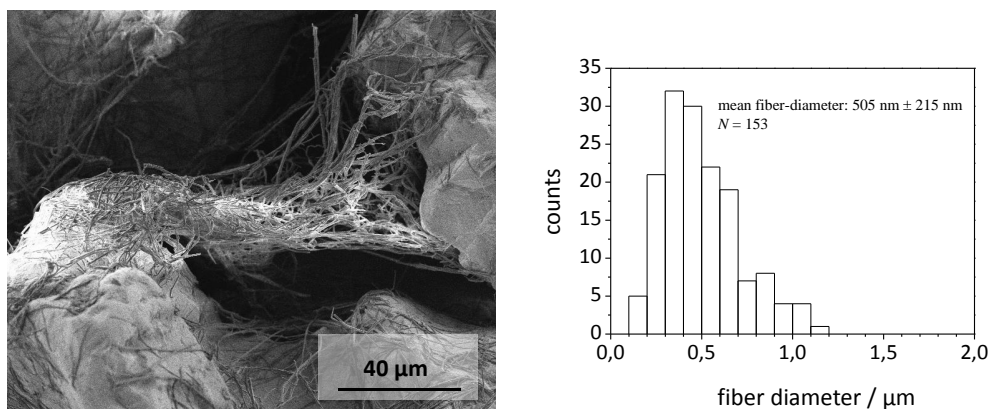


**Figure 5.8:** SEM-Images of supramolecular nanofibers of BTA **7** connecting individual sand particles. Corresponding fiber diameter histogram is based on at least 150 fibers. The mean fiber diameter of the supramolecular nanofibers is 505 nm. Preparation parameters: Solvent: 2 butanone, BTA concentration: 1.0 wt.-%, immersion temperature: 50 °C, cooling temperature: -78 °C, cooling time: 30 min, non-solvent: water, total mass of granulate material: 25 g.

Even though due to the sample preparation, a shift of the individual sand particles relative to each other could not be avoided, the nanofibers still connect the particles. The fiber diameter histogram was prepared in intervals of 100 nm and is based on 153 fiber diameters of individual nanofibers. The mean fiber diameter was found to be 505 nm with a standard deviation of 215 nm. Since the SEM sample was taken from the inside of the granulate material, it is assumed that supramolecular nanofibers are distributed throughout the entire granulate material. This assumption is supported by the remarkable dimensional stability of the material after removal from the container.

### 5.3 Development of a liquid filtration test setup

In order to evaluate the function of the sand - supramolecular nanofiber filters, a custom-made liquid filtration test setup was developed. The development involved two main parts. First, the overall structure of the liquid filtration test setup had to be designed and build that allowed for the filtration of water under pressure and a constant flow rate. The second part corresponds to the development of a custom-made sample holder that is optimized to the selected geometry of the filter units. The experimental setup as well as all details concerning the implementation of the test experiments are described in the following.

#### *Setup for liquid filtration experiments*

A custom-made test setup for liquid filtration testing was developed. The top of **Figure 5.9** is a scheme of the designed test setup for continuous filtration test experiments to remove polymeric micro-particles from water.

The water with micro-particles is kept in a *storage vessel* (30 L), which was equipped with a mechanical stirrer to ensure a homogenous distribution of polymer micro-particles throughout the entire suspension. In addition, clean water is kept in a second *storage vessel* (5 L) that enables purging of the system. A *three-way valve* (PTFE; bore diameter: 3.5 mm; outer diameter connectable tubing: 8 mm; BOLA) allows for the switching between a storage vessel for clean water and a storage vessel for water with micro-particles. All components schematically associated in **Figure 5.9** with solid lines are connected with PTFE-tubes (outer diameter: 8 mm; BOLA) and straight screw-in plug connections featuring a thread connection of  $\frac{1}{4}$ ". A *gear pump* (MCP-Z; Ismatec; pump head No.: MI 0018) allows for the transportation of water through the filtration test setup. If no tubing is connected to the low pressure side of the pump, it is capable of reaching flow rates of up to 5.6 L/min. The maximum differential pressure corresponds to a value of 3.5 bar. A *flow-meter* (FLR-1605A; Omega) in combination with a custom-made *control system* (electronic workshop; University of Bayreuth) provides precise control of the volumetric flow through the entire test setup. The differential pressure, which is the difference in pressure before and after the filtration unit, can be measured with two installed *pressure transducers* (PAA33X-V-10; Omega). A *detector* (Welas 2100 FL; PALAS) at the end of the filter test setup is used for the online determination of the particle size distribution as well as the particle number being in the water after passing through the setup. A particle range with sizes between 0.6 and 29  $\mu\text{m}$  is detectable. The detector requires a consistent volumetric flow without any significant variations as well as a minimum flow of 500 mL/min. The detector is connected to an analyzing unit

(Welas digital 2000, PALAS). All data are recorded on a *Laptop*. The filtered water was gathered in a collection vessel.

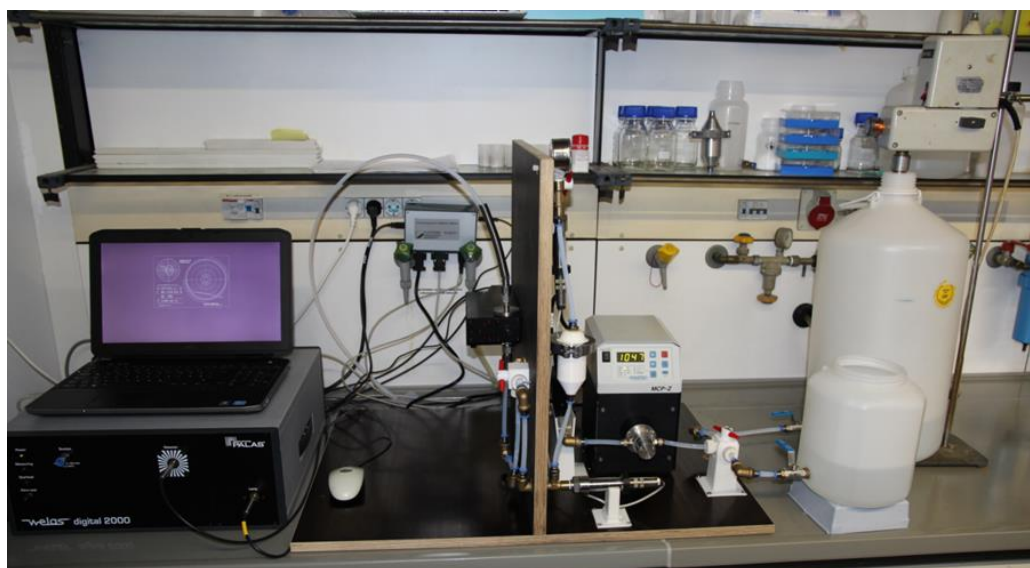
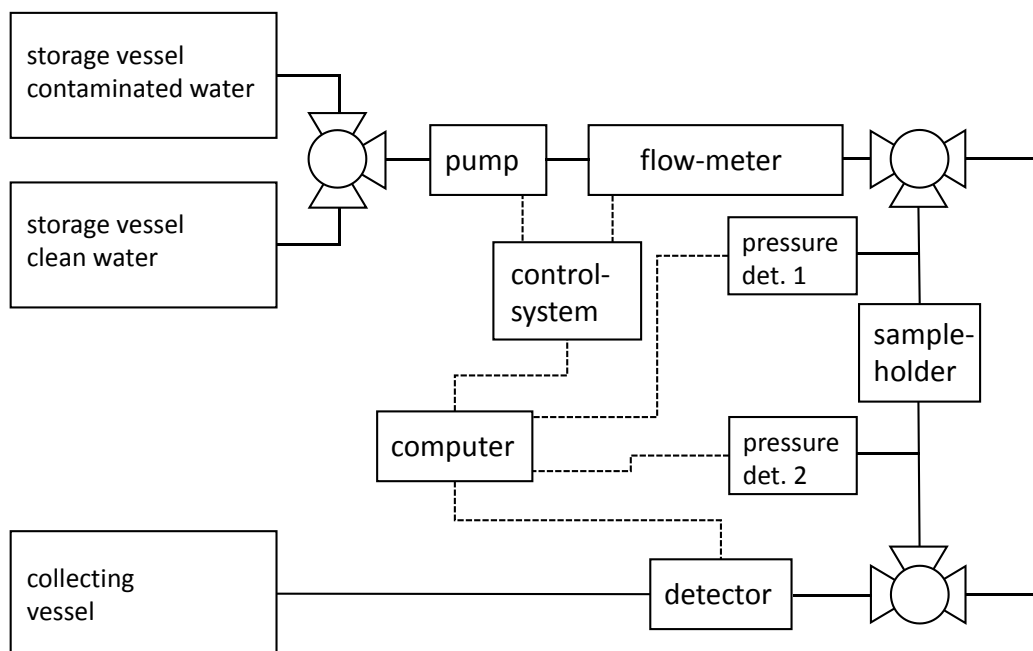


**Figure 5.9:** Top: Scheme of the test setup for the evaluation of filter units by means of liquid filtration performance of polymeric micro-particles from water. Bottom: Photographic image of the liquid filtration test setup.

### *Sample holder*

In the course of the project, a sealable and pressure resistant sample holder for filtration test experiments of prepared filter units had to be designed. During the development of the preparation process to sand - supramolecular nanofiber filters, a variety of different geometries were tested.

The use of many different filter geometries during the project required the possibility to quickly adapt a sample holder to a new geometry. To enable these quick changes, 3D printing technique based on fused deposition modelling (FDM) was utilized to prepare suitable sample holders. Polylactic acid (PLA) was selected as material for manufacturing of the sample holders. To illustrate the development of such a sample holder, **Figure 5.10** displays a technical drawing and a photographic image of an early version of such a sample holder consisting of different individual components. The technical drawing corresponds to the 3D-printed objects that were further modified after the printing process was completed. A hole with a diameter of 4 mm was drilled through the sample holder along the longitudinal axis after the manufacturing process was finished. This opening enabled purging the sample holder. The 14 mm opening in the top and the bottom part were equipped with straight screw-in plug connections featuring a thread connection of  $\frac{1}{4}$ ". The connection was mounted by the use of multicomponent glue. The bottom part of the sample holder was equipped with a semi-circle shaped indentation to provide enough space to place a polymer sealing ring with a diameter of the cross section of 5.4 mm into this indentation to improve the contact between the sealing ring and the PLA material of the sample holder. By pressing the top and the bottom part together with a clamping ring, the sample holder was sealed and pressure resistant. However, the selected container geometry shown in **Figure 5.10** had some disadvantages due to technical reasons. First, the particle detector at the end of the test setup requires a minimum volumetric flow of 500 mL/min. Considering the small diameter of the container, differential pressures building up during the filtration process were reaching the limit of the gear pump and other parts on the setup. In consequence, the sample holder had to be developed further.

The previously described film canister as container with an inner diameter of 30 mm, an outer diameter of 32 mm and a bottom area of 7.06 cm<sup>2</sup> was selected to provide the final geometry for the filter unit. The sample holder was modified to the geometry shown in **Figure 5.11**. The bottom part of the sample holder was produced via 3D printing technique and equipped with a straight screw-in plug connection connectable to tubing with an outer diameter of 8 mm. As material, this version of the sample holder was also made of polylactic acid. A filter cartridge consisting of a container and the prepared material was first placed in an inner centering ring typically used in vacuum technology. In

addition, it was equipped on the outside with an additional sealing ring and placed in the bottom part of the sample holder.

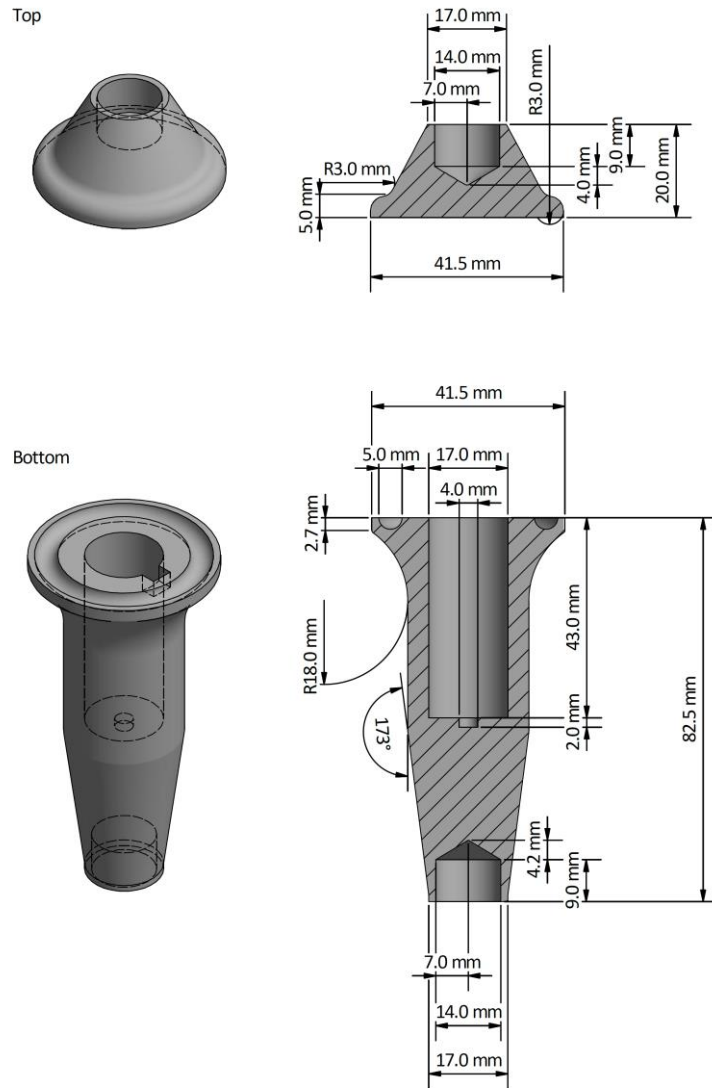


**Figure 5.10:** Technical drawing and photographic images of an early version of a custom-made sample holder for filter units prepared inside a polymer cartridge. The bottom part of the sample holder was manufactured by utilization of 3D printing and equipped with a straight screw-in plug connection. A filter cartridge was placed in the bottom part of the sample holder being equipped with a sealing ring. The top part of the sample holder is placed on top of the filter cartridge and sealed with a clamping ring.

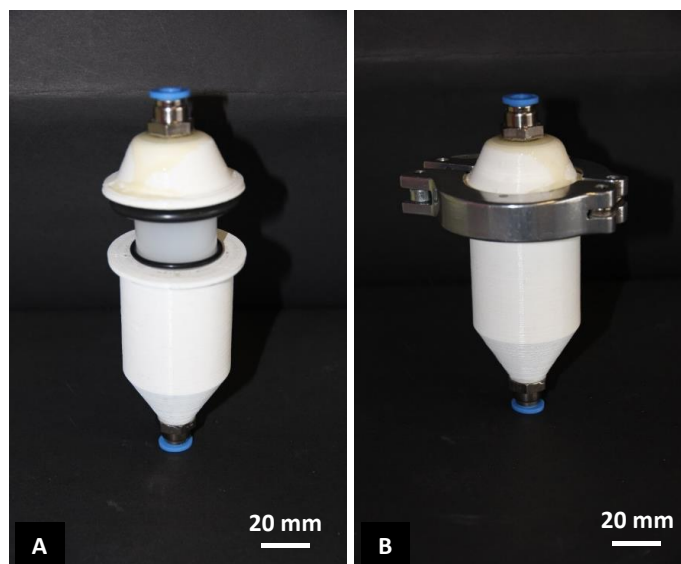
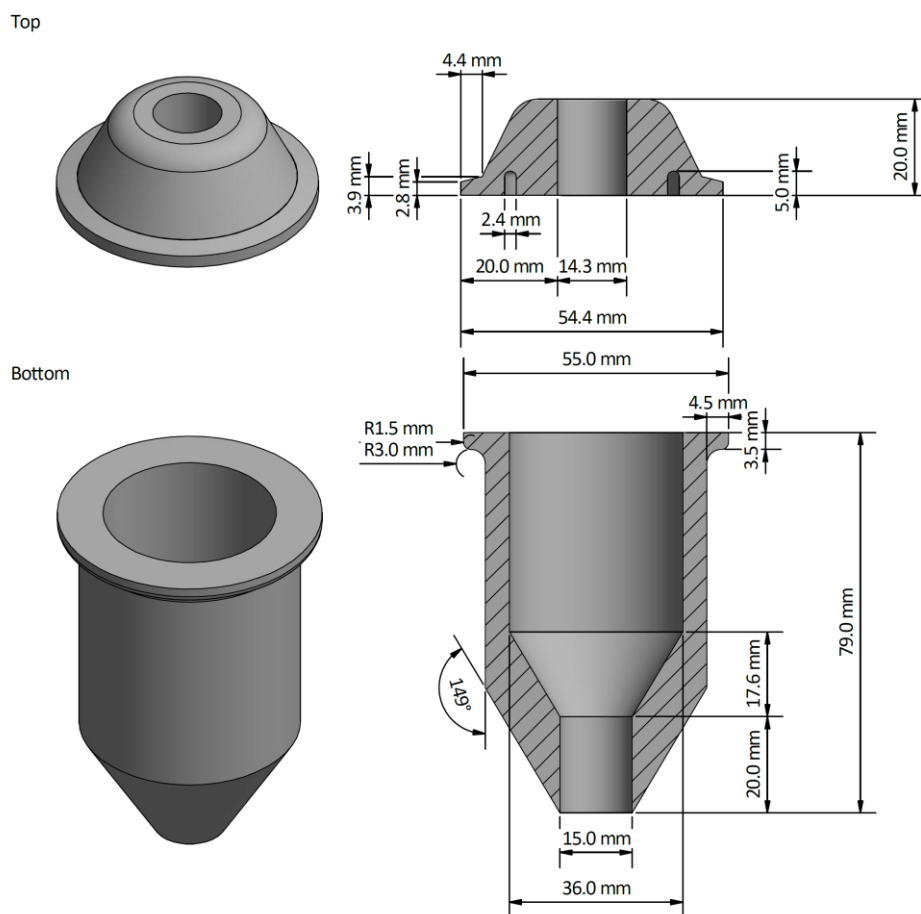


**Figure 5.11:** Technical drawing and photographic images of the final version of a custom-made sample holder that allows the easy exchange of the filter containers. The bottom and the top part of the sample holder was manufactured by utilization of 3D printing and equipped with a straight screw-in plug connection. A container is placed in the bottom part of the sample holder being equipped with a sealing ring and an inner centering ring. The top part of the sample holder is placed on top of the filter cartridge and sealed with a clamping ring.

Analogous to the bottom part, the top part of the sample holder was also fabricated by 3D printing and placed on top of the filter container (**Figure 5.11**). The sample holder can be sealed with a clamping ring pressing both parts together providing pressure resistance of at least 1.5 bar. As shown in **Figure 5.9**, two three way valves (PTFE; bore diameter: 3.5 mm; outer diameter connectable tubing: 8 mm; BOLA) allowed for disconnection of the sample holder from the rest of the test rig. The application of a continuous water flow at elevated pressures as well as the possibility to quickly exchange the filter containers is realized with this sample holder.

One basic requirement for the function a liquid filtration test setup is the possibility to purge the filter unit with water including polystyrene micro-particles as test contamination at a constant flow rate and under pressure. Therefore, an experiment to demonstrate the applicability of the developed setup was performed. A container filled with 25 g of sand and including the filter paper was placed in the sample holder and purged with water with micro-particles at a constant flow rate of 500 mL/min. The evolution of the differential pressure during the experiment is displayed in **Figure 5.10**. It was found that the differential pressure remains constant during the measurement with values of around 150 mbar. The applied volumetric flow rate during such an experiment is directly proportional to the differential pressure. The observed results demonstrate that the volumetric flow rate is stable, because the differential pressure remains constant during the whole measurement. Also in 24 h experiments, the volumetric flow rate was kept constant.

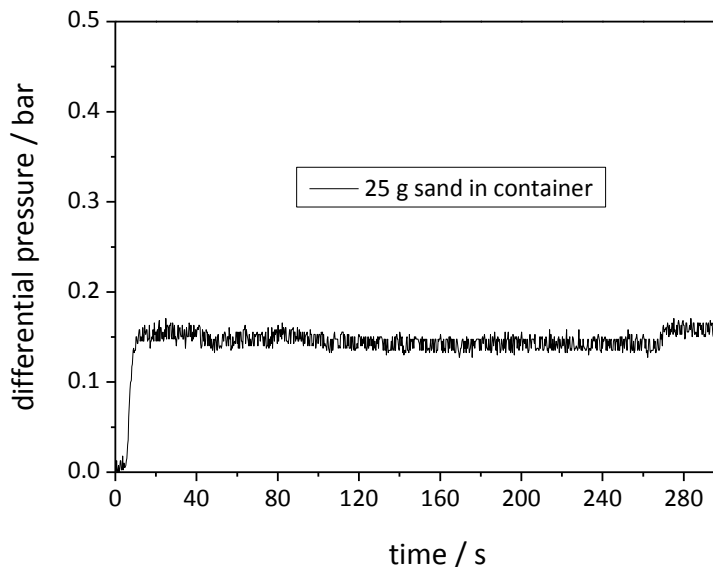


**Figure 5.12:** Time dependence of the differential pressure during filtration process of a container filled with 25 g of pure sand including the filter paper. Measuring parameters: Total mass of granulate material: 25 g, Volumetric flow rate: 500 mL/min, Total volume filtered: 2.5 L, Filter area: 7.06 cm<sup>2</sup>.

*Filtration of polymer micro-particles as model system*

Evaluation of the filtration efficiency of a prepared sand - supramolecular nanofiber filter was performed as follows. First, a suspension of polymer micro-particles in water was prepared by adding 25  $\mu\text{L}$  of a 10 wt.-% suspension of polystyrene particles (mean diameter: 1.1  $\mu\text{m}$ ; Aldrich) to 30 L of water. These particles were selected because many bacteria exhibit sizes in the range of 1  $\mu\text{m}$ . **Figure 5.13** shows an SEM image of the employed particles after drying of the suspension. The suspension was continuously stirred for at least 30 min with a mechanical stirrer. Constant stirring during the entire measuring process provided a homogeneous suspension. The particle size-distribution as well as the particle number of a defined amount of the pure suspension was measured. Experiments were performed with total volumes of either 2.5 L or 10 L. Therefore, the suspension was conducted through the liquid filtration test setup at a volumetric flow rate of 500 mL/min with an empty container placed inside the sample holder.

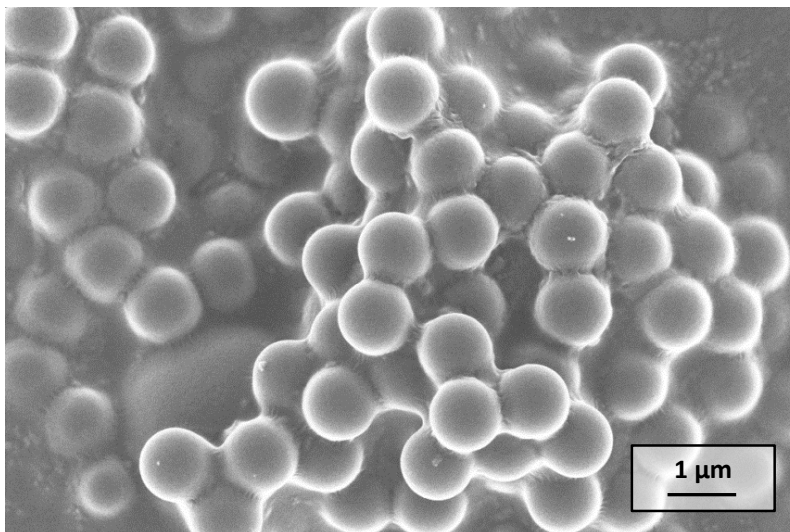


**Figure 5.13:** Overview SEM image of polystyrene micro-particles that were used for filtration test experiments by suspending these particles in water. The particles feature an average diameter of 1.1  $\mu\text{m}$ .

Subsequently, a prepared sand - supramolecular nanofiber filter was placed in the sample holder and sealed with the clamping ring. Before the actual measurement, remaining particles in the system of a previous test had to be removed. The filter unit was purged with pure water for 2.5 min featuring a volumetric flow rate of 500 mL/min. In addition, the purging of the filter unit ensures that remaining air bubbles in the system were also removed. Then, the actual filtration measurement started. This measurement was performed with a volumetric flow of 500 mL/min and a total volume of 2.5 L of water with micro-particles. Recording of particle size distributions and particle numbers before and after the filtration process allowed to determine the filtration efficiency of a filtration unit.

As example, **Figure 5.14** displays the initial particle size distribution of the total number of particles recorded prior to filtration with only an empty container placed in the sample holder in a total volume of 10 L at a volumetric flow rate of 500 mL/min. Particles with sizes ranging from 0.6  $\mu\text{m}$  to 29  $\mu\text{m}$  were detected. The micro-particle suspension was prepared by addition of 0.025 mL of a 10 wt.-% suspension of polystyrene micro-particles to a total volume of 30 L of water. The recorded particle size distribution was found to be unimodal and the determined particle sizes are in very good agreement with provided data by the supplier. Micro-particles were detected in the range from 0.8  $\mu\text{m}$  to 1.3  $\mu\text{m}$ . The filtration efficiencies are only calculated within this particle-size range. All particle-size distributions displayed in this chapter represent the total number of particles counted in the total volume.

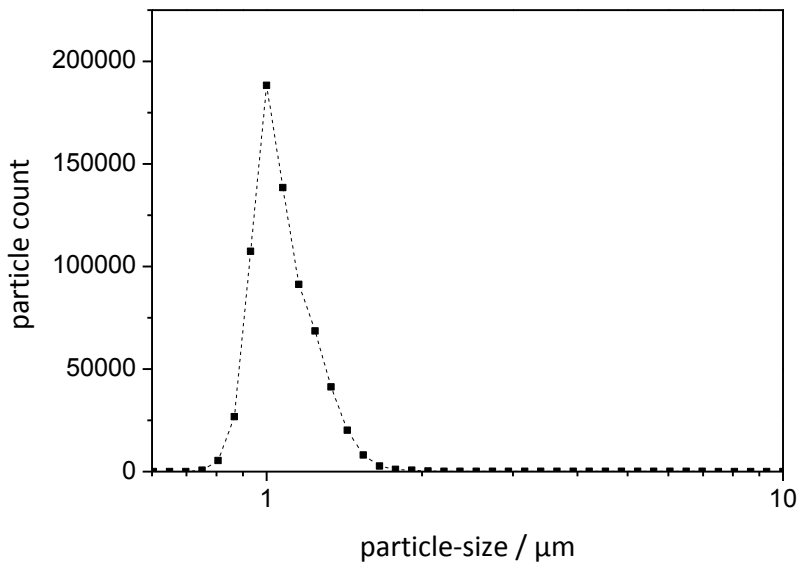


**Figure 5.14:** Particle size distribution of the total number of particles of the suspension of polystyrene micro-particles in water. The data correspond to the initial particle size distribution before filtration in a total volume of 10 L. Measuring parameters: Volumetric flow rate: 500 mL/min, Total volume measured: 10 L, Measuring time: 20 min, Filter area: 7.06  $\text{cm}^2$ .

*Filtration performance of polymer micro-particles from water*

Filter media to remove solid particles from fluids are usually characterized by two fundamental criteria. On the one hand, each filtration unit has to be able to efficiently remove particles from the fluid featuring the selected dimensions. On the other hand, the filtration process requires the fluid mixture to be forced through the filter unit by applying an external pressure. Therefore, filter media are normally characterized by a difference in pressure that is measured before and after the filtration unit at a certain volumetric flow rate. This difference is commonly referred to as the differential pressure as described in chapter 1. In addition, monitoring the differential pressure during the filtration process provides information concerning the stability of the filter. These two characteristics were evaluated with the custom-made liquid filtration test setup.

The earlier described sand - supramolecular nanofiber filters were investigated in liquid filtration test experiments.

For the evaluation of the filtration performance of the prepared filter units, the total number of particles and the particle size distributions of the polymer micro-particles in the suspensions were recorded before the filtration measurement and during the entire filtration process. In both cases, the same amount of the suspension was analyzed. Therefore, the initial particle size distribution of the polymer micro-particle suspension was measured by pumping the suspension through the liquid filtration test setup with an empty container being employed. These two particle size distributions and particle numbers allows for the calculation of the corresponding filtration efficiency in the investigated particle size range.

As reference, a filtration unit only containing 25 g of the sand and the filter paper on the bottom of the container, but without supramolecular nanofibers was investigated. **Figure 5.15** displays the corresponding particle size distributions of the total number of particles recorded of the suspension before filtration and after filtration with a filter unit containing 25 g of sand on top the filter paper. The filter area of the unit was 7.06 cm<sup>2</sup> and the filtration process was performed at a volumetric flow rate of 500 mL/min. During this specific measurement, the total volume passing through the filter unit was 10 L. It was found that only a minor reduction of the number of particles was observed. 704204 particles were detected in the suspension before the filtration measurement. The corresponding value after filtration with a filter unit containing 25 g of sand and the filter paper was 597596. In consequence, the total number of particles detected was reduced by around 15% utilizing the filtration unit containing only sand without nanofibers. These results prove no significant filtration effect of just sand and the filter paper on the bottom of the filter container.

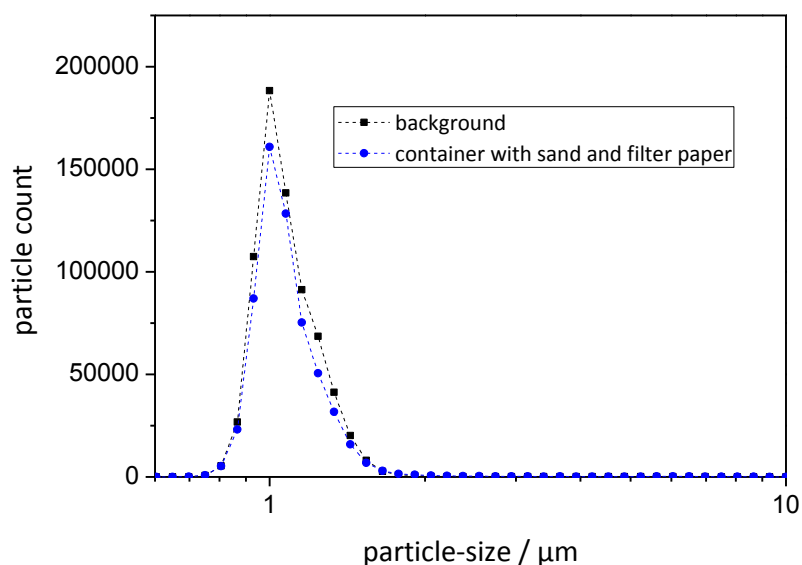


**Figure 5.15:** Particle size distributions of the total number of particles of a suspension of polystyrene particles in water. The black curve corresponds to the initial particle size distribution before filtration with a total volume of 10 L. The blue curve was recorded during the filtration measurement of the suspension by a container filled with 25 g of pure sand including the filter paper at the bottom of the container. Measuring parameters: Volumetric flow rate: 500 mL/min, Total volume filtered for each curve: 10 L, Filter area: 7.06 cm<sup>2</sup>.

In the following, filter units containing sand and supramolecular nanofibers based on 1,3,5-benzenetrisamides were prepared and subjected to the same liquid filtration test experiments. **Figure 5.16** displays the two cumulative particle size distributions recorded during filtration test experiments of a total volume of 10 L for each curve. The black curve corresponds to the distribution and the total number of particles of the initial suspension of polymer micro-particles. The filter unit was prepared from a 1.0 wt.-% solution of BTA **7** from 2-butanone as described before. The filter unit was placed in the sample holder and 10 L of water with micro-particles were filtered at a volumetric flow rate of 500 mL/min. The red curve is the distribution of remaining particles in the water after filtration with a filter unit containing the sand and supramolecular nanofibers. As shown in **Figure 5.16**, by utilization of sand - supramolecular nanofiber filters the particle size distribution of the remaining polymer micro-particles in the filtrate is significantly reduced compared to the initial suspension. 662782 particles were detected in the suspension before the filtration measurement and the corresponding value after filtration with a filter unit containing 25 g of sand with supramolecular nanofibers was 52452. The total number of particles in a volume of 10 L was reduced by around 90%. These results clearly demonstrate that the incorporation of supramolecular nanofibers inside

granulate material leads to a filter unit that is suitable to remove particles with diameters of around 1.1  $\mu\text{m}$  from water.

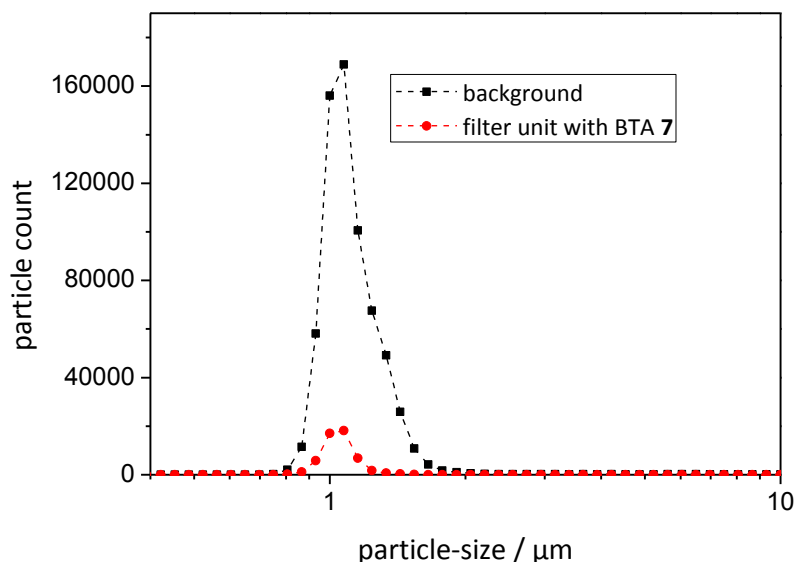


**Figure 5.16:** Particle size distributions of the total number of particles of a suspension of polystyrene particles in water. The black curve corresponds to the initial particle size distribution before filtration measured in a volume of 10 L. The red curve was recorded after filtration of the suspension by a container filled with a prepared combination of supramolecular nanofibers of BTA **7** and the granulate material. Filter unit preparation parameters: Solvent: 2-butanone, BTA concentration: 1.0 wt.-%, Immersion temperature: 50 °C, Cooling temperature: -78 °C, Cooling time: 30 min, Non-solvent: water, Total mass of granulate material: 25 g. Measuring parameters: Volumetric flow rate: 500 mL/min, Total volume filtered for each curve: 10 L, Filter area: 7.06  $\text{cm}^2$ .

#### *Differential pressure during the filtration process*

Apart from monitoring of the total number of particles and the corresponding particle size distributions, the pressure of the system during the filtration process before and after the sample holder was monitored. Due to the relatively large inner diameter of the tubing installed in the liquid filtration test setup (7 mm) and an inner diameter of 32 mm inside the sample holder, the resulting differential pressure before and after the sample holder without any inserted filtration unit is close to zero and can be neglected under the standard measuring conditions. Employment of a filtration unit that either contains pure sand or the sand - supramolecular nanofiber material leads to an increase in the differential pressure. **Figure 5.17** displays recorded differential pressures during a filtration test experiment with a total volume of 2.5 L. The black curve corresponds to the pressure building up by inserting a filter unit containing 25 g of pure sand, while the red curve refers to a measurement with a

filtration unit that contained sand with supramolecular nanofibers. Both measurements were performed at a volumetric flow rate of 500 mL/min.

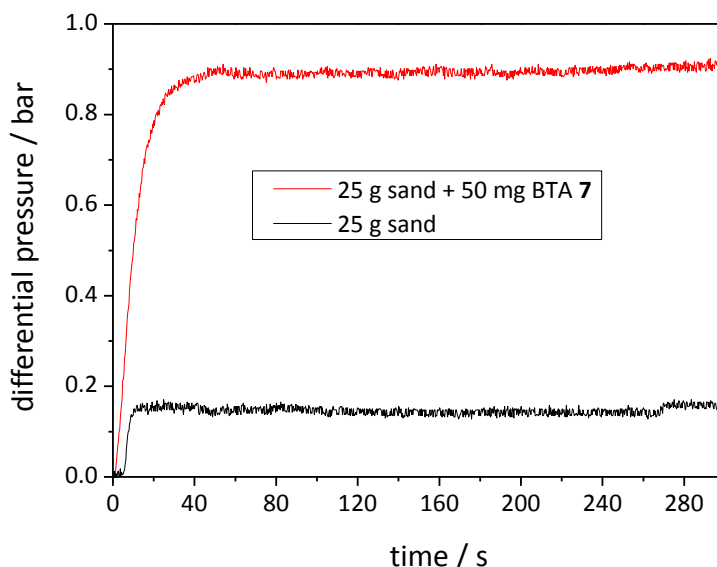


**Figure 5.17:** Evolution of differential pressure during filtration experiments of water with micro-particles. Black curve: Differential pressure of a container filled with 25 g of pure sand (black curve). Red curve: Differential pressure of a filter unit with supramolecular nanofibers of BTA 7 and sand. Filter unit preparation parameters: Solvent: 2-butanone, BTA concentration: 1.0 wt.-%, Immersion temperature: 50 °C, Cooling temperature: -78 °C, Cooling time: 30 min, Non-solvent: water, Total mass of granulate material: 25 g. Measuring parameters: Volumetric flow rate: 500 mL/min, Total volume filtered: 2.5 L, Filter area: 7.06 cm<sup>2</sup>.

Two important findings can be derived from the data shown in **Figure 5.17**. Due to the introduction of supramolecular nanofibers inside the granulate material, the differential pressure is significantly increased to a value of around 900 mbar compared to the filtration unit that only contains 25 g of pure sand with a differential pressure of only 150 mbar. This result reveals that the connection of the individual sand particles by self-assembled supramolecular nanofibers leads to smaller pore sizes of the sand with supramolecular fibers compared to the initial granulate material without any supramolecular material, which greatly increases the filtration performance to remove polymer micro-particles from water. In addition, the differential pressure of the filtration unit containing sand with supramolecular nanofibers remains constant during the whole measurement, which indicates that it is sufficiently stable under the selected testing conditions. If a significant amount of supramolecular nanofibers would be damaged during the process, the differential pressure would decrease during the filtration process and approach the differential pressure of pure sand.

However, potential real life applications of such a filtration unit might require a stability that exceeds a total volume of 2.5 L being filtered over a time period of 5 min. Even though the supramolecular material exhibits a very low solubility in pure water, constant exposure of this material to a flow of water might damage the network of self-assembled fibers by solving only minor fractions of the supramolecular material. Therefore, a 24 h measurement was performed to evaluate the long term stability of the system by purging the filtration unit with pure water at a constant volumetric flow rate of 500 mL/min. **Figure 5.18** shows the monitored differential pressure during the stability test (red curve). Even though the pressure varies slightly over time, the value of the pressure does not fall below a value of 900 mbar indicating that the nanofiber network was still present. After purging the unit for 24 h, the sample was removed from the sample holder and the material was stirred with a spatula. During this process, the nanofiber network that connected the individual sand particles was destroyed by shifting the particles relative to each other. Subsequently, the filter unit was placed back into the sample holder and purged for another two hours with pure water at a volumetric flow rate of 500 mL/min.

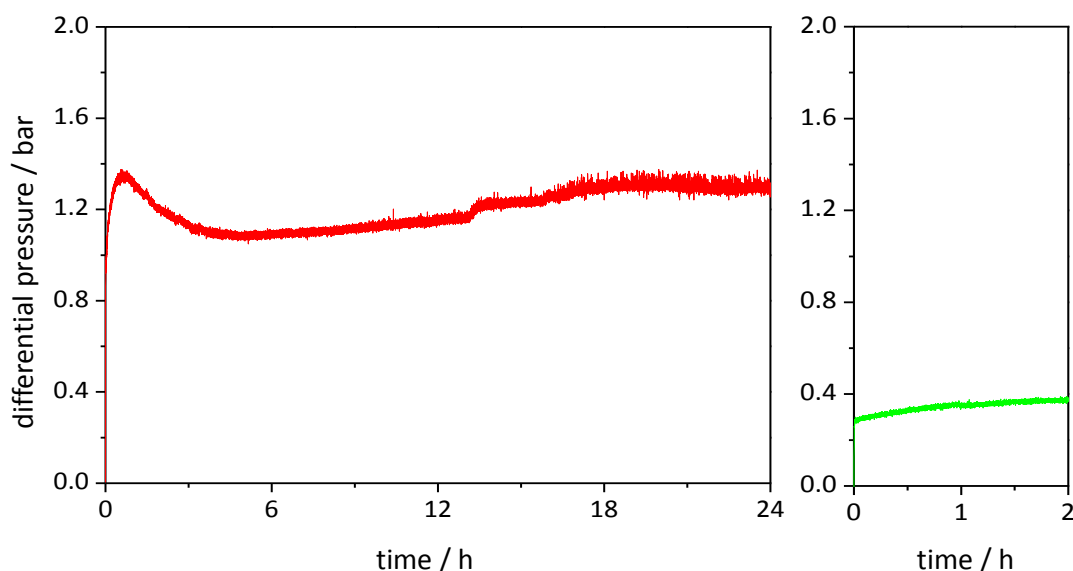


**Figure 5.18:** 24 h measurement of the differential pressure of a container filled with sand and supramolecular nanofibers of BTA **7** (left). In this case, pure water was purged through the sample without any particles present. After 24 h, the filter unit was stirred with a spatula to crack the remaining network of the supramolecular nanofibers. This sample was then placed again in the filter test setup and purged for additional 2 h (right). Measuring parameters: Volumetric flow rate: 500 mL/min, Filter area: 7.06 cm<sup>2</sup>.

It was found that the remaining differential pressure after reinsertion of the filter unit only reached a value of around 300 mbar, which is in the range of 25 g of just pure sand. This result proves that the

supramolecular nanofibers are remarkably stable. Even after the filtration unit has been purged over a period of time of 24 h an intact nanofiber network was still present.

### *Preparation of sand - supramolecular nanofiber filters from solutions with different concentrations*

So far, all prepared combinations of supramolecular nanofibers with a granulate material were processed from a solution of BTA 7 in 2-butanone at a concentration of 1.0 wt.-%. All these samples exhibited dimensional stability and very good filtration efficiency to remove polymer micro-particles from water. However, to gain a deeper insight of the required amounts of nanofibers in such a material to obtain a dimensionally stable filter, experiments were performed with varying concentrations of BTA 7 in the immersion solution. Apart from the BTA concentration, all units were prepared under identical conditions. Different concentrations of BTA 7 in the immersion solution result in different supramolecular nanofiber contents. The containers containing 25 g of the granulate material were immersed at a temperature of 50 °C, placed in polymer bags and subsequently cooled to -78 °C for 30 min. The solvent 2-butanone was replaced by water. To evaluate the dimensional stability of the samples, each unit was dried at room temperature and it was carefully removed from the containers.

Considering the solution uptake of the granulate material in the containers, the preparation from a 1.0 wt.-% solution yields around 50 mg of remaining BTA in the filter units. Corresponding amounts for other investigated concentrations are 40 mg (0.8 wt.-%), 30 mg (0.6 wt.-%) and 20 mg (0.4 wt.-%). **Figure 5.19** shows a photographic image of prepared samples that were dried and carefully removed from the container. The sample prepared from a solution containing 0.4 wt.-% of BTA 7 almost completely fell apart and exhibited no dimensional stability. Increasing the nanofiber content by utilizing a solution with 0.6 wt.-% of BTA 7, a sand - nanofiber combination that is partially stable is obtained. The inner part of the material appears to be most stable, which may be attributed to the sample preparation. Further increase of the nanofiber content appears to yield even more stable samples. While the sample prepared from a 0.8 wt.-% solution appears to be mostly stable except for some regions that were close to the wall of the container during the preparation, the sample prepared using the highest BTA-concentration of 1.0 wt.-% shows to be almost fully stable. These results indicate that a minimum of supramolecular material is required to yield a homogeneously distributed nanofiber network throughout the entire granulate material to generate a stable network of supramolecular nanofibers in the sand. A BTA concentration in the immersion solution of 1.0 wt.-% appears to be most suitable to obtain dimensionally stable structures.



**Figure 5.19:** Photograph combinations of supramolecular nanofibers and sand prepared with different BTA concentrations in the immersion solutions: 0.4 wt.-%, 0.6 wt.-%, 0.8 wt.-%, 1.0 wt.-%. Preparation parameters: Solvent: 2-butanone, Immersion temperature: 50 °C, Cooling temperature: -78 °C, Cooling time: 30 min, Non-solvent: water, Total mass of granulate material: 25 g.

In addition to the evaluation of the dimensional stability, filtration test experiments were performed. In contrast to previously shown results, these experiments only involved filtration of a total volume of 2.5 L at a constant flow rate of 500 mL/min. **Figure 5.20** shows particle size dependent filtration efficiency curves of units containing different contents of supramolecular nanofibers. Due to the particle size distribution of the selected polystyrene micro-particles, the filtration efficiency was only calculated for particles with diameters between 0.8  $\mu\text{m}$  and 1.3  $\mu\text{m}$ . Each curve displayed in the figure is based on at least 4 individual filtration test experiments of independently prepared samples.

It was found that samples that were prepared from 0.1 wt.-% solutions with a resulting nanofiber content of only 5 mg do not show any significant filtration efficiency. Even though samples prepared from 0.4 wt.-% solutions of BTA **7** in 2-butanone do not exhibit dimensional stability, polymer micro-particles can be removed from water at efficiencies of up to 90%. Further increase of the nanofiber content only results in minor improvements of the filtration efficiency. Independently of the nanofiber content, no filtration efficiency beyond 90% could be detected.

This finding might be attributed to the custom-made measuring process using the developed liquid filtration test setup and the corresponding filtration test procedure. In the course of filtration experiments, the water with micro-particles was conducted through mainly the same tubing than the filtered water. The tubing exhibited an inner diameter of 7 mm and the volumetric flow rate of the fluid was 500 mL/min. Under these conditions, the flow profile of the fluid is laminar and particles transported through these tubes may be partially deposited on the walls of the tubing. While measuring the filtered water, these particles may detach from the walls and get detected at the end of the test setup. Even with extensive purging of the test setup, these particles could not be fully

removed. In consequence, filtration efficiencies of fully 100% cannot be reached by the use of this setup.

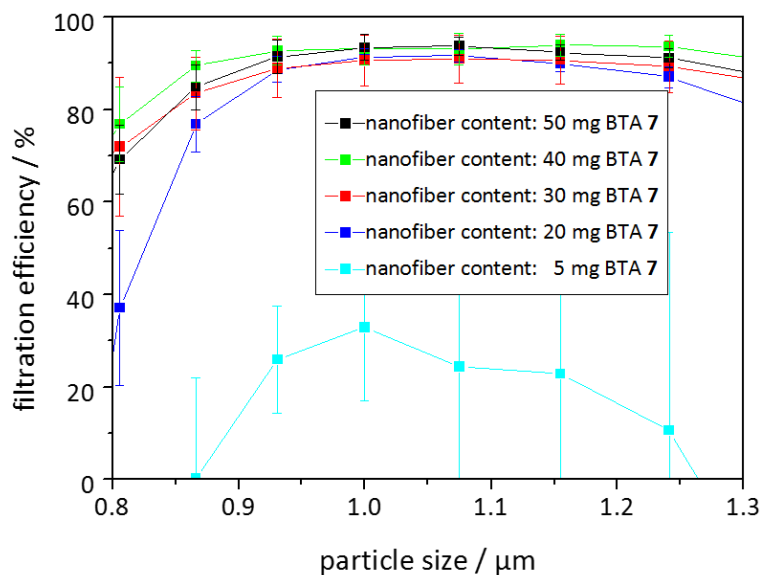


**Figure 5.20:** Particle size dependent filtration efficiencies of filter units with different contents of supramolecular nanofibers of BTA 7 inside 25 g of sand. Each curve displayed contains different amounts of BTA nanofibers and is based on a minimum of 5 independently prepared samples and filtration measurements. Preparation parameters: Solvent: 2-butanone, Immersion temperature: 50 °C, Cooling temperature: -78 °C, Cooling time: 30 min, Non-solvent: water, Total mass of granulate material: 25 g. Measuring parameters: Volumetric flow rate: 500 mL/min, Total volume filtered: 2.5 L, Filter area: 7.06 cm<sup>2</sup>.

#### 5.4 Filtration of *E.coli* bacteria from water

To this point, all filter units were only investigated by means of liquid filtration of polymer micro-particles from water until an optimized system was identified. Subsequently, these units were subjected to liquid filtration test experiments to remove *E. coli* bacteria from water. These experiments were performed in cooperation with the DWI – Leibniz Institute for Interactive Materials at the RWTH in Aachen.

The filtration test experiments were performed in a two-step process. First, a suspension of bacteria in water was filtered through a prepared filtration unit. Second, bacterial growth test experiments were performed to determine the exact bacteria concentrations before and after filtration.

##### *Implementation of filtration process*

The experiments were performed in two different sessions. During the first session, a set of experiments was performed by testing of filtration units that only contained 25 g of sand without any supramolecular material. During the second session, only the filtration performance of samples containing supramolecular nanofibers was tested. Samples and experiments of both sessions were subjected to the complete preparation process. Only the reference experiments were performed without any supramolecular material.

For the first session, samples that only contained 25 g of pure sand were treated by previously described processing conditions, while any microbial contamination was avoided. The specific preparation parameters were: Solvent: 2-butanone, immersion temperature: 50 °C, cooling temperature: -78 °C, cooling time: 30 min, non-solvent: water, total mass of granulate material: 25 g. For filtration test experiments, suspensions of *E. coli* strains were incubated at 37 °C in nutrient solution consisting of Mueller-Hinton Broth (Beef infusion: 2 g/L; casein peptone (acidic hydrolysate): 17.5 g/L; corn starch: 1.5 g/L; pH value: 7.4) for 18 h to provide a suspension with a known bacteria concentration of around  $10^9$  CFU/mL. By dilution of this stock suspension with a 0.9 wt.-% solution of NaCl in water, four different suspensions were prepared with *E. coli* concentrations of  $2.4 \times 10^3$  CFU/mL,  $2.4 \times 10^4$  CFU/mL,  $2.4 \times 10^5$  CFU/mL and  $2.4 \times 10^6$  CFU/mL (CFU = colony forming units).



**Figure 5.21:** Photograph of the testing procedure to evaluate the efficiency of prepared filter units to remove *E. coli* from water.

To enable purging of the samples, each unit was placed in a sample holder as previously described. In contrast to earlier versions, this sample holder comprised of aluminum and was equipped with a female luer lock fitting at the top part. A dosing syringe (0.5 - 5 ml; Sartorius) exhibiting a male luer lock connection was connected to the sample holder and used to pump water through the prepared sample as depicted in **Figure 5.21**.

Each unit was first purged with 25 mL of a 0.9 wt.-% solution of NaCl in water to remove potential remaining microbial contamination. 15 mL was assumed to be the dead volume of the dosing syringe, the corresponding tubing and the filtration unit in combination with the sample holder. Therefore, 15 mL of the corresponding suspension of *E. coli* in water was pumped through the unit to replace the clean solution of NaCl by contaminated water. Afterwards, 50 mL of the contaminated suspension was filtered into a sterile Erlenmeyer flask (see **Figure 5.12**). This filtrate was then used for bacterial growth tests, which will be discussed in detail later.

The second session included testing of units that contained sand with supramolecular nanofibers. These samples were subjected to the complete preparation process. The specific preparation parameters were: Solvent: 2-butanone, BTA concentration: 1.0 wt.-%, immersion temperature: 50 °C, cooling temperature: -78 °C, cooling time: 30 min, non-solvent: water, total mass of granulate material: 25 g. Suspensions of *E. coli* were prepared according to the first session with resulting *E. coli* concentrations of  $1.8 \times 10^3$  CFU/mL,  $1.5 \times 10^4$  CFU/mL,  $1.9 \times 10^5$  CFU/mL and  $1.5 \times 10^6$  CFU/mL. The filtration process itself was performed in an identical way for both sessions.

*Time dependent bacterial growth curves*

Evaluation of the filter units by means of filtration efficiency to remove *E. coli* from water required bacterial growth tests of samples of the initial bacterial suspensions as well as of the filtered suspensions. Two different methods of testing were performed to determine the microbial content of each tested suspension.

First, time dependent bacterial growth curves were recorded on a Multiwell Reader (Infinite 2000 Pro; Tecan). Therefore, different samples were prepared on a 96 space well plate. **Table 5.1** shows all samples that were investigated during the first session of the filtration experiments. Each suspension was tested twice in two different wells. All wells except for those containing the leaching control experiments, were filled with 20  $\mu\text{L}$  of the corresponding suspension and 180  $\mu\text{L}$  of a nutrient solution (0.5 wt.-% peptone from caseine and 0.3 wt.-% meat extract in water). Bacterial growth was followed for 20 h with cycles of 30 min during incubation at 37 °C and shaking for 1000 s at 100 rpm per cycle. After each cycle the optical density of each suspension inside a well was measured, which reflects the total number of *E. coli* bacteria present in the sample.

The series involved two experiments to verify that the samples were sterile and were not contaminated with bacteria in the course of the preparation process. During this test, the samples were purged with a sterile solution of NaCl in water (0.9 wt.-%) and the filtrate was tested on bacterial growth. In addition, each of the four initially prepared *E. coli* suspensions was investigated. Eight prepared filter units were tested by means of filtration of *E. coli* from water, whereas the filtration of each suspension was tested twice in independent experiments and each sample was only used once.

**Table 5.1:** Prepared samples on the 96 space well plate during the first session of bacterial filtration test experiments. The first column refers to the specific samples tested. The second column corresponds to the concentration of *E. coli* bacteria in the filtered suspension. Two independent bacteria growth curves were recorded in two separate wells for each sample.

Sample	<i>E. coli</i> concentration of filtered water	Number of wells
Sterile control – 1	0 CFU/mL	2
Sterile control – 2	0 CFU/mL	2
Initial suspension	$2.4 \times 10^3$ CFU/mL	2
Filtered by sand - 1	$2.4 \times 10^3$ CFU/mL	2
Filtered by sand - 2	$2.4 \times 10^3$ CFU/mL	2
Initial suspension	$2.4 \times 10^4$ CFU/mL	2
Filtered by sand - 3	$2.4 \times 10^4$ CFU/mL	2

Sample	<i>E. coli</i> concentration of filtered water	Number of wells
Filtered by sand - 4	$2.4 \times 10^4$ CFU/mL	2
Initial suspension	$2.4 \times 10^5$ CFU/mL	2
Filtered by sand - 5	$2.4 \times 10^5$ CFU/mL	2
Filtered by sand - 6	$2.4 \times 10^5$ CFU/mL	2
Initial suspension	$2.4 \times 10^6$ CFU/mL	2
Filtered by sand - 7	$2.4 \times 10^6$ CFU/mL	2
Filtered by sand - 8	$2.4 \times 10^6$ CFU/mL	2

**Table 5.2** displays all samples prepared on the well plate during the second session of the filtration test experiments. To ensure that no potential antibacterial components were leaching out of the filter units, *E. coli* contaminated water was added to the filtrate of the sterile control samples and the resulting mixtures were analyzed in separate wells. The corresponding wells were filled with 20  $\mu$ L of the filtrate from sterile control experiments, 20  $\mu$ L of *E. coli* suspension ( $10^6$  CFU/mL) and 160  $\mu$ L of nutrient solution.

**Table 5.2:** Prepared samples on the 96 space well plate during the second session of bacterial filtration test experiments. The first column refers to the specific sample that was investigated by the bacterial growth test. The second column corresponds to the *E. coli* concentration of the filtered suspension. The leaching experiments were performed without any bacteria in the filtered water, but *E. coli* were added afterwards. Preparation parameters: Solvent: 2-butanone, BTA concentration: 1.0 wt.-%, immersion temperature: 50 °C, cooling temperature: -78 °C, cooling time: 30 min, non-solvent: water, total mass of granulate material: 25 g.

Sample	<i>E. coli</i> conc. of filtered water	Number of wells
Sterile control – 1	0 CFU/mL	2
Sterile control – 2	0 CFU/mL	2
Leaching – 1	<i>E. coli</i> added to filtered sterile water	2
Leaching – 2	<i>E. coli</i> added to filtered sterile water	2
Initial suspension	$1.8 \times 10^3$ CFU/mL	2
Filtered by sand with nanofibers – 1	$1.8 \times 10^3$ CFU/mL	2
Filtered by sand with nanofibers – 2	$1.8 \times 10^3$ CFU/mL	2
Initial suspension	$1.5 \times 10^4$ CFU/mL	2
Filtered by sand with nanofibers – 3	$1.5 \times 10^4$ CFU/mL	2
Filtered by sand with nanofibers – 4	$1.5 \times 10^4$ CFU/mL	2
Initial suspension	$1.9 \times 10^5$ CFU/mL	2

## Sand - supramolecular nanofiber filters for the removal of bacteria from water

Sample	<i>E. coli</i> conc. of filtered water	Number of wells
Filtered by sand with nanofibers – 5	$1.9 \times 10^5$ CFU/mL	2
Filtered by sand with nanofibers – 6	$1.9 \times 10^5$ CFU/mL	2
Initial suspension	$1.5 \times 10^6$ CFU/mL	2
Filtered by sand with nanofibers – 7	$1.5 \times 10^6$ CFU/mL	2
Filtered by sand with nanofibers – 8	$1.5 \times 10^6$ CFU/mL	2

### *Colony counting experiments*

Apart from the time dependent measurements of bacterial growth utilizing the Multiwell-Reader, colony counting experiments on ST1-Agar plates were performed. Therefore, 50  $\mu$ L of each initial *E. coli* suspension as well as of the filtrates were dropped on Agar plates. The suspensions were dried and subsequently incubated at 37 °C overnight. Colony counting on the plates of bacterial suspensions and filtrates allows for calculation of the filtration performance of samples containing supramolecular nanofibers.

### *Results of filtration experiments to remove E. coli bacteria from water*

One major objective of this project was the employment of supramolecular nanofibers inside a granulate material to create a unit that is capable of removing microbial contaminations from water to provide a new approach to potential future water treatment solutions. Therefore, the optimized system that has been characterized by the custom-made liquid filtration test setup was subjected to filtration test experiments with suspensions of *E. coli* bacteria in water. As reference, filter units containing only 25 g of plain sand without any supramolecular nanofibers were also tested in filtration experiments.

The experiments involved two independent parts. First the 50 mL of a suspension of *E. coli* with a known concentration were filtered through a filter unit utilizing a dosing syringe and the custom-made sample holder. The second part involved the microbial investigation of the filtrates as well as the initial suspensions. These investigations were performed in two individual experiments. Monitoring of time dependent bacterial growth curves and bacterial growth on agar plates with subsequent colony counting were the two independent analyzing methods.

For the measurement of time dependent bacterial growth, a sample of each suspension was mixed with a nutrient solution and incubated at 37 °C for 20 h. Optical density of the mixture was recorded in time intervals of 30 min (1800 s). In consequence, 40 data points (40 cycles) were monitored for

each sample. **Figure 5.22** displays the time dependent bacterial growth curves of suspensions of *E. coli* before filtration (blue curve) and the corresponding curves after filtration with a filtration unit that only contained 25 g of pure sand. It was found that the bacterial growth of the filtrates (orange and grey curves) is slightly retarded compared to the initial suspension.

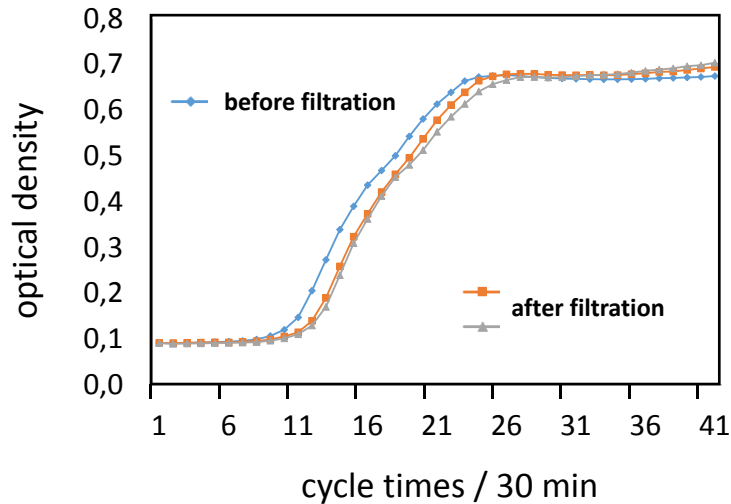


**Figure 5.22:** Bacterial growth curves of a suspension of *E. coli* in water before and after filtration with a filter unit that contained 25 g of pure sand. The samples were subjected to the full preparation process without any BTA in the immersion solution. The initial *E. coli* concentration was  $2.4 \times 10^6$  CFU/mL and the total volume filtered was 50 mL. Filter unit preparation parameters: Solvent: 2-butanone, Immersion temperature: 50 °C, Cooling temperature: -78 °C, Cooling time: 30 min, Non-solvent: water, Total mass of granulate material: 25 g.

This result shows that the filter unit that contains just pure sand does separate some of the bacteria from the water. In cooperation with the DWI - Leibniz-Institute for interactive materials (Aachen), a filtration efficiency by orders of magnitude was derived. This calculation is based on calibration measurements with different concentrations of *E. coli* bacteria. The recorded difference in bacterial growth corresponds to a reduction of bacteria by less than one order of magnitude. This result is referred to as a reduction by “< log 1”. Experiments were performed with four different concentrations of  $2.4 \times 10^3$  CFU/mL,  $2.4 \times 10^4$  CFU/mL,  $2.4 \times 10^5$  CFU/mL and  $2.4 \times 10^6$  CFU/mL. Independently of the concentration of the filtered suspension, the filtration efficiency corresponded always to a reduction of < log 1 (less than 90%). In terms of microbiology, these reference filter units can be classified as ineffective for the separation of *E. coli* from water due to the fact that bacteria can still reproduce after the filtration process. Sterile control samples revealed, that no contamination of the filter units was present before the filtration test.

In addition, prepared filter units from a solution of BTA **7** in 2-butanone with a concentration of 1.0 wt.-% were subjected to bacterial filtration experiments. During the preparation process, any microbial contamination was avoided. **Figure 5.23** displays exemplarily the corresponding time dependent bacterial growth curves for filtration with units containing supramolecular nanofibers and with an *E. coli* concentration of  $1.8 \times 10^6$  CFU/mL in the initial suspension. It was found that the bacterial growth is significantly retarded compared to the growth originating from the initial suspension.

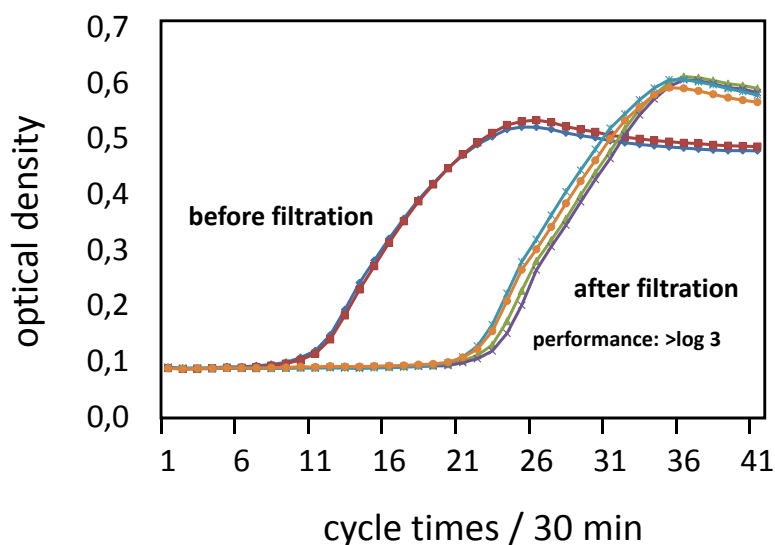


**Figure 5.23:** Bacterial growth curves of a suspension of *E. coli* in water before and after filtration with a filter unit of supramolecular nanofibers of BTA **7** inside 25 g of sand. The initial *E. coli* concentration was  $1.8 \times 10^6$  CFU/mL and the total volume filtered was 50 mL. Preparation parameters: Solvent: 2-butanone, BTA concentration: 1 wt.-%, Immersion temperature: 50 °C, Cooling temperature: -78 °C, Cooling time: 30 min, Non-solvent: water, Total mass of granulate material: 25 g.

The difference in bacterial growth corresponds to a reduction of *E. coli* concentration by  $> \log 3$ , which corresponds to filtration efficiency of more than 99.9%. In consequence, the introduction of supramolecular nanofibers inside the granulate material creates a material that exhibits a filtration effect that allows for the removal of the *E. coli* bacteria from water. Apart from the results exemplarily shown in **Figure 5.22** and **Figure 5.23**, three additional concentrations of *E. coli* were filtered by units that either contain 25 g of pure sand or the sand - supramolecular nanofibers combination. **Table 5.3** shows an overview of filtration efficiencies derived from time dependent bacterial growth curves for all investigated concentrations of *E. coli* in water.

**Table 5.3:** Filtration efficiencies of filter units containing either 25 g of sand or prepared filter units to remove *E. coli* from water at different initial concentrations. Preparation parameters: Solvent: 2-butanone, BTA concentration: 1 wt.-%, Immersion temperature: 50 °C, Cooling temperature: -78 °C, Cooling time: 30 min, Non-solvent: water, Total mass of granulate material: 25 g

Filter unit	Initial concentration	Volume tested	Filtration efficiency
25 g of sand	$2.4 \times 10^3$ CFU/mL	50 mL	< 90%
	$2.4 \times 10^4$ CFU/mL		< 90%
	$2.4 \times 10^5$ CFU/mL		< 90%
	$2.4 \times 10^6$ CFU/mL		< 90%
Sand with supramolecular nanofibers	$1.5 \times 10^3$ CFU/mL		≈ 100%
	$1.9 \times 10^4$ CFU/mL		≈ 100%
	$1.5 \times 10^5$ CFU/mL		99.9% - 100%
	$1.8 \times 10^6$ CFU/mL		99.9%

In all cases, the total volume filtered was 50 mL. It was found that no significant filtration performance was determined for any of the samples containing only 25 g of sand. Even though the bacterial growth has been slightly retarded, the reduction was always below one order of magnitude ( $< \log 1$ ). By utilization of the prepared units with supramolecular nanofibers in filtration experiments, microbial contamination was significantly reduced in the filtrates. The results indicate that there might be a concentration dependence of the initial bacteria suspensions on the resulting filtration performance. The filtrates of suspensions with initial concentrations of  $10^3$  CFU/mL and  $10^4$  CFU/mL did not show any bacterial growth after filtration proving the filtrates to be completely free of microbial contamination. Filtration of a suspension containing *E. coli* at a concentration of  $10^5$  CFU/mL results in an efficiency between 99.9% and 100%. The highest concentration of bacteria always showed remaining bacteria in the filtrates. This filtration performance might be enhanced by increasing the residence time of bacteria inside the filter unit during the filtration process. This enhancement can for example be achieved by adjustment of the geometry of the filtration unit or the amount of granulate material being equipped in the current unit.

In addition to the time dependent bacterial growth curves, samples of 50  $\mu$ L from each filtrate as well as the initial suspensions were placed on agar plates and incubated overnight. Colony counting of the samples allowed for the calculation of the filtration efficiency of the unit filled with sand as well as with the samples containing supramolecular material.

**Table 5.4** displays the resulting filtration efficiency values obtained by colony counting experiments. By analysis of the different filtrates, it was found that units filled with 25 g of sand without any supramolecular material do reduce the microbial contamination by around 50% independently of the initial concentration of bacteria in the filtered suspension. This is in very good agreement with the results from the time dependent bacterial growth curves. By utilization of a prepared unit with supramolecular nanofibers, the filter effect of the units is significantly increased. Even though the filtration efficiency does not reach 100% for any of the investigated concentrations, the filtration performance is strongly increased and therefore it is in good agreement with previous results.

**Table 5.4:** Filtration efficiencies of filter units containing either 25 g of sand or filter units containing nanofibers to remove *E. coli* from water at different initial concentrations. Preparation parameters: Solvent: 2-butanone, BTA concentration: 1 wt.-%, Immersion temperature: 50 °C, Cooling temperature: -78 °C, Cooling time: 30 min, Non-solvent: water, Total mass of granulate material: 25 g

Filter unit	Initial concentration	Filtration efficiency from colony counting
25 g of sand	$2.4 \times 10^3$ CFU/mL	48%
	$2.4 \times 10^4$ CFU/mL	53%
	$2.4 \times 10^5$ CFU/mL	51%
	$2.4 \times 10^6$ CFU/mL	49%
Sand with supramolecular nanofibers	$1.5 \times 10^3$ CFU/mL	99.0%
	$1.9 \times 10^4$ CFU/mL	99.9%
	$1.5 \times 10^5$ CFU/mL	99.0%
	$1.8 \times 10^6$ CFU/mL	98.7%

Filtration experiments with *E. coli* bacteria revealed a remarkable filtration performance of the prepared filter units containing the supramolecular nanofibers, while results from two independent analyzing methods were found to be in very good agreement.

## 5.5 Conclusion

This chapter reports on the preparation of dimensionally stable combinations of sand and supramolecular nanofibers based on the self-assembly of 1,3,5-benzenetrisamides that can be utilized in filtration applications. The work focused especially on the ability of the filter units to remove microbial contamination such as *E. coli* bacteria from water. Therefore, an easy multistep preparation process was developed for the *in situ* preparation of material inside a suitable container to create a filtration unit that can be used for subsequent filtration test experiments.

The prepared filter units were characterized by means of dimensional stability as well as SEM analysis. It was found that by utilization of the developed preparation process, supramolecular nanofibers can be prepared throughout a granulate material such as sand to establish a network connecting the individual sand particles featuring dimensional stability. Concentration dependent studies demonstrated that a minimum of the supramolecular material has to be present to obtain a fully stable structure. Only 50 mg of supramolecular nanofibers of BTA **7** with a mean nanofiber diameter of around 500 nm in 25 g of sand are already sufficient. This amount corresponds to a mass content of only 0.2 wt.-% in the dried samples.

Employed in the selected containers, filtration units were prepared and intensively studied by means of their filtration performance. Therefore, a custom-made liquid filtration test setup was designed and built that allowed for the purging of the units with water under pressure. Filtration test experiments with a suspension of polymer micro-particles in water were carried out. A custom-made sample holder was designed and by application of 3D-printing technique optimized to the selected geometry of the filtration unit. Filter testing revealed that the introduction of supramolecular nanofibers inside sand yields a structure, which is capable of removing polymer micro-particles with an average diameter of 1.1  $\mu\text{m}$ . Monitoring of the differential pressure before and after the filter unit demonstrated that the units remain stable during the filtration process. Compared to containers that only contained the pure granulate material without any supramolecular fibers, the prepared filter units exhibited an increased differential pressure indicating that the pore sizes of the material were reduced by the supramolecular nanofibers. Even under exposure of the filter units to filtration conditions for 24 h, a remarkable pressure stability of up to 1.2 bar was demonstrated. Concentration dependent experiments showed that even with lower contents of supramolecular nanofibers down to 0.4 wt.-% a filtration effect can be observed.

Once the preparation process was optimized and the filtration properties were characterized on the liquid filtration test setup, filtration units containing the nanofibers of BTA **7** in sand were subjected to

liquid filtration tests with suspensions of *E. coli* in water. 50 mL of four different suspensions with varying concentrations were filtered and the filtrates were analyzed by two different methods. Time dependent monitoring of the bacterial growth showed significant reduction of *E. coli* by filtration. Filtration efficiencies between 99.9% and 100% were obtained depending on the initial concentration of the suspension. Results obtained from colony counting experiments on agar plates were found to be in very good agreement with the time dependent bacterial growth curves.

It has been shown that the formation of supramolecular nanofibers provides a possibility to introduce fibrous structures into a complex porous structure. In consequence, supramolecular nanofibers based on the self-assembly of 1,3,5-benzenetrisamides have been successfully employed inside a granulate material and it has been shown that the resulting filter units have a great potential in real life filtration applications.

## 6 Summary

The *in situ* preparation of supramolecular nanofibers based on the self-assembly of 1,3,5-benzenetrisamides (BTAs) from solution is the essential element of the scientific work performed during this thesis. These BTAs are based on a symmetrically substituted benzene-core connected to three amide moieties which can be substituted with a vast number of different groups. By proper selection of these substituents, important properties of the BTAs can be tailored. Most important for this thesis is the solubility at elevated temperatures and the aggregation behavior upon cooling and evaporation of a BTA solution.

Three different chapters utilizing the supramolecular bottom-up approach to prepare nanofibers are covered in this thesis. The topic of each chapter involves basic scientific challenges, also in connection with potential applications. The thesis addresses the following topics:

- *Self-assembly of alkoxy-substituted 1,3,5-benzenetrisamides under controlled conditions*
- *Supramolecular nanofibers for air filtration applications*
- *Sand - supramolecular nanofiber filters for the removal of bacteria from water*

In the chapter "***Self-assembly of alkoxy-substituted 1,3,5-benzenetrisamides under controlled conditions***", the influence of processing parameters on the morphology of supramolecular nanofibers from solution is investigated. The self-assembly results are strongly influenced by the molecular structure of the selected BTA, the BTA starting concentration or the selected processing solvent. The self-assembly experiments are typically performed preparing a clear solution of a BTA in a selected solvent at elevated temperatures and applying an external influence to start the self-assembly process such as a temperature change (e.g. cooling).

In a first step, a custom-made experimental setup was built to control processing parameters and to allow for a series of self-assembly experiments under controlled conditions. Changes in temperature, especially cooling of a BTA solution, were selected to initiate the formation of supramolecular nanofibers. The investigations focused on the influence of controlled mechanical stirring during the self-assembly process and possibilities to control the resulting fiber morphology by variation of the cooling and the stirring conditions. The heat transfer during the cooling process was theoretically described to understand the influences of mechanical stirring on the cooling process.

Based on a series of five different alkoxy-substituted 1,3,5-benzenetrisamides, *N,N',N''*-tris(1-methoxybutan-2-yl)benzene-1,3,5-tricarboxamide (BTA **4**) in a solvent mixture of water and isopropanol (80:20) at a concentration of 0.05 wt.-% was identified as the most suitable system. This

system showed the best temperature dependent solubility behavior and the best fiber formation from solution with respect to length and diameter.

During the *first series of experiments under controlled conditions*, the *mechanical stirring velocity was varied*, while other processing parameters were kept constant. The results demonstrated that the experiments were highly reproducible. Preliminary, it was found that an increase in the stirring velocity results in a decrease of the mean fiber diameter and the fiber diameter distributions were found to be narrower. However, analysis of the corresponding temperature profiles for different stirring velocities confirmed an improved cooling performance of the BTA solution by increasing the stirring velocity. Beyond a stirring velocity of 150 rpm, only minor changes of the temperature profile during cooling were found. The differences in supramolecular nanofiber morphology and the dependence of the cooling process on the mechanical stirring demonstrates that the nanofiber morphology obtained from these experiments is *mainly dependent on variations of the cooling process*. Above a stirring velocity of 150 rpm, only minor changes of the fiber morphology were detected, which relates to changes of the temperature profile above 150 rpm.

A *second series of experiments* was performed by *variation of the applied cooling temperature*. It was found that the supramolecular nanofiber-morphology can also be controlled by variation of the applied cooling temperature and a constant mechanical stirring velocity. It was revealed that the mechanical stirring has no direct influence on the supramolecular nanofiber morphology. Changes in mechanical stirring velocity only influence the nanofiber morphology by a parallel change in the cooling process.

The second part "***Supramolecular nanofibers for air filtration applications***" involved the preparation and characterization of nanofiber-microfiber composites based on the self-assembly of BTAs from solution inside a polymer microfiber nonwoven scaffold. In contrast to the previous chapter, the preparation of nanofiber-microfiber composites involves cooling as well as evaporation of the solvent.

The research performed within this chapter can be divided into two main sections. The *first section* involves the preparation of nanofiber-microfiber composites from solutions with three different BTAs: *N,N',N''-tris(2-ethylhexyl)-benzene-1,3,5-tricarboxamide* (BTA **6**), *N,N',N''-tris(6-methylheptyl)-benzene-1,3,5-tricarboxamide* (BTA **7**) and *N,N',N''-tris(3-methylbutyl)-benzene-1,3,5-tricarboxamide* (BTA **8**). A polyester/viscose nonwoven was selected as microfiber scaffold. Samples were processed from different solvents such as 2-butanone, isopropanol and ethanol. The temperature dependent solubility behavior of each BTA and solvent combination was investigated and demonstrated the importance of this behavior on the resulting supramolecular fiber morphology inside the prepared

composites. It was found that BTA and solvent combinations featuring a high solubility of the BTA appear to be less favorable for the preparation of supramolecular nanofiber microfiber composites.

Different series of nanofiber-microfiber composites were prepared and subsequently characterized by methods like SEM analysis or filtration test experiments to remove particulate matter from air. Concentration dependent experiments to prepare composites from 2-butanone showed that a BTA concentration of 1.0 wt.-% is usually sufficient to obtain a homogeneous distribution of nanofibers throughout the voids of the nonwoven scaffold. Corresponding filtration test experiments to remove particulate matter (iso fine dust) from air demonstrated that these nanofiber-microfiber composites can reach remarkable high filtration efficiencies. Several repetitions of these experiments revealed the high reproducibility of this fast and easy preparation process. In addition, some selected composites were analyzed by capillary flow porometry. The results demonstrate that composites containing BTA **8** exhibited rather broad pore size distributions compared to composites containing BTA **7** and the results relate to observed filtration efficiencies. Experiments with variations of the selected processing solvent demonstrated that composites prepared from 2-butanone exhibit the most homogeneously distributed supramolecular nanofibers throughout the voids of the nonwoven scaffold compared to composites prepared from isopropanol or ethanol. The preparation process to obtain supramolecular nanofiber-microfiber composites is very sensitive to the selected processing parameters such as the processing solvent or the molecular structure of the selected BTA. IR-spectroscopic investigations confirmed that the supramolecular nanofibers inside the nonwoven material consist of supramolecular columns based on threefold directed hydrogen bond formation of the BTAs.

In summary, the results presented in this section demonstrate that *supramolecular nanofibers have a great potential for air filtration applications and the resulting morphology of the composites can be tailored by proper selection of the processing parameters.*

In the second section of this chapter, the preparation of nanofiber-microfiber composites was extended for the first time to a BTA with alkoxy-substituent processed from a mixture of water and isopropanol (60:40). As scaffold, a technical polyester nonwoven was used to prepare composites. Concentration dependent experiments demonstrated that mean fiber diameters were uniformly in the range from 500 to 650 nm. The samples prepared inside the technical polyester nonwoven exhibit filtration efficiencies between 50 and 80% with differential pressures of only 57 Pa. Comparing the filtration performance of these composites to those from the first part using the model nonwoven, the differential pressure here is more than one order of magnitude lower. By proper selection of the processing parameters and materials, the *preparation concept to obtain nanofiber-microfiber*

*composites for filtration applications is not limited to the previously used polyester/viscose model nonwoven and can be tailored towards a specific application.*

The last chapter "***Sand - supramolecular nanofiber filters for the removal of bacteria from water***" covers the development of a process for the *in situ* preparation of supramolecular nanofibers inside a granulate material for liquid filtration applications. Therefore, two main issues had to be solved. The first issue addresses the preparation and subsequent characterization of a filter unit containing a dimensionally stable filter material that was capable of removing solid particles from water. The second part involved the development of a liquid filtration test setup that allowed for the evaluation of the filtration performance of prepared units by means of filtration efficiency and differential pressure during the filtration process and subsequent filtration test experiments to remove microbial contamination from water.

Sea sand was selected as granulate material and by implementation of an immersion process in a BTA solution at elevated temperatures followed by subsequent cooling and solvent replacement, a dimensionally stable material of sand with supramolecular nanofibers was obtained. Only 50 mg of the supramolecular nanofibers were found to fully connect individual sand particles throughout a total mass of 25 g of sand. SEM analysis demonstrated that the supramolecular mean fiber diameter in the voids of the sand is around 500 nm. The filtration performance was first tested on the developed custom-made liquid filtration test setup to remove polystyrene micro-particles with a mean diameter of 1.1  $\mu\text{m}$  from water. The results showed that depending on the amount of supramolecular material inside the sand, around 90% of the micro particles were removed. In a 24 h measurement of liquid filtration, the supramolecular nanofiber network inside the granulate material is stable. After all preparation parameters were optimized, filtration test experiments were performed to remove *E. coli* bacteria from water at different microbial contaminations. *The prepared filter units exhibited a remarkable filtration efficiency of up to 100% to remove bacteria from water depending on the initial microbial concentration.*

## 7 Zusammenfassung

Die Selbstassemblierung von 1,3,5-Benzoltrisamiden (BTAs) zur Präparation von supramolekularen Nanofasern ist ein essentieller Bestandteil der wissenschaftlichen Arbeiten, die im Rahmen dieser Dissertation durchgeführt wurden. BTAs bestehen aus einem symmetrisch substituierten Benzolkern und in den Positionen 1, 3 und 5 befinden sich Amidgruppen, die ihrerseits wiederum mit verschiedensten chemischen Seitengruppen substituiert sein können. Durch die Wahl geeigneter Substituenten können wichtige Eigenschaften der BTAs angepasst werden. Von besonderer Bedeutung sind dabei sowohl die Löslichkeit in verschiedenen Lösungsmitteln bei erhöhten Temperaturen als auch das Aggregationsverhalten durch Kühlen und Verdampfen des Lösungsmittels.

Diese Arbeit umfasst drei verschiedene Kapitel. In jedem dieser Kapitel wird ein sogenannter „bottom-up“-Ansatz zur Präparation eindimensionaler Nanofasern basierend auf der supramolekularen Selbstassemblierung untersucht. Dabei befasst sich jedes Kapitel mit grundlegenden wissenschaftlichen Fragestellungen, aber auch mit möglichen Anwendungen der untersuchten Systeme. Die drei Kapitel werden im Folgenden vorgestellt:

- *Self-assembly of alkoxy-substituted 1,3,5-benzenetrisamides under controlled conditions*
- *Supramolecular nanofibers for air filtration applications*
- *Sand - supramolecular nanofiber filters for the removal of bacteria from water*

In dem Kapitel „***Self-assembly of alkoxy-substituted 1,3,5-benzenetrisamides under controlled conditions***“ wird der Einfluss von Prozessparametern auf die Selbstassemblierung aus Lösung und die Morphologie entstehender supramolekularer Nanofasern unter kontrollierten Bedingungen untersucht. Die Ergebnisse werden dabei stark durch Faktoren wie beispielsweise die molekulare Struktur des BTAs, das gewählte Lösungsmittel oder die Konzentration beeinflusst. Üblicherweise wird zur Durchführung von derartigen Experimenten zunächst eine klare Lösung des BTAs benötigt. Anschließend wird durch einen äußeren Einfluss, wie zum Beispiel durch Kühlen der Lösung, der Selbstassemblierungsprozess gestartet.

Zunächst musste ein Versuchsaufbau entwickelt werden, der die Kontrolle über sämtliche Prozessparameter ermöglicht. Der äußere Einfluss zum Start der Selbstassemblierung war das Kühlen einer BTA-Lösung. Die Untersuchungen konzentrierten sich auf einen möglichen Einfluss durch mechanisches Rühren der Lösung während der Selbstassemblierung auf die entstehende Morphologie der supramolekularen Fasern. Da Wärmeaustauschprozesse ein wichtiger Bestandteil dieser

Experimente sind, wurde der Einfluss des mechanischen Rührens auf den Kühlvorgang theoretisch beschrieben.

Ausgehend von fünf verschiedenen alkoxy-substituierten 1,3,5-Benzoltriamiden wurde *N,N',N''*-Tris(1-methoxybutan-2-yl)-benzol-1,3,5-tricarboxamid (BTA **4**) in einer Lösungsmittelmischung von Wasser und Isopropanol (80:20) und einer Konzentration von 0,05 Gew.-% als geeignetes System identifiziert. Diese Kombination zeigte das am stärksten ausgeprägte temperaturabhängige Löslichkeitsverhalten und die beste Faserbildung aus Lösung hinsichtlich Länge und Durchmesser der entstehenden Strukturen.

In einer *ersten Reihe von Experimenten unter kontrollierten Bedingungen* wurde die mechanische Rührgeschwindigkeit während der Selbstassemblierung variiert. Alle anderen Parameter wurden konstant gehalten. Die Ergebnisse erwiesen sich als äußerst reproduzierbar. Eine Erhöhung der Rührgeschwindigkeit führte zu einer Verringerung des supramolekularen Faserdurchmessers. Zudem wurden die Verteilungen der Faserdurchmesser enger. Die Analyse zeigte, dass bis zu einer Rührgeschwindigkeit von 150 Umdrehungen pro Minute starke Verbesserungen der Kühlleistung festzustellen waren. Oberhalb dieser Geschwindigkeit konnten jedoch nur noch geringe Änderungen im Temperaturverlauf beobachtet werden. Die Unterschiede in der Morphologie der supramolekularen Fasern und in den Temperaturverläufen zeigten, dass die *Morphologie der Nanofasern hauptsächlich durch Einflüsse auf den Kühlverlauf bestimmt wird*. Oberhalb einer Rührgeschwindigkeit von 150 Umdrehungen pro Minute konnten keine wesentlichen Änderungen im Faserdurchmesser festgestellt werden.

In einer *zweiten Reihe von Experimenten* wurde die außen *angelegte Kühltemperatur variiert* und es wurde beobachtet, dass die supramolekulare Fasermorphologie ebenfalls durch Änderung dieses Parameters beeinflusst werden kann, während die mechanische Rührgeschwindigkeit für alle Experimente gleich blieb. Folglich hat das mechanische Rühren keinen direkten Einfluss auf die supramolekulare Fasermorphologie. Nur durch eine gleichzeitige Änderung des Kühlverlaufs kann ein indirekter Einfluss erzielt werden.

Im zweiten Kapitel „*Supramolecular nanofibers for air filtration applications*“ wurde die Selbstassemblierung von BTAs aus Lösung in einem polymeren Mikrofaservlies zur Präparation von Nanofaser-Mikrofaser-Kompositen untersucht. Im Gegensatz zum ersten Kapitel beinhalten die Experimente sowohl die Kühlung einer BTA Lösung als auch das Verdampfen des Lösungsmittels.

Die Arbeiten werden in zwei Abschnitte unterteilt. Der Erste befasst sich mit der Präparation von Nanofaser-Mikrofaser-Kompositen aus Lösung von drei unterschiedlichen BTAs: *N,N',N''*-Tris(2-

ethylhexyl)-benzol-1,3,5-tricarboxamid (BTA **6**), *N,N',N''*-Tris(6-methylheptyl)-benzol-1,3,5-tricarboxamid (BTA **7**) und *N,N',N''*-Tris(3-methylbutyl)-benzol-1,3,5-tricarboxamid (BTA **8**). Das verwendete Mikrofaservlies war ein Polyester/Viskose-Mischgewebe. Es wurden 2-Butanon, Isopropanol und Ethanol als Lösungsmittel zur Herstellung der Komposite als auch das temperaturabhängige Löslichkeitsverhalten jeder Kombination aus BTA und Lösungsmittel untersucht. Es zeigte sich die enorme Bedeutung dieses Verhaltens auf die entstehende Morphologie der supramolekularen Fasern in den Kompositen. Zu hohe Löslichkeiten der BTAs in den jeweiligen Lösungsmitteln erscheinen weniger geeignet für die Herstellung entsprechender Komposite.

Unterschiedliche Nanofaser-Mikrofaser-Komposite wurden präpariert und durch Rasterelektronenmikroskopie und durch Filtrationstests zur Entfernung von Feinstaub aus Luft charakterisiert. Konzentrationsabhängige Experimente ergaben, dass ein BTA-Anteil von 1.0 Gew.-% in der Lösung ausreichend ist, um einen Komposit mit homogen verteilten Nanofasern in den Poren des Mikrofaservlieses zu erhalten. Entsprechende Filtrationsexperimente demonstrierten bemerkenswert hohe Effizienzen zur Abtrennung von Feinstaub aus Luft (iso fine dust). In wiederholten Experimenten wurde zudem die hohe Reproduzierbarkeit des Prozesses deutlich. Ausgewählte Komposite wurden mittels Kapillarfluss-Porometrie charakterisiert. Dabei wiesen Komposite mit BTA **8** sehr viel breitere Porengrößenverteilungen auf als Komposite mit BTA **7**. Diese Ergebnisse korrelieren mit den Ergebnissen aus den Filtrationsexperimenten. In lösungsmittelabhängigen Experimenten erwies sich 2-Butanon als das geeignetste Lösungsmittel für die Herstellung von homogenen Nanofaser-Mikrofaser-Kompositen im Vergleich zu Isopropanol und Ethanol. Dabei ist der Prozess zur Herstellung der Komposite äußerst sensibel hinsichtlich des gewählten Lösungsmittels oder der molekularen Struktur des BTAs. Durch Infrarotspektroskopie konnte bestätigt werden, dass die supramolekularen Nanofasern in den Kompositen aus Kolumnen basierend auf der Bildung von gerichteten Wasserstoffbrückenbindungen bestehen.

Zusammenfassend wurde in diesem ersten Abschnitt gezeigt, dass *supramolekulare Nanofasern in Kompositen ein großes Potential im Bereich der Luftfiltration aufweisen, und dass die entstehende Morphologie der supramolekularen Fasern stark von der Wahl der Prozessparameter abhängig ist.*

Im zweiten Abschnitt dieses Kapitels wurde die Herstellung von Nanofaser-Mikrofaser-Kompositen auf die Verwendung eines alkoxy-substituierten BTAs (BTA **4**) aus einer Lösungsmittelmischung von Wasser und Isopropanol (60:40) erweitert. Als Mikrofaservlies wurde ein technisches Polyestervlies verwendet. Konzentrationsabhängige Experimente zeigten, dass der mittlere Faserdurchmesser stets im Bereich von 500 bis 650 nm lag. Die Komposite wiesen Filtrationseffizienzen zwischen 50 und 80% bei Differenzdrücken von lediglich 57 Pa auf. Im Vergleich zu Kompositen aus dem ersten Abschnitt

dieses Kapitels ist der Differenzdruck um ca. eine Größenordnung geringer. *Folglich kann das Konzept der Herstellung von Nanofaser-Mikrofaser Kompositen vom Modellvlies aus dem ersten Abschnitt auf weitere Systeme durch die Wahl geeigneter Prozessparameter übertragen und optimiert werden.*

Das letzte Kapitel „**Sand - supramolecular nanofiber filters for the removal of bacteria from water**“ beschäftigt sich mit der Entwicklung eines Herstellungsprozesses zur *in situ* Präparation von supramolekularen Nanofasern innerhalb einer granulären Schüttung zur Anwendung in der Flüssigfiltration. Dabei mussten zwei grundlegende Aufgaben bearbeitet werden. Die Erste entspricht der Herstellung und Charakterisierung einer Filtereinheit, die ein Material beinhalten soll, dass in der Lage ist, feste Mikropartikel aus Wasser abzutrennen. Die zweite Aufgabe beinhaltete die Entwicklung eines Prüfstands zur Wasserfiltration, der die Bewertung hinsichtlich Filtrationseffizienz sowie Druckverlust der Filtereinheiten ermöglicht. Später wurden diese Filtereinheiten zur Abtrennung von Bakterien aus Wasser eingesetzt.

Als granuläre Schüttung wurde Seesand gewählt und durch Anwendung des entwickelten Prozesses konnte ein formstabiles Material aus Sand und supramolekularen Nanofasern hergestellt werden. Der Prozess umfasste einen Tauchvorgang der Schüttung in eine BTA-Lösung bei erhöhten Temperaturen gefolgt von einer Kühlung und dem Austausch des Lösungsmittels. Lediglich 50 mg der supramolekularen Nanofasern reichten aus, um 25 g der Sandpartikel miteinander zu verbinden und ein formstabiles Material zu ergeben. Rasterelektronenmikroskopische Analysen zeigten supramolekulare Nanofasern mit einem mittleren Durchmesser von 500 nm in den Zwischenräumen des Sandes. Die Filtrationsleistung wurde zunächst mit dem entwickelten Prüfstand untersucht. Dabei wurden Mikropartikel aus Polystyrol mit einem Durchmesser von 1,1 µm aus Wasser filtriert. In Abhängigkeit des Anteils supramolekularer Nanofasern konnten Effizienzen bis zu 90% erreicht werden. Selbst nach einer Filtrationszeit von 24 h war immer noch ein stabiles Netzwerk aus supramolekularen Nanofasern in der Schüttung vorhanden. Nachdem alle Parameter zur Herstellung der Filtereinheiten optimiert waren, wurden Filtrationsexperimente zur Abtrennung von *E. coli* Bakterien aus Wasser bei unterschiedlichen Keimbelastungen durchgeführt. *Die hergestellten Filtereinheiten wiesen Filtrationseffizienzen von bis zu 100%, abhängig von der zu filtrierenden Bakterienkonzentration, auf.*

## 8 Appendix

### 8.1 Materials and Methods

The synthesis of the individual 1,3,5-benzenetrisamides investigated in the course of this thesis was performed by Sandra Ganzleben, Jutta Failner, Rika Schneider and Doris Hanft. The analytical data presented for BTAs 6, 7 and 8 are based on the work of Timme.<sup>[163]</sup>

*Scanning electron microscopy* (SEM) investigations were performed on a Zeiss 1530 equipped with a field emission cathode. Images were taken utilizing a SE2 detector and an accelerating voltage of 2 kV.

<sup>1</sup>H-NMR and <sup>13</sup>C-NMR spectra were measured utilizing a Bruker Ultrashield 300. The corresponding frequencies were 300 MHz for 1H-NMR measurements and 75 MHz for 13C-NMR measurements. Evaluation of the obtained data was performed by utilization of a suitable software MestReNova (Mestrelab Research S.L., version 6.1.0-6224). The solvent signals were used as internal reference.

*Thermogravimetric analysis* (TGA) was performed on a Mettler Toledo TGA/SDTA 851e. Data were recorded with a scan rate of 10 K/min in a temperature range from 30 to 700 °C. All measurements were conducted under nitrogen atmosphere.

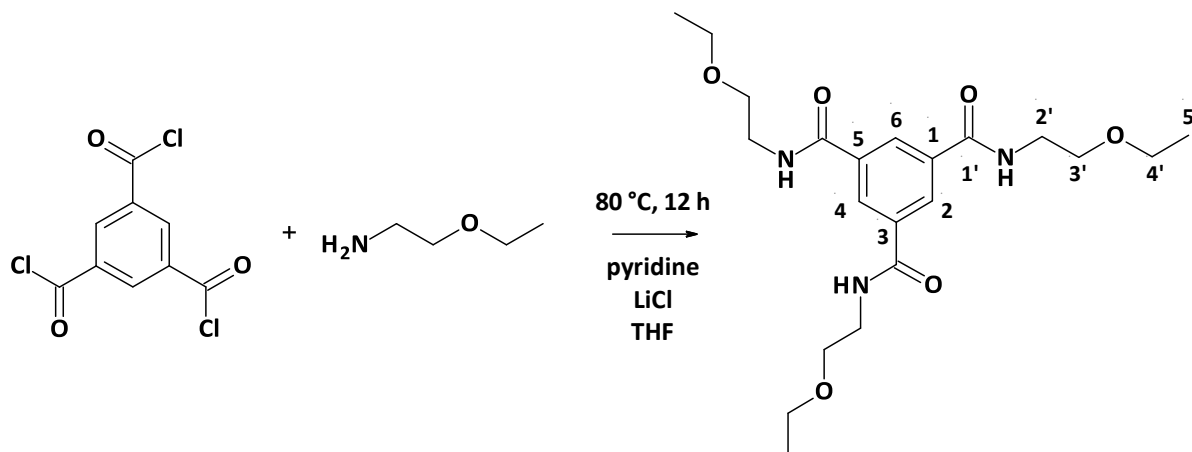
*Differential scanning calorimetry* (DSC) was measured on a Perkin Elmer Diamond DSC with a scan rate of 10 K/min. Each measurement was performed in a high pressure DSC pan. The investigated temperature range was selected according to the corresponding to the data obtained by TGA analysis.

*XRD measurements* were carried out on a Huber Guinier diffractometer 600 that was equipped with a Huber germanium monochromator 611 to provide CuK<sub>α</sub>-radiation ( $\lambda=154.051$  pm). All samples were analyzed in a range from 0.5 to 15°. A custom-made furnace was implemented into the experimental setup that allowed for the investigation of each sample in a temperature range from room temperature to 250 °C. The samples were prepared in glass capillaries with a diameter of 1.5 to 2 mm.

## 8.2 Synthesis and analytical data of *N,N,N'*-tris(2-ethoxyethyl)benzene-1,3,5-tricarboxamide

Identifier: (BTA 1) (LK 1)

Synthesis:



To a solution of 2-ethoxyethanamine (7.8 mL; 74 mmol; 3.2 eq), pyridine (5 mL; 62.1 mmol; 3.3 eq) and a spatula tip of LiCl in THF (150 mL) was added 1,3,5-benzenetricarbonyl trichloride (6 g; 23 mmol; 1 eq) slowly at 0 °C under argon atmosphere. The reaction mixture was stirred overnight at 80 °C and the solvent was removed in vacuo. The residue was dissolved in methylenchloride (100 mL) and the organic phase was washed with HCl (2 M; 2 x 40 mL) and brine and dried over Na<sub>2</sub>SO<sub>4</sub>. The crude product was recrystallized from MeOH/EE (1:9), washed with diethyl ether and dried in vacuo to yield the product as a white solid (7.9 g; 18.6 mmol; 81%).

Characterization:

<sup>1</sup>H-NMR (300 MHz; DMSO; δ): 8.72 (m; 3-H; N-H), 8.41 (s; 3-H; H<sub>2</sub>, H<sub>4</sub>, H<sub>6</sub>), 3.51 – 3.41 (m; 18-H; H<sub>2</sub>, H<sub>3</sub>, H<sub>4</sub>), 1.15 (t; J = 6,8 Hz; 9-H; H<sub>5</sub>).

<sup>13</sup>C-NMR (75 MHz; DMSO; δ): 166.0 (C-1'), 135.3 (C-1, C-3, C-5), 129.0 (C-2, C-4, C-6), 68.7 (C-3'), 65.9 (C-4'), 40.8 (C-2'), 15.6 (C-5').

MS (m/z, %): 423 (3), 394 (9), 377 (57), 352 (9), 335 (100), 306 (12), 289 (8), 263 (11), 248 (8), 219 (6), 202 (15), 173 (4), 146 (10), 133 (7), 103 (11), 75 (19), 72 (82), 44 (48).

*Thermogravimetric analysis:*

- 5% decrease of mass at 350 °C.

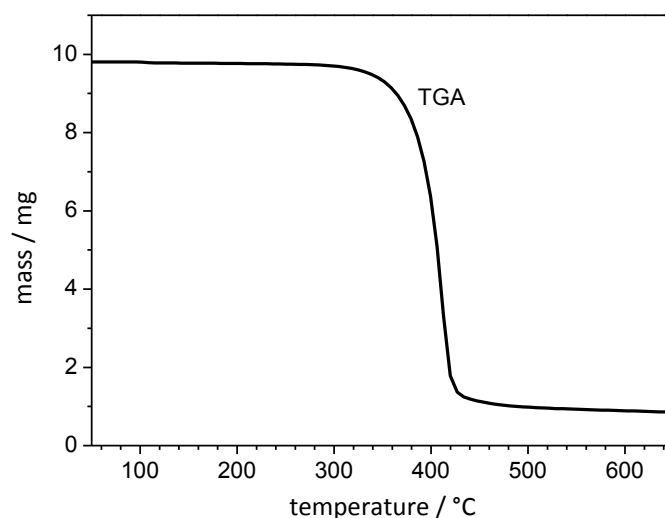


**Figure 8.1:** Thermogravimetric analysis curve of *N,N',N''*-tris(2-ethoxyethyl)benzene-1,3,5-tricarboxamide (BTA 1). TGA data were recorded at a scanning rate of 10 K/min at temperatures ranging from 30 to 700 °C.

*Differential scanning calorimetry:*

- 1<sup>st</sup>-heating curve: Phase transition at 117 °C (39 kJ/mol)
- No recrystallization upon cooling

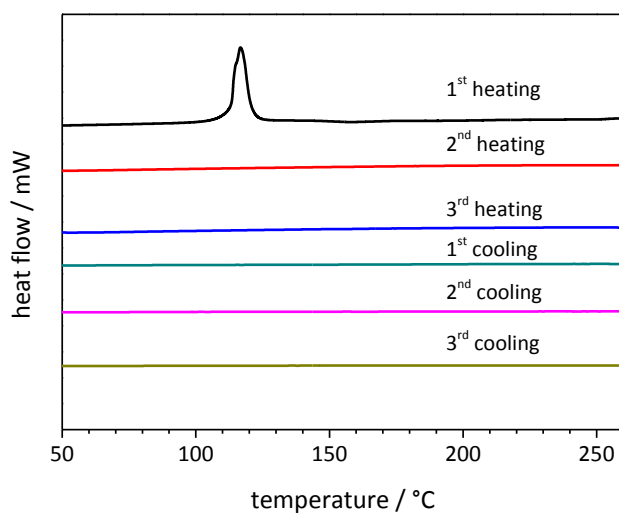


**Figure 8.2:** DSC heating and cooling scans of *N,N',N''*-tris(2-ethoxyethyl)benzene-1,3,5-tricarboxamide (BTA 1). DSC data were recorded at a scanning rate of 10 K/min at temperatures ranging from 20 to 280 °C.

*X-Ray analysis:*

- Data show no crystalline structure after heating beyond 125 °C and cooling back to RT.

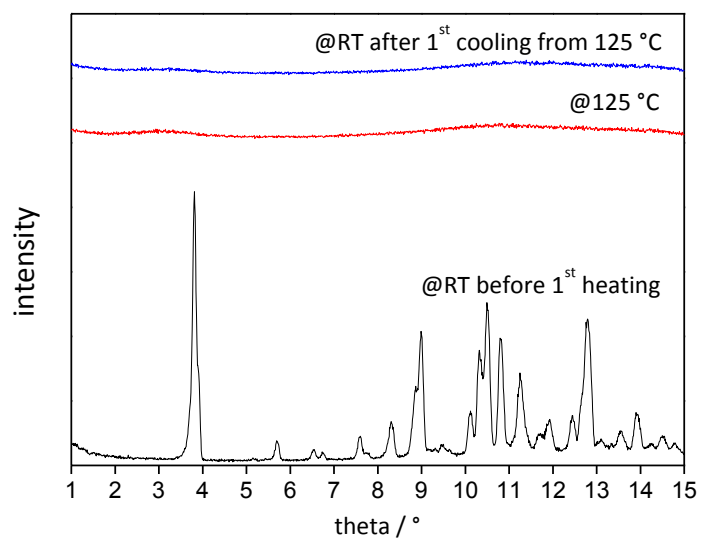
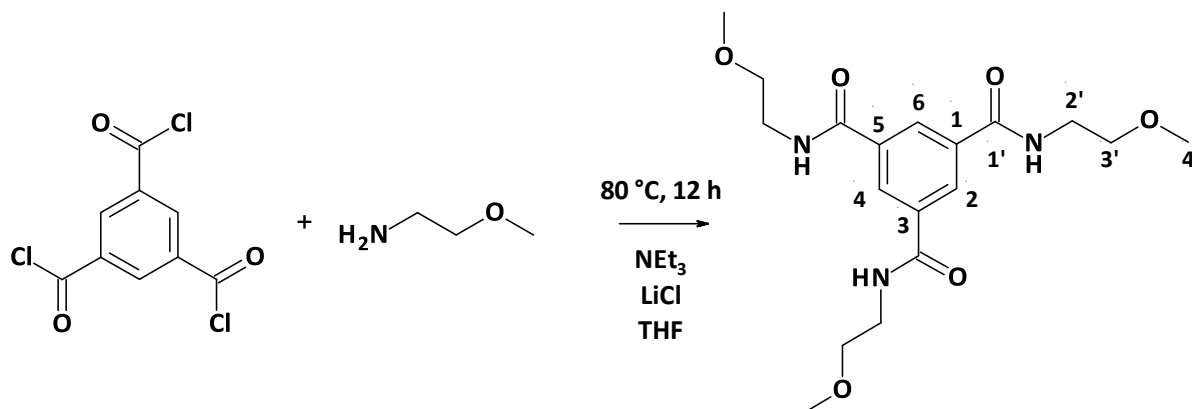


**Figure 8.3:** X-Ray diffraction diagrams of BTA 1 at different temperatures.

### 8.3 Synthesis and analytical data of *N,N,N'*-tris(2-methoxyethyl)benzene-1,3,5-tricarboxamide

Identifier: (BTA 2) (LK 2)

Synthesis:



To a solution of 2-methoxyethanamine (11 mL; 126 mmol; 3.3 eq), triethylamine (12 mL; 87 mmol; 2.29 eq) and a spatula tip of LiCl in THF (100 mL) was added benzene-1,3,5-tricarbonyl trichloride (10 g; 38 mmol; 1 eq) slowly at 0 °C under argon atmosphere. The reaction mixture was stirred overnight under reflux and then the solvent was removed in vacuo. The residue was dissolved in methylenchloride (200 mL) and the organic phase was washed with HCl (2 M; 2 x 40 mL) and brine and dried over Na<sub>2</sub>SO<sub>4</sub>. The crude product was recrystallized from ethanol (10 mL) and dried in vacuo to yield the product as a white solid (13 mmol; 35%).

Characterization:

<sup>1</sup>H-NMR (300 MHz; DMSO; δ): 8.74 (m; 3-H; N-H), 8.40 (s; 3-H; H<sub>2</sub>, H<sub>4</sub>, H<sub>6</sub>), 3.50 – 3.45 (m; 12-H; H<sub>2</sub>, H<sub>3</sub>), 3.28 (s; 9-H; H<sub>4</sub>).

<sup>13</sup>C-NMR (75 MHz; DMSO; δ): 166.0 (C-1'), 135.2 (C-1, C-3, C-5), 129.0 (C-2, C-4, C-6), 70.8 (C-3'), 58.4 (C-4'), 39.6 (C-2').

MS (m/z, %): 381 (3), 349 (24), 307 (100), 275 (4), 249 (11), 234 (5), 205 (6), 176 (3), 145 (3), 117 (2), 103 (4), 75 (7), 58 (10), 46 (8).

*Thermogravimetric analysis:*

- 5% decrease of mass at 364 °C.

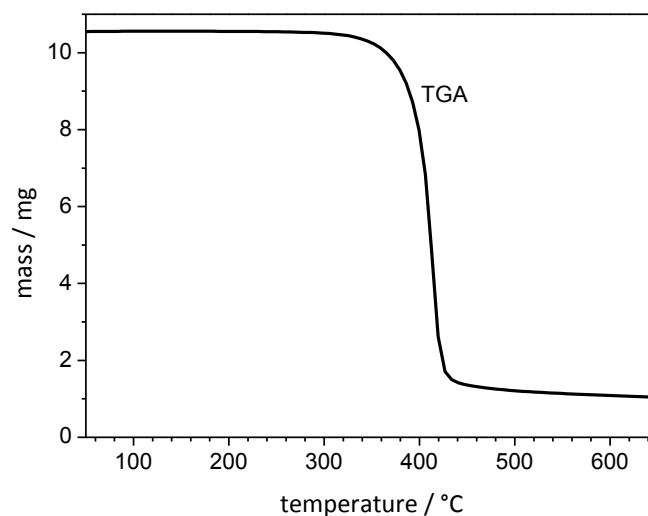


**Figure 8.4:** Thermogravimetric analysis curve of *N,N',N''*-tris(2-methoxyethyl)benzene-1,3,5-tricarboxamide (BTA 2). TGA data were recorded at a scanning rate of 10 K/min at temperatures ranging from 30 to 700 °C.

*Differential scanning calorimetry:*

- 1<sup>st</sup>-heating curve: Phase transition at 158 °C (37 kJ/mol).
- Shift of phase transition in 2<sup>nd</sup> (155 °C, 36 kJ/mol) and 3<sup>rd</sup> (155 °C, 36 kJ/mol) heating curve.
- 2 phase transitions in 2<sup>nd</sup> cooling curve. 120 °C (24 kJ/mol) and 65 °C (2 kJ/mol)

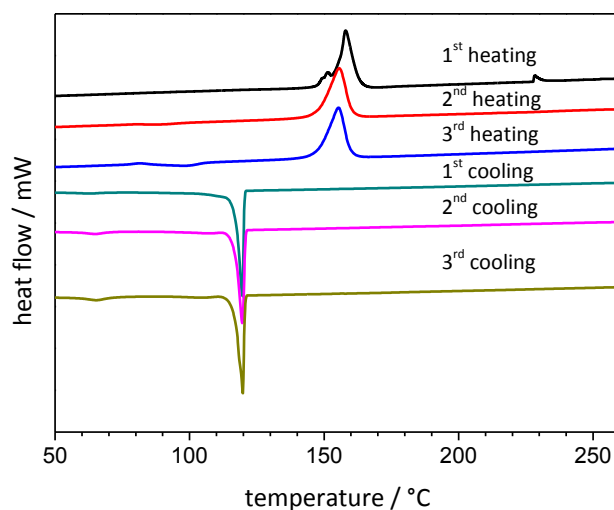


**Figure 8.5:** DSC heating and cooling scans of *N,N',N''*-tris(2-methoxyethyl)benzene-1,3,5-tricarboxamide (BTA 2). DSC data were recorded at a scanning rate of 10 K/min at temperatures ranging from 20 to 275 °C.

*X-Ray analysis:*

- No crystalline structure at 180 °C.
- No change in crystalline structure between room temperature and 90 °C.
- Different structure before and after cooling from 180 °C.

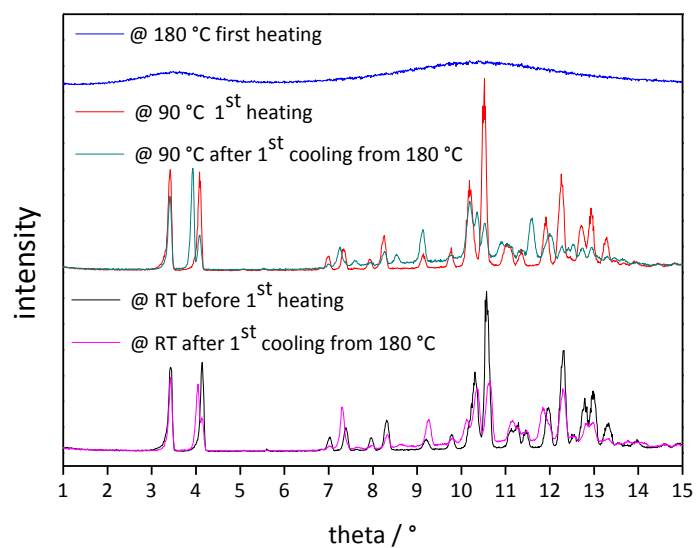
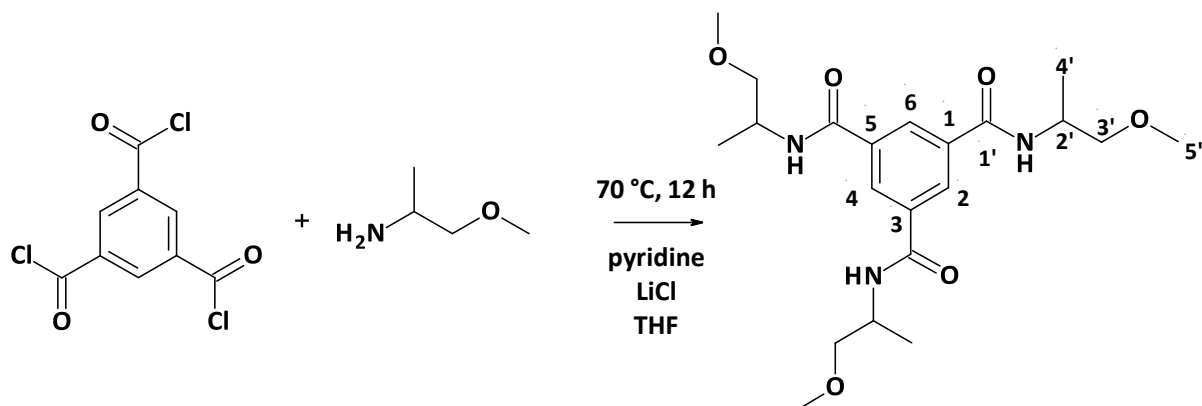


**Figure 8.6:** X-Ray diffraction diagrams of BTA 2 at different temperatures.

#### 8.4 Synthesis and analytical data of *N,N',N''*-tris(1-methoxypropan-2-yl)benzene-1,3,5-tricarboxamide

Identifier: (BTA 3) (LK 3)

Synthesis:



To a solution of 1-methoxy-2-propylamine (5.5 mL; 56 mmol; 3.50 eq), pyridine (5 mL; 62.1 mmol; 3.88 eq) and a spatula tip of LiCl in THF (150 mL) was added benzene-1,3,5-tricarbonyl trichloride (4.24 g; 16 mmol; 1 eq) slowly at 0 °C. The reaction mixture was stirred overnight at 70 °C and then the solvent was removed in vacuo. The residue was dissolved in methylenchloride (100 mL) and the organic phase was washed with HCl (2 M; 2x 40 mL) and brine and dried over Na<sub>2</sub>SO<sub>4</sub>. The crude product was recrystallized from ethanol (100 mL) and dried in vacuo to yield the product as a white solid (5.82 mmol; 35%).

Characterization:

<sup>1</sup>H-NMR (300 MHz; DMSO; δ): 8.53 (d; *J* = 8.0 Hz; 3-H; N-H), 8.35 (s; 3-H; H<sub>2</sub>, H<sub>4</sub>, H<sub>6</sub>), 4.20 (q; *J* = 6.6 Hz; 3-H; H<sub>2</sub>), 3.40 – 3.30 (m; 6-H; H<sub>3</sub>'), 3.35 (s; 9-H; H<sub>5</sub>'), 1.15 (d; *J* = 6,8 Hz; 9-H; H<sub>4</sub>').

<sup>13</sup>C-NMR (75 MHz; DMSO; δ): 165.61 (C-1'), 135.46 (C-1, C-3, C-5), 129.06 (C-2, C-4, C-6), 75.36 (C-3'), 58.56 (C-5'), 45.09 (C-2'), 17.77 (C-4'1).

MS (*m/z*, %): 392 (6), 379 (32), 353 (14), 336 (100), 220 (4), 45 (5).

*Thermogravimetric analysis:*

- 5% decrease of mass at 333 °C.

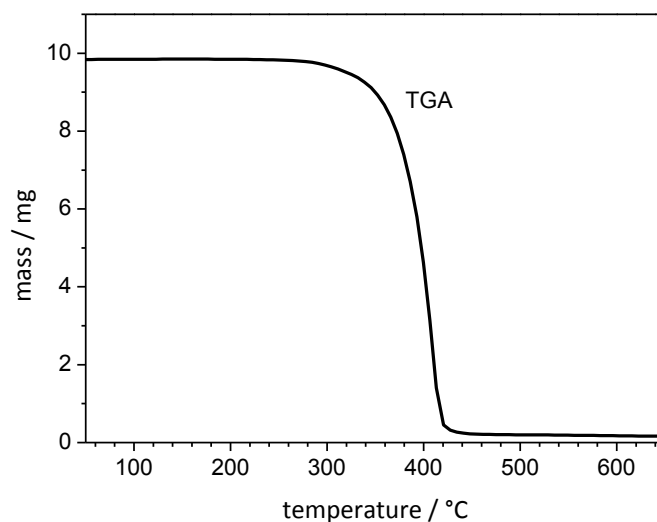


**Figure 8.7:** Thermogravimetric analysis curve of *N,N',N''*-tris(1-methoxypropan-2-yl)benzene-1,3,5-tricarboxamide (BTA 3). TGA data were recorded at a scanning rate of 10 K/min at temperatures ranging from 30 to 700 °C.

*Differential scanning calorimetry:*

- 1<sup>st</sup>-heating curve: Phase transition at 312 °C (44 kJ/mol).
- Shift of phase transition temperature to 306 °C in 2<sup>nd</sup> and 3<sup>rd</sup> heating curve

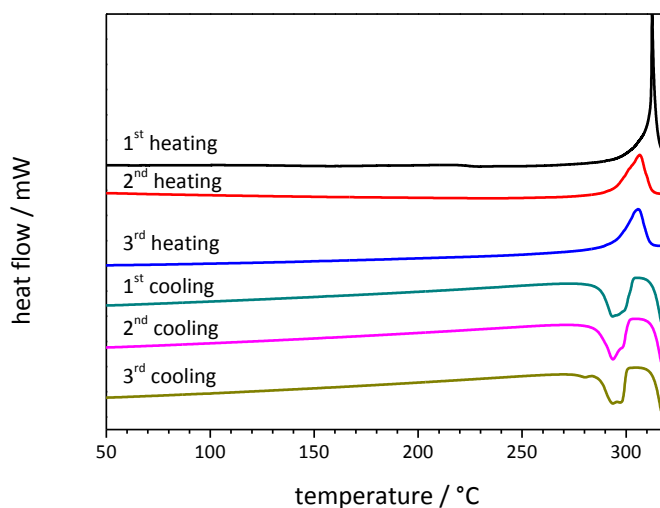


**Figure 8.8:** DSC heating and cooling scans of *N,N',N''*-tris(1-methoxypropan-2-yl)benzene-1,3,5-tricarboxamide (BTA 3). DSC data were recorded at a scanning rate of 10 K/min at temperatures ranging from 20 to 320 °C.

X-Ray analysis:

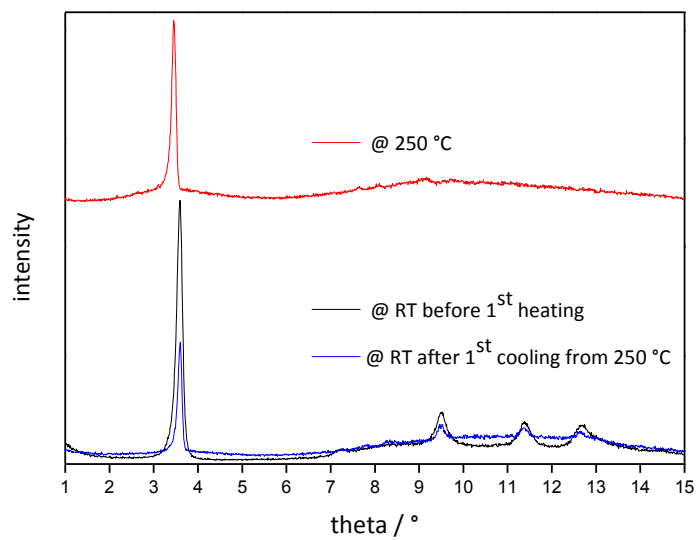
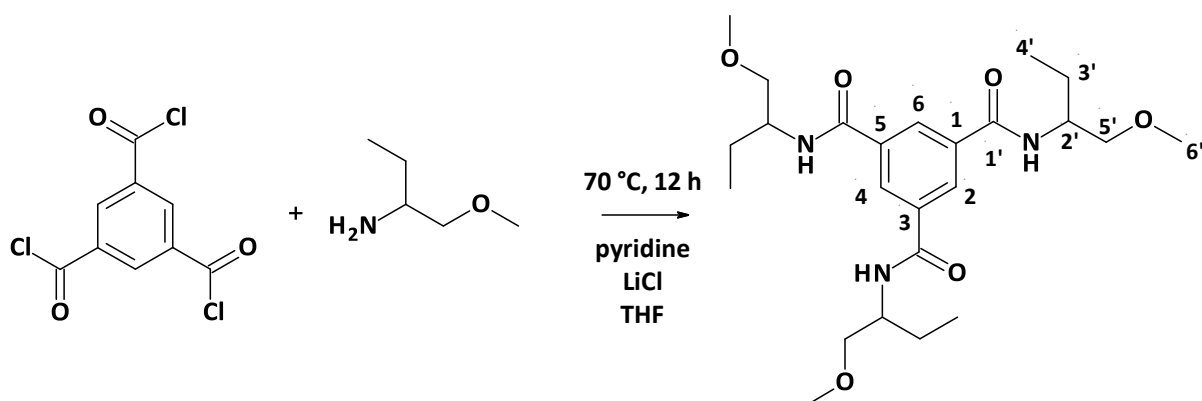


**Figure 8.9:** X-Ray diffraction diagrams of BTA 3 at different temperatures.

## 8.5 Synthesis and analytical data of *N,N',N''*-tris(1-methoxybutan-2-yl)benzene-1,3,5-tricarboxamide

Identifier: (BTA 4) (LK 4)

Synthesis:



To a solution of 2-amino-1-methoxybutane (8 mL; 70 mmol; 3.50 eq), pyridine (7 mL; 86,7 mmol; 4.34 eq) and a spatula tip of LiCl in THF (150 mL) was added benzene-1,3,5-tricarbonyl trichloride (5.55 g; 20 mmol; 1 eq) slowly at 0 °C under argon atmosphere. The reaction mixture was stirred overnight at 70 °C and then the solvent was removed in vacuo. The residue was dissolved in methylenchloride (100 mL) and the organic phase was washed with HCl (2 M; 2x 40 mL) and brine and dried over Na<sub>2</sub>SO<sub>4</sub>. The crude product was recrystallized from ethanol (100 mL) and dried in vacuo to yield the product as a white solid (6.18 mmol; 31%).

Characterization:

<sup>1</sup>H-NMR (300 MHz; DMSO; δ): 8.45 (d; *J* = 8.0 Hz; 3-H; N-H), 8.37 (s; 3-H; H<sub>2</sub>, H<sub>4</sub>, H<sub>6</sub>), 4.06 (m; 3-H; H<sub>2</sub>'), 3.42 – 3.32 (m; 6-H; H<sub>5</sub>'), 3.26 (s; 9-H; H<sub>6</sub>'), 1.62 – 1.49 (m; 6-H; H<sub>3</sub>'), 0.89 (d; *J* = 6.8 Hz; 9-H; H<sub>4</sub>').

<sup>13</sup>C-NMR (75 MHz; DMSO; δ): 166.10 (C-1'), 135.53 (C-1, C-3, C-5), 129.06 (C-2, C-4, C-6), 74.33 (C-5'), 58.58 (C-6'), 50.86 (C-2'), 24.39 (C-3'), 11.03 (C-4').

MS (*m/z*, %): 436 (3), 421 (49), 381 (13), 364 (100), 349 (2), 317 (3), 277 (4), 262 (4), 233 (5), 206 (3), 172 (2), 160 (4), 132 (2), 86 (6), 75 (6), 46 (14).

*Thermogravimetric analysis:*

- 5% decrease of mass at 338 °C.

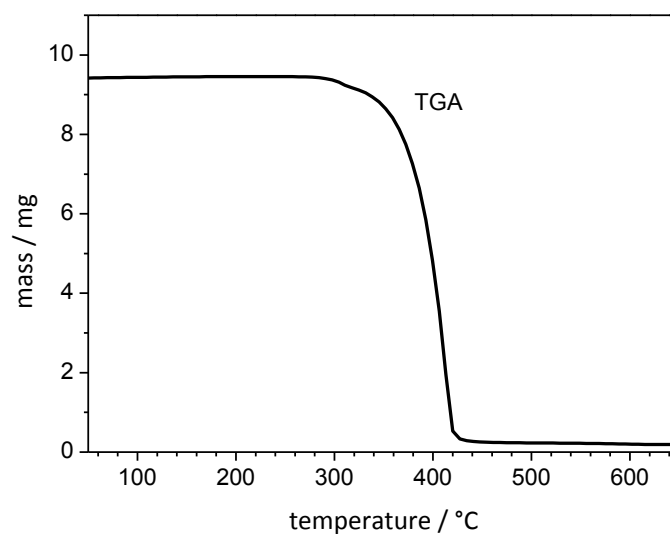


**Figure 8.10:** Thermogravimetric analysis curve of *N,N,N''*-tris(1-methoxybutan-2-yl)benzene-1,3,5-tricarboxamide (BTA 4). TGA data were recorded at a scanning rate of 10 K/min at temperatures ranging from 30 to 700 °C.

*Differential scanning calorimetry:*

- 1<sup>st</sup>-heating curve: Phase transition at 324 °C (45 kJ/mol).
- Shift of phase transition temperature to 318 °C in 2<sup>nd</sup> and 3<sup>rd</sup> heating curves

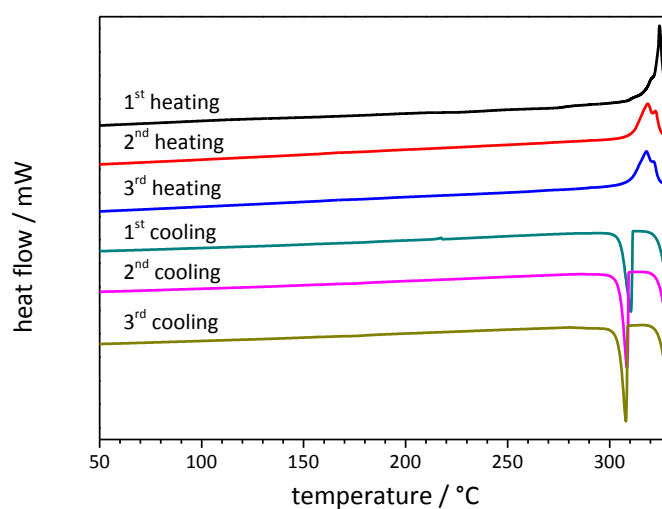


**Figure 8.11:** DSC heating and cooling scans of *N,N,N''*-tris(1-methoxybutan-2-yl)benzene-1,3,5-tricarboxamide (BTA 4). DSC data were recorded at a scanning rate of 10 K/min at temperatures ranging from 20 to 330 °C.

*X-Ray analysis:*

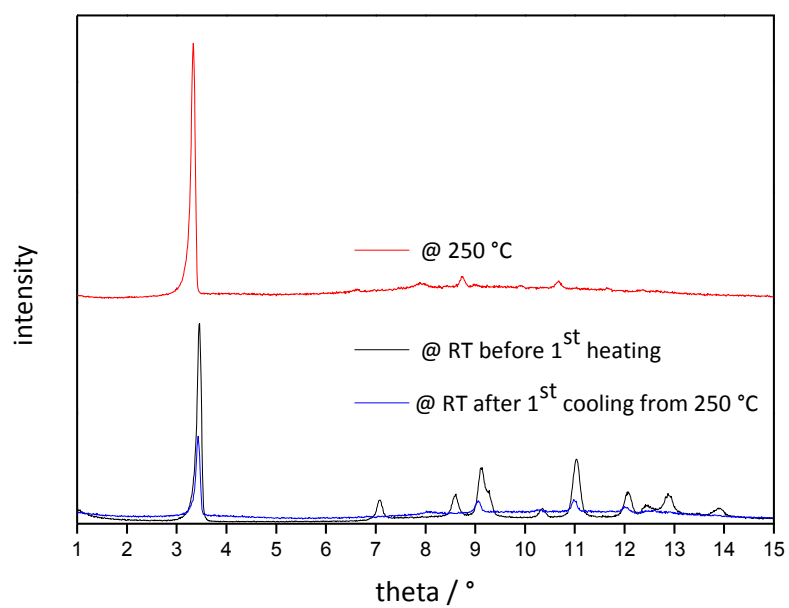
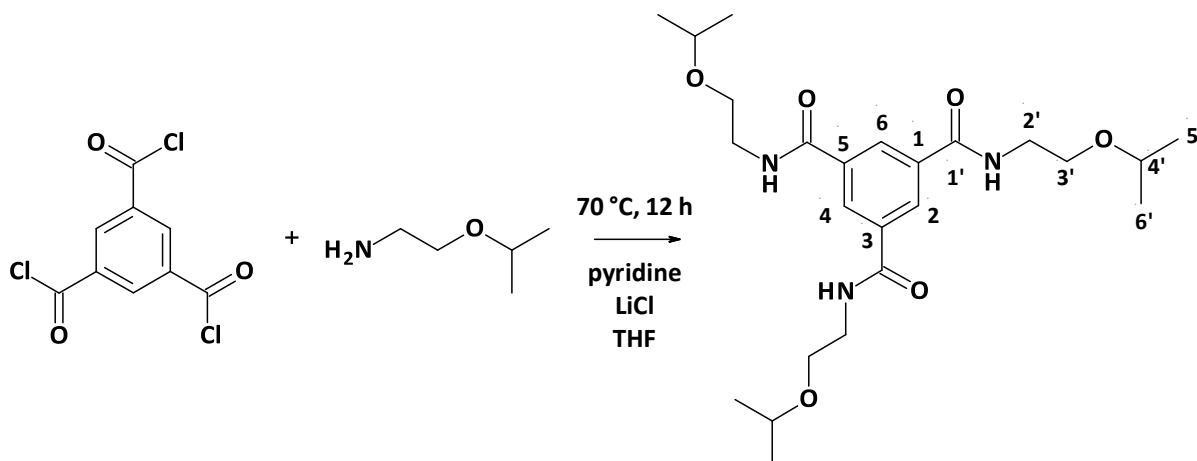


**Figure 8.12:** X-Ray diffraction diagrams of BTA 4 at different temperatures.

## 8.6 Synthesis and analytical data of *N,N',N''*-tris(2-isopropoxyethyl)benzene-1,3,5-tricarboxamide

Identifier: (BTA 5) (LK 5)

Synthesis:



To a solution of 2-amino-ethyl-isopropylether (5 mL; 40.7 mmol; 3.4 eq), pyridine (5 mL; 62.1 mmol; 5.2 eq) and a spatula tip of LiCl in THF (150 mL) was added benzene-1,3,5-tricarbonyl trichloride (3.28 g; 12 mmol; 1 eq) slowly at 0 °C under argon atmosphere. The reaction mixture was stirred overnight at 70 °C and then the solvent was removed in vacuo. The residue was dissolved in methylenchloride (100 mL) and the organic phase was washed with HCl (2 M; 2x 40 mL) and brine and dried over Na<sub>2</sub>SO<sub>4</sub>. The crude product was purified via column chromatography (silica gel 60, 10% MeOH/EE) to yield the product as a white solid (8.41 mmol; 70%).

<sup>1</sup>H-NMR (300 MHz; DMSO; δ): 8.69 (m; 3-H; N-H), 8.40 (s; 3-H; H<sub>2</sub>, H<sub>4</sub>, H<sub>6</sub>), 3.60 – 3.40 (m; 18-H; H<sub>2</sub>, H<sub>3</sub>, H<sub>4</sub>), 1.10 (d; *J* = 6,1 Hz; 18-H; H<sub>5</sub>, H<sub>6</sub>).

<sup>13</sup>C-NMR (75 MHz; DMSO; δ): 166.0 (C-1'), 135.3 (C-1, C-3, C-5), 129.0 (C-2, C-4, C-6), 71.3 (C-4'), 66.2 (C-3'), 40.5 (C-2'), 22.5 (C-5', C-6').

MS (*m/z*, %): 465 (4), 422 (78), 405 (100), 380 (28), 363 (66), 336 (48), 320 (27), 277 (16), 262 (35), 235 (10), 202 (31), 191 (13), 161 (7), 146 (17), 104 (30), 86 (32), 58 (21), 43 (56).

*Thermogravimetric analysis:*

- 5% decrease of mass at 353 °C.

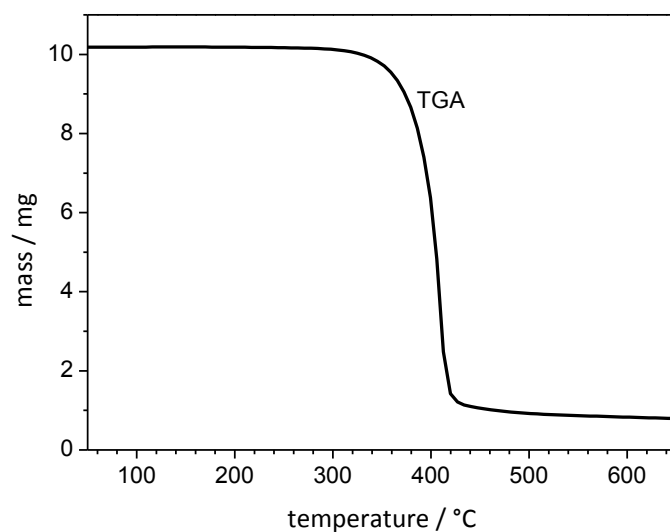


**Figure 8.13:** Thermogravimetric analysis curve of *N,N',N''*-tris(2-isopropoxyethyl)benzene-1,3,5-tricarboxamide (BTA 5). TGA data were recorded at a scanning rate of 10 K/min at temperatures ranging from 30 to 700 °C.

*Differential scanning calorimetry:*

- 1<sup>st</sup>-heating curve: 2 Phase transitions at 65 °C (2 kJ/mol) and 127 °C (23 kJ/mol).

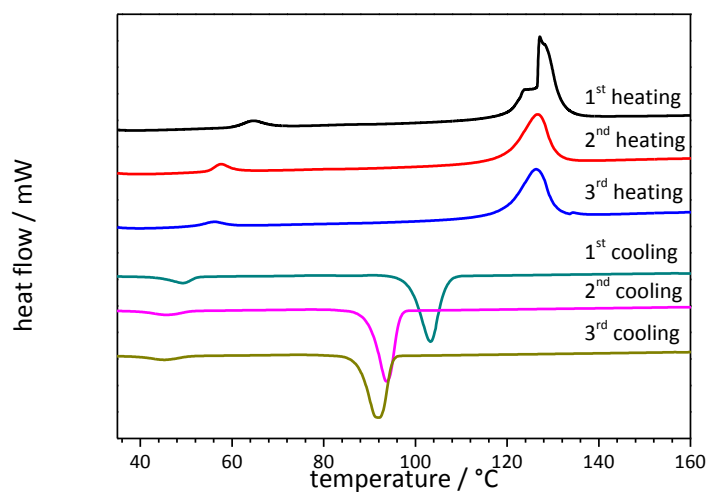


**Figure 8.14:** DSC heating and cooling scans of *N,N',N''*-tris(2-isopropoxyethyl)benzene-1,3,5-tricarboxamide (BTA 5). DSC data were recorded at a scanning rate of 10 K/min at temperatures ranging from 20 to 180 °C.

X-Ray analysis:

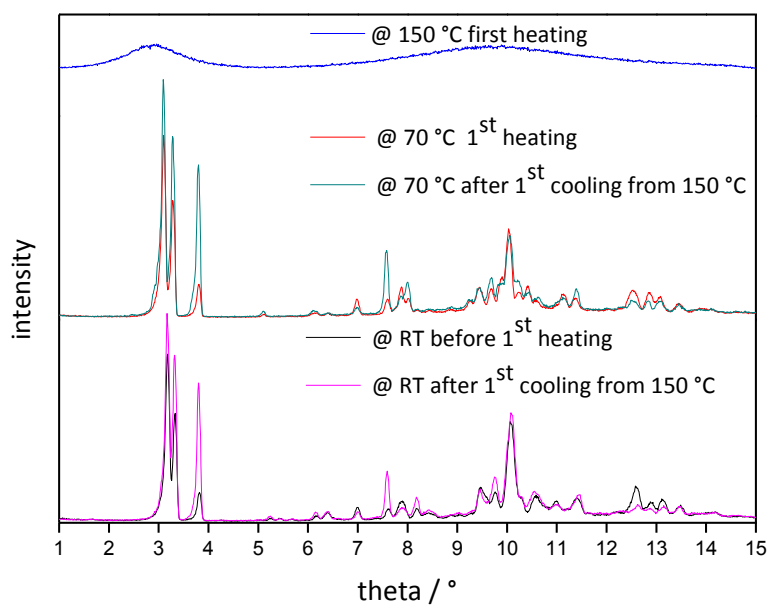
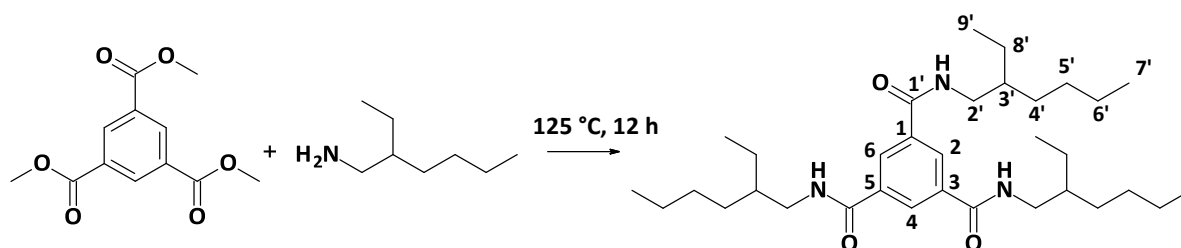


**Figure 8.15:** X-Ray diffraction diagrams of BTA 5 at different temperatures.

## 8.7 Synthesis and analytical data of *N,N',N''*-tris(2-ethylhexyl)benzene-1,3,5-tricarboxamide

Identifier: (BTA 6) (SG417)

Synthesis:



A mixture of 2-ethylhexylamine (49 mL; 297.5 mmol; 5 eq) and trimethyl-1,3,5-benzenetricarboxylate (15 g; 59.5 mmol; 1 eq) was stirred over night at 125 °C. Then the reaction mixture was cooled to room temperature and acetone (200 mL) was added and stirred for 30 min. Filtration yielded the product as a white solid (40.1 mmol; 67.4%).

Characterization:

<sup>1</sup>H-NMR (300 MHz; CDCl<sub>3</sub>+CF<sub>3</sub>COOD; δ): 11.69 (s; 3-H; N-H), 8.67 (s; 3-H; H<sub>2</sub>, H<sub>4</sub>, H<sub>6</sub>), 3.48 (d; *J* = 6.6 Hz; 6-H; H<sub>1</sub>), 1.69 (m; 3-H; H<sub>2</sub>), 1.48 – 1.15 (m; 24-H; H<sub>3</sub>, H<sub>4</sub>, H<sub>5</sub>, H<sub>7</sub>), 1.0 – 0.8 (m; 18-H; H<sub>6</sub>, H<sub>8</sub>).

Thermogravimetric analysis:

- 5% decrease of mass at 360 °C.

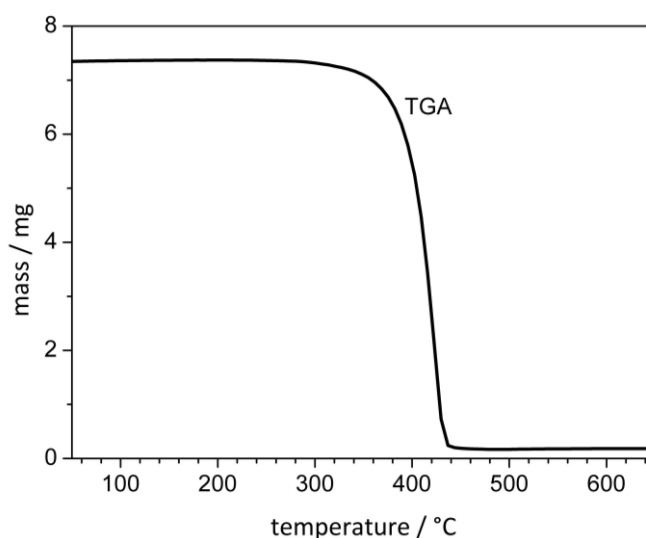


**Figure 8.16:** Thermogravimetric analysis curve of *N,N',N''*-tris(2-ethylhexyl)benzene-1,3,5-tricarboxamide (BTA 6). TGA data were recorded at a scanning rate of 10 K/min at temperatures ranging from 30 to 700 °C.

---

*Differential scanning calorimetry:*

- 1<sup>st</sup>-heating curve: 2 reversible phase transitions at 241 °C (0.18 kJ/mol) and 291 °C (46 kJ/mol)

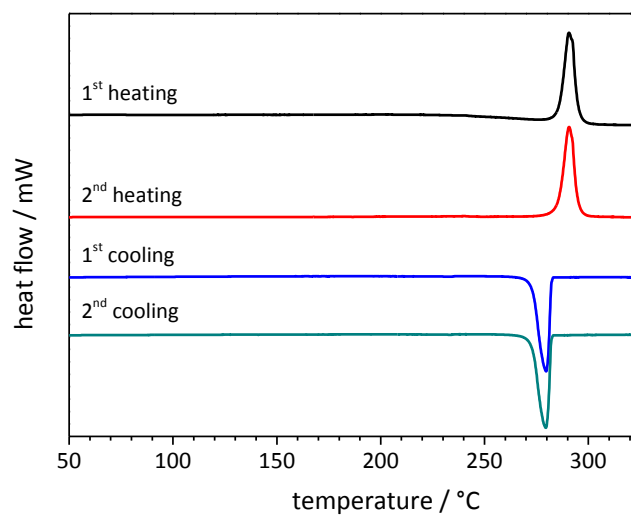
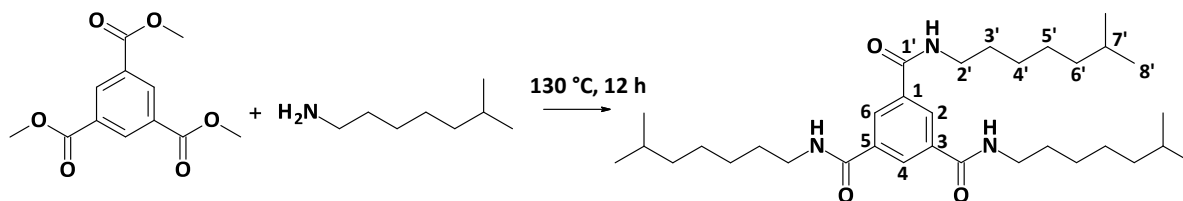


**Figure 8.17:** DSC heating and cooling scans of *N,N',N''*-tris(2-ethylhexyl)benzene-1,3,5-tricarboxamide (BTA 6). DSC data were recorded at a scanning rate of 10 K/min at temperatures ranging from 35 to 330 °C.

## 8.8 Synthesis and analytical data of *N,N',N''*-tris(6-methylheptyl)benzene-1,3,5-tricarboxamide

Identifier: (BTA 7) (JF 114)

Synthesis:



A mixture of 6-methylheptylamine (100 g; 770 mmol; 4 eq) and trimethyl-1,3,5-benzenetricarboxylate (48.8 g; 190 mmol; 1 eq) was stirred over night at 130 °C under argon atmosphere. Then the reaction mixture was cooled to room temperature and hexane (800 mL) was added and stirred for 15 min. The crude product was purified by recrystallization from methanol to yield the product as a white solid (81 mmol; 43%)

Characterization:

$^1\text{H-NMR}$  (300 MHz; DMSO;  $\delta$ ): 8.62 (s; 3-H; N-H), 8.35 (s; 3-H;  $\text{H}_2$ ,  $\text{H}_4$ ,  $\text{H}_6$ ), 3.20 (t;  $J = 5.7$  Hz; 6-H;  $\text{H}_2'$ ), 1.64 – 1.45 (m; 3-H;  $\text{H}_7'$ ), 1.42 – 1.14 (m; 8-H;  $\text{H}_3'$ ,  $\text{H}_4'$ ,  $\text{H}_5'$ ,  $\text{H}_6'$ ), 0.87 (t;  $J = 6.8$  Hz; 6-H;  $\text{H}_8'$ ).

Thermogravimetric analysis:

- 5% decrease of mass at 336 °C.

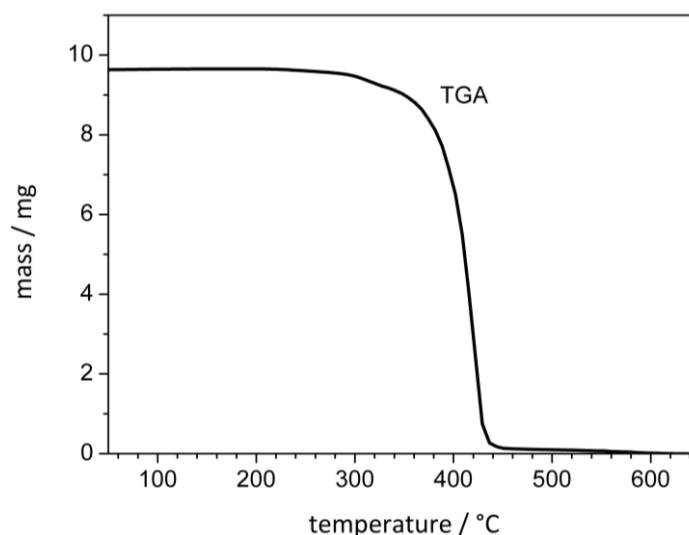


**Figure 8.18:** Thermogravimetric analysis curve of *N,N',N''*-tris(6-methylheptyl)benzene-1,3,5-tricarboxamide (BTA 7). TGA data were recorded at a scanning rate of 10 K/min at temperatures ranging from 30 to 700 °C.

---

*Differential scanning calorimetry:*

- 1<sup>st</sup>-heating curve: 2 reversible phase transitions at 240 °C (0.12 kJ/mol) and 291 °C (48 kJ/mol)

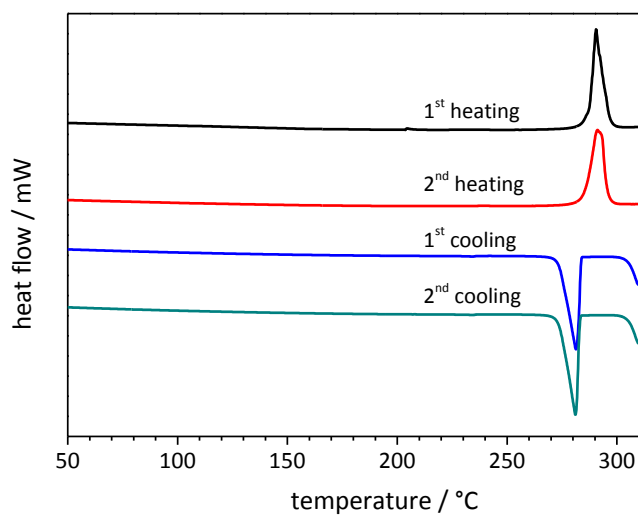
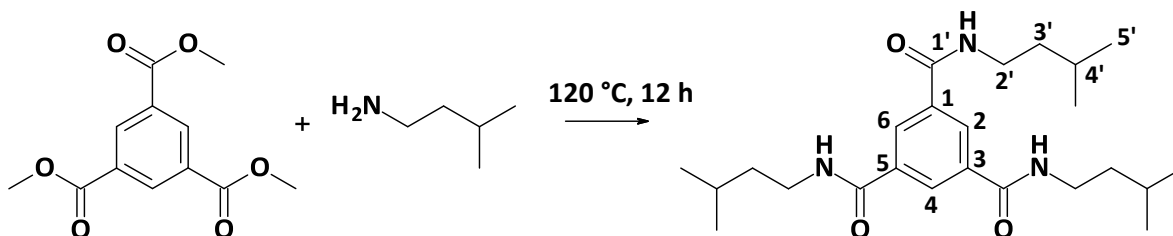


**Figure 8.19:** DSC heating and cooling scans of *N,N',N''*-tris(6-methylheptyl)benzene-1,3,5-tricarboxamide (BTA 7). DSC data were recorded at a scanning rate of 10 K/min at temperatures ranging from 25 to 305 °C.

**8.9 Synthesis and analytical data of *N,N',N''*-tris(3-methylbutyl)benzene-1,3,5-tricarboxamide**

Identifier: (BTA 8) (SG 127)

Synthesis:



A mixture of 3-methylbutylamine (104.6 g; 1200 mmol; 5 eq) and trimethyl-1,3,5-benzenetricarboxylate (60.5 g; 240 mmol; 1 eq) was stirred over night at 120 °C under argon atmosphere. Then the reaction mixture was cooled to room temperature and dispersed in water. Filtration yielded the product as a white solid (482 mmol; 86.2%).

Characterization:

$^1\text{H-NMR}$  (300 MHz; DMSO;  $\delta$ ): 8.64 (t;  $J = 5.4$  Hz, 3-H; N-H), 8.35 (s; 3-H;  $\text{H}_2$ ,  $\text{H}_4$ ,  $\text{H}_6$ ), 3.30 (dd;  $J = 13.0$ , 6.8 Hz; 6-H;  $\text{H}_2'$ ), 1.71 – 1.52 (m, 3-H;  $\text{H}_4'$ ), 1.43 (q;  $J = 7.1$  Hz; 6-H;  $\text{H}_3'$ ), 0.90 (d;  $J = 7.1$  Hz; 18-H;  $\text{H}_5'$ ).

Thermogravimetric analysis:

- 5% decrease of mass at 329 °C.

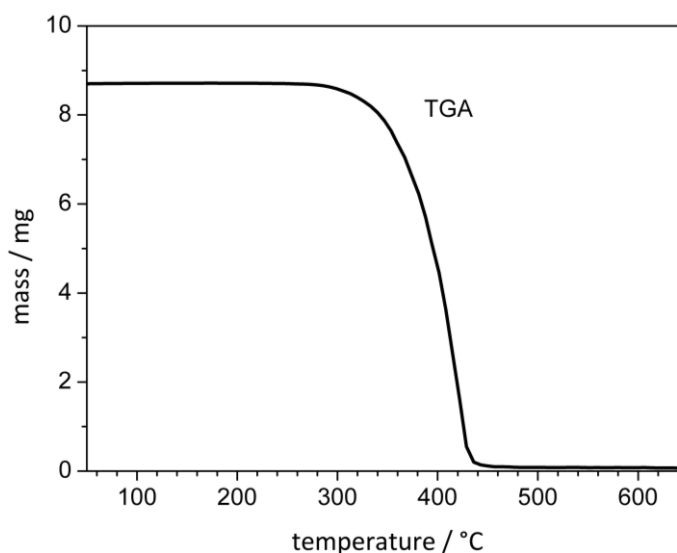


**Figure 8.20:** Thermogravimetric analysis curve of *N,N',N''*-tris(3-methylbutyl)benzene-1,3,5-tricarboxamide (BTA 8). TGA data were recorded at a scanning rate of 10 K/min at temperatures ranging from 30 to 700 °C.

---

*Differential scanning calorimetry:*

- 1<sup>st</sup>-heating curve: 2 reversible phase transitions at 211 °C (3 kJ/mol) and 272 °C (34 kJ/mol)

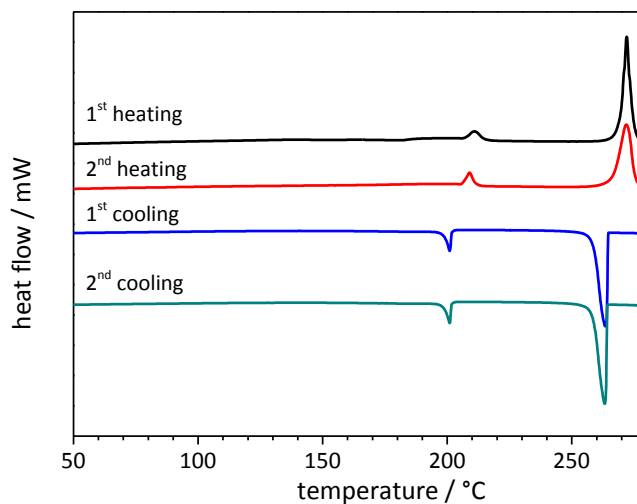


**Figure 8.21:** DSC heating and cooling scans of *N,N',N''*-tris(3-methylbutyl)benzene-1,3,5-tricarboxamide (BTA 8). DSC data were recorded at a scanning rate of 10 K/min at temperatures ranging from 25 to 290 °C.

---

**9 References**

- [1] D. B. Purchas, K. Sutherland, *Handbook of filter media*, Elsevier Advanced Technology, Oxford **2002**.
- [2] P. J. Brown, K. Stevens (Eds.), *Nanofibers and nanotechnology in textiles*, CRC Press, Boca Raton **2007**.
- [3] I. M. Hutten, *Handbook of nonwoven filter media*, Elsevier/BH, Amsterdam **2007**.
- [4] S. Agarwal, A. Greiner, J. H. Wendorff. Electrospinning of Manmade and Biopolymer Nanofibers-Progress in Techniques, Materials, and Applications; *Adv. Funct. Mater.* **2009**, *19*, 2863–2879.
- [5] R. Nayak, R. Padhye, I. L. Kyratzis, Y. B. Truong, L. Arnold. Recent advances in nanofibre fabrication techniques; *Text. Res. J.* **2011**, *82*, 129–147.
- [6] J. H. Wendorff, A. Greiner, S. Agarwal, *Electrospinning: Materials, processing, and applications*, Wiley-VCH, Weinheim **2012**.
- [7] H. J. Koslowski, *Dictionary of man-made fibers: Terms, figures, trademarks*, Deutscher Fachverlag, Frankfurt am Main **2010**.
- [8] C. J. Luo, S. D. Stoyanov, E. Stride, E. Pelan, M. Edirisinghe. Electrospinning versus fibre production methods: from specifics to technological convergence; *Chem. Soc. Rev.* **2012**, *41*, 4708–4735.
- [9] J. W. Steed, J. L. Atwood, *Supramolecular chemistry*, Wiley VCH, Chichester **2009**.
- [10] U. Boudriot, R. Dersch, A. Greiner, J. H. Wendorff. Electrospinning approaches toward scaffold engineering--a brief overview; *Artif. Organs* **2006**, *30*, 785–792.
- [11] M. M. Demir, M. A. Gulgun, Y. Z. Menciloglu, B. Erman, S. S. Abramchuk, E. E. Makhaeva, A. R. Khokhlov, V. G. Matveeva, M. G. Sulman. Palladium Nanoparticles by Electrospinning from Poly(acrylonitrile- co -acrylic acid)-PdCl<sub>2</sub> Solutions. Relations between Preparation Conditions, Particle Size, and Catalytic Activity; *Macromolecules* **2004**, *37*, 1787–1792.
- [12] M. Graeser, E. Pippel, A. Greiner, J. H. Wendorff. Polymer Core-Shell Fibers with Metal Nanoparticles as Nanoreactor for Catalysis; *Macromolecules* **2007**, *40*, 6032–6039.
- [13] X.-H. Qin, S.-Y. Wang. Filtration properties of electrospinning nanofibers; *J. Appl. Polym. Sci.* **2006**, *102*, 1285–1290.
- [14] P. Heikkilä, A. Taipale, M. Lehtimäki, A. Harlin. Electrospinning of polyamides with different chain compositions for filtration application; *Polym. Eng. Sci.* **2008**, *48*, 1168–1176.
- [15] S. A. Theron, A. L. Yarin, E. Zussman, E. Kroll. Multiple jets in electrospinning; *Polymer* **2005**, *46*, 2889–2899.

## References

---

- [16] R. L. Shambaugh. A macroscopic view of the melt-blowing process for producing microfibers; *Ind. Eng. Chem. Res.* **1988**, *27*, 2363–2372.
- [17] T. Nakajima, K. Kajiwara (Eds.), *Advanced fiber spinning technology*, Woodhead Publishing, Cambridge **1994**.
- [18] G. Ward. Meltblown nanofibres for nonwoven filtration applications; *Filtr. Seperat.* **2001**, *38*, 42–43.
- [19] C. J. Ellison, A. Phatak, D. W. Giles, C. W. Macosko, F. S. Bates. Melt blown nanofibers; *Polymer* **2007**, *48*, 3306–3316.
- [20] A. Podgórski, A. Bałazy, L. Gradoń. Application of nanofibers to improve the filtration efficiency of the most penetrating aerosol particles in fibrous filters; *Chem. Eng. Sci.* **2006**, *61*, 6804–6815.
- [21] M. Lalagiri, G. Bhat, V. Singh, S. Parameswaran, R. J. Kendall, S. Ramkumar. Filtration Efficiency of Submicrometer Filters; *Ind. Eng. Chem. Res.* **2013**, *52*, 16513–16518.
- [22] A. Jackiewicz, A. Podgórski, L. Gradoń, J. Michalski. Nanostructured Media to Improve the Performance of Fibrous Filters; *KONA* **2013**, *30*, 244–255.
- [23] X. Zhang, Y. Lu. Centrifugal Spinning; *Polym. Rev.* **2014**, *54*, 677–701.
- [24] Y. Lu, Y. Li, S. Zhang, G. Xu, K. Fu, H. Lee, X. Zhang. Parameter study and characterization for polyacrylonitrile nanofibers fabricated via centrifugal spinning process; *Eur. Polym. J.* **2013**, *49*, 3834–3845.
- [25] L. Ren, R. Ozisik, S. P. Kotha, P. T. Underhill. Highly Efficient Fabrication of Polymer Nanofiber Assembly by Centrifugal Jet Spinning; *Macromolecules* **2015**, *48*, 2593–2602.
- [26] L. C. Palmer, S. I. Stupp. Molecular self-assembly into one-dimensional nanostructures; *Accounts Chem. Res.* **2008**, *41*, 1674–1684.
- [27] X. Li, Y. Kuang, H.-C. Lin, Y. Gao, J. Shi, B. Xu. Supramolecular Nanofibers and Hydrogels of Nucleopeptides; *Angew. Chem. Int. Ed.* **2011**, *50*, 9365–9369.
- [28] T. Aida, E. W. Meijer, S. I. Stupp. Functional supramolecular polymers; *Science* **2012**, *335*, 813–817.
- [29] E. Mattia, S. Otto. Supramolecular systems chemistry; *Nat. Nanotechnol.* **2015**, *10*, 111–119.
- [30] J. Meeuwissen, J. N. H. Reek. Supramolecular catalysis beyond enzyme mimics; *Nature Chem.* **2010**, *2*, 615–621.
- [31] M. Raynal, P. Ballester, A. Vidal-Ferran, van Leeuwen, Piet W N M. Supramolecular catalysis. Part 1: non-covalent interactions as a tool for building and modifying homogeneous catalysts; *Chem. Soc. Rev.* **2014**, *43*, 1660–1733.

## References

---

- [32] M. Raynal, P. Ballester, A. Vidal-Ferran, van Leeuwen, Piet W N M. Supramolecular catalysis. Part 2: artificial enzyme mimics; *Chem. Soc. Rev.* **2014**, *43*, 1734–1787.
- [33] V. Balzani. Supramolecular photochemistry; *Tetrahedron* **1992**, *48*, 10443–10514.
- [34] M.-O. M. Piepenbrock, G. O. Lloyd, N. Clarke, J. W. Steed. Metal- and anion-binding supramolecular gels; *Chem. Rev.* **2010**, *110*, 1960–2004.
- [35] Schenning, Albertus P H J, E. W. Meijer. Supramolecular electronics; nanowires from self-assembled pi-conjugated systems; *Chem. Commun.* **2005**, 3245–3258.
- [36] X. Yan, M. Zhou, J. Chen, X. Chi, S. Dong, M. Zhang, X. Ding, Y. Yu, S. Shao, F. Huang. Supramolecular polymer nanofibers via electrospinning of a heteroditopic monomer; *Chem. Commun.* **2011**, *47*, 7086–7088.
- [37] X. Yan, D. Xu, X. Chi, J. Chen, S. Dong, X. Ding, Y. Yu, F. Huang. A multiresponsive, shape-persistent, and elastic supramolecular polymer network gel constructed by orthogonal self-assembly; *Adv. Mater.* **2012**, *24*, 362–369.
- [38] G. Du, E. Moulin, N. Jouault, E. Buhler, N. Giuseppone. Muscle-like supramolecular polymers: integrated motion from thousands of molecular machines; *Angew. Chem. Int. Ed.* **2012**, *51*, 12504–12508.
- [39] H. Xing, H. Wang, X. Yan, X. Ji. A responsive supramolecular metallogel constructed by coordination-driven self-assembly of a crown ether-based [3]pseudorotaxane and a diplatinum(II) acceptor; *Dalton T.* **2015**, *44*, 11264–11268.
- [40] P. Wei, X. Yan, F. Huang. Supramolecular polymers constructed by orthogonal self-assembly based on host-guest and metal-ligand interactions; *Chem. Soc. Rev.* **2015**, *44*, 815–832.
- [41] J. C. Ma, D. A. Dougherty. The Cation– $\pi$  Interaction; *Chem. Rev.* **1997**, *97*, 1303–1324.
- [42] B. Xia, B. Zheng, C. Han, S. Dong, M. Zhang, B. Hu, Y. Yu, F. Huang. A novel pH-responsive supramolecular polymer constructed by pillar[5]arene-based host–guest interactions; *Polym. Chem.* **2013**, *4*, 2019.
- [43] G. A. Jeffrey, *An Introduction to Hydrogen Bonding*, Oxford University Press, New York **1997**.
- [44] J. D. Hartgerink, J. R. Granja, R. A. Milligan, M. R. Ghadiri. Self-Assembling Peptide Nanotubes; *J. Am. Chem. Soc.* **1996**, *118*, 43–50.
- [45] W. S. Horne, C. D. Stout, M. R. Ghadiri. A heterocyclic peptide nanotube; *J. Am. Chem. Soc.* **2003**, *125*, 9372–9376.
- [46] N. Ashkenasy, W. S. Horne, M. R. Ghadiri. Design of self-assembling peptide nanotubes with delocalized electronic states; *Small* **2006**, *2*, 99–102.
- [47] A. Brik. Fighting hepatitis C virus with peptide nanotubes; *Chem. Biol.* **2011**, *18*, 1347–1348.

## References

---

- [48] Y. Matsunaga, N. Miyajima, Y. Nakayasu, S. Sakai, M. Yonenaga. Design of Novel Mesomorphic Compounds: N,N',N''-Trialkyl-1,3,5-benzenetricarboxamides; *Bull. Chem. Soc. Jpn* **1988**, *61*, 207.
- [49] L. Brunsveld, A. Schenning, M. Broeren, H. M. Janssen, J. Vekemans, E. W. Meijer. Chiral Amplification in Columns of Self-Assembled N,N',N''-Tris((S)-3,7-dimethyloctyl)benzene-1,3,5-tricarboxamide in Dilute Solution; *Chem. Lett.* **2000**, 292–293.
- [50] A. Timme, R. Kress, R. Q. Albuquerque, H.-W. Schmidt. Phase behavior and mesophase structures of 1,3,5-benzene- and 1,3,5-cyclohexanetricarboxamides: towards an understanding of the losing order at the transition into the isotropic phase; *Chem. Eur. J.* **2012**, *18*, 8329–8339.
- [51] S. Cantekin, de Greef, Tom F A, A. R. A. Palmans. Benzene-1,3,5-tricarboxamide: a versatile ordering moiety for supramolecular chemistry; *Chem. Soc. Rev.* **2012**, *41*, 6125–6137.
- [52] Y. Matsunaga, N. Miyajima, Y. Nakayasu, S. Sakai, M. Yonenaga. Design of Novel Mesomorphic Compounds: N,N',N''-Trialkyl-1,3,5-benzenetricarboxamides; *Bulletin of the Chemical Society of Japan* **1988**, *61*, 207.
- [53] P. J. M. Stals, J. C. Everts, R. de Bruijn, I. A. W. Filot, M. M. J. Smulders, R. Martín-Rapún, E. A. Pidko, de Greef, Tom F A, A. R. A. Palmans, E. W. Meijer. Dynamic supramolecular polymers based on benzene-1,3,5-tricarboxamides: the influence of amide connectivity on aggregate stability and amplification of chirality; *Chem. Eur. J.* **2010**, *16*, 810–821.
- [54] J. Y. Chang, J. H. Baik, C. B. Lee, M. J. Han, S.-K. Hong. Liquid Crystals Obtained from Dislike Mesogenic Diacetylenes and Their Polymerization; *J. Am. Chem. Soc.* **1997**, *119*, 3197–3198.
- [55] A. Bernet, R. Q. Albuquerque, M. Behr, S. T. Hoffmann, H.-W. Schmidt. Formation of a supramolecular chromophore; *Soft Matter* **2012**, *8*, 66–69.
- [56] J. J. van Gorp, Vekemans, Jef A. J. M., E. W. Meijer. C<sub>3</sub>-Symmetrical Supramolecular Architectures; *J. Am. Chem. Soc.* **2002**, *124*, 14759–14769.
- [57] P. P. Bose, M. G. B. Drew, A. K. Das, A. Banerjee. Formation of triple helical nanofibers using self-assembling chiral benzene-1,3,5-tricarboxamides and reversal of the nanostructure's handedness using mirror image building blocks; *Chem. Commun.* **2006**, 3196–3198.
- [58] S. Lee, J.-S. Lee, C. H. Lee, Y.-S. Jung, J.-M. Kim. Nonpolymeric thermosensitive benzenetricarboxamides; *Langmuir* **2011**, *27*, 1560–1564.
- [59] K. Hanabusa, C. Koto, M. Kimura, H. Shirai, A. Kakehi. Remarkable Viscoelasticity of Organic Solvents Containing Trialkyl-1,3,5-benzenetricarboxamides and Their Intermolecular Hydrogen Bonding; *Chem. Lett.* **1997**, 429–430.

## References

---

- [60] M. P. Lightfoot, F. S. Mair, R. G. Pritchard, J. E. Warren. New supramolecular packing motifs: p-stacked rods encased in triply-helical hydrogen bonded amide strands; *Chem. Commun.* **1999**, 1945–1946.
- [61] M. Kristiansen, P. Smith, H. Chanzy, C. Baerlocher, V. Gramlich, L. McCusker, T. Weber, P. Pattison, M. Blomenhofer, H.-W. Schmidt. Structural Aspects of 1,3,5-Benzenetrisamides—A New Family of Nucleating Agents; *Cryst. Growth Des.* **2009**, *9*, 2556–2558.
- [62] C. A. Jiménez, J. B. Belmar, L. Ortíz, P. Hidalgo, O. Fabelo, J. Pasán, C. Ruiz-Pérez. Influence of the Aliphatic Wrapping in the Crystal Structure of Benzene Tricarboxamide Supramolecular Polymers; *Cryst. Growth Des.* **2009**, *9*, 4987–4989.
- [63] L. Rajput, V. V. Chernyshev, K. Biradha. Assembling triple helical amide-to-amide hydrogen bonded columns of tris(4-halophenyl)benzene-1,3,5-tricarboxamides into porous materials via halogen...halogen interactions; *Chem. Commun.* **2010**, *46*, 6530–6532.
- [64] C. Zehe, M. Schmidt, R. Siegel, K. Kreger, V. Daebel, S. Ganzleben, H.-W. Schmidt, J. Senker. Influence of fluorine side-group substitution on the crystal structure formation of benzene-1,3,5-trisamides; *CrystEngComm* **2014**, *16*, 9273–9283.
- [65] R. Q. Albuquerque, A. Timme, R. Kress, J. Senker, H.-W. Schmidt. Theoretical investigation of macrodipoles in supramolecular columnar stackings; *Chem. Eur. J.* **2013**, *19*, 1647–1657.
- [66] M. Schmidt, J. J. Wittmann, R. Kress, D. Schneider, S. Steuernagel, H.-W. Schmidt, J. Senker. Crystal Structure of a Highly Efficient Clarifying Agent for Isotactic Polypropylene; *Cryst. Growth Des.* **2012**, *12*, 2543–2551.
- [67] S. J. Lee, C. R. Park, J. Y. Chang. Molecular aggregation of disklike benzenetricarboxamides containing diacetylenic groups in bulk and organic solvents; *Langmuir* **2004**, *20*, 9513–9519.
- [68] M. de Loos, J. H. van Esch, R. M. Kellogg, B. L. Feringa. C<sub>3</sub>-Symmetric, amino acid based organogelators and thickeners; *Tetrahedron* **2007**, *63*, 7285–7301.
- [69] Y. Yasuda, E. Iishi, H. Inada, Y. Shiota. Novel Low-molecular-weight Organic Gels; *Chem. Lett.* **1996**, 575–576.
- [70] A. Paikar, A. Pramanik, D. Haldar. Influence of side-chain interactions on the self-assembly of discotic tricarboxyamides; *RSC Adv.* **2015**, *5*, 31845–31851.
- [71] D. Kluge, F. Abraham, S. Schmidt, H.-W. Schmidt, A. Fery. Nanomechanical properties of supramolecular self-assembled whiskers determined by AFM force mapping; *Langmuir* **2010**, *26*, 3020–3023.
- [72] D. Kluge, J. C. Singer, J. W. Neubauer, F. Abraham, H.-W. Schmidt, A. Fery. Influence of the molecular structure and morphology of self-assembled 1,3,5-benzenetrisamide nanofibers on their mechanical properties; *Small* **2012**, *8*, 2563–2570.

## References

---

- [73] C. M. A. Leenders, L. Albertazzi, T. Mes, M. M. E. Koenigs, A. R. A. Palmans, E. W. Meijer. Supramolecular polymerization in water harnessing both hydrophobic effects and hydrogen bond formation; *Chem. Commun.* **2013**, *49*, 1963–1965.
- [74] C. M. A. Leenders, T. Mes, M. B. Baker, M. M. E. Koenigs, P. Besenius, A. R. A. Palmans, E. W. Meijer. From supramolecular polymers to hydrogel materials; *Mater. Horiz.* **2014**, *1*, 116–120.
- [75] Z. Shen, T. Wang, M. Liu. Macroscopic chirality of supramolecular gels formed from achiral tris(ethyl cinnamate) benzene-1,3,5-tricarboxamides; *Angew. Chem. Int. Ed.* **2014**, *53*, 13424–13428.
- [76] R. C. T. Howe, A. P. Smalley, A. P. M. Guttenplan, M. W. R. Doggett, M. D. Eddleston, J. C. Tan, G. O. Lloyd. A family of simple benzene 1,3,5-tricarboxamide (BTA) aromatic carboxylic acid hydrogels; *Chem. Commun.* **2013**, *49*, 4268–4270.
- [77] M. K. Müller, L. Brunsveld. A supramolecular polymer as a self-assembling polyvalent scaffold; *Angew. Chem. Int. Ed.* **2009**, *48*, 2921–2924.
- [78] N. Mohmeyer, N. Behrendt, X. Zhang, P. Smith, V. Altstädt, G. M. Sessler, H.-W. Schmidt. Additives to improve the electret properties of isotactic polypropylene; *Polymer* **2007**, *48*, 1612–1619.
- [79] J. Hillenbrand, T. Motz, G. M. Sessler, X. Zhang, N. Behrendt, C. von Salis-Soglio, D. P. Erhard, V. Altstädt, H.-W. Schmidt. The effect of additives on charge decay in electron-beam charged polypropylene films; *J. Phys. D: Appl. Phys.* **2009**, *42*, 65410.
- [80] N. Mohmeyer, B. Müller, N. Behrendt, J. Hillenbrand, M. Klaiber, X. Zhang, P. Smith, V. Altstädt, G. M. Sessler, H.-W. Schmidt. Nucleation of isotactic polypropylene by triphenylamine-based trisamide derivatives and their influence on charge-storage properties; *Polymer* **2004**, *45*, 6655–6663.
- [81] M. Blomenhofer, S. Ganzleben, D. Hanft, H.-W. Schmidt, M. Kristiansen, P. Smith, K. Stoll, D. Mäder, K. Hoffmann. “Designer” Nucleating Agents for Polypropylene; *Macromolecules* **2005**, *38*, 3688–3695.
- [82] P. M. Kristiansen, A. Gress, P. Smith, D. Hanft, H.-W. Schmidt. Phase behavior, nucleation and optical properties of the binary system isotactic polypropylene/*N,N,N'*-tris-isopentyl-1,3,5-benzene-tricarboxamide; *Polymer* **2006**, *47*, 249–253.
- [83] F. Abraham, S. Ganzleben, D. Hanft, P. Smith, H.-W. Schmidt. Synthesis and Structure–Efficiency Relations of 1,3,5-Benzenetrisamides as Nucleating Agents and Clarifiers for Isotactic Poly(propylene); *Macromol. Chem. Phys.* **2010**, *211*, 171–181.

## References

---

- [84] F. Abraham, H.-W. Schmidt. 1,3,5-Benzenetrisamide based nucleating agents for poly(vinylidene fluoride); *Polymer* **2010**, *51*, 913–921.
- [85] F. Richter, H.-W. Schmidt. Supramolecular Nucleating Agents for Poly(butylene terephthalate) Based on 1,3,5-Benzenetrisamides; *Macromol. Mater. Eng.* **2013**, *298*, 190–200.
- [86] Y.-H. Cai, Y. Tang, L.-S. Zhao. Poly(l -lactic acid) with the organic nucleating agent N,N,N '-tris(1 H -benzotriazole) trimesinic acid acetylhydrazide; *J. Appl. Polym. Sci.* **2015**, *132*, 42402.
- [87] X. Zhang, L. Meng, G. Li, N. Liang, J. Zhang, Z. Zhu, R. Wang. Effect of nucleating agents on the crystallization behavior and heat resistance of poly(l -lactide); *J. Appl. Polym. Sci.* **2016**, *133*, 42999.
- [88] H. Misslitz, *Supramolecular Nanofibers Preparation, Structure-Property Relations, and Applications*, Bayreuth **2013**.
- [89] H. Misslitz, K. Kreger, H.-W. Schmidt. Supramolecular nanofiber webs in nonwoven scaffolds as potential filter media; *Small* **2013**, *9*, 2053.
- [90] I. D. Wilson (Ed.), *Encyclopedia of separation science*, Elsevier Science, Amsterdam **2000**.
- [91] K. Schwister (Ed.), *Taschenbuch der Verfahrenstechnik*, Fachbuchverlag Leipzig im Carl-Hanser-Verlag, München **2010**.
- [92] A. Behr, D. W. Agar, J. Jörissen, *Einführung in die Technische Chemie*, Spektrum Akademischer Verlag, Heidelberg **2010**.
- [93] M. Baerns, *Technische Chemie*, Wiley-VCH, Weinheim **2013**.
- [94] K. Sutherland, *A-Z of filtration and related separations*, Elsevier, Oxford **2005**.
- [95] R. J. Wakeman, E. S. Tarleton, *Filtration: Equipment selection modelling and process simulation*, Elsevier, Oxford **1999**.
- [96] G. Viswanathan, D. B. Kane, P. J. Lipowicz. High Efficiency Fine Particulate Filtration Using Carbon Nanotube Coatings; *Adv. Mater.* **2004**, *16*, 2045–2049.
- [97] J. J. Simonis, A. K. Basson. Manufacturing a low-cost ceramic water filter and filter system for the elimination of common pathogenic bacteria; *Phys. Chem. Earth* **2012**, *50-52*, 269–276.
- [98] D. Ren, L. M. Colosi, J. A. Smith. Evaluating the Sustainability of Ceramic Filters for Point-of-Use Drinking Water Treatment; *Environ. Sci. Technol.* **2013**, *47*, 11206–11213.
- [99] P. Li, C. Wang, Y. Zhang, F. Wei. Air filtration in the free molecular flow regime: a review of high-efficiency particulate air filters based on carbon nanotubes; *Small* **2014**, *10*, 4543–4561.
- [100] L. S. Abebe, Y.-H. Su, R. L. Guarrant, N. S. Swami, J. A. Smith. Point-of-Use Removal of *Cryptosporidium parvum* from Water: Independent Effects of Disinfection by Silver

## References

---

- Nanoparticles and Silver Ions and by Physical Filtration in Ceramic Porous Media; *Environ. Sci. Technol.* **2015**, *49*, 12958–12967.
- [101] S.-L. Loo, A. G. Fane, W. B. Krantz, T.-T. Lim. Emergency water supply: a review of potential technologies and selection criteria; *Water Res.* **2012**, *46*, 3125–3151.
- [102] J. S. Apte, J. D. Marshall, A. J. Cohen, M. Brauer. Addressing Global Mortality from Ambient PM<sub>2.5</sub>; *Environ. Sci. Technol.* **2015**, *49*, 8057–8066.
- [103] D. Cho, A. Naydich, M. W. Frey, Y. L. Joo. Further improvement of air filtration efficiency of cellulose filters coated with nanofibers via inclusion of electrostatically active nanoparticles; *Polymer* **2013**, *54*, 2364–2372.
- [104] J. Matulevicius, L. Kliucininkas, D. Martuzevicius, E. Krugly, M. Tichonovas, J. Baltrusaitis. Design and Characterization of Electrospun Polyamide Nanofiber Media for Air Filtration Applications; *J. Nanomater.* **2014**, *2014*, 1–13.
- [105] L. S. Pinchuk, V. A. Goldade, A. V. Makarevich, V. N. Kestelman, *Melt Blowing: Equipment, Technology, and Polymer Fibrous Materials*, Springer, Berlin **2002**.
- [106] A. Fenwick. Waterborne infectious diseases--could they be consigned to history?; *Science* **2006**, *313*, 1077–1081.
- [107] Duke, W. F., R. N. Nordin, D. Baker, A. Mazunder. The use and performance of BioSand filters in the Artibonite Valley of Haiti: a field study of 107 households; *Rural and Remote Health* **2006**, *6*, 570.
- [108] V. A. Oyanedel-Craver, J. A. Smith. Sustainable Colloidal-Silver-Impregnated Ceramic Filter for Point-of-Use Water Treatment; *Environ. Sci. Technol.* **2008**, *42*, 927–933.
- [109] T. Clasen, *Scaling Up Household Water Treatment Among Low-Income Populations*, WHO Press, Geneva **2009**.
- [110] C. C. Lee, C. Grenier, E. W. Meijer, Schenning, Albertus P H J. Preparation and characterization of helical self-assembled nanofibers; *Chem. Soc. Rev.* **2009**, *38*, 671–683.
- [111] M. Liu, L. Zhang, T. Wang. Supramolecular Chirality in Self-Assembled Systems; *Chem. Rev.* **2015**, *115*, 7304–7397.
- [112] C. Rest, R. Kandaneli, G. Fernández. Strategies to create hierarchical self-assembled structures via cooperative non-covalent interactions; *Chem. Soc. Rev.* **2015**, *44*, 2543–2572.
- [113] F. Abraham, *Synthesis and structure-property relations of 1,3,5-benzenetrisamides as nucleating agents for isotactic polypropylene and poly(vinylidene fluoride)*, Monsenstein und Vannerdat, Münster **2010**, PhD thesis, University of Bayreuth.
- [114] Z. K. Nagy, R. D. Braatz. Advances and new directions in crystallization control; *Annu. Rev. Chem. Biomol. Eng.* **2012**, *3*, 55–75.

## References

---

- [115] N. S. Tavare, *Industrial Crystallization: Process Simulation Analysis and Design*, Springer, Boston **1995**.
- [116] A. S. Myerson (Ed.), *Handbook of industrial crystallization*, Butterworth-Heinemann, Boston **2002**.
- [117] Y. Yuan, R.-l. Fan, L. Guo, C.-y. Chen, Q.-q. Zhao. Solubilities of 1,3,2-Dioxaphosphorinane-2-methanol- $\alpha$ ,5,5-trimethyl- $\alpha$ -phenyl-2-oxide in Selected Solvents between 278.15 K and 343.15 K; *J. Chem. Eng. Data* **2015**, *60*, 729–733.
- [118] X. Gao, W.-L. Xue, Z.-X. Zeng, X.-r. Fan. Determination and Correlation of Solubility of N - tert -Butylacrylamide in Seven Different Solvents at Temperatures between (279.15 and 353.15) K; *J. Chem. Eng. Data* **2015**, *60*, 2273–2279.
- [119] Y. Deng, L. Xu, X. Sun, L. Cheng, G. Liu. Measurement and Correlation of the Solubility for 4,4'-Diaminodiphenylmethane in Different Solvents; *J. Chem. Eng. Data* **2015**, *60*, 2028–2034.
- [120] S.-h. Tang, L.-l. Pei, Y. Tian, X.-k. Wang, Z.-l. Sha, Y.-y. Gao, H.-b. Xu, Y. Zhang. Solubility of Sodium Chromate in the NaOH–CH<sub>3</sub>OH–H<sub>2</sub>O System from (278.15 to 343.15) K; *J. Chem. Eng. Data* **2015**, *60*, 1584–1591.
- [121] L. J. Gordon, R. L. Scott. Enhanced solubility in solvent mixtures. I. The system phenanthrene-cyclohexane-methylene iodide; *J. Am. Chem. Soc.* **1952**, *74*, 4138–4140.
- [122] N. Doki, N. Kubota, A. Sato, M. Yokota. Effect of cooling mode on product crystal size in seeded batch crystallization of potassium alum; *Chem. Eng. J.* **2001**, *81*, 313–316.
- [123] H. Seki, N. Furuya, S. Hoshino. Evaluation of controlled cooling for seeded batch crystallization incorporating dissolution; *Chem. Eng. Sci.* **2012**, *77*, 10–17.
- [124] M. Stieß, *Mechanische Verfahrenstechnik - Partikeltechnologie 1*, Springer, Berlin, Heidelberg **2009**.
- [125] Gesellschaft Verfahrenstechnik und Chemieingenieurwesen, *VDI-Wärmeatlas*, Springer, Berlin **2006**.
- [126] G. Emig, E. Klemm, *Technische Chemie: Einführung in die Chemische Reaktionstechnik*, Springer, Berlin, Heidelberg **2005**.
- [127] H. Kuchling, *Taschenbuch der Physik*, Fachbuchverlag Leipzig im Carl Hanser Verlag, München **2011**.
- [128] C. Han, J. P. Lee, E. Lobkovsky, J. A. Porco. Catalytic ester-amide exchange using group (IV) metal alkoxide-activator complexes; *J. Am. Chem. Soc.* **2005**, *127*, 10039–10044.
- [129] P. J. M. Stals, M. M. J. Smulders, R. Martín-Rapún, A. R. A. Palmans, E. W. Meijer. Asymmetrically substituted benzene-1,3,5-tricarboxamides: self-assembly and odd-even effects in the solid state and in dilute solution; *Chem. Eur. J.* **2009**, *15*, 2071–2080.

## References

---

- [130] M. Wegner, D. Dudenko, D. Sebastiani, A. R. A. Palmans, de Greef, Tom F. A., R. Graf, H. W. Spiess. The impact of the amide connectivity on the assembly and dynamics of benzene-1,3,5-tricarboxamides in the solid state; *Chem. Sci.* **2011**, *2*, 2040.
- [131] M. Kampa, E. Castanas. Human health effects of air pollution; *Environ. Pollut.* **2008**, *151*, 362–367.
- [132] World Health Organization, *Health effects of particulate matter*, WHO Regional Office for Europe, Copenhagen **2013**.
- [133] S. Humbert, J. D. Marshall, S. Shaked, J. V. Spadaro, Y. Nishioka, P. Preiss, T. E. McKone, A. Horvath, O. Jolliet. Intake fraction for particulate matter: recommendations for life cycle impact assessment; *Environ. Sci. Technol.* **2011**, *45*, 4808–4816.
- [134] J. S. Apte, E. Bombrun, J. D. Marshall, W. W. Nazaroff. Global intraurban intake fractions for primary air pollutants from vehicles and other distributed sources; *Environmental science & technology* **2012**, *46*, 3415–3423.
- [135] European Environment Agency, *Particulate matter from natural sources and related reporting under the EU Air Quality Directive in 2008 and 2009*, Publications Office of the European Union, Luxembourg **2012**.
- [136] J. M. Panko, J. Chu, M. L. Kreider, K. M. Unice. Measurement of airborne concentrations of tire and road wear particles in urban and rural areas of France, Japan, and the United States; *Atmos. Environ.* **2013**, *72*, 192–199.
- [137] C. A. Pope III. Lung Cancer, Cardiopulmonary Mortality, and Long-term Exposure to Fine Particulate Air Pollution; *JAMA* **2002**, *287*, 1132.
- [138] M. L. Bell, K. Ebisu, K. Belanger. The relationship between air pollution and low birth weight: effects by mother's age, infant sex, co-pollutants, and pre-term births; *Environ. Res. Lett.* **2008**, *3*, 44003.
- [139] C. A. Pope, M. Ezzati, D. W. Dockery. Fine-particulate air pollution and life expectancy in the United States; *N. Engl. J. Med.* **2009**, *360*, 376–386.
- [140] P. Pagano, T. de Zaiacomo, E. Scarcella, S. Bruni, M. Calamosca. Mutagenic Activity of Total and Particle-Sized Fractions of Urban Particulate Matter; *Environ. Sci. Technol.* **1996**, *30*, 3512–3516.
- [141] A. T. Lemos, M. V. Coronas, J. A. V. Rocha, V. M. F. Vargas. Mutagenicity of particulate matter fractions in areas under the impact of urban and industrial activities; *Chemosphere* **2012**, *89*, 1126–1134.
- [142] S. S. Lim, T. Vos, A. D. Flaxman, G. Danaei, K. Shibuya, H. Adair-Rohani, M. A. AlMazroa, M. Amann, H. R. Anderson, K. G. Andrews, M. Aryee, C. Atkinson, L. J. Bacchus, A. N. Bahalim, K.

## References

---

- Balakrishnan, J. Balmes, S. Barker-Collo, A. Baxter, M. L. Bell, J. D. Blore, F. Blyth, C. Bonner, G. Borges, R. Bourne, M. Boussinesq, M. Brauer, P. Brooks, N. G. Bruce, B. Brunekreef, C. Bryan-Hancock, C. Bucello, R. Buchbinder, F. Bull, R. T. Burnett, T. E. Byers, B. Calabria, J. Carapetis, E. Carnahan, Z. Chafe, F. Charlson, H. Chen, J. S. Chen, A. T.-A. Cheng, J. C. Child, A. Cohen, K. E. Colson, B. C. Cowie, S. Darby, S. Darling, A. Davis, L. Degenhardt, F. Dentener, D. C. Des Jarlais, K. Devries, M. Dherani, E. L. Ding, E. R. Dorsey, T. Driscoll, K. Edmond, S. E. Ali, R. E. Engell, P. J. Erwin, S. Fahimi, G. Falder, F. Farzadfar, A. Ferrari, M. M. Finucane, S. Flaxman, F. G. R. Fowkes, G. Freedman, M. K. Freeman, E. Gakidou, S. Ghosh, E. Giovannucci, G. Gmel, K. Graham, R. Grainger, B. Grant, D. Gunnell, H. R. Gutierrez, W. Hall, H. W. Hoek, A. Hogan, H. D. Hosgood, D. Hoy, H. Hu, B. J. Hubbell, S. J. Hutchings, S. E. Ibeanusi, G. L. Jacklyn, R. Jasrasaria, J. B. Jonas, H. Kan, J. A. Kanis, N. Kassebaum, N. Kawakami, Y.-H. Khang, S. Khatibzadeh, J.-P. Khoo, C. Kok, F. Laden, R. Lalloo, Q. Lan, T. Lathlean, J. L. Leasher, J. Leigh, Y. Li, J. K. Lin, S. E. Lipshultz, S. London, R. Lozano, Y. Lu, J. Mak, R. Malekzadeh, L. Mallinger, W. Marcenes, L. March, R. Marks, R. Martin, P. McGale, J. McGrath, S. Mehta, Z. A. Memish, G. A. Mensah, T. R. Merriman, R. Micha, C. Michaud, V. Mishra, K. M. Hanafiah, A. A. Mokdad, L. Morawska, D. Mozaffarian, T. Murphy, M. Naghavi, B. Neal, P. K. Nelson, J. M. Nolla, R. Norman, C. Olives, S. B. Omer, J. Orchard, R. Osborne, B. Ostro, A. Page, K. D. Pandey, C. D. H. Parry, E. Passmore, J. Patra, N. Pearce, P. M. Pelizzari, M. Petzold, M. R. Phillips, D. Pope, C. A. Pope, J. Powles, M. Rao, H. Razavi, E. A. Rehfuss, J. T. Rehm, B. Ritz, F. P. Rivara, T. Roberts, C. Robinson, J. A. Rodriguez-Portales, I. Romieu, R. Room, L. C. Rosenfeld, A. Roy, L. Rushton, J. A. Salomon, U. Sampson, L. Sanchez-Riera, E. Sanman, A. Sapkota, S. Seedat, P. Shi, K. Shield, R. Shivakoti, G. M. Singh, D. A. Sleet, E. Smith, K. R. Smith, N. J. C. Stapelberg, K. Steenland, H. Stöckl, L. J. Stovner, K. Straif, L. Straney, G. D. Thurston, J. H. Tran, R. van Dingenen, A. van Donkelaar, J. L. Veerman, L. Vijayakumar, R. Weintraub, M. M. Weissman, R. A. White, H. Whiteford, S. T. Wiersma, J. D. Wilkinson, H. C. Williams, W. Williams, N. Wilson, A. D. Woolf, P. Yip, J. M. Zielinski, A. D. Lopez, C. J. L. Murray, M. Ezzati. A comparative risk assessment of burden of disease and injury attributable to 67 risk factors and risk factor clusters in 21 regions, 1990–2010; *The Lancet* **2012**, *380*, 2224–2260.
- [143] R. Lozano, M. Naghavi, K. Foreman, S. Lim, K. Shibuya, V. Aboyans, J. Abraham, T. Adair, R. Aggarwal, S. Y. Ahn, M. A. AlMazroa, M. Alvarado, H. R. Anderson, L. M. Anderson, K. G. Andrews, C. Atkinson, L. M. Baddour, S. Barker-Collo, D. H. Bartels, M. L. Bell, E. J. Benjamin, D. Bennett, K. Bhalla, B. Bikbov, A. B. Abdulhak, G. Birbeck, F. Blyth, I. Bolliger, S. Boufous, C. Bucello, M. Burch, P. Burney, J. Carapetis, H. Chen, D. Chou, S. S. Chugh, L. E. Coffeng, S. D. Colan, S. Colquhoun, K. E. Colson, J. Condon, M. D. Connor, L. T. Cooper, M. Corriere, M.

- 
- Cortinovis, K. C. de Vaccaro, W. Couser, B. C. Cowie, M. H. Criqui, M. Cross, K. C. Dabhadkar, N. Dahodwala, D. de Leo, L. Degenhardt, A. Delossantos, J. Denenberg, D. C. Des Jarlais, S. D. Dharmaratne, E. R. Dorsey, T. Driscoll, H. Duber, B. Ebel, P. J. Erwin, P. Espindola, M. Ezzati, V. Feigin, A. D. Flaxman, M. H. Forouzanfar, F. G. R. Fowkes, R. Franklin, M. Fransen, M. K. Freeman, S. E. Gabriel, E. Gakidou, F. Gaspari, R. F. Gillum, D. Gonzalez-Medina, Y. A. Halasa, D. Haring, J. E. Harrison, R. Havmoeller, R. J. Hay, B. Hoen, P. J. Hotez, D. Hoy, K. H. Jacobsen, S. L. James, R. Jasrasaria, S. Jayaraman, N. Johns, G. Karthikeyan, N. Kassebaum, A. Keren, J.-P. Khoo, L. M. Knowlton, O. Kobusingye, A. Koranteng, R. Krishnamurthi, M. Lipnick, S. E. Lipshultz, S. L. Ohno, J. Mabweijano, M. F. MacIntyre, L. Mallinger, L. March, G. B. Marks, R. Marks, A. Matsumori, R. Matzopoulos, B. M. Mayosi, J. H. McAnulty, M. M. McDermott, J. McGrath, Z. A. Memish, G. A. Mensah, T. R. Merriman, C. Michaud, M. Miller, T. R. Miller, C. Mock, A. O. Mocumbi, A. A. Mokdad, A. Moran, K. Mulholland, M. N. Nair, L. Naldi, K. M. V. Narayan, K. Nasser, P. Norman, M. O'Donnell, S. B. Omer, K. Ortblad, R. Osborne, D. Ozgediz, B. Pahari, J. D. Pandian, A. P. Rivero, R. P. Padilla, F. Perez-Ruiz, N. Perico, D. Phillips, K. Pierce, C. A. Pope, E. Porrini, F. Pourmalek, M. Raju, D. Ranganathan, J. T. Rehm, D. B. Rein, G. Remuzzi, F. P. Rivara, T. Roberts, F. R. de León, L. C. Rosenfeld, L. Rushton, R. L. Sacco, J. A. Salomon, U. Sampson, E. Sanman, D. C. Schwebel, M. Segui-Gomez, D. S. Shepard, D. Singh, J. Singleton, K. Sliwa, E. Smith, A. Steer, J. A. Taylor, B. Thomas, I. M. Tleyjeh, J. A. Towbin, T. Truelsen, E. A. Undurraga, N. Venketasubramanian, L. Vijayakumar, T. Vos, G. R. Wagner, M. Wang, W. Wang, K. Watt, M. A. Weinstock, R. Weintraub, J. D. Wilkinson, A. D. Woolf, S. Wulf, P.-H. Yeh, P. Yip, A. Zabetian, Z.-J. Zheng, A. D. Lopez, C. J. L. Murray. Global and regional mortality from 235 causes of death for 20 age groups in 1990 and 2010; *The Lancet* **2012**, *380*, 2095–2128.
- [144] G. Lang, S. Jokisch, T. Scheibel. Air filter devices including nonwoven meshes of electrospun recombinant spider silk proteins; *J. Vis. Exp.* **2013**, e50492.
- [145] E. Krieg, H. Weissman, E. Shirman, E. Shimoni, B. Rybtchinski. A recyclable supramolecular membrane for size-selective separation of nanoparticles; *Nat. Nanotechnol.* **2011**, *6*, 141–146.
- [146] E. Krieg, B. Rybtchinski. Noncovalent water-based materials: robust yet adaptive; *Chem. Eur. J.* **2011**, *17*, 9016–9026.
- [147] E. Krieg, S. Albeck, H. Weissman, E. Shimoni, B. Rybtchinski. Separation, immobilization, and biocatalytic utilization of proteins by a supramolecular membrane; *PLoS one* **2013**, *8*, e63188.
- [148] J. P. S. Cabral. Water microbiology. Bacterial pathogens and water; *Int. J. Environ. Res. Public Health* **2010**, *7*, 3657–3703.
-

## References

---

- [149] World Health Organization, *World health statistics 2014*, WHO Press, Geneva **2014**.
- [150] C. Seas, M. Alarcon, J. C. Aragon, S. Beneit, M. Quiñonez, H. Guerra, E. Gotuzzo. Surveillance of bacterial pathogens associated with acute diarrhea in Lima, Peru; *Int. J. Infect. Dis.* **2000**, *4*, 96–99.
- [151] T. Clasen, W.-P. Schmidt, T. Rabie, I. Roberts, S. Cairncross. Interventions to improve water quality for preventing diarrhoea: systematic review and meta-analysis; *BMJ* **2007**, *334*, 782.
- [152] M. D. Sobsey, C. E. Stauber, L. M. Casanova, J. M. Brown, M. A. Elliott. Point of Use Household Drinking Water Filtration; *Environ. Sci. Technol.* **2008**, *42*, 4261–4267.
- [153] S. Boisson, M. Kiyombo, L. Sthreshley, S. Tumba, J. Makambo, T. Clasen. Field assessment of a novel household-based water filtration device: a randomised, placebo-controlled trial in the Democratic Republic of Congo; *PloS one* **2010**, *5*, e12613.
- [154] P. B. Pavlinac, J. M. Naulikha, L. Chaba, N. Kimani, L. R. Sangaré, K. Yuhas, B. O. Singa, G. John-Stewart, J. L. Walson. Water filter provision and home-based filter reinforcement reduce diarrhea in Kenyan HIV-infected adults and their household members; *Am. J. Trop. Med. Hyg.* **2014**, *91*, 273–280.
- [155] V. Verma, V. A. Arankalle. Virological evaluation of domestic water purification devices commonly used in India emphasizes inadequate quality and need for virological standards; *Trop. Med. Int. Health* **2009**, *14*, 885–891.
- [156] K. G. McGuigan, R. M. Conroy, H.-J. Mosler, M. Du Preez, E. Ubomba-Jaswa, P. Fernandez-Ibañez. Solar water disinfection (SODIS): a review from bench-top to roof-top; *J. Hazard. Mater.* **2012**, *235-236*, 29–46.
- [157] P. Dunlop, J. A. Byrne, N. Manga, B. R. Eggins. The photocatalytic removal of bacterial pollutants from drinking water; *J. Photochem. Photobiol. A Chem.* **2002**, *148*, 355–363.
- [158] S. Yu, T. Lin, W. Chen. Photocatalytic inactivation of particle-associated Escherichia coli using UV/TiO<sub>2</sub>; *RSC Adv.* **2014**, *4*, 31370.
- [159] F. Hossain, O. J. Perales-Perez, S. Hwang, F. Román. Antimicrobial nanomaterials as water disinfectant: applications, limitations and future perspectives; *Sci. Total Environ.* **2014**, *466-467*, 1047–1059.
- [160] T. Clasen, S. Nadakatti, S. Menon. Microbiological performance of a water treatment unit designed for household use in developing countries; *Trop. Med. Int. Health* **2006**, *11*, 1399–1405.
- [161] G. Palmateer, D. Manz, A. Jurkovic, R. McInnis, S. Unger, K. K. Kwan, B. J. Dutka. Toxicant and parasite challenge of Manz intermittent slow sand filter; *Environ. Toxicol.* **1999**, *14*, 217–225.

## References

---

- [162] B. A. Aiken, C. E. Stauber, G. M. Ortiz, M. D. Sobsey. An assessment of continued use and health impact of the concrete biosand filter in Bonao, Dominican Republic; *Am. J. Trop. Med. Hyg.* **2011**, *85*, 309–317.
- [163] A. Timme, *Flüssigkristalline supramolekulare Systeme*, Bayreuth **2012**, PhD thesis, University of Bayreuth.

### Danksagung

Zuallererst möchte ich meinem Doktorvater, Herrn Prof. Hans-Werner Schmidt, für die Möglichkeit danken, dass ich diese Doktorarbeit an dem Lehrstuhl Makromolekulare Chemie I der Universität Bayreuth anfertigen durfte. Dabei bedanke ich mich vor Allem für die interessante und anwendungsbezogene Aufgabenstellung, die Möglichkeit in einem gut ausgestatteten Labor arbeiten zu dürfen sowie für seine Unterstützung bei wissenschaftlichen Diskussionen und Ratschlägen.

Darüber hinaus bedanke ich mich für die finanzielle Unterstützung bei der Deutschen Forschungsgemeinschaft (DFG) im Rahmen des Sonderforschungsbereichs 840 „*Von partikulären Nanosystemen zur Mesotechnologie*“ im Teilprojekt B8 „*Struktur-Eigenschaftskorrelationen und Anwendung von faserförmigen Nanoaggregaten und Nanofasernetzwerken*“.

Des Weiteren bedanke ich mich ebenfalls bei der Arbeitsgemeinschaft industrieller Forschungsvereinigungen „Otto von Guericke“ e.V. (AiF), die im Rahmen des Programms zur Förderung der Industriellen Gemeinschaftsforschung (IGF) vom Bundesministerium für Wirtschaft und Energie aufgrund eines Beschlusses des Deutschen Bundestages diese Arbeit finanziell unterstützt hat (Kapitel 5)

Besonderer Dank gilt zudem Dr. Klaus Kreger, der durch seine stete Unterstützung, Diskussionsbereitschaft und umfassende Fachkenntnis zum Gelingen dieser Arbeit beigetragen hat.

Ich bedanke mich auch bei den technischen Angestellten Jutta Failner, Sandra Ganzleben, Doris Hanft und Rika Schneider für die Synthese und Bereitstellung der untersuchten Trisamide. An dieser Stelle gilt besonderer Dank auch Alexander Kern, der mir durch seine umfangreiche Unterstützung im Bereich der Filtrationstests sowie dem Design und Aufbau des Filterprüfstands und unzähligen weiteren Problemstellungen zur Seite stand.

Zudem bedanke ich mich bei Petra Weiss und Christina Wunderlich für die Unterstützung bei vielen verwaltungstechnischen Problemen.

Besonders bedanke ich mich bei Dr. Beate Förster und Martina Heider für die Einweisung und stete Unterstützung im Bereich der Rasterelektronenmikroskopie.

Ferner bedanke ich mich bei David Nardini, Dominik Skrybeck, Moritz Salzmann, Anna Gräser, Partick Hummel, Felix Krohn und Cathrin Müller, die mir als Hilfwissenschaftler neben ihrem Studium bei den wissenschaftlichen Arbeiten halfen.

## Danksagung

---

Mein Dank gebührt auch allen weiteren Mitarbeitern der Makromolekularen Chemie I und dabei besonders meinem Laborkollegen Christian Bartz für die stete Diskussionsbereitschaft.

Zudem bedanke ich mich auch bei der elektronischen Werkstatt der Universität Bayreuth für die Hilfe bei der Entwicklung des Filterprüfstands zur Flüssigfiltration.

Prof. Martin Möller, Dr. Helga Thomas, Dr. Elisabeth Heine, Dr. Xiaomin Zhu, Rita Gartzten und Lisa Severain am Deutschen Wollforschungsinstitut (DWI) - Leibniz-Institut für Interaktive Materialien e.V. in Aachen danke ich für die gute Zusammenarbeit und die Möglichkeit biologische Bakterienwachstumstests im Rahmen dieser Doktorarbeit durchzuführen.

Mein größter Dank gilt meiner Lebensgefährtin Viola Buchholz, die mir trotz der eigenen laufenden Promotion stets zur Seite stand.

## **(Eidesstattliche) Versicherungen und Erklärungen**

(§ 8 S. 2 Nr. 6 PromO)

*Hiermit erkläre ich mich damit einverstanden, dass die elektronische Fassung meiner Dissertation unter Wahrung meiner Urheberrechte und des Datenschutzes einer gesonderten Überprüfung hinsichtlich der eigenständigen Anfertigung der Dissertation unterzogen werden kann.*

(§ 8 S. 2 Nr. 8 PromO)

*Hiermit erkläre ich eidesstattlich, dass ich die Dissertation selbständig verfasst und keine anderen als die von mir angegebenen Quellen und Hilfsmittel benutzt habe.*

(§ 8 S. 2 Nr. 9 PromO)

*Ich habe die Dissertation nicht bereits zur Erlangung eines akademischen Grades anderweitig eingereicht und habe auch nicht bereits diese oder eine gleichartige Doktorprüfung endgültig nicht bestanden.*

(§ 8 S. 2 Nr. 10 PromO)

*Hiermit erkläre ich, dass ich keine Hilfe von gewerblichen Promotionsberatern bzw. -vermittlern in Anspruch genommen habe und auch künftig nicht nehmen werde.*

.....

Ort, Datum, Unterschrift